VOLUME 36 DECEMBER 1958 NUMBER 12

Canadian Journal of Chemistry

Editor: LÉO MARION

Associate Editors:

HERBERT C. BROWN, *Purdue University*
A. R. GORDON, *University of Toronto*
C. B. PURVES, *McGill University*
Sir ERIC RIDEAL, *Imperial College, University of London*
J. W. T. SPINKS, *University of Saskatchewan*
E. W. R. STEACIE, *National Research Council of Canada*
H. G. THODE, *McMaster University*
A. E. VAN ARKEL, *University of Leiden*

Published by THE NATIONAL RESEARCH COUNCIL

OTTAWA CANADA

CANADIAN JOURNAL OF CHEMISTRY

(*Formerly Section B, Canadian Journal of Research*)

Under the authority of the Chairman of the Committee of the Privy Council on Scientific and Industrial Research, the National Research Council issues THE CANADIAN JOURNAL OF CHEMISTRY and five other journals devoted to the publication, in English or French, of the results of original scientific research. Matters of general policy concerning these journals are the responsibility of a joint Editorial Board consisting of: members representing the National Research Council of Canada; the Editors of the Journals; and members representing the Royal Society of Canada and four other scientific societies.

The Chemical Institute of Canada has chosen the Canadian Journal of Chemistry as its medium of publication for scientific papers.

EDITORIAL BOARD

Representatives of the National Research Council

A. Gauthier, *University of Montreal*
R. B. Miller, *University of Alberta*
H. G. Thode, *McMaster University*
D. L. Thomson, *McGill University*

Editors of the Journals

D. L. Bailey, *University of Toronto*
T. W. M. Cameron, *Macdonald College*
H. E. Duckworth, *McMaster University*
K. A. C. Elliott, *Montreal Neurological Institute*
Léo Marion, *National Research Council*
R. G. E. Murray, *University of Western Ontario*

Representatives of Societies

D. L. Bailey, *University of Toronto*
Royal Society of Canada
T. W. M. Cameron, *Macdonald College*
Royal Society of Canada
H. E. Duckworth, *McMaster University*
Royal Society of Canada
Canadian Association of Physicists
K. A. C. Elliott, *Montreal Neurological Institute*
Canadian Physiological Society
P. R. Gendron, *University of Ottawa*
Chemical Institute of Canada
R. G. E. Murray, *University of Western Ontario*
Canadian Society of Microbiologists
T. Thorvaldson, *University of Saskatchewan*, Royal Society of Canada

Ex officio

Léo Marion (Editor-in-Chief), *National Research Council*
J. B. Marshall (Administration and Awards), *National Research Council*

Manuscripts for publication should be submitted to Dr. Léo Marion, Editor-in-Chief, Canadian Journal of Chemistry, National Research Council, Ottawa 2, Canada.
(For instructions on preparation of copy, see **Notes to Contributors** (inside back cover).)

Proof, correspondence concerning proof, and orders for reprints should be sent to the Manager, Editorial Office (Research Journals), Division of Administration and Awards, National Research Council, Ottawa 2, Canada.

Subscriptions, renewals, requests for single or back numbers, and all remittances should be sent to Division of Administration and Awards, National Research Council, Ottawa 2, Canada. Remittances should be made payable to the Receiver General of Canada, credit National Research Council.

The journals published, frequency of publication, and prices are:

Canadian Journal of Biochemistry and Physiology	Monthly	$3.00 a year
Canadian Journal of Botany	Bimonthly	$4.00 a year
Canadian Journal of Chemistry	Monthly	$5.00 a year
Canadian Journal of Microbiology	Bimonthly	$3.00 a year
Canadian Journal of Physics	Monthly	$4.00 a year
Canadian Journal of Zoology	Bimonthly	$3.00 a year

The price of regular single numbers of all journals is 75 cents.

Canadian Journal of Chemistry

Issued by THE NATIONAL RESEARCH COUNCIL OF CANADA

VOLUME 36 DECEMBER 1958 NUMBER 12

POTATO X VIRUS

PART I. THE SIZE AND SIZE DISTRIBUTION OF POTATO X VIRUS IN TOBACCO SAP[1]

M. E. REICHMANN

ABSTRACT

Assuming an irreversible, random, end-to-end aggregation of a small percentage of potato X virus in tobacco sap, the flow birefringence parameters of such polydisperse systems have been calculated. The extinction angles χ were evaluated for different values of the ratio G/θ_1 (G gradient, θ_1 rotary diffusion constant of non-aggregated virus) for preparations containing between 0 and 15% by weight of aggregated material. A particle length of 6200 Å for the non-aggregated virus particle was derived and an amount of 13–15% aggregated material was estimated.

A partially purified and fractionated preparation of potato X virus was also investigated and an average particle length of 5400 Å was derived. Because of the possible contribution of small fragments, this length was taken as the lower limit.

The flow birefringence – gradient curve indicated that the potato X virus behaves like a rigid particle. No evidence of flexibility was obtained from extinction angle – gradient measurements in the range 0.1–0 M phosphate buffer concentrations at pH 7.2.

INTRODUCTION

The tendency of the elongated plant viruses to aggregate irreversibly in an end-to-end fashion, in the process of isolation and purification, has made it difficult to study the shape and size of these viruses in solution (1, 2, 3, 4). The potato X virus in particular presents a difficult problem, as even the mild treatment of ultracentrifugation renders much of the material insoluble (1, 3). The value of physicochemical studies on such preparations is, therefore, somewhat dubious (5, 6). The most reliable data on the size and size distribution of this virus come from electron microscope studies of untreated plant sap (7, 8), where a uniform particle length of 500 to 525 mμ and 10 mμ thickness is indicated with a small amount of the virus material present in the form of higher end-to-end aggregates of this elementary particle. However, since the information obtained from electron microscopy is pertinent only to the non-hydrated virus and, moreover, breakage or aggregation of particles can occur during the preparation of electron microscopic specimens (9, 10, 11), an investigation of the virus size and size distribution in the hydrated form is highly desirable. This paper deals with an analysis of flow birefringence measurements made on tobacco sap infected with potato X virus. In addition, a partial purification of the virus is described. In the process the aggregated fraction present in the sap was preferentially removed. Flow birefringence measurements on this preparation made it possible to determine the lower limit of the characteristic particle size. The flow birefringence technique is particularly suitable for such studies, because of its great sensitivity to the particle length (12) and because of the absence of flow birefringent material in the sap of healthy tobacco after freezing.

[1]*Manuscript received July 6, 1958.*
Contribution No. 2, Chemistry Division, Science Service, Canada Department of Agriculture Research Laboratory, Vancouver, B.C.

Theory

In the treatment that follows, three assumptions are made: 1. The elementary virus particle (here referred to as monomer) as well as the aggregates (polymers) is sufficiently rigid to be treated as rigid ellipsoids of revolution. 2. The end-to-end aggregation occurs at random. 3. The axial ratio is greater than five. Assumptions 1 and 2 are discussed further in the last section of this paper, while assumption 3 is certainly justified by electron microscopy data (4, 7).

The flow birefringence theory for polydisperse systems has been treated by Sadron (13). The flow birefringence parameters have been evaluated for Gaussian (14) and Montroll–Simha distribution functions (15, 16). In the case of random linear aggregation the distribution function will have a different form. The problem can be treated essentially as one of a bifunctional monomer undergoing condensation polymerization. Flory has treated the distribution of x-mers in such a system, and the weight fraction of x-mers W_x is given by the following expression (17):

$$W_x = xp^{(x-1)}(1-p)^2, \tag{1}$$

where p is the total fraction of material which has undergone polymerization. In the case of rigid particles the above expression also gives the size distribution WL_x:

$$WL_x = L_x/L_1\, p^{(L_x/L_1-1)}(1-p)^2. \tag{2}$$

Here L_x is the length of the x-mer and x has been replaced by L_x/L_1. By carrying out the summation over all x's from 1 to ∞ one can see that the function is normalized. This distribution function can thus be used for a derivation of the flow birefringence parameters: the extinction angle χ and the rotary diffusion constant θ. If the axial ratio of the monomer is greater than five, the rotary diffusion constant varies inversely as the cube of the particle length (16, 18) and the following relationship applies:

$$x = L_x/L_1 = (\theta_1/\theta_x)^{\frac{1}{3}} = (\alpha_x/\alpha_1)^{\frac{1}{3}} = \gamma. \tag{3}$$

Here the α's represent the ratio of the velocity gradient G to the respective rotary diffusion constant. The distribution function can now be expressed in terms of α and p only:

$$W_\gamma = \gamma p^{(\gamma-1)}(1-p)^2, \tag{4}$$

$\gamma = (\alpha_x/\alpha_1)^{\frac{1}{3}}$ can only assume integer values from 1 to ∞.

The extinction angle χ in a polydisperse system is given by the following expression (14, 16):

$$\tan 2\chi = A/B,$$

where

$$A = \sum_{x=1}^{\infty} W_x f(\alpha_x) \sin 2\phi_x,\quad B = \sum_{x=1}^{\infty} W_x f(\alpha_x) \cos 2\phi_x, \tag{5}$$

ϕ_x is the extinction angle of the x-mer, and $f(\alpha_x)$ is a form factor. Both quantities can be found in the tables of Scheraga, Edsall, and Gadd (19). Introducing W_x in terms of α from [4]:

$$A = (1-p)^2 \sum_{\gamma=1}^{\infty} \gamma p^{(\gamma-1)} f(\alpha_x) \sin 2\phi_x \tag{6}$$

$$B = (1-p)^2 \sum_{\gamma=1}^{\infty} \gamma p^{(\gamma-1)} f(\alpha_x) \cos 2\phi_x.$$

For values of p not exceeding 0.15 (less than 15% aggregated material) the series converge rapidly and the fifth term ($\gamma = 5$) does not contribute more than 2% to the sum. A and B and thus χ can be evaluated by neglecting higher terms in the series. Table I gives the values of χ for $\alpha_1 = 0$–4 and for $p = 0.02$–0.15. Figure 1 represents a plot of χ vs. α_1 for various degrees of aggregation p.

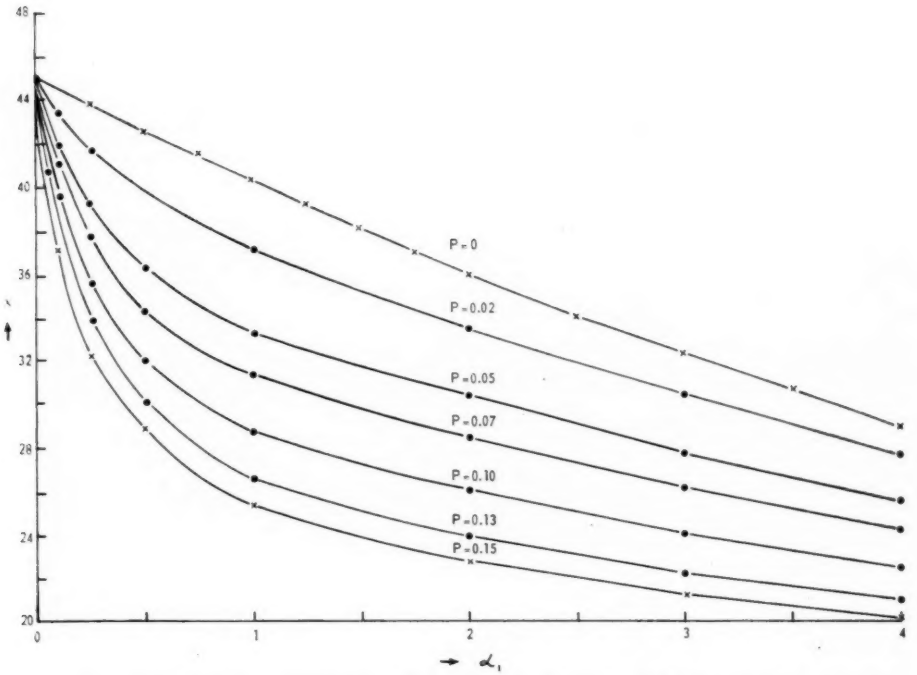

FIG. 1. Extinction angle – gradient curves for polydisperse systems with a Flory distribution function and various fractions p of aggregated material.

For values of α_1 greater than four, α_x becomes too large and the values of $f(\alpha_x)$ and ϕ_x in the tables of reference (19) are somewhat dubious. This, however, does not matter, as the largest deviations from the monodisperse curve $p = 0$ occur in the region of low α's. From the best fit of the theoretical and experimental curves in this region the amount of aggregated material p, as well as the rotary diffusion constant of the monomer, θ_1, can be determined. For prolate ellipsoids of revolution (16):

$$\theta = \frac{kT}{\pi\eta L^3}\frac{3}{2}(-1+2\ln 2\beta)$$

where k is Boltzman's constant, T is the absolute temperature, η is the solvent viscosity, and β is the axial ratio. The length of the monomeric virus particle has been calculated from this equation assuming $\beta = 60$ (4, 7). L_1 and θ_1, however, are not very sensitive to the axial ratio β, because of the logarithmic dependency.

TABLE I

VALUES OF EXTINCTION ANGLES χ AT VARIOUS VALUES OF α_1 (see text) FOR FLORY DISTRIBUTION FUNCTIONS CONTAINING A FRACTION p OF HIGHER AGGREGATES

$p = 0.02$		$p = 0.05$		$p = 0.07$	
α_1	χ	α_1	χ	α_1	χ
0.05	44.23	0.05	43.22	0.05	42.51
0.10	43.50	0.10	42.00	0.10	41.03
0.25	41.71	0.25	39.13	0.25	37.63
0.50	39.62	0.50	36.29	0.50	34.35
1.00	37.14	1.00	33.34	1.00	31.27
2.00	33.55	2.00	30.35	2.00	28.50
3.00	30.40	3.00	27.82	3.00	26.27
4.00	27.69	4.00	25.56	4.00	24.26
$p = 0.10$		$p = 0.13$		$p = 0.15$	
α_1	χ	α_1	χ	α_1	χ
0.05	41.68	0.05	40.61	0.05	40.02
0.10	39.51	0.10	38.07	0.10	37.12
0.25	35.61	0.25	33.83	0.25	32.64
0.50	32.02	0.50	30.04	0.50	28.81
1.00	28.66	1.00	26.50	1.00	25.26
2.00	26.07	2.00	23.91	2.00	22.77
3.00	24.16	3.00	22.23	3.00	21.21
4.00	22.50	4.00	21.00	4.00	20.10

MATERIAL AND METHODS

Preparation of Sap

One-month-old tobacco seedlings were infected with a severe potato X strain, isolated from a single lesion on *Gomphrena globosa*.* Two weeks after inoculation the young leaves were harvested and kept frozen overnight. They were then thawed at 5° C and squeezed in a mortar with a pestle. The sap was centrifuged for 45 minutes at 3500 r.p.m. All the operations were carried out in a cold room (0–5° C), and the brown color of the supernatant sap was not strong enough to interfere with the flow birefringence measurements. The extinction angles at various gradients were measured with a flow birefringence apparatus manufactured by the Rao Instrument Company, Brooklyn 5, New York (20, 22).

For more accurate measurements the sap was concentrated in a Petri dish in a desiccator to $\frac{1}{4}$ of its original volume. This did not change the values of the extinction angles. Dilutions were made with distilled water. The amount of birefringence was never less than 10° expressed in terms of the phase difference (which is twice the angular rotation of the Senarmont compensator). Under these conditions the isoclines were sharp enough to permit a reproducibility of at least 0.8° at gradients of 40 sec^{-1} or higher. The reproducibility on different preparations was also very good provided plants of approximately the same age were used. Sap from plants older than a month from the date of inoculation was deeper in color, and therefore no reliable data could be obtained. There was, however, some indication of the presence of more aggregated material than in younger plants.

Partial Purification and Fractionation

Fresh sap from tobacco plants infected with potato X virus was made 0.05 *M* in phosphate buffer pH 5.7, and centrifuged at 4000 r.p.m. for 40 minutes. Twenty-five

*The author is greatly indebted to Dr. N. S. Wright of the Plant Pathology Section of this laboratory for the supply of virus material.

grams of celite (Johns-Manville, Analytical Filter Aid) was mixed with 250 ml of supernatant sap and poured into a 45-mm diameter glass column with a fritted glass plate bottom. Mild suction was applied. The first 40 ml of sap that came through were recycled. No flow birefringence could be detected in the sap that passed through the column subsequently. The column was washed thoroughly with 0.05 *M* phosphate buffer pH 5.7. Distilled water was then used to elute the virus. Most of the virus came off the column in the first 20 ml of the eluent. About 70% of the virus was recovered. The solution was faintly yellow indicating the presence of impurities. In the Spinco ultracentrifuge a peak corresponding to the virus and a small shoulder near the meniscus were observed. This shoulder failed to separate after 45 minutes at 50,000 r.p.m. Electrophoretic patterns in 0.05 *M* phosphate buffer pH 7.0, taken with a model H Spinco Electrophoresis-Diffusion Apparatus, showed two components. In addition to a sharp, slow-moving peak corresponding to the virus, a faster-moving diffuse peak was present (Fig. 2).

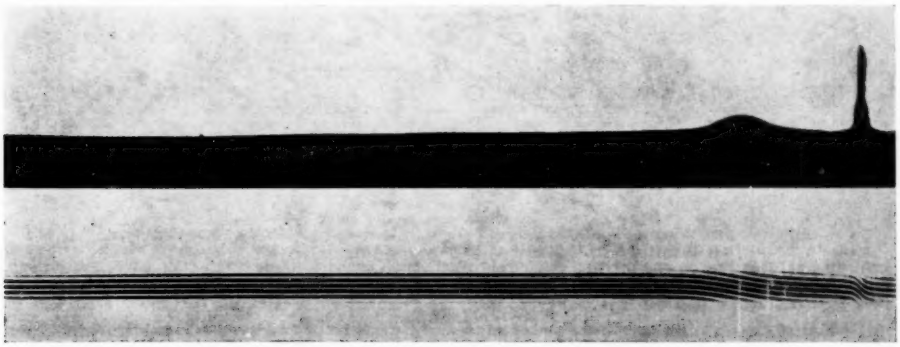

FIG. 2. Electrophoretic pattern of potato X virus after partial purification on celite column. Descending boundary, movement from right to left.

Subsequent purifications on a celite column were made by diluting the aqueous virus solution with 0.05 *M* phosphate buffer pH 5.7 to approximately the same virus concentration as in the sap, and repeating the procedure described above. The impurities present after the first purification could not be removed by additional treatment; also, the virus yields were much lower in the subsequent treatments than in the first one.

For flow birefringence measurements all solutions of the celite-treated virus were dialyzed against distilled water and centrifuged at 4000 r.p.m. for 40 minutes.

RESULTS AND DISCUSSION

Figure 3 represents a plot of the extinction angle χ as a function of gradient G for three different sap concentrations. Within experimental error the extinction angle is independent of concentration, indicating that the interactions of the virus particles with each other and with other sap constituents are negligible. Under these conditions the extinction angle is solely a function of particle length and velocity gradient. The solid lines in Fig. 3 are theoretical curves for a Flory distribution function with $\theta_1 = 70$ giving the best fit of the experimental points. The value $\theta_1 = 70$ corresponds to a length of 6200 Å for the monomer. The amount of aggregated material present in this sample can be estimated from Fig. 3 as 13 to 15%.

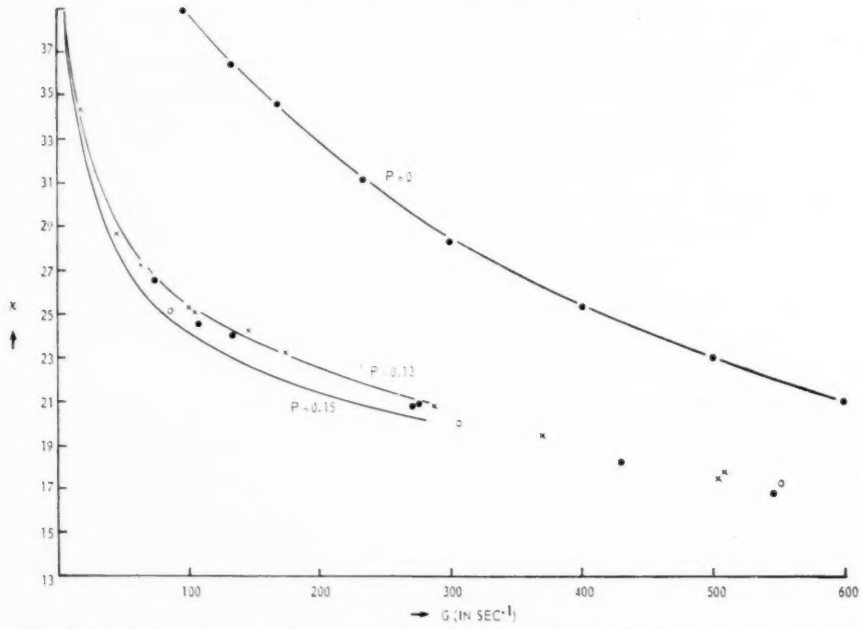

FIG. 3. Extinction angle – gradient curves of sap from potato X infected tobacco: ×, four times concentrated sap; ●, one to one dilution of concentrated sap; ○, one to three dilution of concentrated sap. Solid lines are theoretical curves from Fig. 1 assuming rotary diffusion constant 70.

In Fig. 4 the extinction angle as a function of gradient is plotted for partially purified potato X. Each treatment with celite caused a shift in these curves towards higher extinction angles, accompanied by a decrease in polydispersity features. After the fifth and subsequent absorptions on celite the shift became very minor.

The indication that the virus preparation was becoming less polydisperse excluded the possibility of a random breakage of virus particles. Also, the ultracentrifuge patterns remained unchanged, excluding the possibility of a splitting at specific sites. The most plausible explanation of the shift in the birefringence curves seems to be a preferential absorption of the aggregated materials by the celite column. The rotary diffusion constant of the five times celite-treated material at low gradients (100–200 sec^{-1}) is 60 to 70. Comparing this with the value of 70 derived above for the non-aggregated virus particles, it would seem that this preparation is virtually free of aggregated material. The slight polydispersity could therefore be attributed to shorter fragments present in the sap. Electron microscopy revealed the presence of short fragments in potato X preparations (4, 7, 8). The rotary diffusion constant of the five times celite-treated sample at 800 sec^{-1} is 105. This corresponds to a particle length of 5400 Å for a prolate ellipsoid of revolution. Because of the possibility of a contribution by shorter fragments, the latter value should be considered as the lower limit. Thus the characteristic hydrodynamic length of potato X virus in tobacco would be within the limits of 5400 to 6200 Å.

Curved and kinked potato X virus particles observed under the electron microscope suggested to some authors that a more flexible particle was involved than in the case

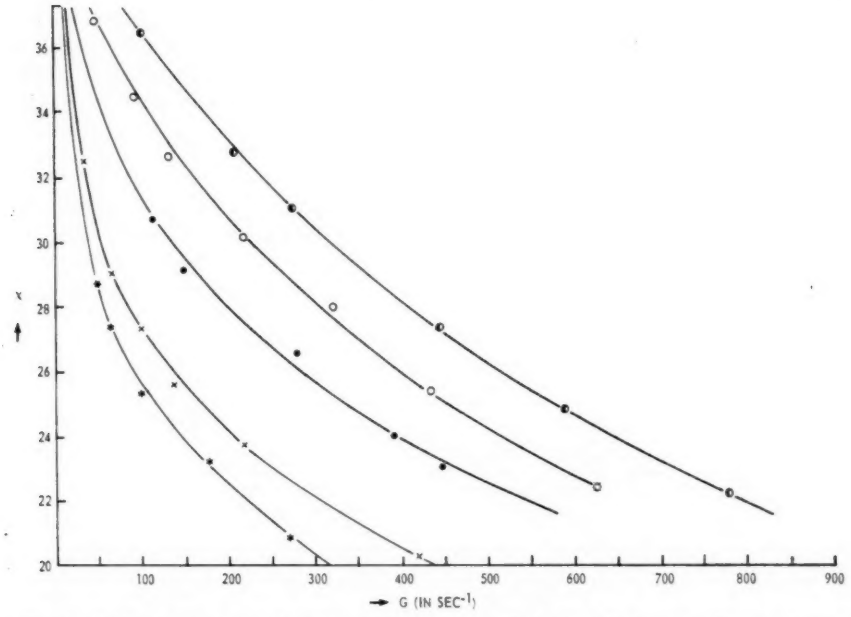

FIG. 4. Extinction angle – gradient curves of partially purified potato X virus on celite columns: •, virus in sap; ×, once; ●, three times; ○, four times; and ◐, five times purified virus.

of the rigid tobacco mosaic virus (21). The difficulty encountered in an interpretation of flow birefringence data in the case of flexible particles (22) merits a closer examination of this problem. Valuable information regarding flexibility can be obtained from birefringence vs. gradient curves. In the case of rigid particles these curves have a downward curvature, the birefringence reaching a saturation value at high gradients (12). Figure 5 shows birefringence curves of potato X virus in sap, corresponding to the extinction angles in Fig. 3. The birefringence is expressed in degrees (twice the angular rotation of the Senarmont compensator), divided by relative concentrations, the most dilute sample being taken as having a concentration of one. The downward curvature is indicative of a rigid particle. Further evidence in support of inflexibility was obtained from extinction angle measurements of sap, dialyzed against distilled water and phosphate buffer pH 7.2, of varying ionic strength. The extinction angle – gradient curves remained unchanged in a range of phosphate concentrations of 0.1–0 *M*, indicating that no measurable stretching of the particles occurred with decreasing ionic strength.

The data on this paper confirm the conclusion from electron microscopy that a definite particle length is characteristic of the potato X virus in tobacco sap. In an earlier publication by Bode and co-workers (7) this characteristic length was given as 5600 to 5800 Å and 6000 to 6200 Å for two different strains of potato X respectively. In a later publication the first value was corrected to 5000 to 5250 Å, owing to previous errors in instrument calibration. A somewhat higher value from flow birefringence studies could be expected because of hydration and the error involved by substituting the cylindrical model with an ellipsoid of revolution (23), although a difference in the virus strains could also be a contributing factor (4, 7).

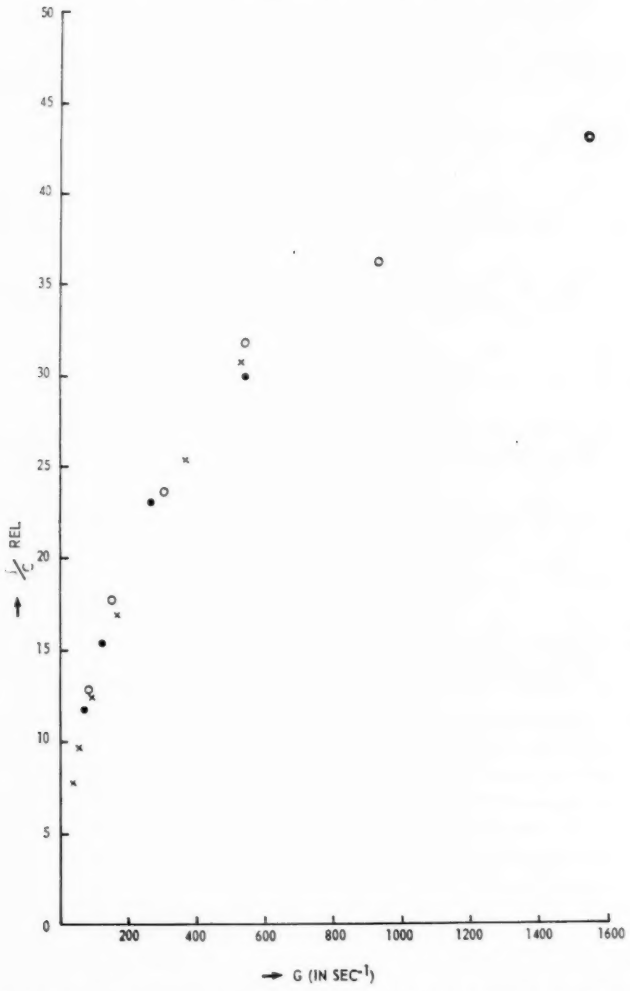

FIG. 5. Birefringence – gradient curves of potato X virus in sap. Points correspond to those given in Fig. 3.

It is difficult to make a comparison of the percentage of aggregated material reported here with that given in the literature. The wide fluctuation, from 23 particles in 651 (3.5%) (7) to 18% (8), is indicative either of great variability with growth conditions and virus strains or artefact formation during the drying processes. On the other hand, the flow birefringence value is open to criticism because of the inherent assumption of a random end-to-end aggregation. This is almost certainly an oversimplification of the mechanism involved. Furthermore the Flory distribution function does not account for fragments smaller than the monomeric unit which are present in all electron microscope mounts and for which there was evidence in the celite-fractionated material. A

close examination of the χ vs. G curves for other distribution functions will show that the curves are not very sensitive to the form of the distribution. Therefore the total amount of aggregated material determined in this way is probably a good estimate as long as the Flory distribution function is an approximate representation of the distribution.

ACKNOWLEDGMENTS

The author wishes to thank Drs. R. E. Fitzpatrick, N. S. Wright, R. Stace-Smith, and P. M. Townsley for their interest, helpful suggestions, and encouragement, and Dr. H. R. MacCarthy for reading the manuscript. The technical assistance of Mr. D. L. Hatt is gratefully acknowledged.

REFERENCES

1. BAWDEN, F. C. Plant viruses and virus diseases. Chronica Botanica Company, Waltham, Mass. 1950.
2. BANDET, J., CROISSANT, O., DERVICHIAN, D. G., JOLY, M., and MOSSE, J. Discussions Faraday Soc. **11**, 236 (1951).
3. LORING, H. S. J. Biol. Chem. **126**, 455 (1938).
4. KLECZKOWSKI, A. and NIXON, H. L. J. Gen. Microbiol. **4**, 220 (1950).
5. LORING, H. S. and WYCKOFF, R. W. G. J. Biol. Chem. **121**, 225 (1937).
6. LAUFFER, M. A. and CARTWRIGHT, T. E. Arch. Biochem. Biophys. **38**, 371 (1952).
7. BODE, O. and KÖHLER, E. Z. Naturforsch. **7b**, 598 (1952).
8. BODE, O. and PAUL, H. L. Biochem. et Biophys. Acta, **16**, 343 (1955).
9. WILLIAMS, R. C. and STEERE, R. L. J. Am. Chem. Soc. **73**, 2057 (1951).
10. RICE, R. V., KAESBERG, P., and STAHMANN, M. A. Biochim. et Biophys. Acta, **11**, 337 (1953).
11. RICE, R. V., KAESBERG, P., and STAHMANN, M. A. Biochim. et Biophys. Acta, **20**, 488 (1956).
12. CERF, R. and SCHERAGA, H. A. Chem. Revs. **51**, 185 (1952).
13. SADRON, C. J. phys. radium, **9**, 381, 384 (1938).
14. SCHERAGA, H. A. J. Chem. Phys. **19**, 983 (1951).
15. MONTROLL, E. W. and SIMHA, R. J. Chem. Phys. **8**, 721 (1940).
16. GOLDSTEIN, M. J. Chem. Phys. **20**, 677 (1952).
17. FLORY, P. J. J. Am. Chem. Soc. **58**, 1877 (1936).
18. COHN, E. J. and EDSALL, J. T. Proteins, amino acids and peptides. Reinhold Publishing Corp., New York. 1943.
19. SCHERAGA, H. A., EDSALL, J. T., and GADD, J. O. J. Chem. Phys. **19**, 1101 (1951).
20. EDSALL, J. T., RICH, A., and GOLDSTEIN, M. Rev. Sci. Instr. **23**, 695 (1952).
21. WYCKOFF, R. W. G. Electron microscopy. Interscience Publishers, Inc., New York. 1949.
22. GOLDSTEIN, M. and REICHMANN, M. E. J. Am. Chem. Soc. **76**, 3337 (1954).
23. BOEDTKER, H. and SIMMONS, N. S. J. Am. Chem. Soc. **80**, 2550 (1958).

OCCURRENCE OF β-DOLABRIN (4-ISOPROPENYLTROPOLONE) IN WESTERN RED CEDAR (THUJA PLICATA DONN.)[1]

J. A. F. Gardner and G. M. Barton

ABSTRACT

The steam-volatile oil of western red cedar contains traces of a fifth tropolone, β-dolabrin (4-isopropenyltropolone), in addition to α-, β-, and γ-thujaplicin and 7-hydroxy-4-isopropyltropolone. The presence of β-dolabrin, previously obtained from Japanese "Hiba" wood by Nozoe, was detected by paper chromatography and proved by isolation of a sample from the steam-volatile oil by a combination of sodium salt precipitation, fractional crystallization, and preparative paper chromatography. The approximate composition of the steam-volatile oil from butt heartwood is given.

INTRODUCTION

The heartwood of western red cedar (*Thuja plicata* Donn.) has been shown to contain up to 1.2% by weight of the three isomeric isopropyltropolones, α-, β-, and γ-thujaplicin (1, 2, 3, 4). Recently, the presence also of a hydroxylated thujaplicin, 7-hydroxy-4-isopropyltropolone (2,7-dihydroxy-4-isopropyl-2,4,6-cycloheptatrien-1-one), was reported (5). This substance, for which the name β-thujaplicinol is now proposed, exhibits the same R_f and violet color reaction on paper chromatograms with ferric chloride as the "unknown enol" detected by Zavarin and Anderson (4) in the tropolone fractions of incense cedar (*Libocedrus decurrens* Torrey) and western red cedar. The occurrence in trace quantities in western red cedar of still another tropolone derivative, β-dolabrin (4-isopropenyltropolone), first detected by Nozoe *et al.* (6) in "Hiba" wood (*Thujopsis dolabrata* Sieb. et Zucc.), has now been proved.

During examination of the steam-volatile oil of western red cedar in this laboratory by the paper chromatographic technique of Zavarin and Anderson (4), the spot corresponding to β-thujaplicinol was observed to be usually elliptical, and sometimes, depending on temperature conditions, two barely separated spots were obtained. One of these gave the violet reaction with ferric chloride typical of β-thujaplicinol and the other of slightly greater R_f had a green-brown reaction similar to that of the thujaplicins. The R_f's and color reactions of this latter substance and its azo dye prepared by the method of Zavarin and Anderson (7) indicated it might be β-dolabrin.

In view of the importance of establishing the identity of trace components of wood extractives from the taxonomic viewpoint, proof of the presence of β-dolabrin in western red cedar was provided by isolating a sample. Because only trace quantities were involved according to the paper chromatograms, this presented considerable difficulty but was achieved by applying a combination of sodium salt precipitation and fractional crystallization to the tropolone fraction of the steam-volatile oil. This procedure provided, in addition to samples and approximate yields of the other components, residual solutions enriched in α-thujaplicin and β-dolabrin. From these, a sample of β-dolabrin was isolated by preparative paper chromatography. The material isolated had m.p. 55–56° C and showed no mixed melting point depression with an authentic sample, m.p. 56–57° C. The R_f's and ultraviolet absorption spectra of the two samples were identical. The infrared absorption spectra were also identical and showed strong bands at 1608, 1557,

[1]*Manuscript received August 1, 1958.*
Contribution from the Vancouver Laboratory, Forest Products Laboratories of Canada, a Division of the Forestry Branch, Department of Northern Affairs and National Resources. Presented at the 133rd National Meeting, American Chemical Society, San Francisco, U.S.A., April 14–18, 1958.

1470, and 1435 cm^{-1}, characteristic of the tropolone nucleus, and also two at 892 and 1407 cm^{-1}, typical of asymmetrically disubstituted ethylenes (8).

The above result shows that western red cedar as well as "Hiba" wood contains β-dolabrin. Since "Hiba" wood also contains α- and β-thujaplicin (9), there are at least three tropolones common to these species of the different genera *Thuja* and *Thujopsis* of the family Cupressaceae.

Previous analytical work (3) had shown that light-colored wood from the outer butt of mature trees had the highest content of tropolones. The composition of oil steam-distilled from freshly cut shavings of butt heartwood selected for its light straw color, estimated from yields and paper chromatographic analysis of fractions obtained, is recorded in Table I. It is, of course, to be expected that the yield and composition of the oil will vary considerably with the source of the wood (3). For optimum yields, it is necessary to distill the wood immediately after conversion to shavings because of the high volatility of the oil.

TABLE I

COMPOSITION OF STEAM-VOLATILE OIL OF WESTERN RED CEDAR BUTT HEARTWOOD (0.82% YIELD)

Components	Percentage of oil	Percentage of wood
Methyl thujate, other neutrals	21.1	0.17
Thujic acid	10.4	0.08
Tropolones	68.5	0.56
β-Thujaplicinol*	8	0.07
γ-Thujaplicin*	24	0.20
β-Thujaplicin*	35	0.30
α-Thujaplicin*	1	0.01
β-Dolabrin*	0.04	0.0003

*Figures for the individual tropolones are approximate, being derived from crude yields and quantitative paper chromatography of mother liquors.

EXPERIMENTAL

Melting points were determined on a Fisher–Johns melting point apparatus and are uncorrected. Infrared absorption spectra were determined on a Beckman Model IR-4 Infrared Spectrophotometer at the Fisheries Experimental Station, Vancouver, B.C. Ultraviolet absorption spectra were determined with a Beckman D.U. Spectrophotometer.

Steam Distillation of Light-colored Western Red Cedar Shavings

Butt-wood spalts selected for light straw color were reduced to shavings in a planer and steam-distilled immediately. Approximately 6 liters of aqueous distillate were collected per kilogram of shavings. The distillate was extracted five times with a sixth of its volume of chloroform and the extract concentrated under reduced pressure to leave a yellow oil. From 11.987 kg of shavings (moisture content 20.0%) 79 g or 0.82% based on the moisture-free wood were obtained.

Preparation of Tropolone Mixture

Steam-distilled oil (103 g) in chloroform (300 ml) was extracted with 1 *N* sodium hydroxide solution (6×50 ml) and back-extracted with chloroform. The chloroform solution was dried over anhydrous sodium sulphate and the solvent removed under reduced pressure to leave crude methyl thujate (21.8 g).

The alkaline solution was acidified and extracted with chloroform (3×100 ml). The

chloroform solution was than extracted with saturated aqueous sodium bicarbonate solution (5×50 ml). Acidification of the bicarbonate solution precipitated crude thujic acid (10.7 g). The chloroform solution, after extraction with bicarbonate, was washed with water and dried over anhydrous sodium sulphate, filtered, and the solvent removed. The residual oil was distilled under reduced pressure to yield the semicrystalline tropolones (66.0 g).

Fractionation of Tropolone Mixture

The tropolone mixture was dissolved in hot 3 *N* sodium hydroxide (350 ml) and the solution cooled. The deposited yellow sodium salts were filtered using a rubber dam to remove excess filtrate.

The caustic filtrate was acidified with 6 *N* sulphuric acid, extracted with chloroform, and the solvent removed to yield crude β-thujaplicinol.

The sodium salts were acidified with 6 *N* sulphuric acid in the presence of chloroform. Removal of the solvent from the chloroform layer left the mixed thujaplicins. The thujaplicin mixture (5.2 g approx. 40% γ-, 60% β-thujaplicin with traces of α-thujaplicin and β-dolabrin), and anhydrous sodium acetate (2.5 g) were refluxed in sodium-acetate-saturated ethanol (50 ml) for 1 hour. The solution was cooled to room temperature and the precipitated yellow sodium salt and excess sodium acetate removed by filtration. The precipitated salts were enriched with respect to γ-thujaplicin (approx. 75% γ-, 15% β-), while the filtrate was enriched with β-thujaplicin (approx. 70% β-, 30% γ-, traces of α-thujaplicin and β-dolabrin). Regeneration of the thujaplicins from the salts, and the filtrate and recrystallization from ligroin–chloroform and ligroin gave respectively γ- and β-thujaplicin. The mother liquors were combined to yield a solution, enriched with α-thujaplicin and β-dolabrin, on which the sodium acetate – sodium salt precipitation was repeated. This in turn yielded more γ- and β-thujaplicin and mother liquors which were combined for isolation of β-dolabrin.

Isolation of β-Dolabrin by Preparative Paper Chromatography

The qualitative technique of Zavarin and Anderson (4) was adapted. Sheets of Whatman No. 1 paper (6 in. × 22½ in.) were impregnated with 17% by volume of phosphoric acid, spotted with 0.2 ml of a chloroform solution (0.08 g/ml) of the residue from removal of solvent from the mother liquors above, and developed with iso-octane–toluene (3:1). The β-dolabrin zones were located by ultraviolet light, excised, and Soxhlet-extracted with petroleum ether (30–60° C) under a carbon dioxide atmosphere. Solvent removal left crystals (0.019 g from 45 sheets) which were triturated with a minimum of petroleum ether (30–60° C), filtered, and dissolved in petroleum ether (30–60° C). Slow evaporation of the solution yielded yellow crystals, m.p. 56–57° C, mixed melting point with authentic dolabrin 56–57° C. The ultraviolet and infrared absorption spectra of the isolated material and authentic β-dolabrin were identical. ν_{max}^{KBr} in cm^{-1}: 3240, 1628, 1608, 1557, 1494, 1470, 1435, 1406, 1313, 1274, 1257, 1230, 958, 911, 892, 823.

ACKNOWLEDGMENTS

The authors are indebted to MacMillan & Bloedel Ltd. and Canadian Forest Products Ltd. for samples of western red cedar, and to Professor Tetsuo Nozoe for a sample of β-dolabrin with its ultraviolet absorption spectrum. Miss Shirley McKelvey assisted with the experimental work.

REFERENCES

1. Anderson, A. B. and Gripenberg, J. Acta Chem. Scand. **2**, 644 (1948).
2. Erdtman, H. and Gripenberg, J. Acta Chem. Scand. **2**, 625 (1948).

3. MACLEAN, H. and GARDNER, J. A. F. Forest Prods. J. **6**, 510 (1956).
4. ZAVARIN, E. and ANDERSON, A. B. J. Org. Chem. **21**, 332 (1956).
5. GARDNER, J. A. F., BARTON, G. M., and MACLEAN, H. Can. J. Chem. **35**, 1039 (1957).
6. NOZOE, T., TAKASE, K., and OGATA, M. Chem. & Ind. 1070 (1957).
7. ZAVARIN, E. and ANDERSON, A. B. Ber. 545 (1955).
8. BELLAMY, L. J. The infrared spectra of complex molecules. Methuen & Co. Ltd., London. 1954. pp. 44, 46.
9. NOZOE, T., YASUE, A., and YAMANE, K. Proc. Japan Acad. **27**, 15 (1951).

LIGHT-SCATTERING STUDIES OF COPOLYMERS

I. EFFECT OF HETEROGENEITY OF CHAIN COMPOSITION ON THE MOLECULAR WEIGHT[1]

W. Bushuk[2] and H. Benoît

ABSTRACT

The classical light-scattering theory for polymer solutions is extended to solutions of copolymers which may be polydisperse in chain composition as well as in molecular weight. It is shown that much too high molecular weights will result from light-scattering data for copolymers owing to fluctuations in chain composition; the magnitude of this effect increases rapidly as the absolute value of the refractive index increment approaches zero. The methods for determining the usual weight-average molecular weight and polydispersity of composition are described.

The theory was tested with experimental results on: (1) a mixture of polystyrene and poly(methylmethacrylate), considered as a copolymer with the highest possible polydispersity of composition; (2) a high conversion, statistical copolymer of styrene and methylmethacrylate (copolymer I); and (3) a block copolymer of the same monomers (copolymer II). The apparent molecular weight for copolymer I ($M_w = 1.83\times10^5$) varied markedly with refractive index increment in much the same way as the total molecular weight for the mixture. The molecular weight of copolymer II ($M_w = 1.20\times10^6$) remained essentially constant in the same series of solvents. The polydispersities of composition obtained were 0.72 and 0.05 for copolymer I and II respectively compared with the maximum possible value equal to 1.0.

INTRODUCTION

Since the demonstration by Debye (1) that the amount of light scattered by solutions of high polymers is related to the mass of the solute molecules, light scattering has rapidly become one of the standard methods for the determination of molecular weights of macromolecules. The application of this technique to copolymers has not been equally successful. On one occasion (2) the molecular weight obtained for a sample of GR–S (butadiene–styrene copolymer) was found to vary with refractive index of the solvent and it was suggested that this might be due to heterogeneities in the composition of the particular sample. Similar anomalous molecular weights were obtained in this laboratory for other types of copolymers (3). Accordingly, it seemed desirable to study the problem of light scattering by copolymers and the use of this technique for the determination of molecular parameters both from theoretical and experimental viewpoints.

The theoretical treatment for the molecular weights of copolymers given in this paper is similar to that indicated by Stockmayer *et al.* (4) except that the final equations are arranged in somewhat more useful form. A preliminary report of the present study has already been published (5).

To test the theory, experimental data are presented for solutions of mixtures of polystyrene (PS) and poly(methylmethacrylate) (PMM) and two types of styrene–methylmethacrylate copolymers. These polymers were selected primarily because of the large difference between the refractive indices of the two homopolymers, polystyrene and poly(methylmethacrylate).

THEORETICAL

Introduction

In a homopolymer all the scattering elements scatter in the same manner; in a copolymer there may be two or more types of scattering elements depending on the number of monomer types that make up the copolymer. The treatment given here considers

[1]*Manuscript received August 5, 1958.*
Contribution from the Centre de Recherches sur les Macromolécules, Strasbourg, France, with financial assistance from the National Research Council of Canada.
[2]*Present address: Grain Research Laboratory, Winnipeg 2, Canada.*

only the binary copolymers, although it could be readily extended to include copolymers comprising more than two monomer types. The equations derived are completely general in that they are applicable to statistical, block, or graft copolymers, which may be polydisperse in mass as well as in composition.

Specific Refractive Index Increment

It is assumed that the refractivity of a copolymer is a simple sum of the refractivities of the two component homopolymers. As pointed out by Stockmayer *et al.* (4) this should be particularly true for block copolymers and probably does not introduce a very large error when applied to statistical copolymers. Accordingly, if c_A is the concentration of type A (polymer or monomer) and c_B is the concentration of type B, the refractive index of a solution of this copolymer (or mixture of homopolymers) will take on the value:

$$n = n_0+(dn/dc)_A c_A+(dn/dc)_B c_B, \quad [1]$$

where n_0 is the index of the pure solvent and the dn/dc are the specific refractive index increments for the components indicated. In this paper the two components A and B will be taken as polystyrene and poly(methylmethacrylate) respectively.

If the total concentration is $c = c_A+c_B$, then the increment for the solution will be

$$dn/dc = (n-n_0)/c = [(dn/dc)_A c_A+(dn/dc)_B c_B]/(c_A+c_B). \quad [2]$$

As has been verified on numerous occasions, equation [2] incorporates the fact that the specific refractive index increment of a solution of polymer depends only on the weight concentration and not on the molecular weight.

To simplify the notation set $(dn/dc)_A = \nu_A$; $(dn/dc)_B = \nu_B$; and $dn/dc = \nu$; and $x = c_A/(c_A+c_B)$ the weight fraction of component A. With this notation

$$\nu = x\nu_A+(1-x)\nu_B. \quad [3]$$

Accordingly the specific refractive index for a solution of copolymer in any solvent can be calculated if the composition of the copolymer and the increments for the corresponding homopolymers for the same solvent are known accurately.

Theory for Particles Small Compared with the Wavelength of Light

General

According to classical theory on light scattering, the excess scattering due to the solute particles of mass M, concentration c, and having ν for the specific refractive index increment (expressed in terms of the usual Rayleigh ratio R, extrapolated to zero concentration) can be put in the form

$$R = K'\nu^2 cM, \quad [4]$$

where $K' = (2\pi^2\eta_0^2)/(\lambda^4 N)$, in which η_0 is the refractive index of solvent, λ is the wavelength of the incident light in vacuum, and N is Avogadro's number. If the particles are polydisperse in molecular weight, M then becomes the weight-average molecular weight.

Now consider a solution of a copolymer which may show polydispersity of chain composition in addition to polydispersity of molecular weight. Assuming additivity of scattered intensities from the different scattering elements, equation [4] can be put in the form

$$R = K'\sum \nu_i^2 c_i M_i, \quad [5]$$

where c_i is the concentration of molecules of mass M_i and composition x_i. The refractive

index increment for this composition ν_i is defined by equation [3]. To separate the effects of heterogeneity of composition and molecular weight it would probably be clearer to use a double sum in equation [5]; that is, to characterize the species of molecular weight M_i by its compositions x_{ij}. However the writing can be simplified by using a single summation without affecting the rigorousness of the mathematical treatment. It is necessary only to keep in mind that it is possible to have different values of i for the same molecular weight.

The intensity of the scattered light that is actually measured is given by

$$R = K'\nu_0^2 c M_{ap}, \qquad [6]$$

where ν_0 is the average refractive index increment that is obtained by the usual methods of measurement and M_{ap} is the molecular weight that is obtained from the data by the standard method of extrapolation to zero concentration.

Equating the intensities given by equations [5] and [6] the molecular weight takes on the value

$$M_{ap} = \sum \nu_i^2 c_i M_i / \nu_0^2 c = (1/\nu_0^2) \sum \nu_i^2 \gamma_i M_i, \qquad [7]$$

where γ_i is defined as the relative concentration of molecules of composition x_i.

Equation [7] defines the molecular weight that is obtained experimentally for a polymer for which the component molecular species may exhibit different specific refractive index increments in a single solvent. This molecular weight will be referred to henceforth as the apparent molecular weight.

The significance of equation [7] can be best demonstrated by expanding the sum for specific cases to which it can be applied. The most important of these from the viewpoint of the present investigation is the copolymer of heterogeneous chain composition. This will be discussed first. The general equations obtained will then be applied to two special cases, the copolymer of homogeneous chain composition and a binary mixture of homopolymers.

Copolymer of Heterogeneous Composition

If $\nu_i \neq \nu_0$, which is the case when the composition of different molecules is different, equation [7] can be expanded to a more practical form by substituting for ν_i its value given by equation [3]. The new equation for the apparent molecular weight becomes

$$M_{ap} = (\nu_A\nu_B/\nu_0^2)\sum\gamma_i M_i + [\nu_A(\nu_A-\nu_B)/\nu_0^2]\sum\gamma_i M_i x_i^2 + [\nu_B(\nu_B-\nu_A)/\nu_0^2]/\sum\gamma_i M_i(1-x_i)^2. \qquad [8]$$

Equation [8] can be simplified further by introducing the equalities: $\sum\gamma_i M_i = M_w$; $\sum\gamma_i M_i x_i^2 = x_0 M_A$; and $\sum\gamma_i M_i(1-x_i)^2 = (1-x_0)M_B$. M_w is the weight-average molecular weight of the copolymer, M_A and M_B are defined as the weight-average molecular weights of the parts of the copolymer formed of monomer A and B respectively, and x_0 is the over-all average weight fraction of component A.

$$M_{ap} = (\nu_A\nu_B/\nu_0^2)M_w + [\nu_A(\nu_A-\nu_B)/\nu_0^2]\, x_0 M_A + [\nu_B(\nu_B-\nu_B)/\nu_0^2](1-x_0)M_B. \qquad [9]$$

Equations [8] and [9] show that if the copolymer is of heterogeneous chain composition, the molecular weight of the particular sample, obtained from light-scattering data, will depend on the refractive index of the solvent and, as will be seen later, this dependence is related to the degree of heterogeneity. It is therefore quite possible to obtain an infinitely high apparent molecular weight as the scattering may not necessarily be zero, when the average refractive index increment is zero, owing to heterogeneity of the sample.

From measurements in three solvents it should be possible, in principle, to solve for the

three parameters M_A, M_B, and M_w from which the composition of the copolymer can be verified. From the same three sets of measurements it is also possible to obtain information on the degree of heterogeneity of composition.

The quantitative determination of the degree of polydispersity of chain composition becomes more feasible if equation [7] is expanded by a slightly different notation from that used to obtain equations [8] and [9]. In this case set

$$\delta x_i = x_i - x_0 \tag{10}$$

where δx_i is the deviation in composition of molecules of type i from the average composition, x_0. According to this notation, equation [3] for the refractive index increment takes on the form

$$\nu_i = \nu_0 + \delta x_i(\nu_A - \nu_B) \tag{11}$$

and the equation for the apparent molecular weight becomes

$$M_{ap} = M_w + 2(\nu_A - \nu_B)/(\nu_0)\sum \gamma_i M_i \delta x_i + (\nu_A - \nu_B)^2/(\nu_0^2)\sum \gamma_i M_i \delta x_i^2. \tag{12}$$

It can be shown that equation [12] is equivalent to equation [9] by substituting in the former the following equalities,

$$2\sum \gamma_i M_i \delta x_i = (1-x_0)(M_w - M_B) - x_0(M_w - M_A) \tag{13}$$

$$\sum \gamma_i M_i \delta x_i^2 = x_0(1-x_0)(M_A + M_B - M_w).$$

These relations are derived by substituting the value for δx_i given by equation [10] and expanding the sums indicated.

By introducing two new parameters P and Q, equation [12] becomes

$$M_{ap} = M_w + 2P[(\nu_A - \nu_B)/\nu_0] + Q[(\nu_A - \nu_B)/\nu_0]^2, \tag{14}$$

in which P and Q are equal to $\sum \gamma_i M_i \delta x_i$ and $\sum \gamma_i M_i \delta x_i^2$ respectively. To plot equation [14] it is convenient to divide both sides of the equation by M_w.

According to equation [14], if M_{ap} is plotted against $(\nu_A - \nu_B)/\nu_0$, which varies with the refractive index of the solvent, the points should describe a parabola from which the values of the parameters M_w, P, and Q can be estimated. The value of M_w should agree with the value obtained from equation [9]. The other two parameters are related to the heterogeneity in composition of the sample by the definitions given above and should be constant for a particular copolymer. In general, the values of P and Q will vary between the following limits:

$$-x_0 M_w \leqslant P \leqslant (1-x_0)M_w,$$

$$0 \leqslant Q \leqslant M_w[1 - x_0(1-x_0)].$$

If the copolymer is monodisperse in mass or if the distribution of chain composition is independent of molecular weight, equation [14] simplifies further since under such conditions $P = 0$ and Q can only take on values between 0 and $x_0(1-x_0)M_w$. The maximum value of Q can only be realized with a mixture of two homopolymers.

The parameter Q/M_w for a specific copolymer may be defined as a quantitative measure of the polydispersity of chain composition. Accordingly the ratio of the value of Q/M_w, determined either graphically or by a direct calculation, to the maximum possible value, $x_0(1-x_0)$, seems to be a convenient index of the polydispersity in chain composition which can be used as an additional parameter for characterizing copolymers.

Copolymer of Homogeneous Composition

If the copolymer molecules are of uniform composition then $\nu_i = \nu_0$ for all values of i, $\delta x_i = 0$ and equation [12] gives

$$M_{ap} = M_w, \tag{15}$$

where M_w is the usual weight-average molecular weight. That is, for a copolymer of homogeneous chain composition, the molecular weight obtained from light-scattering data will be independent of the refractive index of the solvent.

For this special case, equations [13] give $M_A = x_0 M_{ap}$ and $M_B = (1-x_0)M_{ap}$. These relations can then be used to determine the weight-average molecular weights of the two components of the copolymer.

Solution Containing Two Homopolymers

For a system comprising two homopolymers A and B, of molecular weights M_A and M_B and relative concentrations γ_A and γ_B, equations [7], [9], or [14] give

$$M_{ap} = (\nu_A^2\gamma_A M_A + \nu_B^2\gamma_B M_B)/\nu_0^2. \tag{16}$$

Equation [16] shows that for a mixture of homopolymers the apparent molecular weight will depend on the refractive index of the solvent and in general will not be equal to the usual weight-average molecular weight. In a solvent with refractive index intermediate between those of the two polymers, concentrations can be selected so that the average refractive index increment will be zero. However the solution will still show positive scattering. The apparent molecular weight will then become infinite. For a solvent having the same refractive index as either component, equation [16] will give the weight-average molecular weight of the other component.

It is of interest to examine what happens to the parameters P and Q in this special case. The summations in the definitions of these parameters given above can be readily expanded to give

$$\begin{aligned} P &= x_0(1-x_0)(M_A - M_B) \\ Q &= x_0(1-x_0)[(1-x_0)M_A + x_0 M_B]. \end{aligned} \tag{17}$$

Equations [17] show that when the polymers are of the same mass, P will be zero as in the case of monodisperse (in mass) copolymers. If $M_A \neq M_B$, but are of the same order of magnitude, P will still be small compared with Q. This will not be true always and P can actually have values greater than those of Q when M_A and M_B are very different, that is, when the sample has a very broad distribution of molecular weight as well as of composition.

Theory for Particles of Size Comparable to the Wavelength of Light

If the dimensions of the solute molecules are greater than approximately $1/20\ \lambda$, the same type of destructive interference in the scattered light will result in the case of copolymers as with homopolymers. It is therefore necessary to make a correction for this interference in the usual manner by extrapolating to zero angle according to the method of Zimm (6). The value of the molecular weight so obtained will be the apparent molecular weight of the copolymer for the particular solvent used.

MATERIALS AND METHODS

Solvents

Solvents used for the light-scattering and the viscosity measurements were purified

by several distillations. The 1-bromonaphthalene remained slightly yellow even after two distillations; however, it did not absorb any light at the wavelength used for the light-scattering measurements. The solvents and other pertinent data are listed in Table I.

TABLE I

LIST OF SOLVENTS AND OTHER PERTINENT DATA

Solvent	$n(20°; 5460$ Å)	ν_A (PS) (cc g^{-1})	ν_B (PMM) (cc g^{-1})
Butanone	1.3856	0.220	0.111
Dioxane (p)	1.4280	0.168	0.068
Carbon tetrachloride	1.4677	0.146	0.023
Benzene	1.5056	0.106	−0.010
Chlorobenzene	1.5293	0.079	−0.026
Bromobenzene	1.5641	0.042	−0.058
1-Bromonaphthalene	1.6628	−0.051*	−0.147*

*Measured on the Zeiss Interferometer.

Polymers

The polystyrene used was a fraction of medium molecular weight obtained from a polydisperse polymer prepared at ordinary temperatures in the presence of an inhibitor. It was fractionated from benzene solution by precipitation by methanol. The polymer was dried in vacuum at 60° C. Its molecular weight and intrinsic viscosities in a number of solvents are listed in Table II which will be given in conjunction with a subsequent section.

The poly(methylmethacrylate) was of commercial origin (Plexiglass). It was purified by a single precipitation from a 2% solution in butanone by methanol followed by drying in vacuum at 60° C. Its molecular weight and intrinsic viscosities in a number of solvents are given in Table II.

TABLE II

SUMMARY OF RESULTS ON MIXTURES

65% PS of $M_w = 8.10\times10^5$; 35% PMM of $M_w = 6.88\times10^5$; M_w of mixture $= 7.67\times10^5$

Solvent	ν_0 (cc g^{-1})	$M_{sp}\times10^{-5}$	M_{sp}/M_w	$[\eta]$(cc g^{-1}) PS	$[\eta]$(cc g^{-1}) PMM
Butanone	0.180	7.67	1.00	82	64
Dioxane (p)	0.133	7.69	1.00	—	—
Benzene	0.065	9.46	1.23	168	97
Chlorobenzene	0.044	34.7	4.52	—	—
Bromobenzene	0.007*	292	38.1	124	89
1-Bromonaphthalene	−0.088†	21.4	2.80	126	92

*Calculated: $\nu_0 = 0.65(0.042)+0.35(-0.058)$.
†Measured on the Zeiss Interferometer.

Copolymer I was a statistical copolymer of styrene and methylmethacrylate prepared by using benzoyl peroxide as initiator. The copolymerization was allowed to proceed to about 95% conversion. It was then redissolved in benzene, precipitated by the addition of methanol, and dried in the usual manner. The composition of this copolymer was 68% PS and 32% PMM, as determined from the specific refractive index increments in five solvents. Combustion analysis gave its composition as 70% PS and 30% PMM.

Copolymer II was a block copolymer of styrene and methylmethacrylate. It was

prepared by the method of Szwarc (7) in which the polystyrene was the living radical. Its composition from combustion analysis (and refractive index increments) was 70% PS and 30% PMM. It was used without further purification.

Methods

Solutions were prepared by weighing a predetermined quantity of polymer directly into a volumetric flask and making up to volume with dust-free solvent. Prior to the light-scattering measurements, portions of this solution of concentration c were diluted to $\frac{3}{4}c$, $\frac{1}{2}c$, and $\frac{1}{4}c$. Two samples of pure solvent (one to rinse the pipette used to transfer the dust-free solvent and the solutions) and the four solutions were centrifuged at 25,000g, for 1 hour to remove dust. With some of the higher density solvents it was necessary to filter the solutions through a fritted-glass filter prior to centrifugation.

Light-scattering measurements were made on a photometer described by Wippler and Scheibling (8) using the green mercury line (5460 Å) and pure benzene as the calibration standard. All experiments were made at 25±1° C. After the usual refractive index and volume corrections, the data were treated according to the extrapolation method of Zimm (6) using measurements ranging from 30 to 150° to the incident at the four concentrations shown above. Except where indicated otherwise, the refractive index increments were measured on a Pulfrich Refractometer with a divided cell using the green mercury line.

Molecular weights were calculated using the value of Carr and Zimm (9) for the Rayleigh ratio of benzene (16.3×10^{-6} for 5461 Å at 25° C). It was assumed that the correction factor owing to depolarization was negligible.

Viscosities were measured in a capillary viscometer described by Vallet (10). Viscometers with capillary diameters were selected so that the flow time for the pure solvent was at least 100 seconds.

RESULTS AND DISCUSSION

The most feasible way to test the theory developed above is to study the variation of the apparent molecular weight with refractive index of the solvent. The extent of this variation, in turn, depends on the degree of heterogeneity in chain composition of the copolymer. Accordingly, it should be possible in this manner to determine the effect of the variations in chain composition on the molecular weight determined by light scattering in any specific solvent.

The first series of light-scattering experiments were made on solutions of two homopolymers, comprising 65% PS and 35% PMM of the total polymer concentration. Two features of these solutions make these experiments significant. First, they are most suitable for testing the theory, since their compositions and refractive index increments are known accurately, and second, they can be regarded as solutions of copolymer having the greatest possible heterogeneity of chain composition.

Table II gives the results for the mixture in a series of solvents. The fourth column gives the ratio of the molecular weight obtained from the Zimm plot (M_{ap}) and the weight-average molecular weight calculated from the composition and the weight-average molecular weights of the homopolymers listed at the top of Table II. The viscosities are given as an additional characterization of the polymers used.

To illustrate the variation of the apparent molecular weight with refractive index of solvent, it is convenient to plot the ratio M_{ap}/M_w as a function of the index. Figure 1 shows such a plot of the data of Table II. Experimental data are shown as circles; the solid line represents a corresponding plot for which M_{ap} was calculated from equation

[16]. The agreement between theory and experiment is satisfactory considering the large experimental errors inherent in the measurements on solutions with very small refractive index increments.

The results for the copolymer I (statistical copolymer) are summarized in Table III. In this case the ratio M_{ap}/M_w was determined using the value of M_w (given later in Table V) calculated from equation [14] with the values of M_{ap} listed in Table III. The three unknowns of equation [14], M_w, P, and Q, were evaluated by solving three simultaneous equations. The value of M_w calculated in this manner is strongly dependent on the values for the refractive index increments for the two component polymers in the series of solvents used. Determination of the latter quantities involves a fairly large experimental error particularly in the cases where the increment is very small. Accordingly, it would probably be just as correct, and less laborious, to use for M_w the value of M_{ap} obtained with the solvent having the highest index increment (butanone).

TABLE III

SUMMARY OF RESULTS ON COPOLYMER I
Composition: Combustion analysis, 70% PS+30% PMM
Index increments, 68% PS+32% PMM

Solvent	ν_0 (cc g^{-1})	$M_{ap}\times10^{-5}$	M_{ap}/M_w
Butanone	0.185	2.21	1.20
Dioxane (ρ)	0.136	2.49	1.36
Carbon tetrachloride	0.103	2.81	1.53
Benzene	0.068	3.32	1.81
Chlorobenzene	0.045	9.59	5.24
Bromobenzene	0.010*	26.4	14.42

*Calculated: $\nu_0 = 0.68(0.042)+0.32(-0.058)$.

Figure 2 gives the plots of M_{ap}/M_w as a function of the solvent refractive index. The circles represent data for copolymer I and the points those for copolymer II which will be discussed later. The lines represent points for which M_{ap}/M_w was calculated from equation [14] for the corresponding experimental conditions and the values of Q/M_w indicated. The second term of the right hand side of equation [14] was not included in the calculations for this plot, since it was found that when M_{ap} was plotted against $(\nu_A-\nu_B)/\nu_0$ the slope at $(\nu_A-\nu_B)/\nu_0 = 0$, which is equal to 2P, was essentially zero.

Figure 2 demonstrates clearly a marked variation in the apparent molecular weight of copolymer I with index of solvent. Even in the case of benzene, which is commonly used as solvent, the value of the apparent molecular weight is much higher than the true weight-average molecular weight.

Another method of plotting the data of Fig. 2 is demonstrated in Fig. 3. Here M_{ap}/M_w is plotted as a function of $(\nu_A-\nu_B)/\nu_0$. According to equation [14] the points in such a plot should fall on a parabola. One difficulty with using this plot is to find solvents that will give negative values of $(\nu_A-\nu_B)/\nu_0$. 1-Bromonaphthalene is one such solvent for styrene–methylmethacrylate copolymers; unfortunately measurements on copolymer I in this solvent could not be made owing to shortage of the copolymer. From Fig. 3 it is possible to estimate the value of Q/M_w that will best fit the experimental data. The value of this parameter for copolymer I is approximately 0.15. This result indicates an exceptionally high heterogeneity of chain composition, since the highest possible value that Q/M_w could have is 0.22.

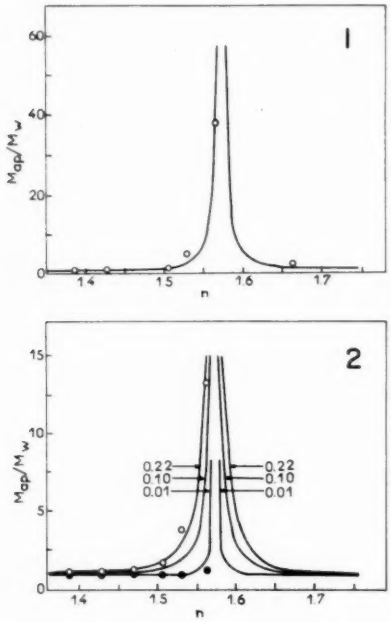

FIG. 1. Apparent (total) molecular weight of mixture comprising 65% PS and 35% PMM (expressed as M_{ap}/M_w) vs. refractive index of solvent. Circles, experimental data; lines, M_{ap} calculated from equation [16].

FIG. 2. Apparent molecular weight (M_{ap}/M_w) vs. refractive index of solvent. Experimental data: circles, copolymer I; points, copolymer II. Lines represent values of M_{ap} calculated from equation [14] with $P = 0$ and Q/M_w as indicated.

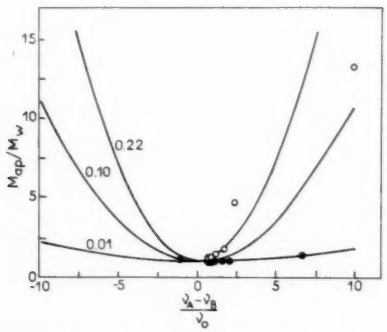

FIG. 3. Apparent molecular weight (M_{ap}/M_w) vs. $(\nu_A-\nu_B)/\nu_0$. Experimental data: circles, copolymer I; points, copolymer II. Lines represent data calculated from equation [14] with $P = 0$ and Q/M_w as indicated.

The high heterogeneity of composition found for copolymer I may seem somewhat contrary to the suggestion by Stockmayer (11) that the instantaneous distribution of chain composition of copolymers can be described by a very narrow Gaussian distribution curve. This is probably true in the case of low conversion copolymers (4); however, it

seems that high conversion copolymers may show considerable heterogeneity of chain composition. Indeed, the theory of copolymerization (12) does predict that high conversion copolymers will in general be of heterogeneous chain composition. It does not seem likely that copolymer I could be a mixture of copolymer and homopolymer of either type A or B.

A further remark is necessary regarding the merits of the two methods of plotting the experimental data shown by Figs. 2 and 3. Figure 2 gives a very striking demonstration of the extent of variation in the apparent molecular weight with the refractive index of the solvent. The deviation of M_{ap}/M_w from unity for the various solvents is related to the degree of heterogeneity of chain composition. To obtain a quantitative measure of this heterogeneity graphically, the plot of Fig. 3 is more useful than that of Fig. 2.

Table IV summarizes the light-scattering results on copolymer II (block copolymer). For this copolymer, the value of M_{ap}/M_w is equal to unity, within experimental error, for all the solvents used. Accordingly, it is concluded that copolymer II is of reasonably uniform chain composition. Whether this is generally true for copolymers prepared by the Szwarc method or whether the homogeneous composition can be attributed to the high degree of polymerization will have to be ascertained by further experiments. The results for copolymer II were plotted in Figs. 2 and 3 for the purpose of comparison.

TABLE IV

SUMMARY OF RESULTS ON COPOLYMER II

Composition: 70% PS+30% PMM

Solvent	ν_0 (cc g^{-1})	$M_{ap}\times10^{-6}$	M_{ap}/M_w
Butanone	0.195	1.42	1.18
Dioxane (p)	0.139	1.15	0.96
Carbon tetrachloride	0.116	1.39	1.16
Benzene	0.074	1.40	1.16
Chlorobenzene	0.051	1.30	1.08
Bromobenzene	0.015*	1.91	1.59
1-Bromonaphthalene	−0.096†	1.74	1.45

*Calculated: $\nu_0 = 0.70(0.042)+0.30(-0.058)$.
†Measured on the Zeiss Interferometer.

As indicated in the theoretical section, it should be possible to determine the weight-average molecular weights of the fractions comprising part A and B of the copolymer. The values obtained for the two copolymers used in this study are given in Table V. The values for M_A and M_B listed were calculated from equation [9] taking the values for M_{ap} from Fig. 2 for n equal to 1.49 where $\nu_B = 0$ and 1.61 where $\nu_A = 0$.

TABLE V

SUMMARY OF DERIVED DATA FOR COPOLYMERS I AND II

Copolymer	M_A	M_B	M_w	P/M_w	Q/M_w	Q/Q_{max}
I	1.74×10^5	0.82×10^5	1.83×10^5	0.01	0.16	0.72
II	0.84×10^6	0.36×10^6	1.20×10^6	0.00	0.01	0.05

Table V also gives the values of M_w, P/M_w, and Q/M_w. These were calculated from equation [14] using the values of M_{ap} for all the solvents used and listed in Tables III and IV.

It may be seen that for copolymer II, which seems to be of reasonably homogeneous composition, the sum of the molecular weights of the components is equal to the molecular weight of the copolymer. This is not true for copolymer I in which case M_w is related to M_A and M_B by equation [16].

As found by graphical interpolation, the value of P (actually P/M_w) for copolymer I is considerably smaller than that of Q (Q/M_w). Accordingly, omission of the term containing P when using equation [14] seems to be justified. The calculated value of Q/M_w is in satisfactory agreement with that obtained by the graphical method.

The last column of Table V gives the ratio Q/Q_{max} where Q_{max} is calculated from the relation $x_0(1-x_0)$, which for both copolymers is approximately 0.22. This ratio may be taken as the quantitative measure of the heterogeneity of chain composition as compared with the maximum possible value equal to unity. Expressed in this manner, the heterogeneity of composition values are 0.72 and 0.05 for copolymer I and II respectively.

As an application of the findings presented in this paper, it should be possible to study the variation of chain composition of copolymers as a function of conversion during copolymerization by means of light scattering. Information of this type may be of considerable value in the interpretation of copolymerization kinetics.

ACKNOWLEDGMENTS

One of the authors (W.B.) wishes to make the following grateful acknowledgments. To Professor C. Sadron, Director, Centre de Recherches sur les Macromolécules, Strasbourg, for making available the facilities of the laboratory and for his kind interest throughout the project; to the professional members and the technicians of the same laboratory for their co-operation, assistance, and advice during the period the author spent at the laboratory; to the National Research Council of Canada for the financial assistance in form of an Overseas Postdoctorate Fellowship; to the Royal Society of Canada for the Rutherford Memorial Fellowship.

The authors wish to thank Drs. Banderet and Rempp of the Centre de Recherches sur les Macromolécules for providing copolymers I and II respectively.

REFERENCES

1. Debye, P. J. Phys. & Colloid Chem. **51**, 18 (1947).
2. Tremblay, R., Rinfret, M., and Rivest, R. J. Chem. Phys. **20**, 523 (1952).
3. Weill, G. Private communication.
4. Stockmayer, W. H., Moore, L. D., Jr., Fixman, M., and Epstein, B. N. J. Polymer Sci. **16**, 517 (1955).
5. Bushuk, W. and Benoît, H. Compt. rend. **246**, 3167 (1958).
6. Zimm, B. H. J. Chem. Phys. **16**, 1099 (1948).
7. Szwarc, M. Nature, **178**, 1168 (1956).
8. Wippler, C. and Scheibling, G. J. chim. phys. **51**, 201 (1954).
9. Carr, C. I., Jr. and Zimm, B. H. J. Chem. Phys. **18**, 1616 (1950).
10. Vallet, G. Ph.D. Thesis, Strasbourg. 1952.
11. Stockmayer, W. H. J. Chem. Phys. **13**, 199 (1945).
12. Alfrey, T., Jr., Bohrer, J. J., and Mark, H. Copolymerization. Interscience Publishers, Inc., New York. 1952. Chap. VII.

SUR LA SYNTHÈSE DE FORMYLDIPHÉNYL ÉTHERS POLYSUBSTITUÉS[1]

R. CONSTANTIN[2] ET P. L'ÉCUYER

RÉSUMÉ

Bon nombre de formyldiphényl éthers ont été synthétisés en faisant réagir certains phénols avec la 2-chloro-5-nitrobenzaldéhyde ou la 3-nitro-4-chlorobenzaldéhyde. Plusieurs l'ont été en condensant le tosylate de la 5-nitrovanilline ou de la 4-hydroxy-3-nitrobenzaldéhyde avec divers phénols. Ces derniers ne donnent pas d'éthers avec la 2-chloro-5-nitrobenzaldéhyde; mais, cependant, les phénolates alcalins réagissent avec cette aldéhyde en solution alcoolique diluée. Par une série de réactions, les 2,2′-diméthoxy-4,4′-diformyl-6-nitro-, 2,2′-diméthoxy-4,4′-diformyl-, 2,2′-diméthoxy- 4,4′-bis-(β-carboxyvinyl)- et 2,2′-diméthoxy-4,4′-bis-(β-carboxyéthyl)-diphényl éthers ont été préparés.

Le travail de Purves (1) sur la synthèse de la papavérine et de la papavéraldine par la méthode de Pomeranz–Fritsch nous a fait imaginer que le 2,3′,4′-triméthoxy-6-formyldiphényl éther (I) pourrait servir de matière première à la préparation de la cularine. Le désir de préparer cette aldéhyde nous a conduits à l'étude des méthodes de synthèse des formyldiphényl éthers polysubstitués.

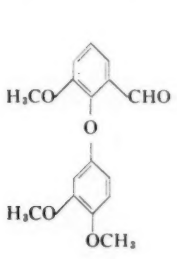

I

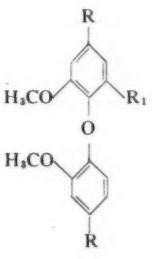

II

R = CHO, $CH{=}CH_2{-}CO_2H$ ou $CH_2{-}CH_2{-}CO_2H$
R_1 = H ou NO_2

La préparation d'éthers diphényliques à partir d'un phénol et de chlorobenzènes convenablement activés a déjà été décrite par Grundon et Perry (2). Nous avons obtenu plusieurs formyldiphényl éthers en faisant réagir la 2-chloro-5-nitrobenzaldéhyde ou la 3-nitro-4-chlorobenzaldéhyde avec le phénol approprié en solution alcoolique diluée contenant 1 équivalent d'hydroxyde de sodium. Les rendements varient selon la nature et la position des groupes substituants (Tableau I).

Hems et quelques collaborateurs (3) avaient auparavant constaté que le tosylate du 2,4-dinitrophénol peut remplacer le 2,4-dinitrochlorobenzène dans les réactions de celui-ci avec un phénol pour donner aussi naissance à des diphényl éthers. Nous avons de cette façon préparé bon nombre de formyldiphényl éthers en condensant le tosylate de la 5-nitrovanilline ou de la 4-hydroxy-3-nitrobenzaldéhyde avec divers phénols dans la pyridine.

[1]*Manuscrit reçu le 11 juillet, 1958.*
Contribution du Département de Chimie, Faculté des Sciences, Université Laval, Québec, P.Q. Ce mémoire est tiré de la thèse de doctorat de R. Constantin.
[2]*Adresse actuelle: Département d'Agriculture, Section des Sciences, Division de la Chimie, Ottawa, Canada.*

TABLEAU I

INFLUENCE DE LA NATURE ET DE LA POSITION DES GROUPES SUBSTITUANTS DANS LE PHÉNOLATE DE SODIUM SUR LE RENDEMENT DE SES RÉACTIONS (1 HEURE) AVEC LES FORMYLNITROCHLOROBENZALDÉHYDES EN SOLUTION AQUEUSE

	Rendement, %	
Phénolate	2-Nitro-4-formylchlorobenzène	2-Formyl-4-nitrochlorobenzène
2-Méthoxy	50.5	48
4-Méthoxy	52	53
3-Formyl	48	59
4-Formyl	25	30
2-Méthoxy-5-formyl	56.5	65
2-Méthoxy-4-formyl	15	5
2-Nitro	0	—
3-Nitro	49	—
4-Nitro	0	—
2-Méthoxy-3-nitro-5-formyl	22	—

Que l'on fasse réagir avec un phénol le tosylate d'un phénol ou un chlorobenzène convenablement activé, nous avons vérifié que le rendement de la réaction dépend de la durée de celle-ci. Il augmente graduellement jusqu'à un maximum qui s'obtient pour un temps de réaction allant de 60 à 90 minutes et décroît ensuite rapidement, lorsqu'on chauffe plus longtemps (Fig. 1).

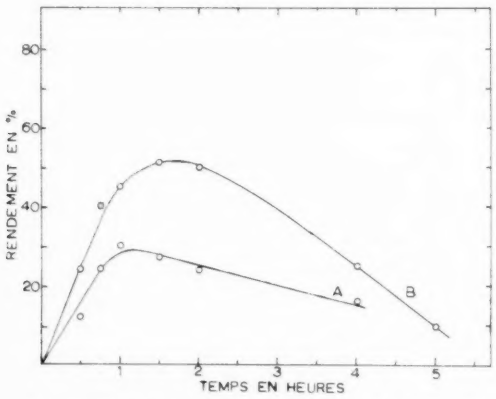

FIG. 1. Rendement de la réaction de 1 mole de guaïacol avec 3 moles de l'ester tosylique de la 5-nitrovanilline (A) ou de la 3-nitro-4-chlorobenzaldéhyde (B) en fonction du temps.

Quoique la réaction des formylchlorobenzènes ou des tosylates de phénols activés avec les phénols permette d'obtenir nombre de formyldiphényl éthers, il semble bien que la réaction de Hems ne va pas quand le groupement formyle est voisin du chlore ou du groupe oxytosyle, comme c'est le cas pour le 2-formyl-4-nitrochlorobenzène, par example. Il en est ainsi également pour la réaction d'Ullmann lorsque, en plus de la situation précédente, l'autre position voisine du chlore est occupée par un groupement méthoxyle. Par ailleurs, la réaction du tosylate de la 5-nitrovanilline ou de la 5-nitro-*o*-vanilline ne donne qu'une transestérification avec les phénolates alcalins. Nous avons cependant

réussi la condensation de la 2-chloro-5-nitrobenzaldéhyde avec les phénolates de sodium en milieu alcoolique dilué; mais nous n'avons pas réussi à obtenir la 2-chloro-3-méthoxy-5-nitrobenzaldéhyde pour préparer I.

Enfin, la condensation de la vanilline avec l'ester tosylique de la 5-nitrovanilline dans la pyridine a donné le 2,2′-diméthoxy-4,4′-diformyl-6-nitrophényl éther (II; R = CHO, $R_1 = NO_2$). Nous avons réduit celui-ci par le chlorure stanneux en 2,2′-diméthoxy-4,4′-diformyl-6-aminodiphényl éther et éliminé la fonction amine dans ce dernier en diazotant en présence d'acide hypophosphoreux pour isoler le 2,2′-diméthoxy-4,4′-diformyldiphényl éther (II; R = CHO, R_1 = H). En condensant celui-ci avec l'acide malonique dans la pyridine nous avons synthétisé le 2,2′-diméthoxy-4,4′-bis-(β-carboxy-vinyl)-diphényl éther (II; R = CH=CH—CO_2H, R_1 = H) dont la réduction par le nickel Raney a donné le 2,2′-diméthoxy-4,4′-bis-(β-carboxyéthyl)-diphényl éther (II; R = CH_2—CH_2—CO_2H, R_1 = H).

PARTIE EXPÉRIMENTALE*

Esters tosyliques de formylnitrophénols

Tout en agitant mécaniquement et en maintenant la température au-dessous de 5°, on ajoute du chlorure de *p*-toluènesulfonyle (0.11 mole) à une suspension du formylnitrophénol (0.1 mole) dans la pyridine (70 ml). Le tout se dissout et on abandonne la solution à la température ambiante jusqu'à ce qu'un précipité commence à se former. On verse alors le mélange dans environ 300 ml d'eau froide. On essore l'ester et on le lave à l'eau. Il cristallise dans le solvant approprié en lamelles blanches (Tableau II).

TABLEAU II

ESTERS TOSYLIQUES DE PHÉNOLS

Phénol	P.f., °C	Rdt, %	Solvant	Formule	N	
					% calculé	% trouvé
5-Nitrovanilline (2)	144–145	78	Acide acétique	$C_{15}H_{13}O_7NS$	3.98	3.9
5-Nitro-*o*-vanilline	72	74	Éthanol	$C_{15}H_{13}O_7NS$	3.98	4.1
2-Nitro-4-formylphénol	115	84	Éthanol	$C_{14}H_{16}NS$	4.36	4.5

Esters diphényliques dérivés de la 5-nitrovanilline

On bout à reflux pendant 1 heure une solution de tosylate de la 5-nitrovanilline (0.01 mole) et du phénol approprié (0.03 mole) dans de la pyridine (10 ml). On abandonne le mélange réactionnel à la température ambiante et, une fois refroidi, on le verse dans environ 100 ml d'eau froide. On extrait la suspension à l'éther, on lave l'extrait éthéré successivement à l'acide chlorhydrique et à la soude dilués, et enfin à l'eau, puis on l'évapore à siccité. On cristallise l'éther dans le solvant approprié (Tableau III).

Éthers diphényliques dérivés de la 3-nitro-4-hydroxybenzaldéhyde

On peut préparer ces éthers comme précédemment à partir du tosylate de la 3-nitro-4-hydroxybenzaldéhyde (0.01 mole) et du phénol requis (0.03 mole) dans la pyridine (10 ml) (façon de procéder (*a*)), ou bien en chauffant à reflux pendant 1 heure de la 3-nitro-4-chlorobenzaldéhyde (0.01 mole) avec le phénol approprié (0.03 mole) dans la pyridine (10 ml) (façon de procéder (*b*)), ou dans 5 ml d'eau contenant 0.4 g (1 équivalent)

*Les points de fusion ont été pris à l'aide de l'appareil de Johns.

TABLEAU III

2-NITRO-4-FORMYL-6-MÉTHOXYPHÉNYL ARYL ÉTHERS

Groupe aryle	P.f., °C	Rdt %	Solvant	Forme cristalline	Formule	N % calculé	N % trouvé
Phényle	63	29	Éthanol	Lamelles jaunes	$C_{14}H_{11}O_5N$	5.12	4.7
2-Méthoxyphényle (2)	136–137	30	Éthanol	Aiguilles jaunes	$C_{15}H_{13}O_6N$	4.62	4.5
4-Méthoxyphényle	110–111	45	Éthanol	Aiguilles jaunes	$C_{15}H_{13}O_6N$	4.62	4.6
3-Formylphényle	138	39	Éthanol	Prismes blancs	$C_{15}H_{11}O_6N$	4.65	4.8
4-Formylphényle	131.5	32	Éthanol	Prismes blancs	$C_{15}H_{11}O_6N$	4.65	4.7
2-Méthoxy-5-formyl-phényle	167	40	Acide acétique	Prismes blancs	$C_{16}H_{13}O_7N$	4.23	4.4
2-Méthoxy-4-formyl-phényle	155	48	Acide acétique	Lamelles blanches	$C_{16}H_{13}O_7N$	4.23	4.2

d'hydroxyde de sodium (façon de procéder (*c*)). Dans les deux premières façons de procéder (soit (*a*) et (*b*)) on isole les éthers comme on le fait pour les éthers dérivés de la 5-nitrovanilline, tandis que dans la dernière (soit (*c*)) on ne lave l'extrait éthéré qu'à l'eau. On cristallise les éthers dans l'éthanol (Tableau IV).

TABLEAU IV

2-NITRO-4-FORMYLPHÉNYL ARYL ÉTHERS

Groupe aryle	P.f., °C	Rdt, %	Forme cristalline	Formule	N % calculé	N % trouvé
Phényle	48	(*a*) 45	Prismes blancs	$C_{13}H_9O_4N$	5.65	5.3
2-Méthoxyphényle	101.5	(*a*) 55 (*b*) 52 (*c*) 50	Aiguilles blanches	$C_{14}H_{11}O_5N$	5.12	5.0
4-Méthoxyphényle	66	(*a*) 50 (*b*) 50 (*c*) 52	Prismes jaunes	$C_{14}H_{11}O_5N$	5.12	5.3
3-Formylphényle	99	(*a*) 45 (*b*) 45 (*c*) 48	Lamelles blanches	$C_{14}H_9O_5N$	5.16	5.1
4-Formylphényle	93.5	(*a*) 54 (*b*) 70 (*c*) 28	Lamelles blanches	$C_{14}H_9O_5N$	5.16	5.3
2-Méthoxy-5-formylphényle	127	(*a*) 70 (*b*) 65 (*c*) 56	Aiguilles blanches	$C_{15}H_{11}O_6N$	4.65	4.6
2-Méthoxy-4-formylphényle	136	(*a*) 75 (*b*) 80 (*c*) 15	Prismes jaunâtres	$C_{15}H_{11}O_6N$	4.65	4.9
3-Nitrophényle	128	(*a*) 48 (*b*) 49	Aiguilles blanches	$C_{13}H_8O_6N_2$	9.72	9.8
2-Méthoxy-3-nitro-5-formylphényle	190	(*c*) 22	Lamelles blanches	$C_{15}H_{10}O_8N_2$	8.09	8.2

Éthers diphényliques dérivés de la 5-nitrosalicylaldéhyde

Dans une solution de 2-chloro-5-nitrobenzaldéhyde (0.01 mole) dans de l'éthanol (5 ml) on verse une solution du phénol approprié (0.01 mole) dans 5 ml d'eau contenant

0.4 g (1 équivalent) d'hydroxyde de sodium et on fait bouillir à reflux pendant 1 heure. Lorsque le mélange réactionnel est à la température ambiante on le dilue avec de l'eau, on essore l'éther précipité et on le cristallise dans l'éthanol sauf pour le 2'-méthoxy-2,5'-diformyl-4-nitrodiphényl éther qu'on cristallise dans l'acide éthanoique (Tableau V).

TABLEAU V

2-FORMYL-4-NITROPHÉNYL ARYL ÉTHERS

Groupe aryle	P.f., °C	Rdt, %	Forme cristalline	Formule	N	
					% calculé	% trouvé
2-Méthoxyphényle	113	48	Aiguilles blanches	$C_{14}H_{11}O_5N$	5.12	5.2
4-Méthoxyphényle	105	53	Aiguilles blanches	$C_{14}H_{11}O_5N$	5.12	4.9
3-Formylphényle	119–120	59	Prismes jaunâtres	$C_{14}H_9O_5N$	5.16	5.0
4-Formylphényle	131.5	30	Prismes blancs	$C_{14}H_9O_5N$	5.16	5.3
2-Méthoxy-4-formylphényle	71	47	Aiguilles blanches	$C_{15}H_{11}O_6N$	4.65	4.9
2-Méthoxy-5-formylphényle	210	65	Lamelles blanches	$C_{15}H_{11}O_6N$	4.65	4.6

2,2'-Diméthoxy-4,4'-diformyldiphényl éther (II; R = CHO, R_1 = H)

On ajoute 9.93 g (0.03 mole) de 2,2'-diméthoxy-4,4'-diformyl-6-nitrodiphényl éther à une solution de chlorure stanneux (23.0 g) dans 25 ml d'acide chlorhydrique concentré. On agite ce mélange pendant 2 heures à la température ambiante, puis 5 minutes à 80°. On refroidit et on décompose le composé complexe en le versant dans 150 ml d'eau. On essore l'amine, on la dissout dans 50 ml d'acide chlorhydrique dilué (1:1) et on la diazote à 0° par l'addition d'une solution de nitrite de sodium (2.1 g) dans 10 ml d'eau. Tout en agitant cette solution du sel de diazonium et en la maintenant à 0°, on verse lentement 100 ml d'acide hypophosphoreux à 30% préalablement refroidi à 0° et on laisse reposer le tout à cette température pendant 20 heures. On essore le précipité qui s'est formé et on le lave successivement à la soude diluée et à l'eau. Après avoir cristallisé dans un mélange de benzène et d'éther de pétrole, on obtient 6.5 g (76% de la théorie) de 2,2'-diméthoxy-4,4'-diformyldiphényl éther pur sous la forme de prismes blancs de p.f. 123°. Calculé pour $C_{16}H_{14}O_5$: C, 66.9%; H, 4.9%. Trouvé: C, 66.7%; H, 5.1%.

2,2'-Diméthoxy-4,4'-bis-(β-carboxyvinyl)-diphényl éther (R = CH=CH—CO_2H, R_1 = H)

On chauffe au bain-marie pendent 1 heure, puis à reflux durant 5 minutes, un mélange de 2,2'-diméthoxy-4,4'-diformyldiphényl éther (5.8 g, 0.02 mole), d'acide malonique (6.5 g, 0.08 mole), de pyridine (25 ml) et de pipéridine (0.5 ml). On verse ensuite la solution froide sur de la glace (100 g) additionnée de 25 ml d'acide chlorhydrique concentré et on filtre le précipité. On cristallise dans le benzène et on essore 5.9 g (80% de la théorie) de 2,2-diméthoxy-4,4'-bis-(β-carboxyvinyl)-diphényl éther pur sous la forme de cubes jaunâtres de p.f. 225–226°. Calculé pour $C_{20}H_{18}O_7$: C, 64.8%; H, 4.8%. Trouvé: C, 64.4%; H, 4.9%.

2,2'-Diméthoxy-4,4'-bis-(β-carboxyéthyl)-diphényl éther (R = CH_2—CH_2—CO_2H, R_1 = H)

À une solution vivement agitée de 2,2'-diméthoxy-4,4'-bis-(β-carboxyvinyl)-diphényl éther (7.41 g, 0.02 mole) dans 200 ml de soude à 10%, on ajoute, en petites portions et en l'espace de 1 heure, 20.0 g de l'alliage de nickel Raney. On filtre ensuite, on lave le précipité à l'eau et on verse le filtrat dans 10 ml d'acide chlorhydrique concentré. On essore le 2,2'-diméthoxy-4,4'-bis-(β-carboxyéthyl)-diphényl éther et on le cristallise dans

l'éthanol à 50%. L'éther cristallise en aiguilles blanches de p.f. 126°. Rendement: 6.0 g (80% de la théorie). Calculé pour $C_{20}H_{22}O_7$: C, 64.1%; H. 5.9%. Trouvé: C, 63.8%; H, 6.0%.

REMERCIEMENTS

Nous remercions le Conseil National de Recherches du Canada, l'Office de Recherches de la Province de Québec et les Canadian Industries Limited pour des bourses d'études qu'ils ont accordées à l'un de nous (R.C.).

BIBLIOGRAPHIE

1. GUTHRIE, D. A., FRANK, A. W. et PURVES, C. B. Can. J. Chem. **33**, 729 (1955).
2. GRUNDON, H. F. et PERRY, H. J. H. J. Chem. Boc. 3531 (1954).
3. BORROWS, E. T., CLAYTON, J. C., HEMS, B. A. et LONG, A. G. J. Chem. Soc. S190 (1949).

ON THE SPECTRAL RESPONSE OF PHOTOCONDUCTION IN THIN SINGLE CRYSTALS OF ANTHRACENE[1]

J. FERGUSON[2] AND W. G. SCHNEIDER

ABSTRACT

The photoconduction of thin crystals of anthracene (sublimation flakes) has been studied as a function of the wavelength of the incident light as well as the geometry of the "surface cell" arrangement. With spot electrodes on one face of the crystal, the spectral response showed a very pronounced difference depending on whether the electrode face or the opposite face was illuminated. In the latter case the spectral response followed the absorption curve of the crystal, whereas when the electrode face was illuminated the photoconductivity was a minimum at wavelengths corresponding to maximum extinction coefficients of the crystal.

INTRODUCTION

Photoconduction of aromatic compounds has been the subject of a considerable number of recent publications (1–17). One important aspect of this work has been the study of the variation of the photocurrent with wavelength. Carswell (18) first noted that the spectral dependence of the photocurrent in anthracene crystals reproduced the absorption spectrum of the crystal, and Lyons and co-workers (3, 13, 14) have extended these measurements to other compounds. Lyons (4) has suggested a reason for the similarity between the absorption spectrum of the crystal and the spectral dependence of the photocurrent. During the course of an investigation of the absorption and fluorescence spectra of anthracene sublimation crystals (19, 20) we have remeasured the spectral dependence of the photocurrents in these crystals and we find that if particular care is taken to ensure that the electrode material is only on the surface on which the light falls, the spectral dependence does not reproduce the absorption spectrum. The present paper reports these measurements.

EXPERIMENTAL

The anthracene crystals were grown by sublimation in an atmosphere of carbon dioxide. Chromatographically pure anthracene which had been kept in the dark after purification was used. Crystals deliberately contaminated with tetracene were obtained by adding small amounts of tetracene to the anthracene before sublimation.

The sublimation crystals were usually transferred to a clean silica disk so that one of the developed *ab* crystal faces was in contact with the silica disk. The disk provided the necessary support for the very thin crystals. A few measurements were made on thicker crystals (about 3 μ) mounted over a slot cut in a silica disk so that only about one half of the crystal was supported by the disk. These measurements did not differ significantly from those made with the disk supporting all of the crystal.

Aquadag was initially used as the electrode material but it was found that at low light intensities the photocurrent showed an unusually long build-up time and this was eliminated by reverting to electrodes from alkadag. The electrodes were judged to be "good" if no back e.m.f. was found.

At first, electrodes were painted over each end of a crystal and also over part of the

[1]*Manuscript received May 14, 1958.*
Contribution from the Division of Pure Chemistry, National Research Council, Ottawa.
Issued as N.R.C. No. 4934.

[2]*National Research Council Postdoctorate Fellow 1955–57. Present address: Division of Industrial Chemistry, Box 4331, G.P.O., Melbourne, Victoria, Australia.*

silica disk. This produced an apparent variation of the spectral dependence of the photocurrent with crystal thickness. This variation was removed when care was taken to place the electrodes so that contact was made only with one *ab* face of the crystal. This was done by anchoring two flexible wires at diametrically opposite sides of a silica disk and making electrode contact to the exposed *ab* face with alkadag, taking particular care to prevent the electrode material from lapping over the edge of the crystal (see Fig. 1). Two arrangements were then possible, one with the light incident on the exposed *ab* face (electrode side), the other with the light incident on the opposite face.

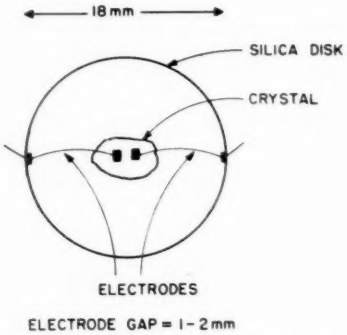

FIG. 1. Diagram of electrode arrangement. The incident light uniformly covered the electrodes and the area between the electrodes.

The silica disk was then mounted on a teflon block inside a brass cell fitted with a silica window. The cell, which could be evacuated, was clamped to a Keithley 200B micromicroammeter. Normally measurements were made in dry air but a few were made in an atmosphere of helium.

The spectral dependences were determined with a Beckman DU Spectrometer as a monochromator. The light source was a 500-watt projection lamp and the radiation was polarized by a sheet of polaroid between the exit slit and the cell. The wavelength knob of the monochromator was driven by a motor and the photocurrent was recorded by a Varian G10 recorder. The intensity dependence of the photocurrent was measured at different wavelengths by using filters of evaporated silver on silica. After the photoconduction measurements had been made the absorption spectrum in polarized light was determined in every case.

The photocurrents were usually in the range 10^{-13}–10^{-12} amp and slit widths varied from 0.05 to 0.4 mm, with 0.2 mm the usual value. No increased "resolution" was found at slit widths below this value.

RESULTS

A. Anthracene Crystals Containing Tetracene

There are two processes taking place after the absorption of light which could possibly complicate the interpretation of the spectral response of the photocurrent. These are the migration of excitation energy and reabsorption of fluorescence. It is important to demonstrate experimentally that migration of energy over a large number of lattice parameters (50–100) is not an essential factor in determining the spectral response. This

can be done simply by deliberately contaminating anthracene with small amounts of tetracene so as to quench the anthracene fluorescence and thereby reduce the mean free path of the exciton. This was done for a series of crystals with increasing tetracene concentration but no change in the polarized spectral response was observed, with either arrangement of electrodes and incident light, from that observed with pure anthracene crystals even when 90% of the emission was from the tetracene. These experiments also proved that reabsorption of fluorescence was not an important factor.

One observation, noted previously (15), is that the magnitude of the photocurrent is decreased markedly by the introduction of the tetracene. This suggests that the process leading to the production of charge carriers is one that does not take place in a time that is very short compared to the lifetime of the excited state, and the formation of charge carriers is thereby inhibited by any interaction which decreases, even slightly, the lifetime of this state.

B. Pure Anthracene Crystals

The spectral responses recorded here were all taken in dry air. Some measurements were made in which the cell was evacuated to 10^{-5} mm Hg and then dry helium introduced at atmospheric pressure. These showed that no significant changes occurred in the spectral response even after continued pumping resulting in appreciable sublimation of the crystals. As mentioned earlier, care was taken to ensure that the anthracene, after purification, was not exposed to light of high intensity so that photooxidation products on the surface of the crystals were kept to a minimum.

It was necessary to correct the spectral response in two ways. First, the intensity of the light incident on the crystal decreased with decreasing wavelengths so correction factors were calculated from the known energy distribution of the light source, the dispersion of the monochromator, and the transmission of the polaroid sheet. Measurements of the photocurrent at different wavelengths with polarized light of varying intensity showed that the photocurrent was directly proportional to the light intensity for both arrangements of light and electrodes. This result is needed to correct the response curves to equal energy input but is more important for an interpretation of the spectral response. Second, the spectral response has to be corrected in regions of the spectrum where the crystal transmits light. This occurs with very thin crystals for wavelengths within the absorption region and for all crystals at wavelengths on the absorption edge. In order to do this the absorption spectrum of each crystal was determined but no measurements of reflection losses were made. Although the latter will be small in regions where the absorption is strong (21) they are very important on the absorption edge when the optical density is less than about 0.2. As the correction factors convert the observed response to equal amounts of absorbed energy, they will be in serious error on the tail of the absorption band because the apparent absorption due to reflection is appreciable, and for this reason the corrected spectral dependences reported here cover only the wavelength region where reflection losses cause no appreciable error to the measured absorption spectrum.

As mentioned in the Experimental section, particular care is required in applying the electrode material to the crystals. If the electrodes are carefully placed only on the exposed *ab* face, then it is found that the spectral dependence depends critically on whether the incident light falls on this surface or on the opposite surface. Figs. 2 and 3 illustrate this behavior.

It was found that with light incident on the surface containing the electrodes the

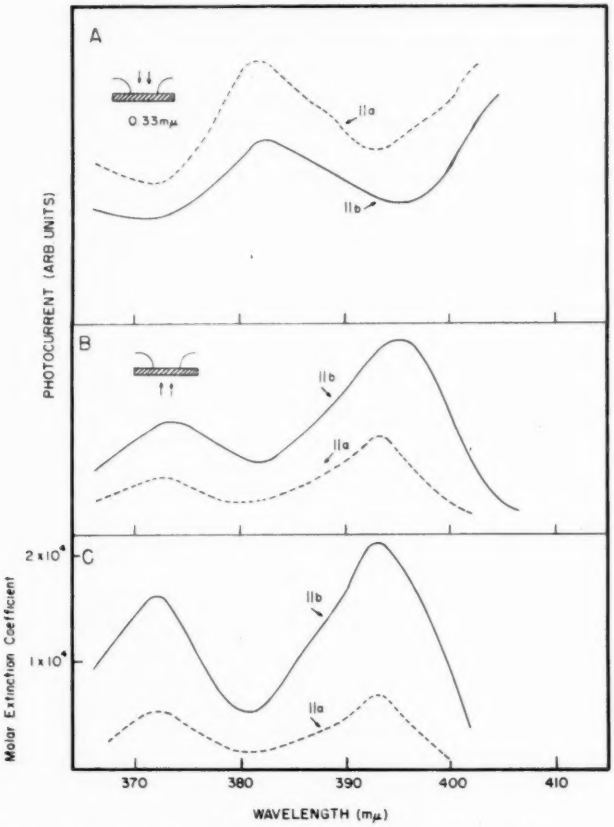

FIG. 2. The spectral dependence of the photocurrent (corrected to equal amounts of absorbed energy) in polarized light of a single anthracene crystal, thickness 0.33 μ; A, light incident on the surface containing the electrodes; B, light incident on the opposite face; C, the absorption spectrum of anthracene crystal (21).

wavelengths of maximum photocurrent correspond to wavelengths of minimum absorption coefficient, and this holds for both crystal polarizations. It is only when the light is incident on the other face that a resemblance is found between the spectral response of the photocurrent and the absorption spectrum of the crystal. In this case the wavelengths of maximum photocurrent correspond to wavelengths of maximum absorption coefficient and, although there is an apparent resemblance between the absorption spectrum and spectral response of the photocurrent, there is not a direct relation between the two. It must be assumed that in earlier reports of the spectral dependence of the surface cell the electrodes were not carefully confined to the surface on which the light was incident.

Measurements of the relative magnitudes of the photocurrents produced in the two arrangements were not made. However, with crystals of thickness about 4 μ mounted on silica and with electrodes not carefully confined to the top surface, i.e. electrode material painted over the crystal and onto the disk, the spectral response showed a resemblance to the absorption spectrum. This arrangement corresponds to electrodes simultaneously

on the front and back surfaces but with unequal distances between the electrodes. As the spectral response appeared similar to the absorption spectrum, we can assume that the arrangement with the electrodes on the back surface gives higher currents in the external circuit than the other arrangement.

A large number of measurements were made of the spectral response of a series of crystals of different thickness with the "true" surface cell arrangement, i.e. light incident

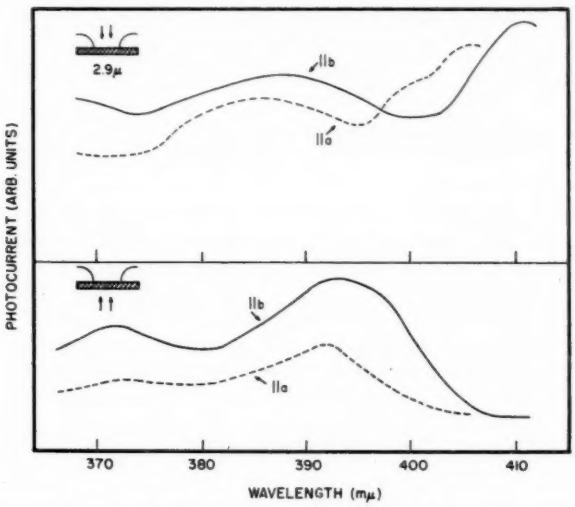

FIG. 3. The spectral dependence of the photocurrent (corrected to equal amounts of absorbed energy) in polarized light of a single anthracene crystal, thickness 2.9 μ. The top two curves were measured with the light incident on the surface containing the electrodes, the bottom two with the light incident on the opposite face.

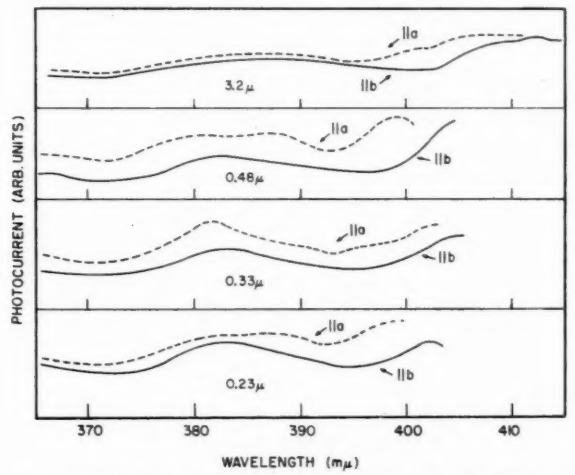

FIG. 4. The spectral dependence (corrected to equal amounts of absorbed energy) of the photocurrents in polarized light of four single anthracene crystals of different thickness, all measured with the light incident on the surface containing the electrodes.

on the face containing the electrodes. Fig. 4 shows some of the results. The crystal thickness ranges from 0.23 to 3.2 μ but there does not appear to be a dependence of the spectral response on crystal thickness. This is not strictly true for the *b* polarization, where there is seen to be a slight shift of the response to longer wavelengths for thicker crystals. This is interpreted as reflecting a modification of the surface energy levels in the thicker crystals (19), so that light absorbed near the surface is of slightly longer wavelength. The *a* polarization also shows variations in relative peak heights, as can be seen, but these show no correlation with crystal thickness.

DISCUSSION

It is apparent from Figs. 2, 3, and 4 that the wavelengths which are most strongly absorbed produce least photocurrent in the "true" surface cell arrangement. The result is striking and suggests immediately that carrier recombination limits the photocurrents in regions of high light absorption. However, the photocurrent is directly proportional to the light intensity and also, if recombination is limiting the photocurrent in these regions, then the spectral response in the arrangement where the light falls on the opposite *ab* face should be similar, whereas maximum photocurrent is found at wavelengths of high absorption coefficient.

Although the results are striking we are not able to interpret them at present. We do, however, make the suggestion that diffusion of charge carriers, hitherto neglected, should be seriously considered in any attempt at an explanation. The surface cell arrangement of electrodes must produce an inhomogeneous field within the crystal and this, coupled with diffusion of carriers, can possibly complicate the spectral dependence.

The parallelism between the spectral response within the absorption region and the absorption edge should be noted. Inside the absorption band we see that wavelengths of minimum light absorption (true surface cell arrangement) produce a higher photocurrent than wavelengths of maximum absorption. If we compare the absorption edge with the absorption band as a whole we see that the former produces a higher photocurrent than the latter, so the general rule appears to be that high photocurrents are obtained in regions of low light absorption. We must not therefore interpret the spectral response of the surface cell to mean that the absorption edge necessarily has a higher efficiency for charge carrier formation. This becomes clear when we compare the two regions in the other arrangement of the light and electrodes, the general rule here being that high photocurrents are obtained in regions of high light absorption.

We would like finally to suggest that considerable care be taken in the interpretation of spectral response curves of organic photoconductors as anthracene is not a unique case. It was shown earlier (22) that the spectral dependence of 9,10-dichloroanthracene is also critically dependent on incident light and electrode geometry. Also we note the attempt to assign the electronic states of the pyrene molecule from measurements of the polarized spectral dependence of single crystals of pyrene (14). The assignment of the lowest excited state is most likely correct but the sense of the polarization ratio as observed in the spectral dependence of the photocurrent is opposite to that found by direct absorption spectroscopy (23). This is then probably a result of some specific sensitivity of the electrode and incident light geometry.

REFERENCES

1. CHYNOWETH, A. G. and SCHNEIDER, W. G. J. Chem. Phys. **22**, 1021 (1954).
2. CHYNOWETH, A. G. J. Chem. Phys. **22**, 1029 (1954).
3. BREE, A. V. and LYONS, L. E. J. Chem. Phys. **22**, 1630 (1954).

4. LYONS, L. E. J. Chem. Phys. **23**, 220 (1955).
5. GOLDSMITH, G. J. Ph.D. Thesis, Purdue Univeristy, Lafayette, Indiana. 1955.
6. BREE, A. V., CARSWELL, D. J., and LYONS, L. E. J. Chem. Soc. 1728 (1955).
7. CARSWELL, D. J. and LYONS, L. E. J. Chem. Soc. 1734 (1955).
8. NORTHRUP, D. C. and SIMPSON, O. Proc. Phys. Soc. **68**, 974 (1955).
9. ZINZER, H. J. Z. Naturforsch. **11a**, 306 (1956).
10. INOKUCHI, H. Bull. Chem. Soc. Japan, **29**, 131 (1956).
11. SCHNEIDER, W. G. and WADDINGTON, T. C. J. Chem. Phys. **25**, 358 (1956).
12. BREE, A. V. and LYONS, L. E. J. Chem. Phys. **25**, 384, 1284 (1956).
13. LYONS, L. E. and MORRIS, G. C. Proc. Phys. Soc. **69**, 1162 (1956).
14. LYONS, L. E. and MORRIS, G. C. J. Chem. Soc. 3648, 3661 (1957).
15. COMPTON, D. M. J., SCHNEIDER, W. G., and WADDINGTON, T. C. J. Chem. Phys. **27**, 160 (1957).
16. LYONS, L. E. Australian J. Chem. **10**, 365 (1957).
17. LYONS, L. E. J. Chem. Soc. 5001 (1957).
18. CARSWELL, D. J. J. Chem. Phys. **21**, 1890 (1953).
19. FERGUSON, J. and SCHNEIDER, W. G. J. Chem. Phys. **28**, 761 (1958).
20. FERGUSON, J. and SCHNEIDER, W. G. Can. J. Chem. **36**, 1070 (1958).
21. BREE, A. V. and LYONS, L. E. J. Chem. Soc. 2663 (1956).
22. BOCK, E., FERGUSON, J., and SCHNEIDER, W. G. Can. J. Chem. **36**, 507 (1958).
23. FERGUSON, J. J. Chem. Phys. **28**, 765 (1958).

KINETICS OF EXCITED MOLECULES

I. KETENE[1]

B. T. Connelly and Gerald B. Porter

ABSTRACT

The primary quantum yield of ketene decomposition was studied as a function of pressure, temperature, and wavelength. The results show that excited vibronic states are formed which may be degraded before dissociation can occur. The ratio of the rate of collisional degradation to the rate of dissociation decreases from 164 liters/mole at 3340 Å to 16.8 liters/mole at 3130 Å.

INTRODUCTION

Previous experiments have shown that the primary quantum yield of ketene decomposition is a function of the wavelength of the absorbed radiation. At 2700 Å Strachan and Noyes (1) found the primary quantum yield to be unity within experimental error, independent of pressure and temperature. At 3650 Å (1) the primary quantum yield, extrapolated to zero pressure of ketene, is much less than unity, decreases as pressure is increased, and increases with increase in temperature.

Following the absorption of 2700 Å radiation and the formation of an excited ketene molecule, dissociation occurs in less time than that required for collision with another molecule, to give a methylene radical and a molecule of carbon monoxide. The methylene radical then attacks another ketene molecule to form ethylene and another carbon monoxide, according to the following mechanism:

$$K + h\nu\ (2700\ Å) = K^m, \qquad [1m]$$

$$K^m = CH_2 + CO, \qquad [2m]$$

$$CH_2 + K = C_2H_4 + CO, \qquad [2m]$$

where K is a ketene molecule, and K^m is a ketene molecule excited by 2700 Å radiation. For each photon absorbed, one molecule of ketene is dissociated and two molecules of carbon monoxide are formed.

Strachan and Noyes (1) found the quantum yield of carbon monoxide formation to be 2.12 ± 0.15. They also found the ratio of the quantum yield of carbon monoxide formation to the quantum yield of ethylene to be 2.2 instead of 2.0 to be expected from reactions [1*m*] and [2*m*].

It is evident therefore that some methylene radicals are involved in another reaction, such as

$$CH_2 + y\,CH_2CO = \text{polymer} + CO.$$

At 3650 Å, the low quantum yields can be attributed to collisional deactivation and internal conversion of the excited ketene molecules (2), according to the following mechanism:

$$K + h\nu\ (3650\ Å) = K^q, \qquad [1q]$$

$$K^q = \text{products}, \qquad [2q]$$

$$K^q = K, \qquad [3q]$$

$$K^q + K = 2K. \qquad [4q]$$

The energy is dissipated in processes [3*q*] and [4*q*] as heat, since no fluorescence has ever been observed.

[1]*Manuscript received July 28, 1958.*
Contribution from the Department of Chemistry, University of British Columbia, Vancouver, B.C.

It is evident from the low quantum yield that reaction [3q] is more rapid than reaction [2q]. As the pressure is increased the rate of reaction [4q] increases from zero to become the dominant process. Extrapolation to zero pressure at 26° C gives a carbon monoxide quantum yield of approximately 0.07. At 3650 Å, therefore, dissociation occurs only after a finite time interval during which the excited ketene molecule may be deactivated.

Kistiakowsky and Mahan (3) found that the primary quantum yield at 3130 Å was independent of pressure and suggested a value of unity. However, they apparently investigated the photolysis over a narrow range of pressures and their results are therefore not conclusive. Investigation of the quantum yield at a number of wavelengths provides the means of determining the relation between the rate of dissociation and the energy of the dissociating molecule. It was therefore decided to investigate the photolysis of ketene at 3130 Å more carefully over a wide range of pressures using a technique whereby quantum yields could be determined accurately. This technique would reveal any small effect of pressure on the primary quantum yield that may have escaped detection in previous work (3).

It was felt that since another mercury-arc line, 3340 Å, occurs between 3130 Å and 3650 Å, precise quantum yield determinations at this wavelength would substantially increase our understanding of the process of deactivation.

EXPERIMENTAL

A medium pressure 100-watt Hanovia mercury-arc lamp was used as the light source for runs at 3130 Å. The lamp was encased in aluminum tubing with $\frac{1}{4}$-in. diameter hole opposite the arc. The lamp was run from a constant voltage regulator (115 volts). For runs at 3340 Å a B.T.H. medium pressure mercury-arc lamp was used. The divergent light beam passed through a combination of two quartz convex lenses.

A filter cell block consisting of two compartments each 2.5 cm long and with quartz windows, together with a 2-mm Corning 9863 filter to exclude visible radiation, was placed between the lenses and the cell. The quartz reaction cell of length 14.8 cm and diameter 3.6 cm was housed in a heated aluminum block in which the temperature could be controlled to within ±0.1° C. The emergent beam was passed through another convex lens and focused on the cathode of an RCA 935 photocell.

The filter solutions used are given in Table I and the respective transmissions at the various wavelengths are shown in Fig. 1. Filters A and B were similar to those of Hunt and Davis (4), although the nickel chloride was omitted. Filter C was similar to that suggested by Kasha (5).

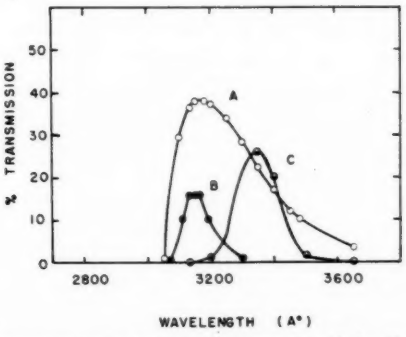

FIG. 1. Percentage transmission against wavelength for filters A, B, and C.

TABLE I
FILTER SOLUTIONS

Filter solution	Potassium biphthalate, g/100 ml 2.5-cm cell	Potassium chromate, g/100 ml 2.5-cm cell	Nickel sulphate hexahydrate, 1-cm cell	Naphthalene in methyl alcohol, g/50 ml 1-cm cell	Glass filters
A	0.08	0.008	—	—	2-cm Corning 9863
B	0.08	0.019	—	—	2-mm Corning 9863
C	—	—	Saturated solution	0.44	2-mm Corning 9863 1-mm Pyrex window

Gas Analyses

Gas analyses were carried out in an all-glass high-vacuum system evacuated by a standard-type oil pump and a single stage mercury diffusion pump. In this system mercury cutoffs were used in place of stopcocks.

The carbon monoxide analysis was performed by allowing the products to flow through successive baths cooled to −78° C, −196° C, −210° C (dry ice – acetone, liquid nitrogen, and solid nitrogen, respectively). The solid nitrogen trap was prepared by pumping on fresh liquid nitrogen for about fifteen minutes.

Ketene was condensed in the first two baths and the ethylene was collected in the solid nitrogen trap. Carbon monoxide was the only product not condensed at −210° C and was measured with a McLeod–Toepler gauge (1).

Diethyl Ketone

Diethyl ketone, used as the internal actinometer for runs at 3130 Å, was fractionally distilled (b.p. 101°). Once on the line, the diethyl ketone was distilled under vacuum and the middle third was retained.

Prior to each run, a quantity of diethyl ketone was transferred from a blackened storage bulb to a dry ice – acetone cooled trap and outgassed three times until all non-condensables and low-boiling gases were removed.

Ketene

Ketene was prepared in the vacuum system by pyrolyzing acetic anhydride (6). Trap-to-trap distillation was performed on the freshly prepared ketene and the middle third retained. Prior to each run, a quantity of ketene was thoroughly outgassed by three distillations similar to those for diethyl ketone. The ketene was stored in a trap immersed in liquid nitrogen to prevent polymerization.

Actinometry

3130 Å

Diethyl ketone was selected for experiments at 3130 Å where the quantum yield of carbon monoxide formation is 1.0 at 100° C (7). The use of an internal actinometer was found to be very convenient because it is devoid of the errors usually associated with external actinometers.

The measurement of the intensity absorbed during a run was performed by the conversion of the current from the photocell into a voltage which was continuously recorded on a 10-mv recorder. The following scale readings were taken:

R_i = cell empty,
R_t = photolyte in cell.

The recorder scale was calibrated using diethyl ketone as an internal actinometer.

Scale readings were taken before and after each run to determine the average R_t. This was necessary because of the fluctuation and decay of the lamp, and polymer formation. R_t was measured continuously during each run.

The difference $R_t - R_t = R_a$ was calibrated in terms of absolute intensity by the measurement of carbon monoxide yields from the photolysis of diethyl ketone at 100° C. It was possible to measure R_a to within $\pm 0.5\%$ and, on averaging the results of a number of diethyl ketone runs, quantum yields of carbon monoxide formation from ketene were obtained within $\pm 3\%$.

At 3130 Å, an external actinometer was also used (8), but because of the large amount of reflection from the glass–air interfaces and because of the suspected polymer on the exit wall of the reaction cell, the values for the absolute intensity of the light were considerably lower than those obtained using diethyl ketone. Twelve runs were performed using potassium ferrioxalate actinometer; consistent results indicated the need for a conversion factor to be applied when the external liquid actinometer was used to estimate the energy absorbed during runs at 3130 Å.

The intensity found from a ferrioxalate run when multiplied by this conversion factor gave the intensity incident to the cell, reproducible to within $\pm 10\%$.

3340 Å

The potassium ferrioxalate actinometer was used for runs at 3340 Å, since no internal actinometer is available for this wavelength. The intensities obtained by this actinometry when multiplied by the conversion factor found previously were used to calibrate the recorder scale. Absorbed intensities were obtained from measurements of R_t, R_t, and R_a, as described previously.

RESULTS

3130 Å

Using filter solution combination A, at low pressures of ketene, a carbon monoxide quantum yield of 1.82 was obtained, whereas at high pressures around one atmosphere, the carbon monoxide quantum yield decreased to 1.08, as shown in Table II. A decrease in the carbon monoxide quantum yield at high pressures was expected.

The results of five diethyl ketone actinometer runs, at pressures ranging from 60 to 155 mm of diethyl ketone, and interspersed between the ketene runs, gave a light intensity of approximately 5.4×10^{14} quanta per second.

Using filter solution combination B, a new series of diethyl ketone actinometer runs gave intensities of approximately 1.6×10^{14} quanta per second. The carbon monoxide quantum yield at low pressures of ketene was 2.0 within experimental error, and at 1 atmosphere a value of 1.18 was obtained as shown in Table II.

Absorbed intensities varied from 0.442×10^{14} quanta per second at 17 mm to 1.911×10^{14} quanta per second at 751 mm. All ketene runs were conducted at 37° C.

It was found that the transmissions at 3130 Å of filters A and B were appreciably lower after 2 weeks' constant use.

3340 Å

The naphthalene in methyl alcohol solutions darkened after only a few hours' exposure to the lamp and its transmission at 3340 Å decreased noticeably. Even when a pyrex window, which absorbs 50% of the light at 3130 Å and 100% of light of shorter wavelengths, was placed in front of the naphthalene solution darkening continued. This effect may have been caused by the attack of methyl alcohol on the adhesive used to bond the quartz windows to the pyrex cell.

TABLE II

PHOTOLYSIS OF KETENE

Run	Pressure of ketene, mm	Length of run, seconds	Intensity absorbed, quanta/second $\times 10^{-1}$	$\phi = \frac{1}{2}\Phi_{CO}$
	3130 Å	Cell temperature	37.0 °C	Filter A
1	35.8	3600	2.305	0.91
5	56.5	1800	2.855	0.93
4	201.6	2700	4.360	0.74
2	402.7	900	4.790	0.59
3	444.5	914	4.580	0.57
7	726.8	1800	4.290	0.54
	3130 Å	Cell temperature	37.0° C	Filter B
14	17.0	3600	0.442	1.03
13	40.8	2460	0.846	1.00
12	57.1	1800	1.029	1.00
11	135.8	2407	1.428	0.94
9	230.3	2400	1.710	0.83
10	679.1	1920	1.584	0.63
8	750.7	2400	1.911	0.59
	3340 Å	Cell temperature	37.0° C	Filter C
18	26.0	180	1.221	0.72
15	39.7	4200	0.771	0.72
16	47.0	1800	2.545	0.51
17	105.3	600	2.825	0.41
20	177.8	390	1.841	0.37
19	384.6	900	2.023	0.21
	3340 Å	Cell temperature	100.0° C	Filter C
24	26.1	180	0.811	0.80
23	56.7	240	1.239	0.74
22	121.8	255	1.579	0.58
21	299.5	600	1.920	0.37

The intensity of the beam as measured using the ferrioxalate actinometer when multiplied by the conversion factor of 2.72 gave an incident intensity of approximately 2.1×10^{15} quanta per second. When related to the recorder, this became 0.87×10^{14} quanta per second per scale division. The carbon monoxide quantum yields were determined at both 37° C and 100° C and the results are summarized in Table II.

DISCUSSION

The photolysis of ketene at 2700, 3130, 3340, and 3650 Å can be explained by the following processes:

$$K + h\nu\ (2700\ Å) = K^m \qquad [1m]$$

$$K + h\nu\ (3130\ Å) = K^n \qquad [1n]$$

$$K + h\nu\ (3340\ Å) = K^p \qquad [1p]$$

$$K + h\nu\ (3650\ Å) = K^q \qquad [1q]$$

$$K^m = \text{products} \qquad [2m]$$

$$K^n = \text{products} \qquad [2n]$$

$$K^p = \text{products} \qquad [2p]$$

$$K^q = \text{products} \qquad [2q]$$

$$K^m = K \qquad [3m]$$

$$K^m = K \quad [3m]$$
$$K^n = K \quad [3n]$$
$$K^p = K \quad [3p]$$
$$K^q = K \quad [3q]$$
$$K^m + K = 2K \quad [4m]$$
$$K^n + K = 2K \quad [4n]$$
$$K^p + K = 2K \quad [4p]$$
$$K^q + K = 2K \quad [4q]$$

where K is a molecule of ketene, and K^m, K^n, K^p, and K^q are excited ketene molecules in order of decreasing vibrational energy. Reactions [1] represent activation; reactions [2] represent product formation; reactions [3] represent internal conversion; and reactions [4] represent collisional deactivation.

It is not implied that the above mechanism which represents the activation and deactivation of excited molecules K^m, K^n, K^p, and K^q formed at wavelengths 2700 Å, 3130 Å, 3340 Å, and 3650 Å is complete. It is obvious that a ketene molecule in vibronic state m can lose its excess energy by a series of vibrational cascades to states n, p, q, etc. until it eventually reaches the equilibrium vibrational state. The number of vibronic states may be 100 or more for a molecule initially in state m. The kinetics of such a process are very complicated and will be treated in a later paper (9).

For simplicity the present discussion will consider only reactions [1], [2], [3], and [4], with rate constants k_1, k_2, k_3, and k_4, to represent the activation, deactivation, and dissociation of excited ketene molecules in states m, n, p, and q.

In general,

$$1/\phi = 1+(k_3/k_2)+k_4[K]/k_2$$

represents the equation obtained by steady-state treatment; ϕ is the primary quantum yield, k_3/k_2 is the intercept in the plot $1/\phi$ against pressure, and k_4/k_2 is the slope in liters/mole.

2700 Å

Strachan and Noyes (1) found that the quantum yield of carbon monoxide formation was approximately two. According to the proposed mechanism the primary quantum yield is thus unity. It is evident, therefore, that over the range of pressures and temperatures used, internal conversion and collision deactivation of the excited ketene molecules is negligible. The only way in which these molecules can lose their excess energy is by dissociation. The observed quantum yields can be explained by the mechanism:

$$[1m], [2m].$$

That internal conversion and collisional deactivation are absent may be seen from the intercept of unity and the zero slope of the plot of $1/\phi$ against pressure.

3130 Å

The primary quantum yield of ketene decomposition at this wavelength appears as an isolated number in several papers devoted to ketene photolyses at other wavelengths (3, 9, 10, 11). However, only the recent work of Kistiakowsky and Mahan (3) gives experimental data. From the limited amount of information given it appears that photolyses were only performed at low pressures, in the region of 20 mm. It was found that the primary quantum yield was independent of pressure and possibly equal to unity.

This research has shown that when light which was not monochromatic but which contained quantities of both 3340 and 3650 Å radiation was used, primary quantum yields of 0.91 at 35.8 mm and 0.54 at 726.8 mm were obtained, as shown in Table II.

The plot of $1/\phi$ against pressure intercepts the axis at approximately 1.1 and has a positive slope. It is likely, therefore, that internal conversion and collisional deactivation of the excited ketene molecule contribute slightly to the deactivation process.

Because of the known low quantum yields at 3650 Å and the suspected low yields at 3340 Å, a new series of experiments was performed using monochromatic 3130 Å radiation. The results of these experiments are shown also in Table II. The primary quantum yield is 1.0 at pressures between 17 and 60 mm, and 0.59 and 750.7 mm.

The plot of $1/\phi$ against pressure is shown in Fig. 2; although the extrapolation to zero pressure is unity, because of experimental error the presence of internal conversion is not entirely excluded from the mechanism. The positive slope of the plot in Fig. 2 indicates the presence of collisional deactivation, and hence the mechanism: [1*n*], [2*n*], [3*n*], [4*n*] may be postulated in which the extent of reaction [3*n*] is very small. k_3/k_2 is approximately zero while $k_4/k_2 = 16.8$ liters/mole.

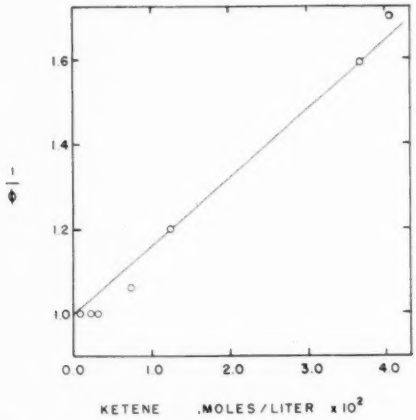

FIG. 2. Dependence of primary quantum yield on concentration at 3130 Å.

The mechanism of ketene decomposition at 3130 Å is intermediate between those postulated for 2700 Å and 3650 Å. From Table II it appears that at low pressures of ketene, every excited ketene molecule dissociates to form products, whereas, at pressures greater than approximately 60 mm, some of the excited molecules lose their energy by collision with unexcited molecules of ketene.

The photolysis at 3130 Å was not extended to higher temperatures because it was thought that little or no significant information would be obtained.

In three experiments the ethylene quantum yield was found to be 1/2.14 of the carbon monoxide quantum yield. This is approximately the same as that found at 2700 Å (1) and 3650 (1, 13).

3340 Å

This research has indicated that for photolyses at 37° C the primary quantum yield is 0.72 at 26 mm and 0.21 at 384 mm. The zero pressure intercept in Fig. 3 is 1.25. The slope of the plot is much steeper than for 3130 Å: 1.64×10^2 liters/mole. This indicates that considerable collisional deactivation of K^p occurs.

Four runs were performed at 100° C and as expected, both the slope and the intercept were smaller than for runs at 37° C. At 26.1 mm the primary quantum yield is 0.80 and

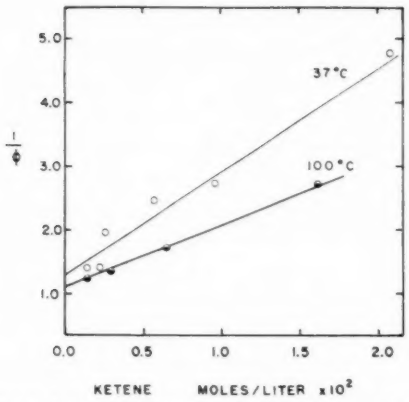

FIG. 3. Dependence of primary quantum yield on concentration at 3340 Å.

at 300 mm equals 0.37. The zero pressure intercept at 100° C is 1.1 and the slope of the straight line is 0.99×10^2 liters/mole, both obtained from Fig. 3. The ratio of the rates of internal conversion to product formation at 100° C is 0.1.

The mechanism for the activation and deactivation of K^p is: [1*p*], [2*p*], [3*p*], and [4*p*], at both 37° C and 100° C. From this information in Table II and Fig. 3, it was possible to estimate approximately the activation energy of reaction [2*p*] from the slope of the plot of $\log_e(k_4/k_2)$ against $1/T$. The slope is $(E_2-E_4)/R$. If E_4 is assumed to be zero, then E_2 is approximately 2 kcal/mole. This value is subject to a large uncertainty.

3650 Å

Strachan and Noyes (1) found a zero pressure intercept of 28 in the plot of reciprocal primary quantum yield against pressure. This corresponds to a primary quantum yield of approximately 0.036 at 26° C. The slope of the linear plot is 4.65×10^4 liters/mole.

Both the intercept and the slope decrease with increasing temperature. The activation energy of reaction [2*q*] is 4.5 kcal/mole.

k_3/k_4 as a Function of Wavelength

At 2700 Å, this ratio is indeterminant. Values of approximately 3×10^{-3}, 1.2×10^{-3}, and 6×10^{-4} all expressed in moles/liter are found for 3130 Å, 3340 Å, and 3650 Å, respectively. It must be emphasized that the values found for 3340 Å and particularly 3130 Å are subject to possible large errors.

k_2/k_4 as a Function of Wavelength

The slope of the plot of reciprocal quantum yield against pressure shows a marked dependence on wavelength, increasing from zero at 2700 Å to 4.65×10^4 liters/mole at 3650 Å. The intermediate values are 16.8 liters/mole at 3130 Å and 1.64×10^2 liters/mole at 3340 Å. It should again be pointed out that the result at 3650 Å was found at 26° C, whereas the other values were obtained at 37° C.

k_2/k_4 is thus 0.06, 0.61×10^{-2}, and 0.22×10^{-4} moles/liter at 3130, 3340, and 3650 Å respectively. In Fig. 4 these values are plotted against the energy of the exciting radiation. The slope increases rapidly as the energy of excitation increases.

If it is assumed that k_4, related to collisional deactivation, is virtually independent of the energy of the radiation, Fig. 4 represents the variation of k_2 with energy of the

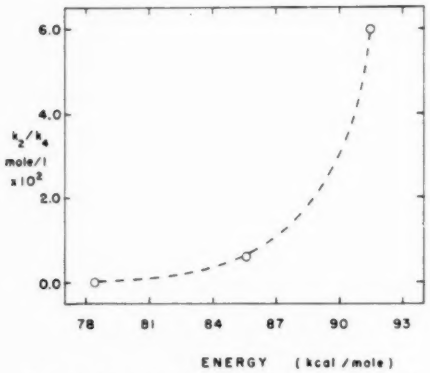

FIG. 4. Variation of k_2/k_4 with energy of excitation.

exciting radiation. It is evident, therefore, that the dissociation rate constant increases rapidly with increasing energy.

A further assumption that k_4 is the collision rate constant, 1.29×10^{11} moles^{-1} liters sec^{-1} calculated for a collision diameter of 3.5 Å, gives absolute values for k_2 of 7.74×10^{9}, 7.87×10^{8}, and 2.84×10^{6} sec^{-1} at 3130, 3340, and 3650 Å, respectively.

Energy of Activation of Reaction [2] as a Function of Wavelength

The apparent energy of activation for the dissociation reaction is 0, 2, and 4.6 (1) kcal/mole at 2700, 3340, and 3660 Å, respectively. The difference in activation energy at 3340 and 3660 Å does not correspond to the difference in energy of the absorbed quanta. The fact that the activation energy changes with wavelength implies the contribution of at least two different dissociation processes. These processes may arise from different electronic states, e.g., singlet and triplet states, whose ratio depends on wavelength. Since ketene neither fluoresces nor phosphoresces, the only evidence for the contribution of a second electronic state is the analogy with other ketones (12).

ACKNOWLEDGMENTS

This research was supported in part by a grant from the National Research Council of Canada, and in part by a grant from the President's Research Fund of the University of British Columbia. One of the authors (B.T.C.) wishes to express his appreciation to the British Columbia Sugar Refining Company for a scholarship for 1957–58.

REFERENCES

1. STRACHAN, A. N. and NOYES, W. A., JR. J. Am. Chem. Soc. **76**, 3258 (1954).
2. PORTER, G. B. J. Am. Chem. Soc. **79**, 827 (1957).
3. KISTIAKOWSKY, G. B. and MAHAN, B. H. J. Am. Chem. Soc. **78**, 2412 (1957).
4. HUNT, R. E. and DAVIES, W. J. Am. Chem. Soc. **69**, 1415 (1947).
5. KASHA, M. J. Opt. Soc. Amer. **38**, 929 (1948).
6. FISHER, G. J., MACLEAN, A. F., and SNIZER, A. W. J. Org. Chem. **18**, 1055 (1953).
7. DAVIS, W. J. Am. Chem. Soc. **70**, 1868 (1948).
8. HATCHARD, C. G. and PARKER, C. A. Proc. Roy. Soc. A, **235**, 518 (1956).
9. PORTER, G. B. and CONNELLY, B. T. To be published.
10. ROSS, W. F. and KISTIAKOWSKY, G. B. J. Am. Chem. Soc. **56**, 1112 (1934).
11. NORRISH, R. G. W., CRONE, R. G., and SALTMARSH, O. D. J. Am. Chem. Soc. **56**, 1644 (1934).
12. NOYES, W. A., JR., PORTER, G. B., and JOLLEY, J. E. Chem. Revs. **56**, 90 (1956).
13. KISTIAKOWSKY, G. B. and ROSENBERG, N. W. J. Am. Chem. Soc. **73**, 321 (1950).

THE SOLUBILITY OF URANIUM PEROXIDE IN ACIDIC AND BASIC MEDIA AT 25° C[1]

KARL H. GAYER AND LANCELOT C. THOMPSON

ABSTRACT

The solubility of uranium peroxide $UO_4 \cdot 2H_2O$ was measured in NaOH and $HClO_4$ solutions. Possible reactions of $UO_4 \cdot XH_2O$ in dilute $HClO_4$ solutions and possible reaction of $UO_4 \cdot XH_2O$ in dilute NaOH solutions are indicated along with the calculated constants. As might be expected, the several oxygens associated with the uranium atom appear to make the hydroxide more acidic than basic.

The purpose of this investigation was to obtain information regarding the reactions of uranium peroxide in dilute sodium hydroxide and dilute perchloric acid. These data should give (1) partial evidence as to the ionic species.

Uranium peroxide has not been investigated in relation to its solubility in acid or base. The literature on this substance is concerned with its preparation and composition.

EXPERIMENTAL

Procedure

The general procedure is similar to that used by Garrett and Heiks (1).

Preparation of Conductivity Water

The preparation of conductivity water is that of Gayer and Woontner (2).

Colorimetric Reagents

A standard uranium solution was prepared by dissolving uranium trioxide $UO_3 \cdot H_2O$ (prepared by hydrolysis of the uranyl acetate) in perchloric acid. Aliquot portions of this solution were used to prepare the color standards. A 10% sodium hydroxide solution was prepared from Baker and Adamson reagent pellets and distilled water. A 20% sodium carbonate solution was prepared with Baker and Adamson anhydrous reagent and distilled water. Baker and Adamson 30% hydrogen peroxide was used in preparing colorimetric solutions.

Determination of pH

The flask necks were broken while enclosed in a rubber membrane and samples were taken using a Beckman 290–78 hypodermic-type glass electrode. Measurements were made with a Beckman Model G meter which was calibrated at pH 4 with 0.05 *M* potassium acid phthalate buffer, at pH 7 with Beckman 3581 buffer, and at pH 10 with boric acid – sodium hydroxide buffer.

Uranium Analysis

The uranium analysis was made with a Beckman Model B spectrophotometer using the $NaOH–Na_2CO_3–H_2O_2$ method to produce the color, as described in *Analytical Chemistry of the Manhattan Project* (3).

Uranium Peroxide $UO_4 \cdot XH_2O$

Pure $UO_4 \cdot XH_2O$ was prepared by adding 30% hydrogen peroxide to a solution of uranium nitrate until precipitation was complete. A small amount of $NaNO_3$ was added

[1]*Manuscript received June 18, 1958.*
Contribution from the Chemistry Department, Wayne State University, Detroit, Michigan. From a dissertation submitted by Mr. Lancelot C. Thompson in partial fulfillment of the requirements for the Doctor of Philosophy degree at Wayne State University.

to the precipitate which was then washed with conductivity water until the washings gave a negative sodium flame test. This material was used in the equilibrium studies.

Uranium Peroxide $UO_4 \cdot 2H_2O$

The peroxide prepared as above was dried at 100°. Analyses of this material corresponded to the formula of the dihydrate. This material was used in the perchloric acid solubility studies and the X-ray analyses.

X-Ray Analyses

The X-ray data obtained on this material compares very favorably with that reported in the literature.

The d values given below were calculated from a, b, c values given in Katz and Rabinowitch (5).

TABLE I

Data of Watt *et al.* (4)		Gayer and Thompson				
d_{obs}	I/I^0	d_{obs}	I/I^0	d_{calc}	Index	% error
5.20	1.00	5.22	1.00	5.22	110	0.000
4.38	0.39	4.38	0.36	4.37	200	0.23
3.77	0.51	3.79	0.52	3.80	101	0.26
3.51	0.55	3.51	0.48	3.50	011	0.28
—	—	3.25	0.26	3.25	020	0.00
2.74	0.32	2.76	0.26	2.76	103	
2.65	0.31	2.66	0.26	2.66	013	
1.95	0.32	1.96	0.26	1.96	112	

Weighed samples of the peroxide prepared in the manner described above and dried at 100° were ignited to U_3O_8 and the percentages of uranium were calculated to be 70.0, 69.8, 69.8. Theoretical percentage of uranium in $UO_4 \cdot 2H_2O$ = 70.4.

From the percentage of uranium analyzed for and the X-ray data it can be seen that the compound prepared above is $UO_4 \cdot 2H_2O$.

THE DATA

The solubility data for uranium peroxide in acid and base solutions are collected in Tables II to IV. Conclusive results could not be obtained in regard to the reactions involved.

TABLE II

SOLUBILITY OF $UO_4 \cdot 2H_2O$ IN $HClO_4$ SOLUTIONS AT 25°*

Initial moles $HClO_4$/1000 g H_2O	Moles uranium/ 1000 g H_2O at equilibrium
2.3×10^{-2}	2.5×10^{-3}
7.0×10^{-2}	6.2×10^{-3}
1.2×10^{-1}	8.6×10^{-3}
1.6×10^{-1}	14.0×10^{-3}
2.0×10^{-1}	16.0×10^{-3}
2.3×10^{-1}	19.0×10^{-3}
2.8×10^{-1}	21.0×10^{-3}
4.2×10^{-1}	33.0×10^{-3}
5.8×10^{-1}	45.0×10^{-3}
8.2×10^{-1}	58.0×10^{-3}

*Each of the above values is actually the average of two experiments which agreed within 10% or less.

TABLE III

EQUILIBRIA OF $UO_4 \cdot XH_2O$ IN $HClO_4$ SOLUTION AT 25°*

Activity of H^+ ion from pH measurements at equilibrium	Moles uranium/ 1000 g H_2O at equilibrium	K_1
1.4×10^{-2}	4.2×10^{-4}	3.1×10^{-2}
1.6×10^{-2}	5.2×10^{-4}	3.3
1.7×10^{-2}	5.7×10^{-4}	3.4
2.1×10^{-2}	7.4×10^{-4}	3.4
2.3×10^{-2}	8.4×10^{-4}	3.6
2.6×10^{-2}	1.0×10^{-3}	3.9
3.4×10^{-2}	1.5×10^{-3}	4.3
	Average $K_1 = 3.6\times10^{-2}$	

*Each of the above values is actually the average of two experiments which agreed within 10% or less.

Equilibria in Acid Solutions

The fair amount of constancy of the equilibrium constant values and the relatively high hydrogen ion concentration at equilibrium suggests the possibility of reaction [1] taking place in solutions of perchloric acid concentration up to about 0.03 molal. The uranium dissolved, however, is proportional to the $[H^+]1.37$. This ratio cannot simply be explained by reaction

[1] $$UO_3(OH)_2 \cdot XH_2O(s) + H^+ \rightleftharpoons UO_4H^+ \cdot XH_2O + H_2O$$

$$K_1 = m_{UO_4H \cdot XH_2O} \cdot \gamma_{UO_4H^+ \cdot XH_2O} / m_{H^+} \cdot \gamma_{H^+} = 3.6\times10^{-2}.$$

One or more competing reactions is probably taking place in the studied acid region. Possibly a peptization of the polymerized solid is taking place.

$$\Delta F^\circ_1 = 1900 \text{ cal/mole}$$

assuming that

$$\gamma_{UO_4H^+ \cdot XH_2O} / \gamma_{H^+} = 1.$$

There is considerable difference of opinion as to the correct formula which should be used for uranium peroxide. We have chosen somewhat arbitrarily $UO_3(OH)_2 \cdot XH_2O$ for the equation in this work. Actually the reactions could be shown with other formulas, since the ratio of H^+ or OH^- to uranium would not be different.

TABLE IV

EQUILIBRIA OF $UO_4 \cdot XH_2O$ IN NaOH SOLUTION AT 25°*

Initial moles NaOH/1000 g H_2O	Activity of OH^- ion per 1000 g H_2O from pH values at equilibrium	Moles uranium per 1000 g H_2O at equilibrium	K_2
5.4×10^{-2}		1.0×10^{-4}	
1.1×10^{-1}	1.3×10^{-2}	1.7×10^{-4}	1.3×10^{-2}
1.8×10^{-1}	2.5×10^{-2}	2.3×10^{-4}	0.9×10^{-2}
2.2×10^{-1}	2.6×10^{-2}	2.5×10^{-4}	0.95×10^{-2}
2.7×10^{-1}	2.8×10^{-2}	3.1×10^{-4}	1.1×10^{-2}
3.2×10^{-1}	3.2×10^{-2}	3.6×10^{-4}	1.1×10^{-2}
3.6×10^{-1}	3.2×10^{-2}	3.8×10^{-4}	1.2×10^{-2}
7.2×10^{-1}		8.2×10^{-4}	
		Average $K_2 = 1.1\times10^{-2}$	

*Each of the above set of values is actually the average of two experiments which agreed within 10% or less.

Equilibria in Basic Solutions

The fair constancy of the equilibrium constant values suggests the possibility of reaction [2] in the concentration region of about 0.05 molal NaOH to 0.7 molal NaOH. The rather high equilibrium pH values would also support this contention. The excessive quantities of hydroxyl ion consumed per dissolved uranium however, precludes the possibility that reaction [2] is the only one taking place in this concentration region. Possibly a peptization of the polymerized solid is occurring. The solubility technique does not lend itself to distinguishing between competing reactions.

[2] $$UO_3(OH)_2XH_2O(s) + OH^- \leftrightharpoons HUO_5^- + XH_2O$$

$$K_2 = m_{HUO_5^-} \times \gamma_{HUO_5^-} / m_{OH^-} \times \gamma_{OH^-} = m_{HUO_5^-} / m_{OH^-} = 1.1 \times 10^{-2}$$
$$\Delta F_2 = 2700 \text{ cal/mole}$$

assuming that

$$\gamma_{HUO_5^-} / \gamma_{OH^-} = 1.$$

Water Solubility

The water solubility of $UO_4 \cdot XH_2O$ was determined from the average of three separate preparations of the oxide. (Each determination was done in duplicate so as to approach equilibrium from undersaturation and oversaturation.) Conductivity water was used as the solvent. The solubility was found to be 1.5×10^{-5} moles uranium peroxide/1000 g water.

ACKNOWLEDGMENTS

The authors gratefully wish to acknowledge the support of the U. S. Atomic Energy Commission Project No. At (11-1)-214 in sponsoring this work. They also wish to thank Mr. George McManus of the Physics Department of Wayne State University for the X-ray analyses.

REFERENCES

1. GARRETT, A. B. and HEIKS, R. E. J. Am. Chem. Soc. **63**, 562 (1941).
2. GAYER, K. H. and WOONTER, L. J. Chem. Educ. **33**, 296 (1956).
3. RODDEN, C. J. Analytical chemistry of the Manhattan project. McGraw-Hill Book Company, Inc., New York. 1950. p. 93.
4. WATT, G. W., ACHORN, S. L., and MARLEY, J. D. J. Am. Chem. Soc. **72**, 3341 (1950).
5. KATZ, J. J. and RABINOWITCH, E. The chemistry of uranium. McGraw-Hill Book Company, Inc., New York. 1951. p. 293.

PHYSICOCHEMICAL STUDIES OF LIGNINSULPHONATES

III. PROPERTIES OF FRACTIONS PREPARED BY SUCCESSIVE SULPHONATION OF PERIODATE LIGNIN[1]

D. A. I. Goring and A. Rezanowich

ABSTRACT

Periodate lignin was sulphonated in stages by a series of short bisulphite cooks. At each stage the soluble ligninsulphonate was removed and purified, and the residue was resulphonated. The 14 fractions thus obtained had constant methoxyl content and ultraviolet absorption coefficients. There was a gradual increase in the sulphur content as the integral reaction time increased, but 26% of the ligninsulphonate possessed a sulphur content of less than 3%. There was a marked increase in both the intrinsic viscosity and rate of solution with increase in reaction time. The mechanism of the sulphonation reaction is discussed in the light of these results.

INTRODUCTION

Many uses of spent sulphite liquor depend on the colloidal and polymeric properties of ligninsulphonate (1, 2, 3, 4, 5). However, information on the size, shape, and configuration of the molecule is scarce.

In an earlier paper in this series, Gardon and Mason (6) demonstrated that ligninsulphonates in spent liquor occurred in a wide range of molecular weights (from 4000 to 60,000). A similar conclusion was reached by McCarthy and co-workers (7), who obtained fractions of ligninsulphonate having molecular weights from 400 to 130,000. In the sulphite process it is possible that the lignin becomes soluble as a uniform monodisperse material. This may be either degraded or condensed during later stages of sulphonation to give the polydispersity observed. It is more likely, however, that lignins extracted at various times during the reaction will differ considerably in molecular weight. The present work is an attempt to study the properties of soluble ligninsulphonates produced at different stages of sulphonation.

The problem was simplified by use of periodate lignin prepared by a method similar to that of Purves and co-workers (8, 9). Periodate lignin, like protolignin, is insoluble in most solvents, and undergoes many of the same reactions (10). The phenyl propane chain is probably not broken during periodate oxidation, although some methoxyl is lost. As a starting material for physical studies it is probably as suitable as any other isolated lignin.

A kilogram of periodate lignin was prepared from white spruce. A large sample was cooked for successive short periods until most of the lignin was dissolved as sulphonate. After each stage of sulphonation the liquor and residue were separated. The residue was recooked and the soluble sulphonate was isolated from the liquor. The purified fractions were characterized by measurement of ultraviolet and visible absorption, methoxyl and sulphur content, and intrinsic viscosity.

A parallel investigation based on the sulphonation of wood was published by McCarthy and co-workers (11, 12) when this manuscript was in preparation. The results obtained are similar, although the present work is on an isolated lignin and is somewhat more detailed.

[1]*Manuscript received March 31, 1958.*
Contribution from the Physical Chemistry Division, Pulp and Paper Research Institute of Canada, Montreal, Que.

Can. J. Chem. Vol. 36 (1958)

EXPERIMENTAL AND RESULTS

Periodate Lignin

A freshly cut, 35-year-old log of white spruce (*Picea glauca* (Moench) Voss) was reduced to a coarse sawdust with a dado circular saw. Six kilograms (dry weight) of the sawdust was subjected to cycles of periodate oxidation and alkaline hydrolysis in a 200-l stainless steel vessel at room temperature. The oxidation liquor was 2500 g of $Na_3H_2IO_6$ dissolved in 60 l of distilled water, the pH being kept at 4 with acetic acid. The hydrolysis liquor was 100 l of 0.1 *N* NaOH. There were usually two or three washings with distilled water after each oxidation and hydrolysis. After the final hydrolysis, it was necessary to neutralize the liquor before washing to reduce the high degree of swelling of the lignin.

Initially, removal of liquors and wash water was easily achieved with large bacterial filter candles. After the third hydrolysis, filtration was ineffective because the filters clogged immediately. At this stage the lignin was allowed to settle overnight when $\frac{4}{5}$ of the supernatant liquid could be removed with a siphon. The final washings were at pH 5–6. The cake of periodate lignin was frozen and the water removed by freeze-drying. The yield on a dry weight basis was 1 kg and represented 64% of the original lignin content of the wood. Some analytical data on this preparation of periodate lignin are given in Table I.

TABLE I

ANALYTICAL DATA ON PERIODATE LIGNIN

Moisture content	= 6%
Yield from wood (dry weight)	= 17.1%
Ash (dry weight)	= 2.4%
Klason lignin (dry weight; ash-free)	= 93.2%
Carbon (dry weight; ash-free)	= 60.8%
Hydrogen (dry weight; ash-free)	= 5.91%
Methoxyl (dry weight; ash-free)	= 12.8%
Sulphur	= Nil
Carbohydrate	= Nil

Sulphonation Procedure

Cooks were made in a stainless steel autoclave of 1200 cc capacity. The autoclave (Fig. 1) was designed to permit rapid heating and cooling as well as positive stirring of the reacting mixture. The vessel was heated to 130° C in 5 minutes by gas burners on the

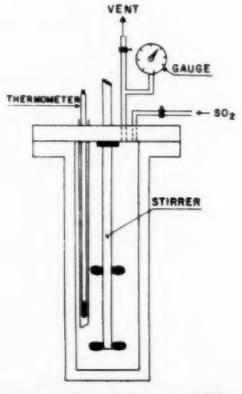

FIG. 1. Stainless steel autoclave used for sulphonation.

bottom and sides. It was cooled to room temperature in 5 minutes by being lowered into a bucket of water. From the initial application of heat to the moment of lowering the vessel into the water, cooks were 30 minutes in duration except for the final two which were for 60 minutes each. Temperature was measured with a thermometer immersed in paraffin in a stainless steel well in the cover. Constant temperature was maintained manually at 130 (±1)° C with a gas burner.

The reaction mixture was stirred with a motor-driven, twin-screw stirrer. The gland on the stirrer was a carbon disk against which a steel disk rotated, the sealing pressure being supplied by the SO_2 in the liquor. At first it was impossible to retain a constant concentration of SO_2 because of slight leakage past the gland. Accordingly, an SO_2 cylinder at 55° C was connected to the autoclave and constant pressure of SO_2 was maintained manually at 115 (±5) p.s.i.g.

The initial sample of periodate lignin, ground to pass 150 mesh, weighed 43 g. The lignin was mixed with 500 cc of distilled water, de-aerated thoroughly by successive evacuation, and soaked overnight. For sulphonation, 500 cc of sodium base acid was added which produced a final concentration of 1% Na and 6% total SO_2. Accurate control of the initial concentration of SO_2 was unnecessary, since the pressure was adjusted in the autoclave at the start of the reaction.

After each sulphonation, the reaction mixture was centrifuged. The insoluble lignin residue was washed with distilled water and recentrifuged, the washings being added to the centrifuged liquor. The residue was then washed into the autoclave with 500 g of distilled water, the liquor was added, and the cook repeated.

Purification

The object of the purification procedure was to secure a neutral sodium ligninsulphonate free from both insoluble debris and excess inorganic ions. The method finally adopted was evolved by trial and error in preliminary experiments.

Cations and anions were removed with the ion-exchange resins Dowex 50-X12 (50–100 mesh) and Dowex 1-X10 (50–100 mesh) respectively.* The centrifuged liquor was stirred with 400 g of regenerated Dowex 50. This treatment removed 90% of the sodium present. The liquor was then evaporated from 1500 cc to 50–100 cc in a rotary vacuum evaporator at 45° C, deionized on columns, neutralized with NaOH to pH 7, and freeze-dried. With some of the later fractions it was necessary to centrifuge at 25,000 g after passage through the columns to remove finely dispersed debris.

Fourteen successive sulphonations were made over a period of 8 hours. Cooking time was 30 minutes for fractions S-1 to S-12 and 1 hour for the final two which are designated fractions S-14 and S-16. The residue after the final reaction was 2.7% of the original weight of the lignin. The total recovery on an ash and sulphur-free basis was 86%.

The rate of solution, R, for each fraction was computed from

[1] R = wt. of fraction (sulphur-free basis)/time of cooking interval.

**In preliminary tests with a purified commercial ligninsulphonate, the columns were found to absorb less than 2% of the lignin based on optical density in the ultraviolet. However, after many of the measurements described later were made, it was found that repassage through the columns removed about 10% by weight of the ligninsulphonate. The sulphur content of the re-ion-exchanged material was virtually unchanged, while the methoxyl content increased by 0.6%. Evidently, material low in methoxyl was being absorbed by the columns. Experiments showed that it was absorbed mostly by the anion-exchange column (Dowex 1-X10) and that it could not be removed by the customary regeneration with 4% of NaOH. It was unlikely that the absorbed material was an inorganic sulphur-containing anion because the sulphur content of the re-ion-exchanged fraction would then decrease. No other type of inorganic anion was introduced during the cooking and purification, and as shown in Table I the ash content of the periodate lignin was relatively low. No correction was made in the original data, except in the case of the second fraction in which 33% by weight was absorbed and the methoxyl content increased from 7.6% to 11.2%.*

As shown in Fig. 2, the rate of solution showed a maximum after 4 hours' cooking. Such a maximum is in fair agreement with other studies on sulphonation. The dotted line in Fig. 2 shows some previous data (13) obtained on a different batch of periodate lignin. For this series, reactions were done in sealed glass bombs at 130° C with a bisulphite solution containing 6% total SO_2 and 1% Mg^{++}. Here the SO_2 content decreased as the sulphonation proceeded, which is probably the cause of the slower rate of solubilization. In general, however, this curve shows the same trends as those obtained in the present study.

The fractional rate of solution, R_F, was calculated from

$$R_F = R/\text{wt. of material cooked.} \qquad [2]$$

In Fig. 3 the fractional rate of solution is plotted together with intrinsic viscosity against cooking time.

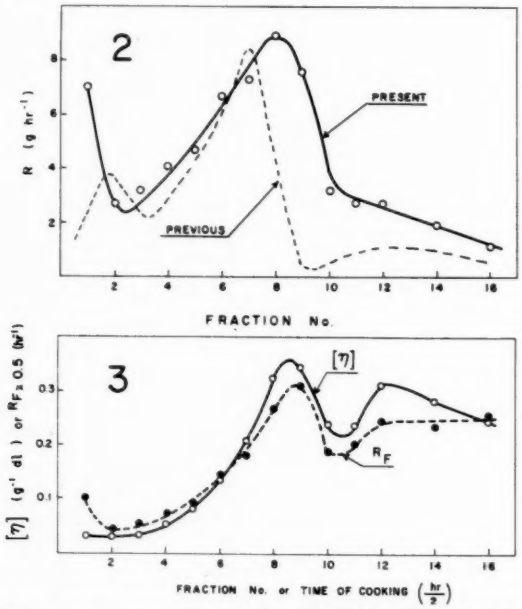

FIG. 2. Rate of solution at various stages of the sulphonation. The dotted line shows similar data from previous experiments. The abscissa units represent half-hourly and hourly intervals in the present and previous series respectively.

FIG. 3. Correlation of R_F and [η] throughout the reaction.

Sulphur Content

Sulphur analyses were made with a Leco apparatus and the results are shown in Fig. 4. Mean error in triplicate determinations was ±2.6%. In previous experiments results with the Leco agreed within ±3% with gravimetric determinations as $BaSO_4$.

Apart from some irregularities in early fractions, there is a gradual rise in sulphur content as the cook proceeds. Some of the early fractions are soluble at a relatively low content of sulphur.

Sulphonation increases the weight of the lignin due to the replacement of —OH by —SO_3Na groups. Therefore values of yields, methoxyl content, and light absorption were adjusted to be based on the weight of unsulphonated lignin.

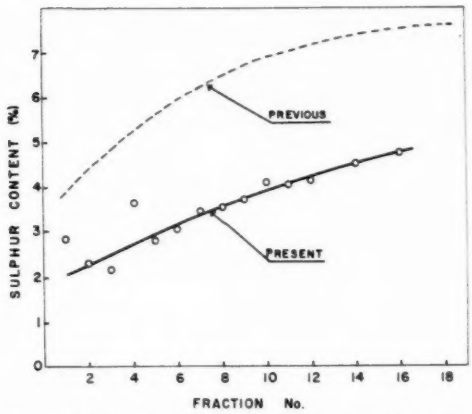

FIG. 4. Sulphur content of fractions at various stages. The dotted line shows similar data from previous experiments. The abscissa units represent half-hourly and hourly intervals in the present and previous series respectively.

Methoxyl Content

The methoxyl content was measured by TAPPI Standard Method 2M43. The mean error in duplicate determinations was ±1%. As shown in Table II the methoxyl content is fairly constant (±5%) and lies between 10 and 12%.

TABLE II

METHOXYL CONTENT AND ULTRAVIOLET ABSORPTION OF FRACTIONS

Fraction	OCH_3 (%)	ϵ_{2800}	ϵ_{2050}
S–1	10.4	12.5	92.9
S–2	11.2	14.2	88.9
S–3	9.9	12.1	87.7
S–4	11.3	13.4	101.9
S–5	10.7	13.5	99.2
S–6	11.1	13.8	99.0
S–7	11.4	15.5	107.4
S–8	11.9	14.5	109.1
S–9	11.7	14.8	102.7
S–10	11.5	14.5	101.8
S–11	11.3	13.6	104.1
S–12	10.4	13.5	100.4
S–14	11.4	14.4	97.5
S–16	9.6	12.9	108.5

Light Absorption

Optical densities were measured in the visible and the ultraviolet with a Beckman DU spectrophotometer using 1-cm quartz cells. Measurements were made in duplicate at wavelengths of 5000 Å, 2800 Å, and 2050 Å with concentrations of 0.2, 0.002, and 0.001 g dl^{-1} respectively. The solvent was 0.1 *M* NaCl.

Absorption was expressed in terms of the coefficient ϵ given by

[3] $$\epsilon = D/cL,$$

where

D = optical density,
c = concentration,
L = length of cell.

As shown in Table II the ϵ values for wavelengths of 2050 Å and 2800 Å are fairly constant. Mean $\epsilon_{2050} = 100.1$ ($\pm 5\%$) cm^{-1} l g^{-1} and mean $\epsilon_{2800} = 13.8$ ($\pm 5\%$)cm^{-1} l g^{-1}. A similar constancy of ultraviolet absorption has been reported by McCarthy and co-workers (7). In the visible absorption at 5000 Å (Fig. 5) a pronounced maximum is noted after 3 hours' cooking, followed by a minimum and then a gradual increase in ϵ.

Intrinsic Viscosity

Viscosity was measured in Ubbelohde viscometers of the type described by Craig and Henderson (14). The dimensions were modified slightly to permit mounting in a Townson and Mercer water bath. Relative temperature changes were held to $\pm 0.005°$ C about the actual temperature of $25 \pm 0.05°$ C. The solvent was 0.1 *M* NaCl. Concentrations ranged from 1.5 to 0.2 g dl^{-1}.

The intrinsic viscosity, $[\eta]$, was obtained as usual by linear extrapolation of η_{sp}/c vs. c to zero concentration (Fig. 6).

The intrinsic viscosities of the fractions are shown in Fig. 3. There is a marked increase in $[\eta]$ with time of cooking up to about 4 hours, after which $[\eta]$ decreases but with another maximum at 6 hours. The correlation between $[\eta]$ and R_F will be discussed later.

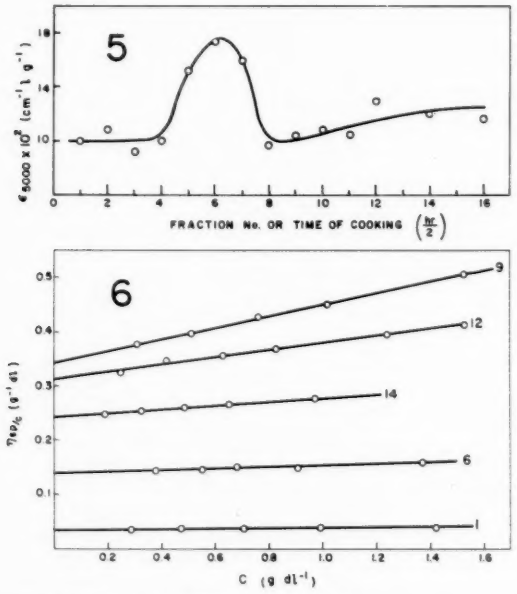

FIG. 5. Light absorption coefficient at 5000 Å at various stages.
FIG. 6. η_{sp}/c vs. c for some of the fractions: lines 1, 6, 9 etc., correspond to fractions S-1, S-6, S-9 etc.

DISCUSSION

As shown in Fig. 4 the sulphur content of the fractions increased with time of sulphonation. The curve suggests a lower rate of sulphonation in the later stages of the reaction in agreement with the results of others (15, 16). It is interesting to note that 26% of the ligninsulphonate possessed a sulphur content of less than 3%, which is generally regarded as the minimum required for solubility (17).

For comparison, the variation of sulphur content of soluble fractions with reaction time, obtained in a previous study (13), is given as the dotted line in Fig. 4. In this case the solubilized lignin was not separated from the reaction mixture but was reacted with the bisulphite solution for the full time of each cook. Both sets of data show an increase of sulphur content with time, but a higher degree of sulphonation of soluble fractions was obtained in the previous series. Rezanowich *et al.* (16) found that if the soluble and insoluble fractions from the same cook were recooked, the soluble portion was sulphonated to a higher degree than the insoluble portion. This is probably the reason why sulphur contents were higher in the previous results.

Comparison of the two series of data suggest that (*a*) some fractions are solubilized at fairly low sulphur contents ($< 3\%$) and (*b*) an appreciable portion of the sulphonation reaction occurs with the ligninsulphonate after it has been rendered soluble.

For all fractions, the ratio of ϵ_{2800} (cm^{-1} l g^{-1}) to methoxyl content (%) was 1.26 ($\pm 3\%$), which is in good agreement with the value 1.30 ($\pm 2\%$) derived for the first seven fractions of Gardon and Mason (6). These authors observed a marked increase of ultraviolet absorption and methoxyl content with molecular weight. In the present work, both ϵ_{2800} and methoxyl content remained constant to $\pm 5\%$ over a wide range of $[\eta]$ and therefore molecular weight. McCarthy and co-workers (11, 18, 19) have also found ϵ_{2800} constant for fractions prepared from non-dialyzable ligninsulphonate by precipitation with ethanol. This contradiction is probably due to a considerable portion of low methoxyl material in the low molecular weight samples of Gardon and Mason. On passing Gardon and Mason's fractions 7 and 8 through the ion-exchange columns, 42% and 70% respectively by weight was lost; methoxyl contents increased respectively from 3.3% and 2.1% to 6.9% and 6.7%. As mentioned earlier, considerably smaller increases in methoxyl content were noted after re-ion exchange of some of the fractions prepared for the present investigation.

From Table II, $\epsilon_{2050}/\epsilon_{2800}$ was 7.26 ($\pm 5\%$) for all fractions. This result supports ϵ_{2050} as a measure of lignin concentration as recommended by Kleinert and Joyce (20). In contrast to the constancy of ϵ_{2050} and ϵ_{2800}, absorption in the visible showed a pronounced maximum after 3 hours' cooking (Fig. 5). In a previous experiment (21) (not reported here in detail) it was found that prolonged cooking (24 hours) of an already sulphonated lignin increased ϵ_{5000} by a factor of 2 while ϵ_{2800} was essentially unchanged. Thus greater visible absorption would be expected in fractions isolated at the end of the reaction; the increase observed after 4 hours is probably due to this effect. However, the initial maximum in ϵ_{5000} suggests that greater visible absorption is characteristic of certain fractions of lignin. Fractions S-5, S-6, and S-7 which give rise to the maximum represented 28% of the material solubilized.

The initial increase in $[\eta]$ with fraction number (Fig. 3) indicates a marked increase in molecular weight as the lignin is made soluble. McCarthy and co-workers (11) have observed a similar increase in molecular weight for lignin sulphonates from spruce and hemlock. The maximum value of $[\eta]$ is 0.34 g^{-1} dl in fraction S-9 compared with the value of 0.075 g^{-1} dl for the highest molecular weight sample of Gardon and Mason (6). Based on the osmotic molecular weights of Gardon and Mason, the molecular weight of fraction S-9 is 250,000. On this basis, 57% of the material solubilized has a molecular weight of over 100,000. These values are somewhat higher than those found by other workers. McCarthy and co-workers (7) quote molecular weights up to 150,000 with about 2% of the lignin above 100,000. The highest value found by Gardon and Mason (6) was 58,000, although the integral distribution indicated values up to 100,000. A

possible reason for the higher molecular weights in the present series was that the lignin, once extracted, was not then subjected to further prolonged sulphonation. In an earlier experiment (21) it was noted that $[\eta]$ fell from 0.10 to 0.04 on resulphonating a lightly cooked ligninsulphonate. Felicetta and McCarthy (12) have demonstrated a similar degradation on prolonged cooking of non-dialyzable ligninsulphonates. Thus it is fairly certain that the soluble lignin is further degraded by the reaction as sulphonation proceeds. The present work indicates that relatively high molecular weights are obtained when the lignin is removed as soon as it is solubilized.

The correlation between the fractional rate of solution and $[\eta]$ (Fig. 3) lends support to the peptization theory of sulphonation proposed by Calhoun, Yorston, and Maass (22). The trends in Fig. 3 suggest that the rate at which lignin is made soluble depends on the molecular weight of the material solubilized. The initial increase in $[\eta]$ and R_F between fractions S-2 and S-9 is accompanied by an increase in the sulphur content (Fig. 4). If condensation reactions are neglected or assumed to occur rapidly, a sulphite cook may be regarded as a simultaneous sulphonation and hydrolysis of the insoluble lignin network. Fragments of lignin produced by the hydrolysis will become soluble as the sulphonation proceeds. The size of a solubilized fragment will be a function of its sulphur content because the lignin only becomes soluble when it acquires hydrophilic sulphonate groups. Thus, as the sulphur content increases, larger and larger fragments produced by the hydrolysis become soluble. The rate of solution thereby increases also.

The decrease in R_F and $[\eta]$ after fraction S-9, in spite of an increase in sulphur content, may be due to the presence of a more cross-linked lignin for which more extensive chain scission would be necessary to set fragments free. Also a more cross-linked molecule would have a lower viscosity for a given molecular weight and would be less soluble for a given sulphur content. If this explanation is correct, fractions of similar molecular weight from early and late in the cook should show clearly defined differences in molecular configuration. Light-scattering and viscometric experiments are now being carried out to investigate this possibility.

It is interesting to note that, in spite of the extremely fine subdivision of the lignin (150 mesh) and the vigorous stirring during the reaction, the rate of delignification is similar to that for the commercial cooking of wood chips. This suggests that diffusion processes have no gross effect on the rate of solution, although the rate at which the dissolved lignin diffuses out of the chip into the liquor is probably affected by the molecular weight of the ligninsulphonate.

ACKNOWLEDGMENTS

The authors wish to acknowledge the assistance of Mr. J. Jaworzyn in much of the experimental work.

REFERENCES

1. Marshall, H. B. Pulp Paper Mag. Can. **53**, No. 5, 125 (1952).
2. Marshall, H. B. and Neate, J. M. Pulp Paper Mag. Can. **54**, No. 7, 125 (1953).
3. Marshall, H. B. and Neate, J. M. Pulp Paper Mag. Can. **54**, No. 9, 113 (1953).
4. Marshall, H. B. and MacDonald, A. Tappi, **38**, No. 7, 165A (1955).
5. Marshall, H. B. and Cunningham, A. I. Tappi, **39**, No. 7, 171A (1956).
6. Gardon, J. L. and Mason, S. G. Can. J. Chem. **33**, 1477 (1955).
7. Felicetta, V. F., Ahola, A., and McCarthy, J. L. J. Am. Chem. Soc. **78**, 1899 (1956).
8. Wald, W. J., Ritchie, P. F., and Purves, C. B. J. Am. Chem. Soc. **69**, 1371 (1947).
9. Smith, D. N. and Purves, C. B. Ind. Eng. Chem. **49**, 1394 (1957).
10. Ritchie, P. F. and Purves, C. B. Pulp Paper Mag. Can. **48**, No. 12, 74 (1947).
11. Nokihara, E., Tuttle, J., Felicetta, V. F., and McCarthy, J. L. J. Am. Chem. Soc. **79**, 4495 (1957).
12. Felicetta, V. F. and McCarthy, J. L. J. Am. Chem. Soc. **79**, 4499 (1957).

13. REZANOWICH, A. Unpublished data.
14. CRAIG, A. W. and HENDERSON, D. A. J. Polymer Sci. **91**, 215 (1956).
15. ALDER, E. and LINDGREN, B. O. Svensk Papperstidn. **55**, 563 (1952).
16. REZANOWICH, A., ALLEN, G. A., and MASON, S. G. Pulp Paper Mag. Can. **58**, No. 10, 153 (1957).
17. BRAUNS, F. E. The chemistry of lignin. Academic Press, Inc., New York. 1952. p. 365–366.
18. MARKHAM, A. E., PENISTON, Q. P., and MCCARTHY, J. L. J. Am. Chem. Soc. **71**, 3599 (1949).
19. MOACANIN, J., FELICETTA, V. F., HOLLER W., and MCCARTHY, J. L. J. Am. Chem. Soc. **77**, 3470 (1955).
20. KLEINERT, T. N. and JOYCE, C. S. Pulp Paper Mag. Can. **58**, No. 10, 147 (1957).
21. GORING, D. A. I. Unpublished data.
22. CALHOUN, J. M., YORSTON, F. H., and MAASS, O. Can. J. Research, B, **17**, 121 (1939).

VOLTAIC CELLS IN FUSED SALTS

PART V. THE SYSTEMS $Sn/SnCl_2$ (KCl–NaCl), $Fe/FeCl_2$ (KCl–NaCl), and $Mn/MnCl_2$ (KCl–NaCl)[1]

S. N. Flengas and T. R. Ingraham

ABSTRACT

Using a Ag/AgCl (KCl–NaCl) reference electrode, the standard electrode potentials of the systems $Sn/SnCl_2$ (KCl–NaCl), $Fe/FeCl_2$ (KCl–NaCl), and $Mn/MnCl_2$ (KCl–NaCl) were determined at 700° C and found to be 0.370 v, 0.520 v, and 1.205 v respectively. In each of the systems the Nernst equation was found to be applicable over the range of concentrations investigated.

The effect of temperature on the electromotive forces of the above cells was measured and the heats of the cell reactions were calculated from the data.

INTRODUCTION

In previous publications in this series (1, 2, 3, 4) standard potentials for several electrode systems in fused salts were reported. To determine the potentials, a silver – silver chloride electrode was used as a null point reference electrode, and an equimolar mixture of sodium and potassium chlorides was used as the solvent for the metallic salts.

In this investigation, the method was applied to the systems tin – stannous chloride, iron – ferrous chloride, and manganese – manganous chloride. These metal chlorides were found to give stable solutions in the alkali chloride – molten salt solvent.

PREPARATION OF MATERIALS

Because the anhydrous metallic salts required in this work were not commercially available, it was necessary to prepare them.

Anhydrous stannous (II) chloride was prepared from the corresponding hydrated salt of analytical grade by heating in a tubular electric furnace at 250° C under a continuous stream of dried gaseous HCl, produced by the action of concentrated H_2SO_4 on concentrated HCl.

Anhydrous ferrous (II) chloride was prepared from National Bureau of Standards certified iron filings by dissolution in concentrated HCl, and recovery of the hydrated ferrous salt by crystallization under an oxygen-free argon cover. The product was filtered under argon and washed with ether. Finally, the light-green hydrated ferrous chloride was dried by heating at 500° C in a stream of dry HCl. In the preparations of stannous chloride and of ferrous chloride, argon was used to flush the apparatus at the beginning and the end of the drying process. The dry divalent chlorides were stable in air and were pelletized without requiring any precautions against oxidation.

Anhydrous manganous (II) chloride was prepared from the corresponding hydrated salt of analytical grade, by heating at 600° C in the presence of a carbon tetrachloride vapor stream which was produced by flash distillation.

The anhydrous salts prepared by the foregoing methods were analyzed and found to be of a purity in excess of 99%. The impurity in each of the chlorides was the corresponding metal oxide.

Very pure (99.99%) tin was used as the liquid indicator electrode in the Sn–Ag voltaic cell. A $\frac{1}{2}$-in. diameter rod of very pure electrolytic iron (99.99%) was used as the indicator

[1]*Manuscript received July 28, 1958.*
Contribution from the Mineral Dressing and Process Metallurgy Division, Mines Branch, Department of Mines and Technical Surveys, Ottawa.

electrode in the Fe–Ag voltaic cell. The manganese metal indicator electrode for the Mn–Ag voltaic cell was prepared from pure electrolytic manganese metal (99.9%) which was remelted and cast into a cylindrical form. The casting was done in a water-cooled arc furnace, operated under reduced argon gas pressure. Platinum wire or tungsten wire was used as the indicator electrode connection to the potentiometer.

EXPERIMENTAL

The experimental technique and the apparatus used to study the tin, iron, and manganese systems were the same as in the previous experiments (3, 4) with solid and liquid metal indicator electrodes and cells under inert gas cover.

The experimental cells were of the type,

$$\begin{array}{c|c|c|c|c|c|c} \text{M} & \multicolumn{2}{c|}{\text{MCl}_2\ (x_2)} & \text{Asbestos} & \multicolumn{2}{c|}{\text{AgCl}\ (x_1)} & \text{Ag} \\ (-) & \multicolumn{2}{c|}{\text{KCl–NaCl (1/1 mole)}} & \text{fiber} & \multicolumn{2}{c|}{\text{KCl–NaCl (1/1 mole)}} & (+) \\ & \multicolumn{2}{c|}{\text{(indicator electrode)}} & & \multicolumn{2}{c|}{\text{(reference electrode)}} & \end{array}$$

where M was respectively tin (pool of liquid metal), iron, and manganese metal, and MCl_2 was respectively $SnCl_2$, $FeCl_2$, and $MnCl_2$ at a mole fraction x_2. The reaction in cells of this type is:

$$[1] \qquad M + 2Ag^+ = M^{2+} + 2Ag.$$

The relationship between the electromotive force and the metal ion concentration in the cell is given by the Nernst equation in the form:

$$[2] \qquad E_{cell} = (E^\circ_{M/M^{2+}} - E^\circ_{Ag/Ag^+}) - (2.303RT/2\mathcal{F})\log(x_2/x_1^2)$$

where $E^\circ_{M/M^{2+}}$ and E°_{Ag/Ag^+} are respectively the standard electrode potential of the half-cells $Sn/SnCl_2$, $Fe/FeCl_2$ or $Mn/MnCl_2$, and $Ag/AgCl$ under the conditions of the experiments.

It will be observed that in equation [2] mole fractions are used instead of activities. The simplification is justified, as will be shown by the subsequent data, only when the activity coefficients or the complexity constants of the species involved in the cell reaction, or both, remain constant over the concentration range investigated. Thus, standard potentials calculated from equation [2] will include the effects due to both activities and complex formation.

From equation [2] it follows that when $\log(x_2/x_1^2)$ is equal to zero, the cell potential is the difference in the standard electrode potentials of the system.

RESULTS

The electromotive forces of the Sn–Ag, Fe–Ag, and Mn–Ag voltaic cells were measured first as a function of the metal ion concentration and then as a function of temperature.

The results of the experiments in which the concentration of the metal ion was varied at constant temperature are given in Table I. A 15 mv correction has been included for thermoelectric effects in the Sn–Ag cell and 9 mv in the Fe–Ag cell. No correction was required in the Mn–Ag cell.

When the electromotive forces of the cells were plotted against the term $\log(x_2/x_1^2)$, as calculated from the data given in Table I, the results were well represented by straight lines as shown in Figs. 1 and 2. The slopes of the experimental lines for Sn–Ag, Fe–Ag, and Mn–Ag systems agree well with the theoretical value for a two-electron electrode process as calculated from equation [2] (0.096, 0.095, and 0.097 as compared with

TABLE I

ELECTROMOTIVE FORCES OF VOLTAIC CELLS AT CONSTANT TEMPERATURE AS A FUNCTION OF THE METAL ION CONCENTRATION AT THE INDICATOR ELECTRODE

(*a*) Sn (−) | $SnCl_2$ (x_2) KCl–NaCl (1/1mole) || AgCl (x_1) KCl–NaCl (1/1 mole) | Ag (+)

Mole fraction of AgCl (x_1)	Mole fraction of $SnCl_2$ (x_2)	t, °C	E_{cell} (volts)
6.235×10^{-2}	6.322×10^{-4}	680	0.453
6.235×10^{-2}	1.433×10^{-3}	680	0.418
6.235×10^{-2}	2.251×10^{-3}	680	0.397
6.235×10^{-2}	4.606×10^{-3}	680	0.366
6.235×10^{-2}	7.585×10^{-3}	680	0.342
6.235×10^{-2}	1.254×10^{-2}	680	0.323

(*b*) Fe (−) | $FeCl_2$ (x_2) KCl–NaCl (1/1 mole) || AgCl (x_1) KCl–NaCl (1/1 mole) | Ag (+)

Mole fraction of AgCl (x_1)	Mole fraction of $FeCl_2$ (x_2)	t, °C	E_{cell} (volts)
6.235×10^{-2}	8.853×10^{-4}	695	0.582
6.235×10^{-2}	2.122×10^{-3}	695	0.546
6.235×10^{-2}	3.771×10^{-3}	695	0.523
6.235×10^{-2}	7.541×10^{-3}	695	0.491
6.235×10^{-2}	1.385×10^{-2}	695	0.467

(*c*) Mn (−) | $MnCl_2$ (x_2) KCl–NaCl (1/1 mole) || AgCl (x_1) KCl–NaCl (1/1 mole) | Ag (+)

Mole fraction of AgCl (x_1)	Mole fraction of $MnCl_2$ (x_2)	t, °C	E_{cell} (volts)
6.235×10^{-2}	5.867×10^{-4}	680	1.284
6.235×10^{-2}	1.391×10^{-3}	680	1.249
6.235×10^{-2}	2.566×10^{-3}	680	1.226
6.235×10^{-2}	4.779×10^{-3}	680	1.200
6.235×10^{-2}	1.087×10^{-2}	680	1.116

the theoretical value of 0.096). In addition, the linearity of the curves in Fig. 1 shows that the activity coefficients or the complexity constants of the species involved in the cell reaction remain constant over the range of concentrations investigated.

The experimental standard electrode potentials for the tin, iron, and manganese systems, as obtained from interpolation at $\log(x_2/x_1^2) = 0$ on the curves in Fig. 1, are given in Table II. In addition, Table II also includes, for comparison, calculated (5) values for the standard potentials of the cell reactions in the absence of solvent.

It should be noted that all potential measurements shown above are equilibrium values. Equilibrium was attained in a few minutes after each change in the metal salt

TABLE II

SUMMARY OF RESULTS

Indicator electrode	Cell reaction in molten KCl–NaCl	t, °C	Standard potential for:	Exptl.* (volts)	Calc.† (volts)
Sn, Sn^{++}	$Sn + 2AgCl = SnCl_2 + 2Ag$	700	$E^\circ_{Sn/Sn^{++}} - E^\circ_{Ag/Ag^+}$	0.370	0.405
Fe, Fe^{++}	$Fe + 2AgCl = FeCl_2 + 2Ag$	700	$E^\circ_{Fe/Fe^{++}} - E^\circ_{Ag/Ag^+}$	0.520	0.305
Mn, Mn^{++}	$Mn + 2AgCl = MnCl_2 + 2Ag$	700	$E^\circ_{Mn/Mn^{++}} - E^\circ_{Ag/Ag^+}$	1.205	1.010

*Experimental values corrected to refer to a temperature of 700° C.

†Potentials calculated from thermodynamic data on the pure salts in the absence of any solvent.

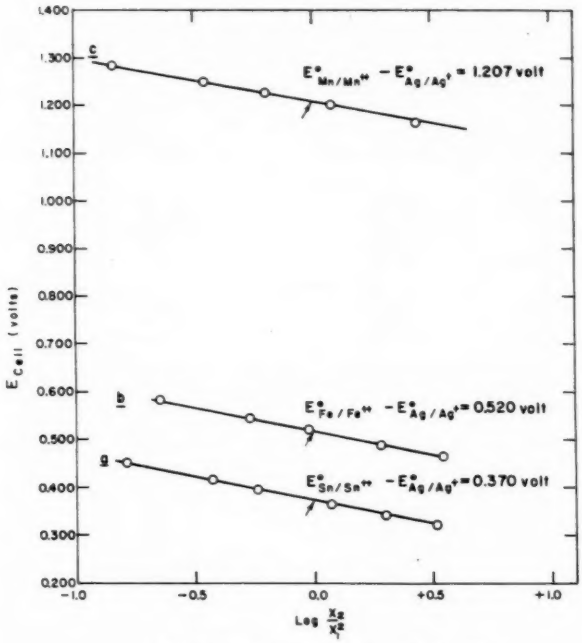

FIG. 1. Electromotive forces of the cells

M	MCl_2 (x_2)	AgCl (x_1)	Ag
(−)	KCl-NaCl (1/1 mole)	KCl-NaCl (1/1 mole)	(+)

as a function of $\log(x_2/x_1^2)$, at constant temperature. M is (*a*) tin, (*b*) iron, and (*c*) manganese. MCl_2 is respectively $SnCl_2$, $FeCl_2$, and $MnCl_2$.

concentration. The potential was very steady and remained practically unchanged when the cells were left overnight.

The effect of temperature change on the electromotive forces of the tin, iron, and manganese cells was investigated next. The results of these experiments are given in Table III. The voltages have been corrected for thermoelectric effects. Also included in Table III are values for the standard potentials at different temperatures, calculated from the data, using equation [2].

From the standard pc tentials, using the procedure previously described (1, 2, 3, 4), it was possible to calculate for various temperatures the equilibrium constants (K) for the cell reactions given in Table II. The results of these calculations are given in Fig. 2, where $\log K$ was plotted against the reciprocal of absolute temperature. The curves are linear over the range of temperature investigated. The best straight lines were calculated by applying the least squares method.

The heat of reactions (ΔH_r) in cells of this type, as calculated according to the van't Hoff equation, is the difference between the heats of formation of the respective chlorides in the presence of the solvent.

The calculated values are:

$$\Delta H_{r(Sn/Sn^{++})} = -23.4 \pm 1.0 \text{ kcal/mole},$$
$$\Delta H_{r(Fe/Fe^{++})} = -27.8 \pm 1.4 \text{ kcal/mole},$$
$$\Delta H_{r(Mn/Mn^{++})} = -61.8 \pm 1.5 \text{ kcal/mole}.$$

TABLE III

EFFECT OF TEMPERATURE ON THE ELECTROMOTIVE FORCES OF THE CELLS

(*a*) Sn (−) | $SnCl_2$ ($x_2 = 3.93\times10^{-3}$) KCl–NaCl (1/1 mole) || AgCl ($x_1 = 6.235\times10^{-2}$) KCl–NaCl (1/1 mole) | Ag (+)

T, ° K	E_{cell} (volts)	$E^\circ_{Sn/Sn^{++}} - E^\circ_{Ag/Ag^+}$ (volts)
	On heating	
946	0.3771	0.3768
996	0.3686	0.3686
1053	0.3600	0.3597
1109	0.3470	0.3467
	On cooling	
1057	0.3598	0.3596
990	0.3710	0.3707
949	0.3779	0.3776

(*b*) Fe (−) | $FeCl_2$ ($x_2 = 3.771\times10^{-3}$) KCl–NaCl (1/1 mole) || AgCl ($x_1 = 6.235\times10^{-2}$) KCl–NaCl (1/1 mole) | Ag (+)

T, ° K	E_{cell} (volts)	$E^\circ_{Fe/Fe^{++}} - E^\circ_{Ag/Ag^+}$ (volts)
	On heating	
968	0.5231	0.5210
1018	0.5199	0.5177
1065	0.5154	0.5131
1106	0.5073	0.5049
1131	0.5047	0.5022
1159	0.5010	0.4985
	On cooling	
1091	0.5147	0.5123
1065	0.5162	0.5139
1033	0.5213	0.5130
981	0.5280	0.5258
954	0.5299	0.5278

(*c*) Mn (−) | $MnCl_2$ ($x_2 = 4.779\times10^{-3}$) KCl–NaCl (1/1 mole) || AgCl ($x_1 = 6.235\times10^{-2}$) KCl–NaCl (1/1 mole) | Ag (+)

T, ° K	E_{cell} (volts)	$E^\circ_{Mn/Mn^{++}} - E^\circ_{Ag/Ag^+}$ (volts)
	On heating	
943	1.204	1.211
953	1.200	1.208
1005	1.193	1.201
1056	1.186	1.194
1122	1.172	1.181
1153	1.168	1.177
	On cooling	
1133	1.170	1.179
1057	1.184	1.192
1037	1.188	1.196
1016	1.193	1.201
995	1.196	1.204
983	1.200	1.208

Following the same procedure, and with the same reservations, as cited previously (1, 2, 3, 4), dissociation constants of complexes of $SnCl_2$, $FeCl_2$, or $MnCl_2$, respectively, in the molten salt solvent, have been calculated as follows:

$$K_{d(SnCl_2\ complex)} = 2.3,$$
$$K_{d(FeCl_2\ complex)} = 5.9\times10^{-3},$$
$$K_{d(MnCl_2\ complex)} = 9.61\times10^{-3}.$$

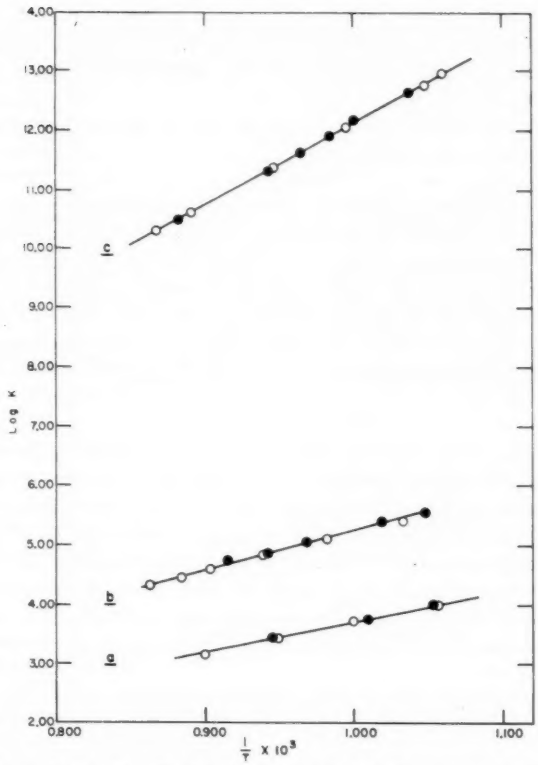

FIG. 2. The variation of log K with the reciprocal of absolute temperature for the systems:

(*a*) Sn (−) | $SnCl_2$ ($x_2 = 3.93\times10^{-3}$) KCl–NaCl (1/1 mole) || $AgCl$ ($x_1 = 6.235\times10^{-2}$) KCl–NaCl (1/1 mole) | Ag (+)

$\Delta H = -23.4\pm1.0$ kcal.

(*b*) Fe (−) | $FeCl_2$ ($x_2 = 3.771\times10^{-3}$) KCl–NaCl (1/1 mole) || $AgCl$ ($x_1 = 6.235\times10^{-2}$) KCl–NaCl (1/1 mole) | Ag (+)

$\Delta H = -27.8\pm1.4$ kcal.

(*c*) Mn (−) | $MnCl_2$ ($x_2 = 4.779\times10^{-3}$) KCl–NaCl (1/1 mole) || $AgCl$ ($x_1 = 6.235\times10^{-2}$) KCl–NaCl (1/1 mole) | Ag (+)

$\Delta H = -61.8\pm1.5$ kcal.

○ with increasing temperature, ● with decreasing temperature.

It is of interest to note that both the iron and manganese complexes in the melt are substantially more stable than that formed by tin.

ACKNOWLEDGMENT

The authors wish to acknowledge the help of Mr. P. Hernandez in constructing the silica apparatus used in the foregoing experiments.

REFERENCES

1. FLENGAS, S. N. and INGRAHAM, T. R. Can. J. Chem. **35**, 1159 (1957).
2. FLENGAS, S. N. and INGRAHAM, T. R. Can. J. Chem. **35**, 1254 (1957).
3. FLENGAS, S. N. and INGRAHAM, T. R. Can. J. Chem. **36**, 780 (1958).
4. FLENGAS, S. N. and INGRAHAM, T. R. Can. J. Chem. **36**, 1103 (1958).
5. HAMER, W. J., MALMBERG, M. S., and RUBIN, B. J. Electrochem. Soc. **103**, 8 (1956).

PHOTOOXIDATION OF BUTENES BY NITROGEN DIOXIDE AT DIFFERENT WAVE LENGTHS[1]

S. Sato[2] and R. J. Cvetanović

ABSTRACT

Photooxidation of butenes by nitrogen dioxide at room temperature has been studied at three different wave lengths: 2288, 2537, and 3261 Å. In the case of butene-1 an abrupt change in the ratios of reaction products is observed between 2537 and 2288 Å: about three times as much α-butene oxide as *n*-butyraldehyde is formed at 2288 Å, while the amounts of these two compounds are almost equal at the longer wave lengths. This discontinuity is ascribed to a difference in the mechanism of reaction with olefinic double bonds of the first excited state, $O(^1D)$, and the ground state, $O(^3P)$, of oxygen atoms. Experimental evidence indicates that there is collisional quenching of $O(^1D)$ to $O(^3P)$ atoms.

Reactions of *cis*- and *trans*-butene-2 and of isobutene are much less reproducible, particularly so that of isobutene, because of the much more readily occurring thermal reaction of the excess nitrogen dioxide present with the epoxides initially formed.

INTRODUCTION

The main features of the reactions between oxygen atoms and olefins have been recently established (1). Mercury-photosensitized decomposition of nitrous oxide was used as the source of oxygen atoms, which were believed to be produced in their ground electronic state. In connection with this work, a study was also made of the reactions of butene-1 and isobutene with oxygen atoms formed by photolysis of nitrogen dioxide at 3660 Å (2). At this wave length there is insufficient energy to produce electronically excited oxygen atoms and the general similarity of the two processes was taken as further evidence that ground state oxygen atoms were formed in the mercury-photosensitized decomposition of nitrous oxide.

It was thought of interest to attempt to study the behavior in similar reactions of the oxygen atoms in their first excited state, $O\ ^1D$, by photolyzing nitrogen dioxide at shorter wave lengths. It is believed (3) that at the wave lengths longer than 2450 Å, oxygen atoms are produced in this process in the ground state and at suitable wave lengths shorter than 2450 Å, in the first excited state. The long wave length threshold for this photolysis has been found to lie between 4047 and 4358 Å (4). The energy difference between 2450 and 4047 Å is 46.0 kcal/mole, which agrees with the energy difference between ^3P and ^1D states of oxygen atoms (45.2 kcal/mole).

In the present work a comparative study has been made of the photooxidation of butenes by nitrogen dioxide at 2288 and 3261 Å, obtained from a cadmium resonance lamp, and at 2537 Å, from a mercury resonance lamp. It would appear from the results obtained with butene-1 that the difference in multiplicity between ^3P and ^1D states of oxygen atoms leads to two distinct mechanisms of their interactions with olefinic double bonds. The usefulness of the reactions of the other butenes in this respect was, unfortunately, greatly reduced because of the considerably greater reactivity of the epoxide formed with excess nitrogen dioxide present and consequent poor reproducibility of the experimental results.

EXPERIMENTAL

Apparatus and experimental procedure used in the present work, as well as the method of purification of nitrogen dioxide, butene-1, isobutene, and *cis*- and *trans*-butene-2 (Phillips reagent grade products), were the same as described previously (2).

[1]*Manuscript received August 15, 1958.*
Contribution from the Division of Applied Chemistry, National Research Council, Ottawa, Canada. Issued as N.R.C. No. 4935.
[2]*National Research Council Postdoctorate Fellow 1956–58.*

A chlorine filter was used to isolate the resonance line of 2288 Å from a cadmium lamp operated at 280±5° C. The emission spectrum, taken with medium quartz Hilger spectrograph, showed that the resonance line at 2288 Å was completely isolated from the stronger resonance line at 3261 Å. A very weak line at 2537 Å was observed, probably owing to a trace of mercury taken into the lamp along with cadmium. The intensity of this mercury resonance line, however, was negligible compared to the intensity of the line at 2288 Å. The light of 3261 Å was obtained from the same cadmium lamp by using a 7–54 Corning glass filter. The light of 2537 Å was obtained from a low pressure mercury resonance lamp and using again a 7–54 Corning glass filter.

Light intensities at the three wave lengths were adjusted by varying the distances of the light sources from the reaction cell and the diameters of the circular light apertures so that almost the same amounts of total reaction products were obtained. The amounts of products were estimated from the gas–liquid chromatography peak areas (2).

A few experiments were carried out in an attempt to measure directly the relative intensities of the light absorbed by nitrogen dioxide at the three wave lengths. The light intensities were so weak that the following technique had to be applied. A very small amount (1 μmole) of nitrogen dioxide and the same amount of butene-1 were taken into the reaction cell and the intensity of transmitted light was followed by means of a photoelectric circuit. Under these conditions the consumption of nitrogen dioxide after 2-hour irradiation was essentially the same at 2288 and 3261 Å (36 and 34%, respectively). The low pressure mercury lamp was not stable enough for this type of measurement.

RESULTS AND DISCUSSION

Photooxidation of Butene-1

Mixtures of 30 mm butene-1 and 3 mm nitrogen dioxide were photolyzed at different wave lengths for 2 hours. The absolute amounts of products formed were not too reproducible and for this reason their ratios are shown in Fig. 1, where the amount of

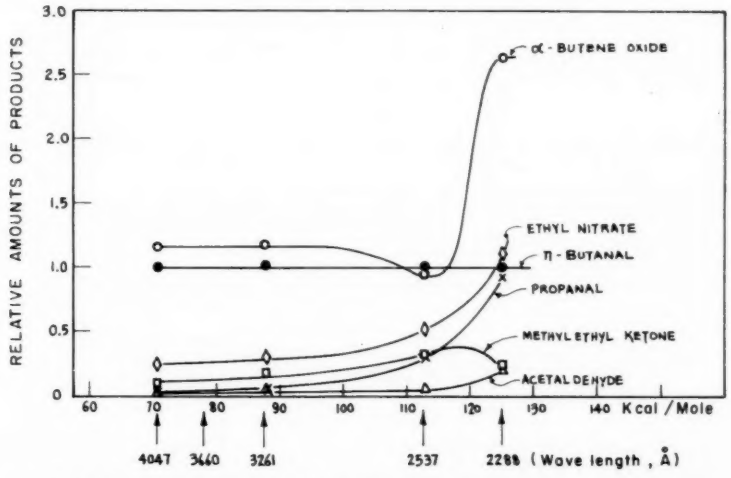

FIG. 1. Relative amounts of products (*n*-butyraldehyde taken as unity) in the photooxidation of butene-1 with nitrogen dioxide at various wave lengths (irradiation time, 2 hours; 30 mm of olefin, 3 mm NO_2; 25±2° C).

n-butyraldehyde is taken as unity.* The ratios were found to be well reproducible. The absolute amount of *n*-butyraldehyde decreased with decreasing wave length and at 2288 Å was approximately about half as great as at 3261 Å.

In Fig. 1, a discontinuity is observed between the wave lengths of 2537 Å and 2288 Å; at 2288 Å the amount of α-butene oxide is about three times as great as that of butanal, while these amounts are almost equal at longer wave lengths. The amount of methyl ethyl ketone gradually increases with decreasing wave length from 4047 Å to 2537 Å, but at 2288 Å it shows a marked decrease. The curves for ethyl nitrate, propanal, and acetaldehyde ascend monotonously with decreasing wave length. These last three compounds are secondary reaction products, while α-butene oxide, butanal, and methyl ethyl ketone are the primary addition products. These results, therefore, suggest that the mechanism of addition of oxygen atoms to butene-1 changes between 2288 Å and 2537 Å. In as much as this conclusion is correct, it can be explained by the difference in the electronic structure of oxygen atoms at the two wave lengths. The continuously increasing amounts of the secondary products, ethyl nitrate, propanal, and acetaldehyde, are, on the other hand, explainable in terms of the increasing amounts of energy with decreasing wave lengths.

The pressure dependence of photooxidation of 3 mm butene-1 by 3 mm nitrogen dioxide with various amounts of nitrogen added has been studied at 2288 Å and the results are shown in Fig. 2. Although there is a certain amount of scatter of the points, the pressure dependence in Fig. 2 is evidently quite different from that observed previously in the photooxidation of butene-1 at 3660 Å (Fig. 3*a* of ref. 2). With increasing total pressure, the amount of α-butene oxide decreases, the amounts of butanal and methyl ethyl ketone show a slight increase, and the secondary products, propanal, ethyl nitrate, and acetaldehyde, rapidly decrease. As the total pressure is increased, the ratios of all the products formed approach those observed at longer wave lengths. The rapid decrease in the

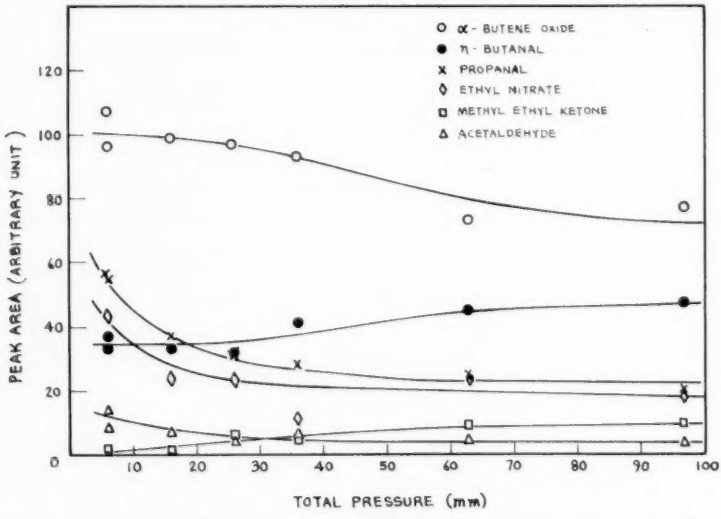

FIG. 2. Amounts of products in the photooxidation of butene-1 with nitrogen dioxide as a function of total pressure (3 mm butene-1, 3 mm NO_2, variable amounts of N_2; irradiation time, 2 hours; 25±2° C).

**The data at 4047 Å were taken from the previous work (4). The total amount of products was approximately equal to that obtained at the other three wave lengths.*

amounts of secondary products is compatible with an increased dissipation of energy by collisions at higher pressures. The trends of the addition products, on the other hand, suggest the simultaneous occurrence of the quenching reaction

$$O(^1D) + M \rightarrow O(^3P) + M. \qquad [1]$$

Photooxidation of Isobutene

Experiments similar to those described for butene-1 have been carried out also with isobutene. As already reported (2), isobutene oxide, which is one of the main products of addition of oxygen atoms to isobutene, was absent because of its rapid thermal reaction with nitrogen dioxide. Moreover, this reaction seemed to be the cause of poor reproducibility. In the case of isobutene, therefore, no significant results were obtained except that with decreasing wave length there was a very pronounced increase in the amount of acetone formed, which became equal to that of isobutyraldehyde at 2288 Å. The mechanism of formation of acetone in the case of isobutene is believed to be analogous to that of propanal in the case of butene-1.

Photooxidation of cis- and trans-Butene-2

The experimental results with *cis*- and *trans*-butene-2 are less reproducible than those with butene-1 but are better than those with isobutene. This is probably because β-butene oxide, one of the main products in the case of butene-2, reacts with nitrogen dioxide at a rate intermediate between those of α-butene oxide and isobutene oxide (5).

The results are summarized in Table I where relative amounts of products are given with methyl ethyl ketone taken as unity. The absolute amount of methyl ethyl ketone appears to increase on passing from longer to the shorter wave lengths, at least in the case of *trans*-butene-2. In these reactions four main addition products are known (1) to be formed: *cis*- and *trans*-β-butene oxide, methyl ethyl ketone, and isobutyraldehyde. The greater part of isobutyraldehyde is formed by combination of free radicals. For this reason this compound would be expected to be much reduced, with simultaneous formation of large amounts of nitro compounds, in the presence of excess nitrogen dioxide used in the present work. As shown in Table I, the four addition products are formed, although *cis*-β-butene oxide and isobutyraldehyde were not separated on the gas chromatographic column used and were not estimated separately. In addition large amounts of nitromethane and methyl nitrate and smaller amounts of acetaldehyde are also formed. The

TABLE I

RELATIVE AMOUNTS OF PRODUCTS (METHYL ETHYL KETONE TAKEN AS UNITY) IN THE PHOTOOXIDATION OF *trans*-BUTENE-2 AND *cis*-BUTENE-2 WITH NITROGEN DIOXIDE

(Irradiation time 2 hours; 30 mm of olefin, 3 mm NO_2; 25±2° C)

Wave length (Å)	AcA	*trans*-BuO	*i*-BuA +*cis*-BuO	CH_2NO_2	MEK	CH_3NO_2
			A. *trans*-Butene-2			
2288	0.5	0.9	0.2	1.2	(1.0)	0.6
2537	0.4	0.8	0.3	0.8	(1.0)	0.6
3261	0.1	0.5	0.1	0.6	(1.0)	0.5
			B. *cis*-Butene-2			
2288	0.4	0.5	0.4	1.9	(1.0)	1.0
2537	0.1	0.6	0.2	0.8	(1.0)	1.0
3261	0.1	0.6	0.3	1.1	(1.0)	0.9

AcA = Acetaldehyde.
BuO = Butene oxide.
BuA = Butyraldehyde.
MEK = Methyl ethyl ketone.

secondary products tend to increase at the lowest wave length used and are similar in that respect to the secondary products observed with butene-1.

It is not possible to say conclusively whether there is an increase in stereospecificity on passing from 2537 to 2288 Å. This uncertainty is due to the relatively poor reproducibility of the figures in Table I, the unknown extent of the thermal reaction with excess nitrogen dioxide of the two epoxides produced, and the fact that *cis*-β-butene oxide was not measured separately. The mean values do suggest an increase in stereospecificity; however, these values are, unfortunately, subject to large uncertainty.

Mechanisms of Addition of Oxygen Atoms (^3P and ^1D) to a Double Bond

According to the spin conservation rule, addition of an oxygen atom in the ground state, $O(^3P)$, to an olefin, which is in a singlet state, should give a triplet state of the activated complex, while the addition of the first excited oxygen atom, $O(^1D)$, should give a singlet state of the activated complex. In agreement with this, when oxygen atoms are produced by the mercury-photosensitized decomposition of nitrous oxide they are most likely in the ^3P state and the initial step of their addition to olefins was, therefore, formulated before (1) as follows:

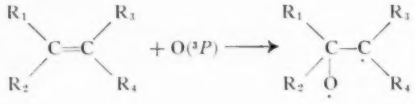

[2]

(A)

Here R stands for an alkyl radical or a hydrogen atom, and the first carbon atom of the double bond is assumed to be "less substituted". The transition complex is a stage in the formation of the biradical (A), which is presumably in the triplet state.

In the case of ^1D oxygen atoms, the activated complex is probably a stage in the following reaction,

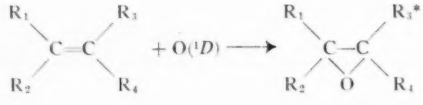

[3]

(B)

where the intermediate (B) should be in the singlet state.

The two intermediates (A) and (B) may undergo internal rearrangements (1). However, both the *cis–trans* isomerization and the migration of R_1 or R_2 to the second carbon atom of the original double bond are likely to be much easier in (A) than in (B) and, therefore, the addition of the $O(^1D)$ atoms should be more stereospecific and should lead to predominant formation of the epoxides. Thus, in the case of butene-1 (where $R_1 = R_2 = R_3 = H$ and $R_4 = C_2H_5$), the relative amount of butanal formed from (A) should be larger than that from (B). This is in agreement with the experimental observation. At the same time, the extent of stereospecificity will depend also on the extent of the quenching reaction [1]. Even when large pressures of the olefin are used and the amount of any other kind of molecules present is negligible, a certain amount of quenching by the olefin itself is likely to occur and the reaction need not be completely stereospecific if the collision yield is smaller than unity. The extent of stereospecificity will then depend on

the average number of collisions of $O(^1D)$ atoms with the olefin before an effective collision takes place. Another factor which is likely to have an effect on the stereospecificity which can be observed under conditions of the present experiments is the high exothermicity of these reactions. As pointed out before (1) the addition products at the moment when they are formed are "hot" and, therefore, the observed stereospecificity will depend to a certain extent on the relative ease of isomerization under such conditions of the particular epoxides formed. Thus, although there is a large quantitative uncertainty in the results obtained with *cis*- and *trans*-butene-2, it is certain that at least in the case of *cis*-butene-2 the addition at 2288 Å is far from being completely stereospecific, i.e. some *trans*-epoxide is still formed. In view of the preceding discussion, however, this should not be taken as an argument against the mechanism proposed here for the addition of $O(^1D)$ atoms to olefins.

Fragmentation Products

Although the complexity of the studied processes precludes a complete explanation of the formation of the fragmentation products, it may be worth while to mention that the amounts of propanal, acetone, and acetaldehyde, in the case of butene-1, isobutene, and butene-2, respectively, increase rapidly with decreasing wave length of the light used for the reaction. It is very likely that these compounds are formed in all these reactions by a similar mechanism. Their formation might perhaps be due, directly or indirectly, to the excited oxygen molecules produced by the reaction of oxygen atoms with nitrogen dioxide (6). This matter, however, requires considerable further investigation.

ACKNOWLEDGMENTS

The authors are indebted to Dr. A. W. Tickner for mass spectrometer analyses, and to the Analytical Section of this Division for the infrared analyses.

REFERENCES

1. CVETANOVIĆ, R. J. Can. J. Chem. **36**, 623 (1958).
2. SATO, S. and CVETANOVIĆ, R. J. Can. J. Chem. **36**, 970 (1958).
3. NOYES, W. A., JR. and LEIGHTON, P. A. The photochemistry of gases. Reinhold Publishing Corp., New York. 1941. p. 400.
4. SATO, S. and CVETANOVIĆ, R. J. Can. J. Chem. **36**, 279 (1958).
5. ELTEKOW, A. Ber. **16**, 395 (1883). Pritchard, J. G. and Long, F. A. J. Am. Chem. Soc. **78**, 2667 (1956).
6. LIPSCOMB, F. J., NORRISH, R. G. W., and THRUSH, B. A. Proc. Roy. Soc. A, **233**, 455 (1955).

SULPHINIC ACIDS AS ANALYTICAL REAGENTS[1]

T. P. FORREST[2] AND D. E. RYAN

ABSTRACT

The "specific" action of sulphinic acids with metal ions is not limited to compounds in which there is direct attachment of the $-SO_2H$ group to an aromatic ring. Since both aliphatic and aromatic sulphinic acids react similarly the assumption that an aromatic group is necessarily co-ordinated to the metal atom through its π system is not valid; the precipitated products are simple salts of the acids. Ferric iron yields at least two products with sulphinic acids. Ceric cerium is reduced in acid solution but an orange-yellow precipitate containing cerium is obtained from acetate-buffered solutions. Naphthalenesulphinic acid may be used to quantitatively precipitate Fe^{+++}, Th^{++++}, Zr^{++++}, U^{++++}, Ti^{++++}, Sn^{++++}, Bi^{+++}, Pd^{++}, Ag^{+}, Hg_2^{++}.

INTRODUCTION

Benzenesulphinic acid, $C_6H_5SO_2H$, and its alkali salts react with ferric salts in solutions of mineral acids to form the slightly soluble orange-yellow ferric benzenesulphinate $(C_6H_5SO_2)_3Fe$ (1). This compound has been stated (2) to be so insoluble that it is formed even in solutions containing fluoride and phosphate ions and that a distinct turbidity occurs in ferric salt solutions so dilute as to yield a scarcely perceptible pink color with thiocyanates. Although various sulphinic acids have been used for the determination and separation of ferric iron (3), Ackerman (4) and Dubsky (5) report that the determination of iron with sulphinic acids is not reproducible.

Tetravalent ions, such as cerium, thorium, uranium, tin, titanium, and zirconium, also react in acid solution to yield precipitates. Feigl (2) reported that, although the sulphinic acids are easily oxidized and ceric salts are powerful oxidizing agents, the compound $(C_6H_5SO_2)_4Ce$ is nevertheless formed in the reaction between these substances. A comparison of the reactivity of benzenesulphinic, benzylsulphinic, and cyclohexylsulphinic acids showed that only benzenesulphinic acid formed slightly soluble salts with the above-mentioned metal ions. These results led to the conclusion that direct attachment of the $-SO_2H$ group to an aromatic ring was necessary and that the phenyl group was co-ordinated to the metal atom through its system of conjugated double bonds. However, Krishna and Singh (3) precipitated ferric iron with *p*-anisylsulphinic acid in which the sulphinic acid group is separated from the aromatic ring by a methylene group.

The present work, therefore, was undertaken to determine the effect of the radical on the analytical behavior of sulphinic acids; this paper records the results of such an investigation.

COMPOUNDS INVESTIGATED

The following sulphinic acids were prepared: benzene, *p*-toluene, β-naphthalene, 2-thiophene, benzyl, cyclohexyl, *n*-hexyl, and *n*-butyl. The aromatic acids were prepared by reducing the corresponding sulphonyl chloride with sodium sulphite (3, 6). Part of the sulphinic acid was removed as a solid and the remainder was extracted with ether from the acidified reaction mixture. The aliphatic acids were prepared by the addition of sulphur dioxide to the Grignard reagent at $-50°$ C (7). The solid magnesium salt thus obtained was decomposed in acid solution and the sulphinic acid extracted with ether.

The ammonium salts, which are more stable than the acids, were prepared by bubbling

[1]*Manuscript received August 29, 1958.*
Contribution from the Department of Chemistry, Dalhousie University, Halifax, N.S., with financial assistance from the National Research Council. Abstracted from the M.Sc. thesis of T.P. Forrest.
[2]*Holder, Canadian Industries Limited Fellowship, 1957–58.*

ammonia through an ethereal solution of the acid. The salts were purified by precipitating the ferric sulphinate, washing with water, and then treating with aqueous ammonia to remove iron as the hydrous ferric oxide; the filtrate was acidified, ether extracted, and the ammonium salt reprecipitated from the ether extract with ammonia.

Properties of Compounds

The aromatic acids were obtained as white solids, the melting points of which are listed in Table I. The aliphatic acids were all obtained as oils which could be solidified at $-10°$ C. Sulphinic acids decompose relatively easily (8); they may be oxidized by air to the sulphonic acid or may disproportionate according to the following equation

$$3RSO_2H \rightarrow RSO_3H + RSOSOR + H_2O.$$

The melting points varied, therefore, due to decomposition incurred in drying the acid and in heating while melting. Benzenesulphinic acid gave melting points varying from 72° to 81° C, although consistent results of 79° to 80° were obtained; literature references (3, 9) give melting points varying from 75° to 85° C.

TABLE I

MELTING POINTS OF SULPHINIC ACIDS

Sulphinic acid	M.p., ° C
Benzene	79–80
p-Toluene	81
2-Thiophene	67
Benzyl	65–68
β-Naphthalene	104–106

The ammonium salts of the aromatic acids were white solids. The butyl and cyclohexyl ammonium sulphinates were obtained as colorless oils, although the cyclohexyl compound solidified slightly below room temperature; the hexyl derivative was obtained as a white, waxy, solid that decomposed to give off ammonia at 35° C.

Ionization constants obtained from potentiometric titration data on the acids showed that they are all fairly strong organic acids. The results obtained for benzenesulphinic acid ranged from 0.96×10^{-2} to 1.28×10^{-2} and for *p*-toluenesulphinic acid from 1.48×10^{-2} to 2.10×10^{-2}. The constants of the aliphatic acids were of the order of 10^{-3}.

Reactions with Metal Ions

Similar reactions were shown by all the sulphinic acids. The reactions were carried out by adding a 2% aqueous solution of the ammonium salt of the sulphinic acid to 0.1 *M* solutions of the metal ions. In dilute acid solution voluminous precipitates were obtained with Ag^{+}, Hg_2^{++}, Hg^{++}, Pd^{++}, Fe^{+++}, U^{++++}, Zr^{++++}. Bi^{+++}, Ti^{++++}, and Sn^{++++} gave good precipitates under these conditions with naphthalene, benzene, and *p*-toluene sulphinic acids but a higher reagent concentration was required for precipitation with the other sulphinic acids. Slight precipitation was obtained with Cu^{++}, Pb^{++}, and Pt^{++++} at reagent concentration above two per cent. From 1 *N* sulphuric acid solution ceric cerium precipitated insoluble oxidation products of the sulphinic acids but an orange-yellow precipitate containing cerium was obtained from acetate-buffered solution. The rare earths were incompletely precipitated from solutions of their salts but were not obtained from solutions above 0.5 *N* in hydrochloric acid. No color or precipitate was noted with the following: Tl^{+}, Ba^{++}, Ca^{++}, Sr^{++}, Mg^{++}, Cd^{++}, Zn^{++}, Co^{++}, Ni^{++}, Fe^{++},

$Al^{\cdot\cdot\cdot}$, $As^{\cdot\cdot\cdot}$, $Sb^{\cdot\cdot\cdot}$, $Rh^{\cdot\cdot\cdot}$, $Ir^{\cdot\cdot\cdot\cdot}$, $As^{\cdot\cdot\cdot\cdot\cdot}$, WO_4'', MoO_4'', VO_4'''. In acid solutions the orange dichromate was reduced to the green chromic ion and the pink color of permanganate was discharged.

Since all the sulphinic acids investigated exhibit the same properties for precipitating metal ions, their selective action is not due to the co-ordination of an aromatic ring to the metal atom through its system of conjugated double bonds. The only significant difference in the products obtained is in their solubilities.

THE IRON REACTION

As previously stated ferric iron has been determined by precipitation of the reportedly very insoluble ferric benzenesulphinate. Use has been made of this reaction to determine iron volumetrically by titration with a standard sulphinic acid solution with dilute thiocyanate as an external indicator (3). However, in the preliminary experiments with ferric iron it was found that, in solutions containing less than 0.5 mg of iron per milliliter, only a yellow to red color developed when the theoretical amount of reagent was added. A red color was obtained on dropwise addition of reagent to more concentrated iron solutions but this color disappeared as the orange-yellow ferric sulphinate separated from solution on the addition of more sulphinic acid; the ferric sulphinate dissolved slowly in ferric chloride solution to regenerate the red color. These results show that, in addition to the insoluble 1:3 ferric benzenesulphinate, there is at least one other product of the reaction. The volumetric method for the determination of iron by sulphinic acids cannot be recommended; although the ferric sulphinate is precipitated from solutions containing more than two milligrams of iron per milliliter the end point is poor and in more dilute solutions a soluble colored complex only is formed.

Table II shows the effects of concentration and acidity on the precipitation of ferric iron by benzenesulphinic acid. The quantity of iron remaining in solution where precipitation occurred was determined colorimetrically with *o*-phenanthroline.

TABLE II

PRECIPITATION OF FERRIC IRON WITH BENZENESULPHINIC ACID

Iron present mg/ml	Acidity	Mole ratio of reagent to iron	Results
0.05	pH 3	10:1	Yellow solution; no precipitate
0.05	pH 3	40:1	Yellow solution; slight precipitation
0.25	pH 3	10:1	Good precipitation; 3.2 p.p.m. iron in filtrate
0.25	0.2 *N* HCl	10:1	Orange solution; slight precipitation
0.40	0.2 *N* HCl	10:1	Good precipitation; 7.4 p.p.m. iron in filtrate
0.60	0.2 *N* HCl	3:1	Red solution; no precipitate
0.60	0.2 *N* HCl	10:1	Good precipitation; 3.7 p.p.m. iron in filtrate

These results show that quantitative precipitation is markedly dependent upon concentration and that best precipitation occurs from slightly acid, relatively concentrated iron solutions. However, precipitates are obtained even in solutions containing as little as 0.05 mg of iron per milliliter provided an extremely large excess of reagent is added ($>40:1$).

In view of the above results an investigation into the statements regarding the extreme insolubility of ferric benzenesulphinate and its formation in the presence of fluoride and phosphate ions was carried out. The solubility was determined by preparing a saturated aqueous solution under nitrogen at 25° C; the iron content of the filtered solution, determined colorimetrically with *o*-phenanthroline, was 4.5×10^{-4} moles per liter after 7

hours and 10^{-3} moles per liter after 4 days. Since dibenzylsulphone was obtained from solutions of ferric benzylsulphinate similarly treated, the increase in solubility on standing is undoubtedly due to some decomposition of the sulphinate. The ferric benzenesulphinate dissolved completely in 1 *M* fluoride and phosphate solutions and no precipitation occurred from neutral solutions containing 20:1 ratio of fluoride or phosphate to iron; in 0.2 *N* acid solutions, however, in which the concentrations of fluoride and phosphate complexes are small, precipitation did take place.

Similar reactions with iron were obtained with the other sulphinic acids; the most insoluble ferric sulphinate was that of naphthalenesulphinic acid. The use of this compound as an analytical reagent is discussed below.

Nature of the Solid Ferric Benzenesulphinate

Analysis of the solid product of the reaction between ferric iron and benzenesulphinic acid, after drying at 110° C, gave 11.69% iron on ignition to the oxide; the theoretical value of $Fe(C_6H_5SO_2)_3$ is 11.65%. A sample, ether-washed and dried at room temperature, lost no weight on drying at 110° C for 2 hours; this result, together with the analysis given above for the dried compound, shows the absence of water of hydration in the precipitated product.

The orange solid was insoluble in ether, ethanol, dioxane, benzene, cyclohexane, chloroform, and carbon tetrachloride but dissolved in glacial acetic acid to give a red solution having a freezing-point depression that indicated complete dissociation. The absorption spectra of this solution, between 400–500 mμ, was identical with that of a solution of ferric nitrate in glacial acetic acid; the compound, therefore, dissociates completely to form the acetate complex.

The magnetic moment of the solid was determined by means of a Guoy balance and found to be 5.7 Bohr magnetons. This value is typical of ferric compounds having five unpaired electrons and shows that no inner orbital bonding has taken place.

The above results suggest that ferric benzenesulphinate is simply a salt of benzenesulphinic acid. Alimarin and Sotnikov (10) have recently concluded, on the basis of the reactivity of benzylsulphinic acid with metal ions, that the products are typical metallic salts of the acids.

THE CERIUM REACTION

Ceric cerium has been reported to react with benzenesulphinic acid to precipitate the ceric sulphinate $Ce(C_6H_5SO_2)_4$ (2); recently, however, the reaction has been stated to be a typical oxidation–reduction reaction yielding RSO_2H and R_2SO_2 with Ce^{+3} remaining quantitatively in solution (10). Our investigation has shown that insoluble white products are obtained on the addition of sulphinic acids to ceric solutions in 1 *N* sulphuric acid; the white product from benzenesulphinic acid addition contained no cerium and recrystallized from benzene as white needles melting, with decomposition, at 192° C; the melting point of diphenyldisulphone, $(C_6H_5SO_2)_2$, is 193° C. Titration of a standard benzenesulphinic acid solution with a 0.1 *M* ceric sulphate solution (1 *N* in H_2SO_4) using ferroin indicator gave a white precipitate; the ceric solution was decolorized and the end point occurred at a molar ratio of 1.8 cerium to 1 sulphinic acid. In acid solutions ceric cerium oxidizes sulphinic acids and is not precipitated, the cerium remaining quantitatively in solution; no precipitation occurred with cerous cerium in 1 *N* sulphuric acid solution.

From ceric solutions buffered at pH 4 with ammonium acetate, however, an orange-yellow precipitate containing cerium is obtained upon addition of sulphinic acids; cerous

cerium is precipitated at pH 4 as a white precipitate. The orange-yellow product obtained from ceric solutions with benzenesulphinic acid varied in composition, part of the product being extractable into ether to give an orange solution. The ether-soluble portion was reprecipitated as an orange solid on the addition of ligroin and gave on analysis, after drying *in vacuo* over boiling methanol, 30.9% Ce. The ether-insoluble portion, after drying in the same manner, gave on analysis 18.15% Ce; the theoretical value for $Ce(C_6H_5SO_2)_4$ is 19.88% Ce. It is evident that a mixture of products is obtained on the addition of sulphinic acids to nearly neutral solutions of ceric cerium.

The reaction of cerium with sulphinic acids depends markedly on the acidity of the solution which controls the oxidation potential of the system. At low acidity ceric cerium is precipitated but not purely as the simple metallic salt of the sulphinic acid whereas in strongly acid solution it is reduced and remains in solution as cerous cerium.

NAPHTHALENESULPHINIC ACID

Since naphthalenesulphinic acid gave the most insoluble precipitates in the preliminary experiments, its usefulness as a reagent for quantitative precipitation of a number of metal ions was briefly investigated. An excess of a 2% aqueous solution of ammonium naphthalenesulphinate was added to solutions of the metal ions, under varying conditions, and the filtrates tested by means of drop reactions for the metal; for the gravimetric results recorded the precipitates were washed with dilute solutions of the reagent and then ignited to the oxide. The results are given in Table III.

TABLE III

PRECIPITATION OF METAL IONS WITH NAPHTHALENESULPHINIC ACID

Metal ion	Conditions	Results
Fe^{+++}	0.05 mg/ml at pH 3	Good precipitation; 1 p.p.m. iron left in filtrate
	0.25 mg/ml in 0.2 *N* HCl	Good precipitation; 1.3 p.p.m. iron left in filtrate
		Benzenesulphinic acid gives no precipitation under the above conditions
Zr^{++++}	0.4 mg/ml in 0.4 *N* HCl	White precipitate; no zirconium detected in filtrate with alizarin
Th^{++++}	1 mg/ml	White precipitate; quantitative in acid solutions, < 5 p.p.m. thorium left in filtrate even in 0.5 *N* HCl
	0.1 mg/ml in 0.2 *N* HCl	Thorium oxide taken, 11.82 mg; recovered 11.87 mg
Ti^{++++}	0.1 mg/ml in 0.2 *N* H_2SO_4	Yellow precipitate; no titanium detected in filtrate with chromotropic acid
	0.05 mg/ml in 0.2 *N* H_2SO_4	Titanium dioxide taken, 7.94 mg; recovered, 7.95 mg
Sn^{++++}	0.3 mg/ml in 0.25 *N* HCl	White precipitate; no tin detected in filtrate by reduction to stannous tin and testing with ferric iron and *o*-phenanthroline
	1 mg/ml in 0.6 *N* HCl	Stannic oxide taken, 12.47 mg; recovered 12.50 mg
U^{++++}	0.1 mg/ml in 0.2 *N* HCl	White precipitate; no uranium detected in filtrate with ferrocyanide
Bi^{+++}	0.1 mg/ml in 0.2 *N* HNO_3	White precipitate; < 5 p.p.m. bismuth determined with stannite and lead solutions
Pd^{++}	0.1 mg/ml in 0.03 *N* HCl	Brown precipitate turned slowly to canary yellow; no palladium detected in filtrate with mercuric iodide in dioxane
	0.1 mg/ml in 0.2 *N* HCl	No precipitate; yellow solution
Hg_2^{++}	0.1 mg/ml in 0.2 *N* HNO_3	White precipitate; no mercury detected in filtrate with iodide
Ag^{+}	1 mg/ml as solution of $AgNO_3$	White precipitate; no silver detected in filtrate with N,N-dimethylaminobenzalrhodanine
	1 mg/ml in 0.5 *N* HNO_3	Greyish precipitate, indicating reduction to metallic silver; silver ion detected in filtrate with N,N-dimethylaminobenzalrhodanine

Naphthalenesulphinic acid quantitatively precipitates a number of metal ions from acid solution and should, therefore, prove useful in the separation and determination of these metals.

REFERENCES

1. THOMAS, J. J. Chem. Soc. **95**, 342 (1909).
2. FEIGL, F. *In* Specific and special reactions. Elsevier Pub. Co., New York. 1940. p. 119.
3. KRISHNA, S. and SINGH, H. J. Am. Chem. Soc. **50**, 792 (1928).
4. ACKERMAN, L. Ind. Eng. Chem., Anal. Ed. **18**, 243 (1946).
5. DUBSKY, J. V., ORAVEC, E., and LANGER, A. Chem. obzor, **12**, 41 (1937); Chem. Abstr. **31**, 5712 (1937).
6. BEATTIE, R. W. and WHITMORE, F. C. J. Am. Chem. Soc. **55**, 1567 (1933).
7. ALLEN, P. J. Org. Chem. **7**, 23 (1942).
8. GILMAN, H. *In* Organic chemistry. Vol. 1. 2nd ed. John Wiley & Sons, Inc., New York. 1947. p. 906.
9. FIELD, L. and GRUNWALD, F. A. J. Org. Chem. **16**, 946 (1951).
10. ALIMARIN, I. P. and SOTNIKOV, V. S. Doklady Akad. Nauk S.S.S.R. **113**, 150 (1957); Chem. Abstr. **51**, 11913 (1957).

INFRARED SPECTRA AND STRUCTURE OF SELENIOUS ACID[1]

MICHAEL FALK[2] AND PAUL A. GIGUÈRE

ABSTRACT

The infrared spectra of selenious acid both crystalline and in solution in water and methanol were recorded from 2 to 30 μ. Assignment of the various frequencies is made on the basis of the crystal structure as determined from X-ray data. It is shown that the molecules have the symmetrical form (*a*), the asymmetrical one (*b*) proposed by Venkateswaran being

(*a*) (*b*)

ruled out. The spectra of solutions in H_2O and D_2O confirm the existence of discrete H_2SeO_3 and D_2SeO_3 molecules with no indication of uncombined SeO_2 molecules even at high concentrations. This behavior is contrasted with that of SO_2 solutions.

INTRODUCTION

Recent spectroscopic investigations (1, 2) have confirmed the absence of measurable quantities of H_2SO_3 molecules in the various phases of the H_2O–SO_2 system. We have now completed a similar study of the H_2O–SeO_2 system prompted by the considerable differences between sulphurous and selenious acids. Unlike SO_2, SeO_2 combines with water to form a definite compound H_2SeO_3 stable both in solution and in the crystalline state. By X-ray diffraction Wells and Bailey (3) have shown that the crystal consists of nearly symmetrical SeO_3 pyramids linked together by strong O–H . . . O bonds. While the present work was in progress Detoni and Hadži (4) reported briefly on the infrared spectrum of the crystalline acid, interpreting their results in terms of molecules having the symmetrical form (*a*). The existence of stable H_2SeO_3 molecules in the solid phase is therefore well established.

The nature of aqueous solutions of selenious acid remained unsettled, however. By analogy with SO_2 persistence of free SeO_2 molecules in these solutions could be suspected. From a Raman study made over twenty years ago Venkateswaran (5, 6) had concluded that solutions of selenious acid present a complex system of two or three molecular species. His interpretation is now untenable as we shall see.

EXPERIMENTAL

Solid films of selenious acid were prepared by evaporating on a polished silver chloride plate solutions of selenium dioxide in chloroform or acetone and then allowing the films to hydrate in air. The latter reaction took place very readily at room temperature and at moderate humidity; once hydrated the films were indefinitely stable under these conditions, showing no tendency to effloresce. Aqueous solutions of selenious acid were prepared by adding weighed amounts of solid anhydrous SeO_2 to H_2O or D_2O. Absolute methanol was used to dissolve the pure crystalline acid. The high-purity sample of selenium dioxide was obtained through the courtesy of Dr. E. M. Elkin, Canadian Copper Refiners, Montreal East. The spectra were recorded by means of a Perkin–Elmer, Model 12-C infrared spectrometer using LiF, NaCl, and CsBr prisms.

[1]*Manuscript received August 26, 1958.*
Contribution from the Department of Chemistry, Laval University, Quebec, Que.
[2]*Present address: Division of Applied Chemistry, National Research Council, Ottawa, Canada.*

RESULTS AND DISCUSSION

The molecular spectra of crystalline selenious acid must be considered first to help decipher those of the solutions.

Solid H_2SeO_3

A composite tracing of the spectrum of selenious acid in the solid state is reproduced in Fig. 1 and the average frequency of the various maxima found in some eighteen films are listed in Table I. Both the frequencies and the relative intensities agree closely

TABLE I

INFRARED BANDS OF CRYSTALLINE H_2SeO_3 AND SeO_2

(Frequencies in cm^{-1})

H_2SeO_3			SeO_2
Ref. 4	This work	Assignments	(ref. 7)
412	403±3 w	δ OSeO	
	425 vw		
			535
			563
			591
	630±2 (sh)		
661	675±2 vs	ν Se–O	
696	715±5 (sh)	SeO_2	716
	787±5 w		
854	849±1 vs	ν Se–O	
	900±15 (sh)	SeO_2	901
			939
1134	1134±1 s	δ SeOH	
1180	1178±2 m	δ SeOH	
2290	2320±15 s	ν O–H	
2940	2900±50 vs	ν O–H	

with the results of Detoni and Hadži (4). For comparison the infrared frequencies of anhydrous SeO_2 (7) are also given. Apart from a few very weak bands presumably due to traces of SeO_2 in the acid, there is no resemblance between the two spectra; nor is there any indication of the H_2O bands in the neighborhood of 1650 and 3300 cm^{-1} usually present in molecular hydrates. Generally speaking, the frequencies below 1000 cm^{-1} may be ascribed to the SeO_3 groups and those above, to the OH groups.

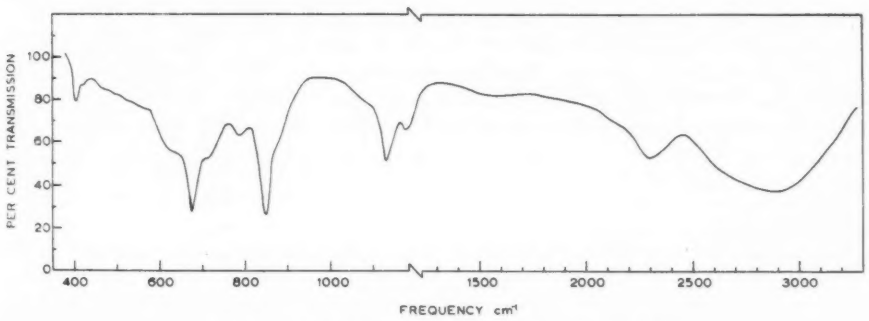

FIG. 1. Infrared absorption of crystalline selenious acid.

The two OH stretching frequencies at 2900 and 2320 cm^{-1} seem quite low compared with that of the free OH (about 3700 cm^{-1}). Such a large downward shift is indicative of strong hydrogen bonding in the crystalline acid and agrees with the short O–H $\cdots$ O distances found by X-ray diffraction, 2.56 and 2.60 Å (3). Correlations have been drawn by various authors between stretching frequencies and hydrogen bond lengths. One of the latest by Nakamoto, Margoshes, and Rundle (8) shows very good agreement for numerous compounds with O–H $\cdots$ O bonds. Taking the latter distance as 2.60 Å in H_2SeO_3, the OH stretching frequency should occur at 2500 cm^{-1}, nearly halfway between the observed values. A second relationship between frequency shift and hydrogen bond distance leads to the same approximate frequency: 3700–1200 = 2500 cm^{-1}. The large splitting between the two stretching frequencies (580 cm^{-1}) must result from the strong coupling of the two OH groups through the heavy selenium atom. In liquid H_2SO_4 the pair of corresponding bands occur at 3000 and 2430 cm^{-1} (9).

It is of interest to inquire where the hydrogen atoms are located in the H_2SeO_3 lattice. Judging from the rather low stretching frequencies one would expect an O–H bond somewhat longer than, for example, in ice: 1.01 Å (10). In fact a rough estimate based on Badgers's rule, using an average frequency of 2600 cm^{-1} leads to a distance of nearly 1.1 Å. On the other hand an empirical relationship between O–H $\cdots$ O distances and O–H bond lengths (8) yields about the same value as in ice. The discrepancy may come from the fact that the hydrogen bonds in the selenious acid crystal are not straight but bent. A neutron diffraction study of this and other mineral acids appears desirable.

The OH bending frequencies also are rather low (1178 and 1134 cm^{-1}) for such a strongly hydrogen-bonded system. Although the influence of hydrogen bonding on the deformation modes is much more complex and obscure than for the stretching modes it usually entails a slight shift toward *higher* frequencies. The situation here is somewhat reminiscent of that in tertiary alcohols (11) where a narrow association band arises near 1100 cm^{-1}. It would seem that even for a bonded hydrogen the bending frequency is strongly dependent on the "resultant mass" on the X atom in the group X–O–H $\cdots$ O.

In view of the small mass of the hydrogen atoms and the strong polarity of the O–H bonds the vibrations of the SeO_3 group can well be analyzed independently. Also for simplicity, a pyramidal configuration with C_{3v} symmetry is assumed since the three Se–O bonds are very nearly equivalent; 1.72, 1.75, and 1.76 Å (3) in the crystalline acid as a result of resonance. The normal Se–O single bond distance is about 1.81 Å (12) and the double bond, 1.68 Å (13). On the basis of that assumption one may expect a symmetrical stretching frequency and a doubly degenerate asymmetrical one. The pair of strong peaks at 849 and 675 cm^{-1} have been rightly assigned to these modes (4). The former has its equivalent at 890 cm^{-1} in the Raman spectra (5); there is, however, no trace in the infrared spectrum of the H_2SeO_3 crystal of any absorption near 600 cm^{-1} corresponding to the intense Raman shift at 597 cm^{-1}. Lastly, we assign the weak maximum at 403 cm^{-1} to a O–Se–O bending rather than a stretching mode as suggested by Detoni and Hadži (4). The other bending frequencies must lie beyond the range covered in this work.

Solutions of H_2SeO_3

The spectra of concentrated solutions of SeO_2 in H_2O and D_2O are shown in Fig. 2 and the frequency of the observed maxima are given in Table II. Progressive dilution of the solutions from 50 to 10% SeO_2 by weight resulted merely in a regular decrease of intensity for all the acid bands. The general resemblance of the spectra of H_2SeO_3 solutions and those of the crystalline acid leaves no doubt that the same species are

TABLE II

INFRARED SPECTRA OF SOLUTIONS OF SELENIOUS ACID
(Frequencies in cm^{-1})

H_2SeO_3 in CH_3OH	SeO_2 in H_2O	SeO_2 in D_2O
434±4 w		
584±4 vs		
670±10 s	682±5 s	670±8 s
920±10 s	894±5 vs	900±16 s
980±10 s	1236±5 s	
2420±20 s	2425±20 s	1820±20 s
2900±100 vs	2980±40 vs	2140±40 vs

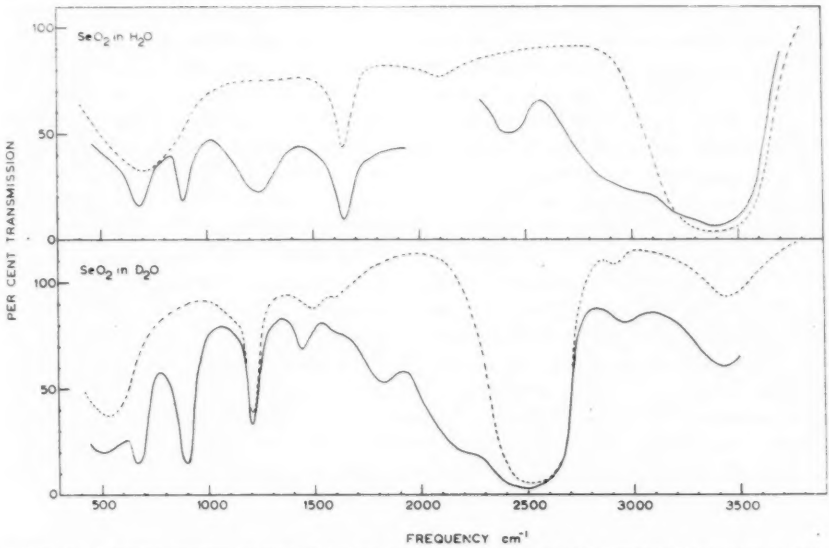

FIG. 2. Infrared spectra of 50% solutions of SeO_2 in H_2O and D_2O. Broken lines refer to the spectra of the pure solvents.

present in both cases. In particular the absence of any bands of uncombined SeO_2 in the solutions is conspicuous. In the deuterated system the OD bending frequency could not be observed as it falls in the region of strong absorption from SeO stretching near 900 cm^{-1}. Shifts of the hydrogen vibrations on passing from the crystal to solutions are not unexpected: it is, however, surprising that the deformation frequency should be shifted to the same extent (about 100 cm^{-1}) and in the same direction as the stretching frequencies.

The only peculiarity in the spectra of methanol solutions was the presence of a fairly strong absorption at 980 cm^{-1} which has no equivalent in either the aqueous solutions or in the crystalline acid. It resulted, no doubt, from oxidation of the alcohol by SeO_2, as shown by appearance, when it was left standing, of the characteristic red coloration of elemental selenium. For that reason these solutions were not studied further.

There is good agreement between our infrared frequencies and the Raman shifts reported by Venkateswaran (5, 6) for selenious acid solutions. For the crystal, however, his spectra have little in common with the present ones. Instead they resemble strangely

the Raman spectra of crystalline SeO_2 (14), which raises the suspicion that his samples were partly dehydrated by heating. From his results Venkateswaran concluded to the existence of two molecular species, a dihydroxyl, symmetrical form (*a*) and an asymmetrical one (*b*), the two being in a state of dynamic equilibrium in proportions varying

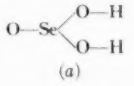

(*a*)

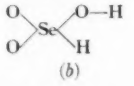

(*b*)

from phase to phase. This is obviously inconsistent with the observed permanence of all the infrared bands of selenious acid both in the solid state and in solutions over a wide range of concentration and temperature (25 to 90° C). In addition the asymmetrical form (*b*) is in contradiction with the X-ray data on the crystal (3) as well as the spectroscopic results of Detoni and Hadži (15) on a series of sulphinic and seleninic acids. Although the 2290 cm^{-1} frequency is of the right magnitude for a Se–H stretching mode (cf. 2260 and 2350 cm^{-1} in H_2Se) the fact that it is shifted to the same extent as the 2900 cm^{-1} frequency on going from crystal to solutions is sufficient proof that both vibrations involve OH groups. Selenium atoms do not normally participate in hydrogen bonding. Lastly, Venkateswaran's assignment of some of the solution bands, particularly that near 900 cm^{-1}, to the biselenite ion $HSeO_3^-$ cannot be correct in view of the very small dissociation constants of selenious acid ($k_1 = 2.4 \times 10^{-3}$ at 25° C).

In conclusion the behavior of selenium dioxide towards water may be contrasted with that of the corresponding oxides of sulphur and tellurium. Whereas SeO_2 displays high affinity for water as exemplified by a great solubility (63% by weight at ordinary temperature) and formation of a well-defined compound stable in the free state and in solutions, SO_2 is only moderately soluble (8.3% by weight) and the solutions contain no detectable amount of H_2SO_3 molecules. The greater polarity of the Se–O bond in the dioxide compared with S–O bond may be partly responsible for the marked difference in properties. This is also apparent in the existence of polymer-like chains in crystalline selenium dioxide (16). As for tellurium dioxide it is quite insoluble in water, and it is doubtful if there exists a definite tellurous acid, H_2TeO_3.

ACKNOWLEDGMENTS

The authors are grateful to the National Research Council for financial help, to the Consolidated Mining and Smelting Co. for a fellowship (M.F.), and to Dr. E. M. Elkin, for a generous sample of very pure selenium dioxide.

RÉSUMÉ

On a étudié les spectres infrarouges de l'acide sélénieux à l'état cristallin et en solution dans l'eau et le méthanol. Les résultats s'accordent avec l'existence de molécules bien définies ayant la formule symétrique

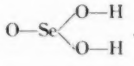

Les spectres des solutions ne révèlent aucune trace de bioxyde de sélénium à l'état libre contrairement au cas du bioxyde de soufre.

REFERENCES

1. Falk, M. and Giguère, P. A. Can. J. Chem. **36**, 1121 (1958).
2. Jones, L. H. and McLaren, F. J. Chem. Phys. **28**, 995 (1958).

3. WELLS, H. G. and BAILEY, M. J. Chem. Soc. **1282** (1949).
4. DETONI, S. and HADŽI, D. J. chim. phys. **53**, 760 (1956).
5. VENKATESWARAN, C. S. Proc. Indian Acad. Sci. A, **3**, 533 (1936).
6. VENKATESWARAN, C. S. Proc. Indian Acad. Sci. A, **7**, 13 (1938).
7. FALK, M. Ph.D. Thesis, Laval University, Quebec, Que. 1958.
8. NAKAMOTO, K., MARGOSHES, M., and RUNDLE, R. E. J. Am. Chem. Soc. **77**, 6480 (1955).
9. MARCUS, R. A. and FRESCO, J. M. J. Chem. Phys. **27**, 564 (1957).
10. PETERSON, S. W. and LÉVY, H. A. Acta Cryst. **10**, 70 (1957).
11. STUART, A. V. and SUTHERLAND, G. B. B. M. J. Chem. Phys. **24**, 559 (1956).
12. SCHOMAKER, V. and STEVENSON, D. P. J. Am. Chem. Soc. **63**, 37 (1941).
13. PAULING, L. Nature of the chemical bond. Cornell Univ. Press, Ithaca, N.Y. 1940.
14. GERDING, H. Rec. trav. chim. **60**, 72 (1941).
15. DETONI, S. and HADŽI, D. J. Chem. Soc. 3163 (1955).
16. MCCULLOUGH, J. D. J. Am. Chem. Soc. **59**, 789 (1937).

THE STRUCTURE OF PYRROLE SALTS AND THE BASIC STRENGTHS OF SOME SIMPLE PYRROLES[1]

E. BULLOCK[2]

ABSTRACT

The infrared spectra of hydrohalide salts of some substituted pyrroles are typical of secondary amine salts. Unlike the free base, cryptopyrrole hydrochloride is easily hydrogenated. The basic strengths of cryptopyrrole and 2,4-dimethylpyrrole are calculated from ultraviolet spectroscopic data.

Contrary to statements in some textbooks and reviews, many substituted pyrroles show considerable basicity (1, 2, 3) and form salts with halogen acids (2, 4, 7, 8). It has been suggested that salt formation is an important step in the acid-catalyzed reactions of pyrroles (1, 2, 3, 5) and the basic property of the heterocyclic nitrogen atom may be a factor in the formation of III-type porphyrins from monopyrroles (6).

The action of dry hydrogen chloride on cryptopyrrole in ether was reported to give a dimer though the conditions were not specified exactly (9). The action of chlorine on a similar solution gave a low yield of a hydrochloride of the pyrrole (8). We obtained a good yield of this stable hydrochloride on treatment of cryptopyrrole in cold ether with dry hydrogen chloride. The salt regenerated the parent base on treatment with sodium acetate solution. The hydrochlorides of 2,4- and 2,5-dimethylpyrrole were isolated similarly but were less stable, especially in contact with the mother liquor. The parent bases could be regenerated from the salts, but after 1–2 hours standing, dimeric compounds were formed. In contact with picric acid solution the picrates of 2,4-dimethylpyrrole and cryptopyrrole behaved similarly; after 4 days the former yielded only the dimer picrate and the latter a mixture of dimer and monomer picrates.

The salts of pyrroles have been formulated as I or II (2, 3, 5) rather than as secondary amine salts, by direct reference to the resonance forms of pyrrole (10). The infrared spectrum of cryptopyrrole hydrochloride (Fig. 2) shows that it is most probably III.

I II III

The spectrum shows no normal $\rangle$NH stretching frequency (cf. Fig. 1, cryptopyrrole band at 3370 cm^{-1}) but has a broad strong band centered at 2630 cm^{-1}. The absence of "immonium" bands (11) at 2100–1980 cm^{-1}, although not conclusive, supports III rather than I or II. Coupled with the disappearance of the $\rangle$NH band, a strong peak appears at 1575 cm^{-1} in the hydrochloride spectrum. Ring vibrations complicate assignments in this region but it seems likely that cryptopyrrole bands at 1597 and 1695 cm^{-1} move to 1650 and 1745 cm^{-1} respectively in the salt and that the 1575 cm^{-1} band is new. This band is considered (12) to be characteristic of the secondary amine salts. The infrared

[1]*Manuscript received August 28, 1958.*
Contribution from the Division of Pure Chemistry, National Research Council, Ottawa, Canada.
Issued as N.R.C. No. 4948.
[2]*National Research Council Postdoctorate Fellow.*

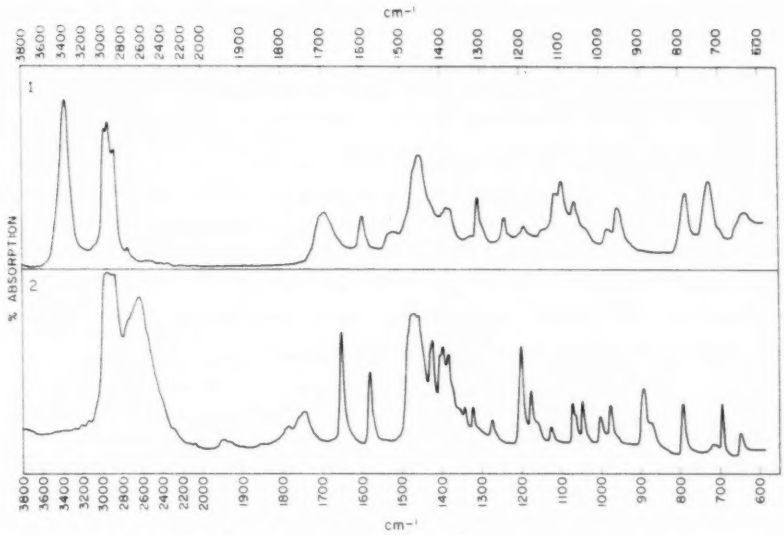

FIG. 1. Cryptopyrrole (thin film).
FIG. 2. Cryptopyrrole hydrochloride (nujol mull).

spectra of hemopyrrole- and cryptopyrrole-dicarboxylic acid hydrobromides show exactly analogous features. The picrates of 2,4-dimethylpyrrole and cryptopyrrole likewise show no normal $\rangle$NH absorption and are probably true salts.*

The ultraviolet spectra of cryptopyrrole and 2,4-dimethylpyrrole in normal hydrochloric acid are consistent with formulation of the salts as *cyclo*-pentadiene analogues (cf. 13). The additional alkyl group in cryptopyrrole causes a bathochromic shift of 11 mμ (λ_{max} 260 mμ compared with 249 mμ) in the main peak.

In neutral or alkaline solution at room temperature and atmospheric pressure, cryptopyrrole is not reduced by hydrogen over Adams' catalyst. In ethanolic hydrochloric acid under these conditions it rapidly takes up 1 mole of hydrogen, further reduction being very slow. The analysis of the product, its behavior with permanganate in acetone, and the infrared spectrum suggest that it is the Δ^2-pyrroline IV (15). As anticipated, the less basic pyrroles V and VI, whose ultraviolet spectra are unchanged by the addition of acid (cf. 14), were not reduced in similar conditions.

The pK_a's of cryptopyrrole and 2,4-dimethylpyrrole were determined by an ultraviolet spectroscopic technique (e.g. 16, 17). Solutions of the bases in various strengths of hydrochloric acid were used, rather than buffer solutions. The error introduced by

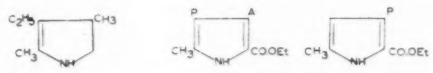

IV V VI

P = $CH_2.CH_2.CO.OEt$
A = $CH_2.CO.OEt$

The author is indebted to a referee for advice on the infrared assignments.

assuming that the pH of the solution is that of the acid is less than 2% for spectroscopic amounts of the base in 0.01 *N* acid.

The pK_a of the conjugate acid to cryptopyrrole is 2.84 and that of 2,4-dimethylpyrrole is 2.12. Allowing 0.7 units of p*K* per alkyl group and neglecting possible "positional" effects, the pK_a of pyrrole is estimated as 0.7. A previous estimate (18) gives the value 0.4. Attempts to measure the pK_a's of variously substituted alkyl pyrroles by other methods are in progress.

From these results it is concluded that: (*a*) In absence of acid, attack of electrophilic reagents may occur at the nitrogen atom of pyrroles. The known structure of the products of such reactions requires that the intermediate rearranges to give α-substituted derivatives. (*b*) In acid solution, the observed catalysis of some pyrrole reactions may be due to salt formation. The $\rangle NH_2^+$ group causes intense polarization of the diene system resulting in high electron density at the 2,5- (α-) positions.

EXPERIMENTAL

Melting points are uncorrected.

Cryptopyrrole Hydrochloride

A solution of the pyrrole (3 g) in dry ether (60 ml) was cooled in an ice bath and saturated with dry hydrogen chloride (3–5 minutes). The precipitated solid was filtered and washed with dry ether (5×20 ml) then dried in a vacuum desiccator over caustic soda. The product (3.2 g) was crystallized from alcohol–ether to large colorless needles, m.p. 109–117 (decomp.). Ehrlich reaction was positive cold. The product is stable *in vacuo* in the dark and is not deliquescent when free of cryptopyrrole (cf. 2, 7). Solutions in water and ethanol are acidic. Calc. for $C_8H_{14}NCl$ (monomer hydrochloride): Cl, 22.33. Calc. for $C_{16}H_{26}N_2Cl$ (dimer hydrochloride): Cl, 12.58. Found: Cl, 21.51. (Dried at room temperature *in vacuo*.) Infrared spectrum (nujol mull): Fig. 1. The spectroscopist reported that the sample became red during the determination. λ_{max} (1 *N* hydrochloric acid): 260 mμ; log ε: 3.56. The material sublimes slowly under water-pump vacuum (60–70° at 12 mm with some decomposition) to a white solid, m.p. 114–117° (decomp.), which slowly turns red on exposure to air.

Regeneration of the Parent Base

A solution of the salt in water was treated with sodium acetate and extracted with ether. The ether layer was washed with water and treated with picric acid. Yellow needles of cryptopyrrole picrate, m.p. 134° alone or mixed with an authentic sample (lit. 137° (20)), were obtained.

2,4-Dimethylpyrrole Hydrochloride

Freshly distilled 2,4-dimethylpyrrole (3.1 g) was dissolved in dry ether (60 ml) and cooled in an ice bath. A rapid stream of dry hydrogen chloride was bubbled through the solution (2–3 minutes) when a semisolid precipitate was formed. The ether was decanted and the product was washed with dry ether (3×50 ml) then taken up in water and neutralized with sodium acetate. The ethereal extract of this solution was washed with water and dried over potassium carbonate. Removal of the ether yielded an almost colorless oil (1.95 g) which distilled almost completely under reduced pressure (b.p. 56.5° at 11 mm).

A sample of the oil was converted to the picrate giving large yellow plates. The picrate is dimorphic showing signs of melting at 56°, accompanied by a collapse of the crystal structure to fine needles, m.p. 92–93° (lit. 91–92° from ethanol–ether (20)).

A sample of the oil was treated with phenyl isothiocyanate and warmed on the steam bath. After 10 minutes the solid product was crystallized from heptane to large yellow needles, m.p. 111–113° (authentic sample 112–114° (19)). Ultraviolet absorption of the pyrrole in acid, λ_{max}: 249 mμ; log ε: 3.43.

2,5-Dimethylpyrrole Hydrochloride

The pyrrole (4.35 g) was treated as above, the colorless oil (1.43 g) liberated from the hydrochloride distilled at 60.0° at 11 mm.

Action of Hydrogen Chloride on α-Methylpyrrole

Under the conditions described above the only product recovered was a solid, probably the dimer.

Reduction of Cryptopyrrole

(*a*) *Acid solution.*—Cryptopyrrole (3.83 g) was dissolved in ethanol (40 ml) saturated with hydrogen chloride and Adams' catalyst (75 mg) was added. The material was hydrogenated at room temperature and atmospheric pressure for 2 hours, after which time 650 ml of hydrogen (almost 50% of theoretical amount for complete reduction) had been absorbed. (In a separate experiment, the uptake was approximately 65% after 6 hours.) The platinum was filtered off over "Celite" and the alcohol removed *in vacuo*. The residue was treated with sodium hydroxide solution (50 ml, 10% w/v) and extracted with ether (3×50 ml). The ethereal extract was washed with water and then re-extracted with a near-saturated solution of potassium dihydrogen phosphate in water (3×50 ml). The yellow phosphate extract was neutralized with sodium hydroxide and the liberated base was collected by further ether extraction (3×50 ml). This ether was well washed with water (5×50 ml), fresh ether being added to maintain the volume of the ethereal layer, and dried over sodium sulphate. Removal of the ether left a pale yellow oil (3.21 g) which gave no Ehrlich reaction. Distillation gave a main fraction, b.p. 152–155° (1.26 g). Calc. for $C_8H_{15}N$: C, 76.79; H, 12.09; N, 11.20. Found: C, 76.50; H, 12.07; N, 11.27. Infrared spectrum (thin film): 3280, 2960, 2890, 1680 (shoulder), 1650, 1550, 1462, 1383, 1305, 1250, 1045, 960 cm^{-1}. α-Naphthylurethane recrystallized from aqueous ethanol. Calc. for $C_{19}H_{22}ON_2$: C, 77.51; H, 7.53; N, 9.52. Found: C, 77.01; H, 7.94; N, 8.95. The picrate, m.p. 157–159°, crystallized in thick needles from ethanol–ether.

(*b*) *Neutral solution.*—In a similar experiment to that described in (*a*) but employing 95% ethanol, no hydrogen was absorbed beyond that required for the catalyst.

(*c*) *Alkaline solution.*—In ethanolic solution containing sodium ethoxide (approximately 2% w/v) the cryptopyrrole absorbed no hydrogen.

Attempted Reduction of Carboxylated Pyrroles

In conditions similar to those given in (*a*) above, cryptopyrrole tricarboxylic acid – triethyl ester (V) and 2-methyl-5-carbethoxypyrrole-4-propionic acid ester (VI) were not reduced.

Determination of pK_a *Values*

Solutions containing spectroscopic amounts of the pyrroles in 1 *N*, 0.1 *N*, and 0.01 *N* hydrochloric acid (0.9–1.7 mg in 25 ml of acid) were prepared and the spectra were recorded from 300 mμ to 208 mμ on a Cary self-recording instrument. The operation of the instrument required approximately 4 minutes, the total time elapsing from completion of the weighing being about 10 minutes. It was found that the spectra were substantially unchanged after 30 minutes' standing, although the solutions became slightly

colored. The spectra of the free bases were recorded in 95% ethanol and the pK_a values were calculated in the usual way (17).

Analyses are by Mr. H. Seguin and the infrared spectra were determined by Mr. R. Lauzon.

REFERENCES

1. TREIBS, A., HERRMANN, E., MEISSNER, E., and KUHN, A. Ann. **602**, 153 (1957).
2. TREIBS, A. and KOLM, H. G. Ann. **606**, 166 (1957).
3. TREIBS, A. and FRITZ, G. Ann. **611**, 162 (1957).
4. STEDMAN, R. J. and MACDONALD, S. F. Can. J. Chem. **33**, 468 (1955).
5. SMITH, G. F. and POTTS, H. A. J. Chem. Soc. 4018 (1957).
6. BULLOCK, E., JOHNSON, A. W., MARKHAM, E., and SHAW, K. B. J. Chem. Soc. 1430 (1958).
7. FISCHER, H., BAUMANN, E., and REIDLE, H. J. Ann. **475**, 205 (1929).
8. PRATESI, P. Gazz. chim. ital. **65**, 658 (1935).
9. FISCHER, H. Ber. **48**, 401 (1915).
10. INGOLD, C. K. Structure and mechanism in organic chemistry. Cornell Univ. Press, Ithaca, N.Y. 1953. p. 176.
11. WITKOP, B. J. Am. Chem. Soc. **76**, 5597 (1954). WITKOP, B., PATRICK, J. B., and KISSMAN, H. M. Chem. Ber. **85**, 949 (1952).
12. HEACOCK, R. A. and MARION, L. Can. J. Chem. **34**, 1782 (1956).
13. POWELL, J. S. and EDSON, K. C. Anal. Chem. **20**, 510 (1948).
14. COOKSON, G. H. J. Chem. Soc. 2791 (1953).
15. LEONARD, N. J. and GASH, V. W. J. Am. Chem. Soc. **76**, 2781 (1954).
16. ALBERT, A., GOLDACRE, R., and PHILLIPS, J. J. Chem. Soc. 2240 (1948).
17. FLEXSER, L. A., HAMMETT, L. P., and DINGWALL, A. J. Am. Chem. Soc. **57**, 2103 (1935).
18. HALL, N. F. J. Am. Chem. Soc. **52**, 5115 (1930).
19. BULLOCK, E. Unpublished work.
20. FISCHER, H. and BARTHOLOMAUS, E. Z. physiol. Chem. **80**, 8 (1912).

DISTRIBUTION OF NUCLEAR CHARGE IN THE PROTON-INDUCED FISSION OF Th^{232} [1]

B. D. Pate,[2] J. S. Foster, and L. Yaffe

ABSTRACT

The cross sections for the independent formation of I^{130}, I^{131}, Te^{131}, I^{132}, and I^{134} and for the cumulative formation of Te^{132}, I^{133}, and I^{135} in the proton-induced fission of Th^{232} have been measured at nine proton energies between 8 and 87 Mev. From these data and from published total chain yield data, charge distribution curves have been obtained. These are compared with published charge distribution curves for uranium fission at energies up to 480 Mev and together they show a shift of the most probable fission product charge toward stability and a widening of the distribution with increasing bombarding energy. These phenomena are interpreted in terms of current models for nuclear reactions.

INTRODUCTION

A voluminous literature exists on the distribution of nuclear mass in the fission process. In spontaneous fission (31) and in the fission of U^{233}, U^{235}, and Pu^{239} with neutrons of thermal energy, the familiar double-peaked distribution, corresponding to a preponderance of asymmetric fission modes, is observed (30). As the energy of bombarding particles is increased the mass distribution in the fission of these and other heavy nuclei becomes more and more symmetric (18, 33) and at sufficiently high energies a singly peaked distribution is observed (19).

About the nuclear charge distribution less is known. Data exist on the distribution from the fission of U^{235} with thermal neutrons (6, 7, 21) and with 14-Mev neutrons (34). Data also exist for the fission of uranium by 170-Mev protons (1), of bismuth by 190-Mev deuterons (10), and of uranium, thorium, and bismuth by 480-Mev protons (16), and there is fragmentary information from other systems. The present work was undertaken to investigate the changes that occur in the charge distribution from proton-induced fission of Th^{232} as the bombarding energy is raised from 8 to 90 Mev, the maximum proton energy of the McGill synchrocyclotron. This energy range is of interest in view of the substantial changes observed in the mass distribution (33). Also in this interval a change presumably begins in the nature of the initial step in nuclear reactions, from simple compound nucleus formation to a mechanism of direct interaction with individual nucleons (29). Thus at the lower energies studied, excitation of the nuclei at the end of the first step of the reaction will be essentially monochromatic whereas at the higher end of the bombarding energy range, a broad spectrum of excitation energies will be produced, with corresponding complexity of the reaction products observed. Ideally, in the determination of a charge distribution, one would wish to measure the independent yields of each of the nuclides in one or more fission chains. This, however, is precluded by the short half-lives of most of the members of any given mass chain. One substitutes a determination of independent yields of accessible nuclides in chains of different mass number, followed by correlation of these data. Correlation is customarily attempted by means of semiempirical or theoretical relationships (6, 7, 21, 27, 35) that

[1]*Manuscript received July 22, 1958.*

Joint contribution from the Radiochemistry Laboratory, Department of Chemistry, and the Radiation Laboratory, Department of Physics, McGill University, Montreal, Que., and the Department of Chemistry, Brookhaven National Laboratory, Upton, Long Island; with financial assistance from the Defence Research Board, the Atomic Energy Control Board of Canada, and the U.S. Atomic Energy Commission.

[2]*Present address: Department of Chemistry, Brookhaven National Laboratory, Upton, Long Island, N.Y.*

give the most probable nuclear charge, Z_p, for a given mass number A. Here Z_p is that charge value at which the peak of the charge distribution occurs, this not necessarily being an integral value. Distribution of yields around the most probable charge is usually assumed to be Gaussian and to be identical for all mass chains. These assumptions appear to be substantiated by much of the experimental evidence.

In the present experiment, yields of some iodine and tellurium nuclides in the mass region 130–135 were measured. The data have been correlated to give a charge distribution in this mass region under the assumptions that the distribution is symmetric about Z_p and that over the mass range investigated Z_p is displaced a constant amount from the Z_A value given by Pappas (21). (Z_A is that charge value, not necessarily integral, corresponding to stability for a given A.) A study over a mass range as small as six units does not provide sufficient data to test theories on the variation of Z_p with A.

EXPERIMENTAL TECHNIQUES AND RESULTS

1. Target and Irradiation

Thorium metal foil of about 190 mg/cm^2 superficial density was employed as the target material and was irradiated in the internal circulating proton beam of the McGill 82-in. synchrocyclotron. In all experiments, but the one at lowest energy, foils were irradiated in stacks of three, and the middle foil was used for the iodine yield determination. Loss of fission fragments by recoil from the target foil was thus compensated for by gain of recoils from the neighboring foils. In the lowest energy bombardment (8 Mev) energy loss considerations precluded the use of more than a single foil.

Upstream from the thorium was a monitor foil, again with a guard foil on both sides. For proton energies of 35 Mev and above, aluminum foils were used and beam intensities monitored via the $Al^{27}(p,3pn)Na^{24}$ reaction. The excitation function given by Hintz and Ramsey (13) was used with the cross-section scale reduced by a factor of 41/49, as indicated by the work of Crandall *et al.* (4). For lower energies copper monitor foils were used, the monitor reaction then being at 8 Mev, $Cu^{63}(p,n)Zn^{63}$ and at 26 Mev, $Cu^{65}(p,pn)Cu^{64}$. Here the cross-section data of Meadows (17) were used, with the appropriate scale correction. The leading edge and the top and bottom edges of the stack of six foils were aligned prior to bombardment by shearing with scissors after the foils had been clamped in the target holder.

The foils were mounted on a water-cooled probe and inserted into the cyclotron tank to a radius appropriate for the desired proton energy, using the data of Kirkaldy (15). Bombardments of 10–20 minutes and beam currents of the order of 10^{15} protons/cm^2 min were employed.

2. Chemical Processing and Measurement

After rapid removal of the target from the cyclotron probe and transfer to the radiochemistry laboratory, the thorium and monitor foils were sheared with scissors from the target clamp. This, together with the preliminary alignment described above, ensured that the monitor and target foils used in the experiment received the same flux. The middle target foil of the stack of three irradiated and likewise the middle monitor foil were selected for processing.

Three timed-separations of iodine activity from the irradiated target foil were accomplished by procedures previously described (8, 14, 34). The target foil was dissolved in concentrated hydrochloric acid, to which a known quantity of iodine (about 10 mg)

in the form of iodide had been added, and the last traces of residue were dissolved by addition of ammonium silicofluoride. The solution was then made up to volume and an aliquot taken for the first iodine separation.

The aliquot was transferred to a separatory funnel and diluted with hydrochloric acid. An equal volume of carbon tetrachloride was then added, followed dropwise by 10% hydrogen peroxide to slight excess. The iodine produced was extracted into the carbon tetrachloride and the phases separated, the time from the end of the bombardment to the separation being noted. The iodine activity was purified by three cycles of extraction of iodine from the carbon tetrachloride layer by a saturated sulphur dioxide solution, followed by acidification of the aqueous extract with 6 *M* nitric acid, reoxidation of the iodine with 1 *M* sodium nitrite solution, and re-extraction into carbon tetrachloride. The iodine was finally extracted from the organic layer with slight excess of SO_2 water, and the aqueous solution made up to volume. Aliquots (1%) were taken and mounted for 4π-counting. The mounts used were 5–10 $\mu g/cm^2$ VYNS films coated with 2–5 $\mu g/cm^2$ of gold (22). A 100 λ aliquot of the separated iodide solution was pipetted, followed by pipette washings, on to the film, followed by 100% excess of 0.1 *M* silver nitrate solution. The resulting colloidal silver iodide solution was then rapidly evaporated to dryness, the time at which the last of the solution disappeared being taken as the time of separation from xenon-daughter activities. The sample was then placed in a 4π-counter and the disintegration rate measured as a function of time by techniques described elsewhere (23, 24, 25, 26). Measurements were made first at 15-minute intervals, later less frequently, and extended for 5 to 6 weeks from the end of bombardment.

Successive 1% aliquots from the separated iodine solution were mounted at intervals, 6-hourly at first, thereafter daily until all 20-hour I^{133} had decayed and no further xenon-daughter activities were being produced.

The time from the end of the bombardment to the first iodine separation was about 20 minutes. Further iodine separations were performed on additional aliquots of the dissolved thorium solution 2–3 hours and again 2–3 days after the end of bombardment. The procedure followed in each case was the same as that described above.

After the elapse of a time interval sufficient to allow substantial decay of iodine activity, semimicrogravimetric determination of iodine as AgI was performed on each of the three iodine solutions, to establish the chemical yields in the separations. The yields averaged about 70% so that the quantity of iodine carrier originally added resulted in less than 100 μg of AgI in the samples used for disintegration rate measurements.

As soon as convenient after the end of the bombardment, the middle monitor foil was dissolved in an appropriate acid, nitric for copper, hydrochloric for aluminum. The solution was made up to volume and a suitable aliquot (0.1–1%) mounted on a VYNS film for 4π-counting, as described above. Counting-rate measurements over several days followed by decay curve analysis allowed the counting rates of 38-minute Zn^{63}, 12.8-hour Cu^{64}, and 15.0-hour Na^{24} at the end of bombardment to be determined.

It is well known that active iodine produced in the fission of uranium and thorium in the form of oxides and oxysalts does not exchange readily with carrier iodide. The chemical separation of iodine activity from uranium metal targets by a procedure involving oxidation of carrier iodide to iodine and extraction into CCl_4 is reported (14) to be 100% complete. It was felt desirable to check this behavior with thorium metal for possible use in the present work. Accordingly, an irradiated thorium metal target was dissolved as above in the presence of iodide carrier. Two aliquots were then taken

and an iodine separation was performed on each. One was treated by the procedure outlined above, and the other by the usual procedure for the separation of iodine from uranium oxysalts (8). The latter involved the oxidation of the iodine to periodate by sodium hypochlorite in sodium hydroxide solution, followed by acidification of the solution with nitric acid and reduction of the iodine to the elementary form with hydroxylamine. Yields from the two separations (after correction for carrier recoveries) were identical within experimental error. Consequently the faster separation by peroxide oxidation of the iodide was adopted, as detailed earlier.

3. Results

The iodine and xenon activities which might be expected to appear in a sample separated from the products of a fission reaction are listed, together with their decay characteristics, see Table I. The list does not include isotopes which, because of their very long or short half-lives, would not be detectable in the present experiments.

TABLE I

DECAY CHARACTERISTICS OF IODINE AND XENON ISOTOPES*

Isotopes	Mode of decay	Half-life	Beta group energies and abundances	Gamma transition energies and abundances
I^{128}	β^-, E.C.	25.0 m	1.125 Mev 2.0% 1.665 Mev 15.5% 2.120 Mev 76.0%	0.455 Mev 17.2% 0.540 Mev 1.8% 0.750 Mev 0.31% 0.990 Mev 0.20%
I^{130}	β^-	12.5 h	0.597 Mev 54% 1.02 Mev 46%	0.409 Mev 8.8% 0.528 Mev 29% 0.660 Mev 26% 0.744 Mev 24% 1.15 Mev 11.8%
I^{131}	β^-	8.05 d	0.250 Mev 2.8% 0.335 Mev 9.3% 0.608 Mev 87.2% 0.815 Mev 0.7%	0.080 Mev 2.2% 0.284 Mev 5.3% 0.364 Mev 80% 0.637 Mev 9% 0.722 Mev 3%
Xe^{131m}	IT	12.0 d	—	0.163 Mev 100%
I^{132}	β^-	2.3 h	0.73 Mev 15% 0.9 Mev 20% 1.16 Mev 23% 1.53 Mev 24% 2.12 Mev 18%	0.528 Mev 10% 0.624 Mev 2.4% 0.673 Mev 37.6% 0.777 Mev 32% 0.96 Mev 8% 1.16 Mev 3.2% 1.40 Mev 4.4% 1.96 Mev 2% 2.2 Mev 1%
I^{133}	β^-	20.9 h	0.5 Mev 6% 1.4 Mev 94%	0.53 Mev 94% 0.85 Mev 5% 1.4 Mev 1%
Xe^{133m}	IT	2.3 d	conv. $e^-(\alpha_k = 4.4)$	0.233 Mev 100%
(Formed in 2.4% of I^{133} decays)				
Xe^{133}	β^-	5.27 d	0.345 Mev 100%	0.081 Mev 100%
I^{134}	β^-	52.4 m	1.6 Mev 70% 2.8 Mev 30%	0.86 Mev 1.10 Mev 1.78 Mev
I^{135}	β^-	6.75 h	0.5 Mev 35% 1.0 Mev 40% 1.4 Mev 25%	1.8 Mev 1.27 Mev
Xe^{135}	β^-	9.2 h	0.55 Mev 3% 0.910 Mev 97%	0.25 Mev 96% 0.36 Mev 0.1% 0.604 Mev 3%

*These data are "best values" derived from Nuclear Science Abstracts, National Research Council, Washington, D.C.

The mixture of activities obtained from each separation was checked for radiochemical purity in two ways.

(*a*) *Gamma-radiation Measurements*

Gamma spectra were observed from suitable aliquots of the iodine activity stock solutions, by means of a $1\frac{1}{2}$ in. × 1 in. NaI (Tl) crystal with a Dumont 6292 photomultiplier, an Atomic Energy of Canada Limited amplifier (AEP 1448), and a single channel pulse-height analyzer. Figure 1 shows the spectra obtained at various times after the end of bombardment from a sample of iodine separated at 24 minutes after the end of bombardment from a thorium target irradiated with 26-Mev protons.

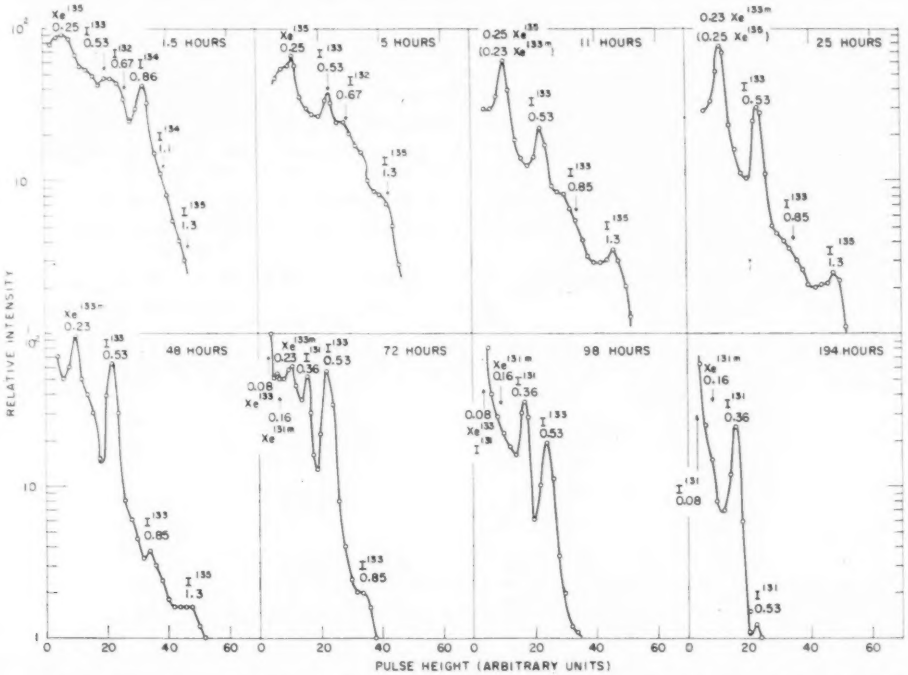

FIG. 1. Gamma spectra of iodine + xenon fission product mixture at various times after the end of bombardment.

The photopeaks are identified as to energy and isotope as indicated, and the positions at which other prominent γ lines in the decay schemes of the various iodine or xenon isotopes would be expected to appear are indicated by arrows.

It is seen that there are no features of the spectra which are inconsistent with the composition of the expected isotope mixture, either as to line energies or intensities. However, these measurements obviously do not constitute a very sensitive test for the presence or absence of activities other than those of iodine or xenon.

(*b*) *Beta-radiation Measurements*

The results of the analysis of beta-activity determinations, which are described below,

constituted a more rigorous check on the effectiveness of the iodine purification procedure. The analysis of the decay curves in terms of the published half-life values in Table I was always successful, and in no case were decay periods observed other than those corresponding to iodine or xenon isotopes. The purification procedure was consequently considered to be satisfactory.

Figure 2 shows the analysis of a typical beta-decay curve obtained with a 4π-counter from iodine samples mounted as AgI as described earlier. The data are for the first sample separated from a target irradiated with 63-Mev protons. The open circles on the curve marked "iodine + xenon activity" represent observations made on a single sample mounted shortly after the end of the separation procedure. (The data presented extend over a 2-week period, but observations continued for a further month to assure positive identification of 8.05-day I^{131}.) The closed circles on the curve marked "iodine activity" represent observations made on a series of samples (one per plotted point) freshly mounted in succession from the stock iodine solution at intervals as described earlier. Since the data plotted were obtained promptly after mounting, they give closely the iodine disintegration rates alone at the times indicated, free of xenon-daughter contributions.

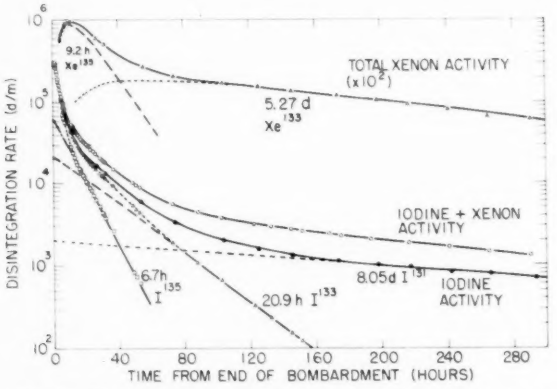

FIG. 2. Beta-decay curve of iodine + xenon fission product mixture.

The standard deviations on disintegration rate measurements were in general less than 1% and always less than the sizes of the plotted points.

The iodine + xenon data are more complete than the pure iodine data, since the mounting of successive samples was time-consuming, and more frequent preparations could not be fitted into the experimental schedule. However, the data can be combined to improve the definition of the pure iodine disintegration rate curve. The points plotted as open triangles on the curve marked "total xenon activity" are the result of the subtraction of one set of observations from the other, with the ordinate multiplied by 100 for reasons of clarity. From 120 hours after bombardment this curve exhibits an exponential decay with a half-period close to 5.27 days, corresponding to Xe^{133}. (The small scatter of the points, each representing a separate sample mounting, confirms the reproducibility of the procedure used.) From the intercept of the 5.27-day line with the ordinate, and from a knowledge of the time of separation and of parent half-life (20.9 hours), the

growth and decay curve of Xe^{133} can be calculated. The early part of this curve is shown as a broken line. Subtraction of this curve from points at abscissa values less than 120 hours gives new points which are well fitted by 9.2-hour Xe^{135} growing from 6.7-hour I^{135}, as indicated by the dashed line. Summing of these two curves gives the smooth total xenon curve. Interpolation from this curve makes possible the determination of xenon-daughter contributions to the total disintegration rate at times other than those at which fresh mountings were made. (Contribution of 2.3-day Xe^{133m} formed in a rare decay mode of I^{133} to the observed xenon activity was apparently not large enough to disturb this method of treatment of the data.)

Subtraction of the interpolated xenon activities from the iodine + xenon data now allows the pure iodine curve to be drawn accurately between the observations made. By the usual method of successive subtractions the iodine decay curves can be analyzed clearly into 8.05-day, 20.9-hour, and 6.7-hour components corresponding to I^{131}, I^{133}, and I^{135} as shown in the figure. In experiments involving proton energies in excess of 74 Mev the data are well fitted by the addition of a 12.5-hour component, corresponding to I^{130}.

After subtraction of these periods, the data at times less than 12 hours from end of bombardment showed an exponential decay with a half-life which varies between 1 and 2 hours, presumably corresponding to a mixture of 52-minute I^{134} and 2.3-hour I^{132}, which the subtraction technique cannot resolve. The resolution is effected by a method originally due to Ford (5), in which the data are fitted to the sum of two exponential terms of the form:

$$A_t = A_1^{\circ} e^{-\lambda_1 t} + A_2^{\circ} e^{-\lambda_2 t},$$

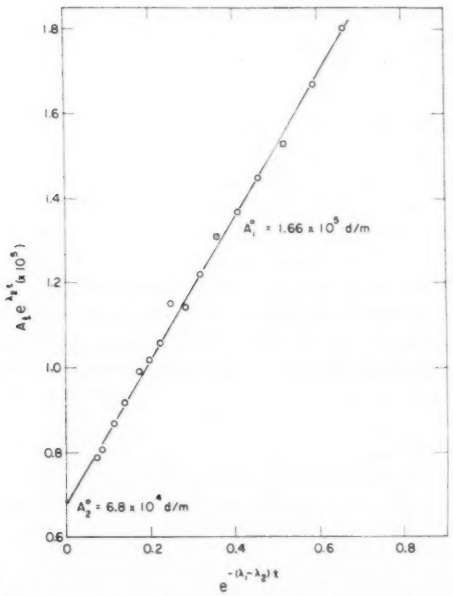

FIG. 3. Ford plot of beta-decay data for I^{132} and I^{134}.

where A_t is the combined activity at time t, and A_1° and A_2° are the initial activities of components 1 and 2. Then.

$$A_t\, e^{\lambda_2 t} = A_2^\circ + A_1^\circ\, e^{-(\lambda_1-\lambda_2)t}.$$

Therefore in a plot of $A_t\, e^{\lambda_2 t}$ versus $e^{-(\lambda_1-\lambda_2)t}$ using the disintegration rate versus time data for A_t and the appropriate decay constants of I^{132} and I^{134} for λ_1 and λ_2, the initial activities of the two isotopes are obtained as the slope of the curve and as the intercept with the ordinate axis respectively.

Figure 3 shows a typical plot of this nature. The success of the fit was in all cases shown by the linear plot obtained, indicating the absence, over the time interval studied, of activities other than the two anticipated. In particular no deviation from linearity at small t values was observed, indicating the absence of 25-minute I^{128} in the samples studied in these experiments. It should be emphasized that the success of the analysis procedure described is probably due in no small degree to the precision of the disintegration rate measurements made by the 4π-counting technique, especially the relative precision of a series of measurements made on the same sample.

TREATMENT OF THE DATA

From the experimental observations described above, two types of cross-section data were obtained. First, from the disintegration rates of given iodine isotopes, measured in samples separated from the irradiated target at times long compared with precursor half-lives, cumulative formation cross sections could be calculated. Secondly, from similar measurements made on samples separated shortly after the end of bombardment, independent formation cross sections for some iodine isotopes and cumulative formation cross sections for some tellurium isotopes could be calculated.

Our method of treatment of the data is essentially similar to that of Wahl (34). It differs in detail, because, particularly at higher bombarding energies, formation cross sections of the observed iodine isotopes are comparable with those of the tellurium precursors. This fact invalidates some of the approximations which are useful at lower energies. Likewise, in the comparison of fractional chain yields for various mass numbers, it is no longer reasonable to assume that iodine cumulative yields represented total yields of the respective masses. With increasing bombarding energies, an increasing fraction of these yields appears at atomic numbers higher than that of iodine. We have used published mass yield curves for the fission of Th^{232}, U^{235}, and U^{238} by projectiles of various energies, together with suitable interpolations and extrapolations, to obtain the variation of total chain fission yield over the mass range studied.

The generalized relationship between the activity $A_n(T, t)$ of the nth member of a decay series, at a time t after the end of a bombardment of duration T, in which the first member is formed at a constant rate r has been given by Rubinson (28) in the form:

$$A_n(T, t) = r \sum_{i=1}^{n} b_i(1-e^{-\lambda_i T})\, e^{-\lambda_i t}$$

where

$$b_i = \prod_{j \neq i} \frac{\lambda_j}{\lambda_j - \lambda_i} (j = 1, 2, \ldots, n)$$

and the λ's are appropriate decay constants.

This expression is useful in the construction of activity vs. time relationships for iodine nuclides, particularly where isomerism exists in the tellurium precursors. Thus in the generalized case of a decay scheme of the form

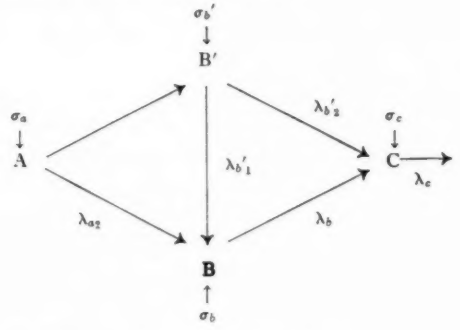

where σ's and λ's are formation cross sections and decay constants respectively (A, B, and C in the present work would be antimony, tellurium, and iodine isotopes), the appropriate expression for the activity of C after given irradiation and decay times may be obtained by summing contributions from the following decay routes:

$$\xrightarrow{\sigma_a} A \xrightarrow{\lambda_{a1}} B' \xrightarrow{\lambda_{b'2}} C$$

$$\xrightarrow{\sigma_a} A \xrightarrow{\lambda_{a1}} B' \xrightarrow{\lambda_{b'1}} B \xrightarrow{\lambda_b} C$$

$$\xrightarrow{\sigma_a} A \xrightarrow{\lambda_{a2}} B \xrightarrow{\lambda_b} C$$

$$\xrightarrow{\sigma_b'} B' \xrightarrow{\lambda_{b'2}} C$$

$$\xrightarrow{\sigma_b'} B' \xrightarrow{\lambda_{b'1}} B \xrightarrow{\lambda_b} C$$

$$\xrightarrow{\sigma_b} B \xrightarrow{\lambda_b} C$$

$$\xrightarrow{\sigma_c} C$$

The assumption is implicit that the tin and earlier precursors of chains in the mass range 130–135 are too short-lived to have been observed in the present experiment. Their formation cross sections may be considered to add to those of the Sb precursors. In each case the rate of formation r in Rubinson's expression is given by

$$r_n = N\sigma_n f$$

where N and f are the number of target nuclei and bombarding particle flux respectively and σ_n is the appropriate cross section. Fortunately, however, it was possible to work with simpler expressions for reasons which will be discussed for each mass number.

A = 130.—I^{130} is shielded by stable Te^{130} from formation by decay of precursors. The activity observed at bombarding energies of 74 Mev and above was therefore due to direct formation. The independent formation cross section was calculated via the simple expression

$$\lambda_a N_a = N\sigma_a f(1-e^{-\lambda_a T})\, e^{-\lambda_a t}.$$

The failure to observe I^{130} at lower energies is assumed to have been due to the larger amounts of I^{135} formed which masked the activity.

A = 131.—The decay scheme (9, 11) of the 131 mass chain up to iodine is as follows:

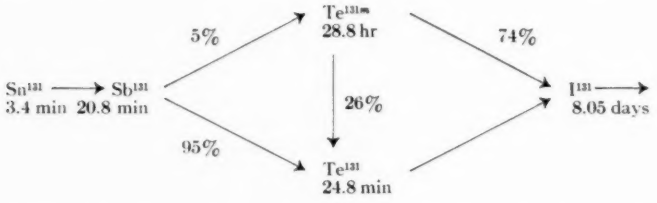

For the purposes of the present work two simplifications were made. First, the 5% branch in the decay of Sb^{131} leading to the metastable state of Te^{131} was neglected in view of the comparatively long half-life of Te^{131m}. Second, the 26% isomeric transition of Te^{131m} was ignored, and all of the decay of this body was taken to proceed directly to I^{131}. This is expected to have little effect on the calculations (34), since, at short times after the end of bombardment, little of the Te^{131m} will have decayed by either path, and after long times the effect of the 24.8-minute half-life of Te^{131} will be negligible.

Thus the approximate decay scheme is now

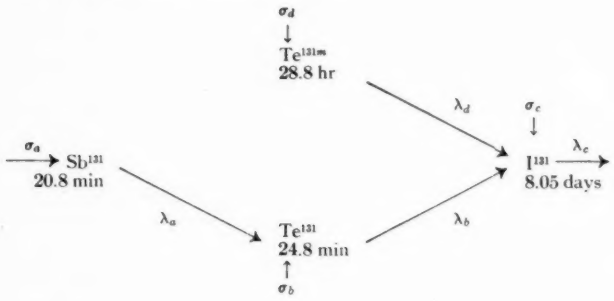

and the corresponding expression for the activity of I^{131}, obtained as outlined above:

$$\lambda_c N_c(T,t) = N\sigma_a f\left[\frac{\lambda_b\lambda_c}{(\lambda_b-\lambda_a)(\lambda_c-\lambda_a)}(1-e^{-\lambda_a T})\,e^{-\lambda_a t}+\frac{\lambda_a\lambda_c}{(\lambda_a-\lambda_b)(\lambda_c-\lambda_b)}(1-e^{-\lambda_b T})\,e^{-\lambda_b t}\right.$$
$$\left.+\frac{\lambda_a\lambda_b}{(\lambda_a-\lambda_c)(\lambda_b-\lambda_c)}(1-e^{-\lambda_c T})\,e^{-\lambda_c t}\right]$$
$$+N\sigma_b f\left[\frac{\lambda_c}{\lambda_c-\lambda_b}(1-e^{-\lambda_b T})\,e^{-\lambda_b t}+\frac{\lambda_b}{\lambda_b-\lambda_c}(1-e^{-\lambda_c T})\,e^{-\lambda_c t}\right]$$
$$+N\sigma_d f\left[\frac{\lambda_c}{\lambda_c-\lambda_d}(1-e^{-\lambda_d T})\,e^{-\lambda_d t}+\frac{\lambda_d}{\lambda_d-\lambda_c}(1-e^{-\lambda_c T})\,e^{-\lambda_c t}\right]$$
$$+N\sigma_c f(1-e^{-\lambda_c T})\,e^{-\lambda_c t}.$$

For each bombarding energy, this expression was used to obtain three equations relating σ_a, σ_b, σ_c, and σ_d by insertion of the decay-constant values for the 131 chain the irradiation time T, the measured values of N and f, and also the three measured

iodine disintegration rates corresponding to the three separation times. A unique solution for the value of σ_c was not obtainable, but an approximate value was obtained by a further series of simplifications.

First, from the data from two samples separated several hours and 3 days respectively after end of bombardment, the values of $\sigma_a+\sigma_b+\sigma_c+\sigma_d$ and of σ_d alone were calculated under the assumptions:

$$\text{(i)}\quad \sigma_d = \sigma_a+\sigma_b+\sigma_c;$$
$$\text{(ii)}\quad \sigma_d = 4\sigma_b;\ \sigma_a = 0;$$
$$\text{(iii)}\quad \sigma_d = 4\sigma_b;\ \sigma_a = \sigma_b;$$
$$\text{(iv)}\quad \sigma_a = \sigma_b = 4\sigma_b.$$

The value of σ_d was assumed to be about four times that of σ_b, as was found by Glendenin (9) in the thermal fission of U^{235}. The value of $\sigma_a+\sigma_b+\sigma_c+\sigma_d$ was found to be unchanged from one assumption to another to within 5% and the value of σ_d to within somewhat smaller limits.

By means of an average of the values calculated, an upper limit on σ_b was now calculated under the extreme assumption that $\sigma_a = \sigma_c = 0$, and an upper limit on σ_c, under the assumption that $\sigma_a = \sigma_b = 0$. Calculations were also made for σ_b and σ_c under the intermediate assumptions $\sigma_a = \sigma_b = \sigma_c$ and $\sigma_a = 0$, $\sigma_b = \sigma_c$. From these results mean values were obtained for σ_b and σ_c together with some indication of the magnitude of the associated uncertainty. The uncertainty in the I^{131} formation cross section (σ_c) and in that for Te^{131} ($\sigma_b+\sigma_d$) from this source was far greater than the uncertainties arising from other sources in the experimental technique.

A = 132.—The decay scheme is as follows:

$$\underset{2\text{ min}}{Sb^{132}} \longrightarrow \underset{77.7\text{ hr}}{Te^{132}} \longrightarrow \underset{2.26\text{ hr}}{I^{132}}$$

In the present experiment, the time between the end of the irradiation and the first iodine separation was long compared with the Sb^{132} half-life. Consequently only a cumulative cross section for Te^{132} was obtained, together with an independent formation cross section for I^{132}. The appropriate activitity–time expression is

$$\lambda_b N_b(T,t) = N\sigma_a f\left[\frac{\lambda_b}{\lambda_b-\lambda_a}(1-e^{-\lambda_a T})\,e^{-\lambda_a t}+\frac{\lambda_a}{\lambda_a-\lambda_b}(1-e^{-\lambda_b T})\,e^{-\lambda_b t}\right] + N\sigma_b f(1-e^{-\lambda_b T})\,e^{-\lambda_b t}.$$

A = 133.—The 133 chain decay scheme is as follows (20):

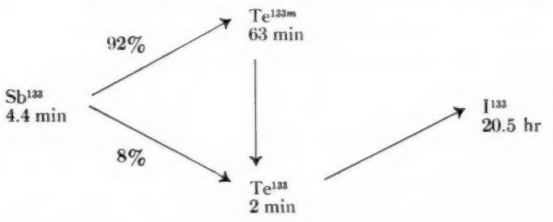

Again, the time of 20 minutes between end of bombardment and the first iodine separation made it impossible to obtain independent yield information about I^{133} or about the Te^{133}

ground state. Consequently, only cumulative formation cross sections for I^{133} were calculated, using disintegration rate data from samples separated 3 days after the end of bombardment and the expression given above under $A = 130$.

A = 134.—From the decay scheme

$$\underset{0.8\text{ min}}{Sb^{134}} \longrightarrow \underset{44.5\text{ min}}{Te^{134}} \longrightarrow \underset{52.4\text{ min}}{I^{134}}$$

it is clear that the 20-minute separation time was in this case too long compared with the Sb^{134} half-life and indeed rather long compared with the Te^{134} half-life for the purposes of obtaining accurate independent yield data. However, the data from the 20-minute and 2–3-hour separations were analyzed using the activity–time expression given for the 132 chain, and independent formation cross sections calculated for I^{134}.

A = 135.—The precursors of I^{135} are not known and are presumably of very short half-life. Therefore, only a cumulative cross section for this isotope was obtained in this work, by means of the activity–time expression given above under $A = 130$.

RESULTS

The results of the analysis outlined above are presented in Figs. 4, 5, and 6 in the form of excitation functions, independent or cumulative formation cross sections being designated σ_{ind} or σ_{cum} respectively. Also on these figures are included, for comparison, excitation function data of Tewes and James (33) for the total proton-induced fission, with an ordinate scale as indicated to the right of the figure. The initial rise with energy of all the cross sections measured in this work is clearly associated with the corresponding rise in the total fission cross section. The decreasing cross sections at higher energies reflect the broadening and shift of the charge distribution, which will be demonstrated below.

The uncertainties associated with the cross-section data presented are estimated to

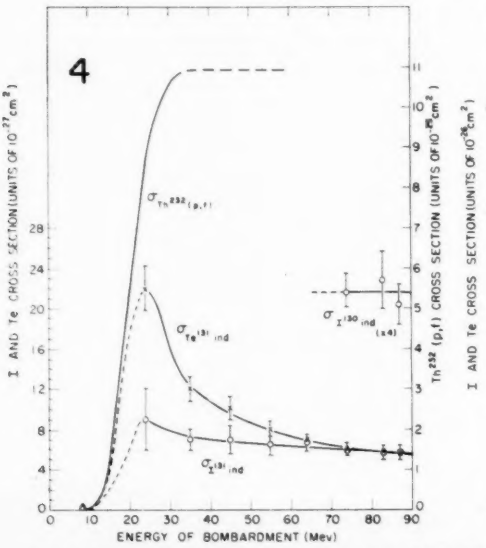
4
I AND Te CROSS SECTION (UNITS OF 10⁻²⁷ cm²)
Th²³² (p,f) CROSS SECTION (UNITS OF 10⁻²⁵ cm²)
ENERGY OF BOMBARDMENT (Mev)
σ Th²³² (p,f)
σ Te¹³¹ ind
σ I¹³⁰ ind (x4)
σ I¹³¹ ind
5
I AND Te CROSS SECTION (UNITS OF 10⁻²⁸ cm²)
Th²³² (p,f) CROSS SECTION (UNITS OF 10⁻²⁵ cm²)
ENERGY OF BOMBARDMENT (Mev)
σ Th²³² (p,f)
σ Te¹³² cum
σ I¹³² ind

FIG. 4. Excitation functions for production of I^{130}, I^{131}, and Te^{131} in Th^{232} (p,f) reaction.
FIG. 5. Excitation functions for production of Te^{132} and I^{132} in Th^{232} (p,f) reaction.

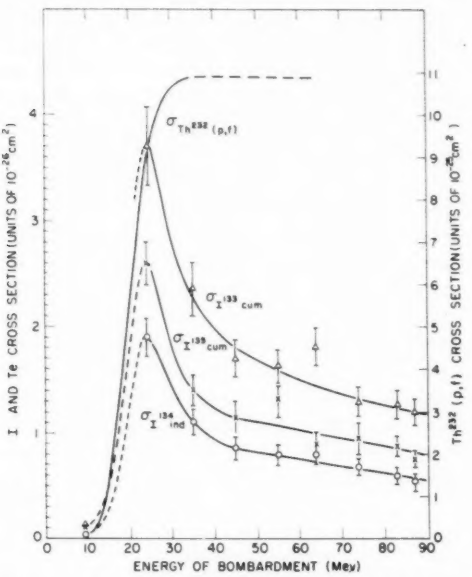
I AND Te CROSS SECTION (UNITS OF 10⁻²⁶ cm²)
Th²³² (p,f) CROSS SECTION (UNITS OF 10⁻²⁵ cm²)
ENERGY OF BOMBARDMENT (Mev)
σ Th²³² (p,f)
σ I¹³³ cum
σ I¹³⁵ cum
σ I¹³⁴ ind
0 10 20 30 40 50 60 70 80 90
0 1 2 3 4
0 1 2 3 4 5 6 7 8 9 10 11

FIG. 6. Excitation functions for production of I^{133}, I^{134}, and I^{135} in Th^{232} (p,f) reaction.

be as follows: the exact proton energy at which the bombardment was made is uncertain due to energy spread in the cyclotron beam and to uncertainties in the calculated value of the energy loss in the target itself (2). Nevertheless, the beam energy was probably known to 2–5 Mev. The uncertainty in the cross-section values results from uncertainties in the original disintegration rate measurements (<1%), in the graphical decay curve analysis and associated extrapolations (5–10%), and from sources described earlier in the treatment of the activity data. The over-all uncertainty is thought to be 15–20%.

The cross-section data were converted into charge distribution curves for five bombarding energies by means of the mass yield data available in the literature and the total Th^{232} (p,f) cross-section data of Tewes and James (33) and of Steiner and Jungerman (32). The product of the fission yield for a given mass A and the total fission cross section gives the cumulative formation cross section for mass A. The division of the independent formation cross section for a given isobar of mass A by this cumulative formation cross section then gives that fraction of the mass chain formed directly as the particular isobar. These fractional values for the various iodine and tellurium nuclides were correlated in a plot versus the nuclide's displacement from stability along the isobaric chain. The assumptions implicit in such a correlation are that the distribution of yields along a chain is the same for chains of different mass, and that the displacement from stability of the charge value at which the highest yield occurs is independent of chain mass. Both assumptions are probably reasonable over the narrow region of mass (130–135) studied.

Tewes' and James' data (33) for the proton-induced fission of Th^{232} at energies of 8.0 and 21.1 Mev were used in conjunction with our data at 8 and 24 Mev, the mass yield data at 8 Mev being further checked by interpolation between the data of Wahl (34) on the 0-Mev (thermal) and 14-Mev neutron-induced fission of U^{235}. In the treatment of data in this paper at energies of 45 Mev and above, we have assumed that over the

mass range 130–135 the total chain yield was independent of mass number and energy at a value close to that indicated by Newton (18). Consideration of his results and of mass yield data at much higher energy (19) indicates that this assumption is probably not in error over the present energy range by more than $\pm 10\%$.

The error introduced by using mass yield data from projectile target systems other than the Th^{232} + proton system is probably small. The mass range studied in this work includes nuclides on the heavy peak of the fission yield curve, the position and height of which changes little with changing target mass number and like parameters.

The charge distribution curves for 8-, 24-, 45-, 64-, and 87-Mev proton energies are shown in Fig. 7, in which the fraction of the chain yield is plotted as ordinate against $Z_A - Z$ as abscissa, where Z_A is the Z-value corresponding to the minimum potential energy (maximum beta stability) for a given A (21). In this plot neutron-excess nuclides lie to the right of the figure and neutron-deficient ones to the left. The location of the Gaussian distribution plotted in each case was determined so that the area under it summed to unit total chain yield, and also so that the independent yields of Te^{132}, I^{133}, and I^{135} and their precursors, as obtained from the curve, summed to a value for the corresponding cumulative yields close to that measured experimentally. This latter is a sensitive criterion for location of the curve, and renders it much more certain than is at first apparent.

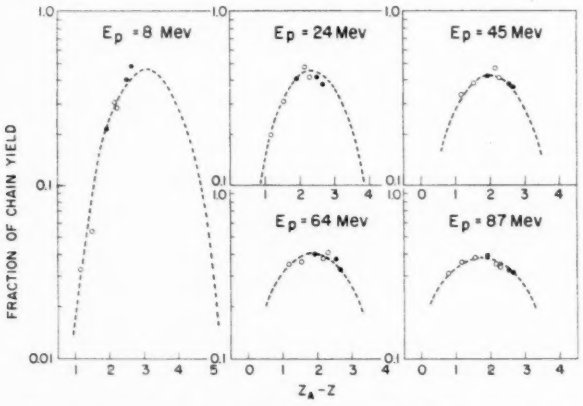

FIG. 7. Charge distribution curves in the Th^{232} (p,f) reaction at proton energies between 8 and 87 Mev.

The five charge distributions are shown assembled on Fig. 8, together with the curve of Glendenin (7) and Pappas (21) for thermal fission of U^{235}, of Wahl (34) for 14-Mev fission of U^{235}, of Aagaard *et al.* (1) for the 170-Mev proton-induced fission of uranium, and of Lavrukhina and Krasavina (16) for the 480-Mev proton-induced fission of uranium. The yield data of Aagaard *et al.* have been converted to a charge distribution in the manner outlined above, and those of Lavrukhina and Krasavina have been renormalized to give a distribution summing to unit chain yield. The position of the 170-Mev curve on the ordinate scale below the other curves is due to the fact that Aagaard *et al.* fitted their data to a wider distribution than those used by the other authors. The position of their curve on the abscissa scale in relation to the others presented, which is of more significance, is not affected by the normalization to unit chain yield.

In Table II the displacement of the maximum of the charge distribution from stability and the "half-width" of the distribution are tabulated with bombarding energy.

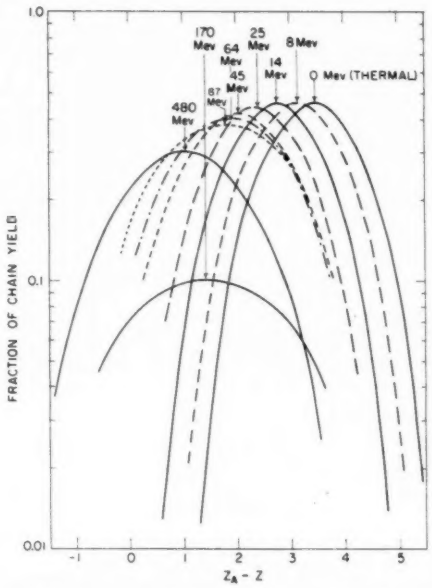

FIG. 8. Assembled charge distribution curves for thorium and uranium fission between 0 and 480 Mev bombarding energy.

DISCUSSION

The data in Table II show two effects. With increasing energy of bombarding particle, the charge distribution is observed to move towards stability, rapidly at first and then more slowly at higher energies. Secondly, while the width of the distribution remains approximately constant up to 25 Mev, at higher energies it shows evidence of increasing with increasing energies.

These effects may be rationalized in terms of a two-step model for nuclear reactions. In this model the projectile undergoes an initial rapid ($\sim 10^{-21}$ second) interaction with the target nucleus. The interaction will be predominantly the formation of a compound nucleus (3) for energies up to approximately 50 Mev. As the energy is raised above 50 Mev interaction with individual nucleons (12, 29) associated with prompt ejection of some nucleons becomes increasingly important. After this initial stage has terminated, the excitation energy deposited is dissipated in a second slower stage, largely by a particle-emission process described as nuclear evaporation, with which fission competes in heavy nuclei.

The shift of the charge distribution with increasing energy, which corresponds to a decrease in neutron/proton ratio of the fission products studied, is then interpreted as reflecting a decrease in the n/p ratio for the nuclide undergoing fission. This will be caused by increasing particle evaporation (predominantly neutron emission at moderate energies with heavy targets) prior to fission. Alternatively, the decrease in the n/p ratio of the fission products may, to some extent, be due to neutron evaporation after fission.

TABLE II

DISPLACEMENT OF CHARGE DISTRIBUTION MAXIMUM AND HALF-WIDTH OF DISTRIBUTION AS A FUNCTION OF BOMBARDING ENERGY

Bombarding energy (Mev)	Displacement of distribution maximum (units of Z)	Half-width of distribution (units of Z)
0	3.4	2.2
8	3.1	2.2
14	2.7	2.2
25	2.4	2.2
45	2.0	2.5
64	1.9	2.8
87	1.8	3.2
170	1.4	—
480	1.0	3.0

An increased width of charge distribution at higher energies is expected from the same picture, since a proliferation of both nuclear cascade and nucleon evaporation would lead to a wider distribution of fissioning nuclei and hence wider distribution of n/p values in the fission products.

Detailed interpretation in terms of calculations based on models of the nuclear cascade and nucleon evaporation processes will be presented in the succeeding paper.

REFERENCES

1. AAGAARD, P., ANDERSSON, G., BURGMAN, J. O., and PAPPAS, A. C. J. Inorg. & Nuclear Chem. **5**, 105 (1957).
2. ARON, W. A., HOFFMAN, B. G., and WILLIAMS, F. C. U.S. Atomic Energy Comm. Rept. AECU-663 (1951).
3. BOHR, N. Science, **86**, 161 (1937).
4. CRANDALL, W. E., MILLBURN, G. P., PYLE, R. V., and BIRNBAUM, W. Phys. Rev. **101**, 329 (1956).
5. FORD, G. P. Private communication to A. C. Wahl (ref. 34).
6. GLENDENIN, L. E., CORYELL, C. D., and EDWARDS, R. R. Phys. Rev. **75**, 337 (1949).
7. GLENDENIN, L. E. Ph.D. Thesis, Massachusetts Institute of Technology, Cambridge, Mass. 1949.
8. GLENDENIN, L. E. and METCALF, R. P. Natl. Nuclear Energy Ser. Vol. 9, Div. IV, Paper 278, Book 3 (1951).
9. GLENDENIN, L. E. Private communication. 1957.
10. GOECKERMANN, R. H. and PERLMAN, I. Phys. Rev. **76**, 628 (1949).
11. HEBB, E. Phys. Rev. **97**, 987 (1955).
12. HEISENBERG, W. Naturwiss. **25**, 749 (1937).
13. HINTZ, N. M. and RAMSEY, N. F. Phys. Rev. **88**, 19 (1952).
14. KATCOFF, S., DILLARD, C. R., FINSTON, H., FINKLE, B., SEILER, J. A., and SUGARMAN, N. Natl. Nuclear Energy Ser. Vol. 9, Div. IV, Paper 280, Book 3 (1951).
15. KIRKALDY, J. S. Ph.D. Thesis, McGill University, Montreal, Que. 1953.
16. LAVRUKHINA, A. K. and KRASAVINA, L. D. J. Nuclear Energy, **5**, 236 (1957).
17. MEADOWS, J. W. Phys. Rev. **91**, 885 (1953).
18. NEWTON, A. S. Phys. Rev. **75**, 17 (1949).
19. O'CONNOR, P. R. and SEABORG, G. T. Phys. Rev. **74**, 1189 (1948).
20. PAPPAS, A. C. Phys. Rev. **87**, 162 (1952).
21. PAPPAS, A. C. Ph.D. Thesis, Massachusetts Institute of Technology, Cambridge, Mass. 1953.
22. PATE, B. D. and YAFFE, L. Can. J. Chem. **33**, 15 (1955).
23. PATE, B. D. and YAFFE, L. Can. J. Chem. **33**, 610 (1955).
24. PATE, B. D. and YAFFE, L. Can. J. Chem. **33**, 929 (1955).
25. PATE, B. D. and YAFFE, L. Can. J. Chem. **33**, 1656 (1955).
26. PATE, B. D. and YAFFE, L. Can. J. Chem. **34**, 265 (1956).
27. PRESENT, R. D. Phys. Rev. **72**, 7 (1947).
28. RUBINSON, W. J. Chem. Phys. **17**, 542 (1949).
29. SERBER, R. Phys. Rev. **72**, 1114 (1947).
30. STEINBERG, E. P. and FREEDMAN, M. S. Natl. Nuclear Energy Ser. Vol. 9, Div. IV, Paper 219, Book 3 (1951).
31. STEINBERG, E. P. and GLENDENIN, L. E. Phys. Rev. **95**, 431 (1954).
32. STEINER, H. M. and JUNGERMAN, J. A. Phys. Rev. **101**, 807 (1956).
33. TEWES, H. A. and JAMES, R. A. Phys. Rev. **88**, 860 (1952).
34. WAHL, A. C. Phys. Rev. **99**, 730 (1955).
35. WAY, K. and WIGNER, E. P. Phys. Rev. **73**, 1318 (1948).

FISSION OF EXCITED HEAVY NUCLEI[1,2]

B. D. PATE

ABSTRACT

The results of published calculations on the prompt nuclear cascade and nuclear evaporation processes are combined with some assumptions regarding the nuclear fission process and fission widths to calculate the average neutron-to-proton ratios of fission products from Th + 8-Mev protons, Th + 87-Mev protons, and U + 450-Mev protons. Comparison of the results with experimental data indicates that the fission charge distribution mode characterized by the equal charge displacement hypothesis, hitherto considered a low energy phenomenon, persists in uranium and thorium up to the highest energy studied. There is also some evidence that fission occurs in excited heavy nuclei before complete de-excitation by particle emission, in agreement with other experimental work.

A. INTRODUCTION

Particle evaporation (30) and fission predominate during the de-excitation of heavy nuclei excited to energies above a few million electron volts. These two processes are expected to compete at each step during the de-excitation in the sense of the following scheme (25):

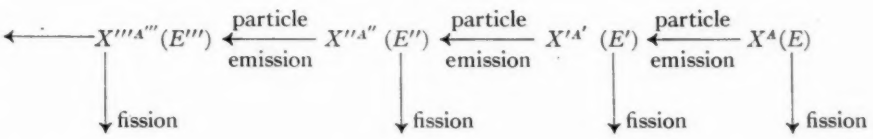

in which a nucleus of mass A excited to energy E evaporates particles to form successively nuclei of masses A', A'', etc. and energies E', E'' . . . with fission as an alternative to each particle evaporation step. The decrease in excitation energy per step, $E-E'$, $E'-E''$, etc., equals the binding energy of the particle evaporated plus, in each case, the (variable) kinetic energy it carries off. The fragments from the fission of a nucleus of a given excitation energy E will themselves share in some way an excitation energy close to E, and may de-excite by further particle emission.

The relative probability that a nucleus in a given energy state de-excites via a specific reaction path is commonly described in terms of a partial "width" of the state for that reaction. Thus the competition between fission and particle emission from a given nucleus at a given energy may be expressed as a ratio Γ_f/Γ_{evap}, where Γ_f is the fission width and Γ_{evap} is a sum of particle emission widths

$$\Gamma_{evap} = \Gamma_n+\Gamma_p+\Gamma_d+\Gamma_t+\Gamma_\alpha+ \ldots \quad .$$

The ratio is expected to be a function of nuclear charge, mass, and excitation energy.

Fission-evaporation competition has been the subject of a number of previous studies, among the more recent being investigations with transuranium nuclei excited to energies up to 40 Mev (27, 28), and with thorium bombarded with protons of energies up to 100 Mev (3).

[1]*Manuscript received July 22, 1958.*
Contribution from the Chemistry Department, Brookhaven National Laboratory, Upton, Long Island, New York.
[2]*Research performed under the auspices of the U.S. Atomic Energy Commission.*

Interpretation of the experimental data is complicated by several factors aside from the complexity of a reaction scheme such as that illustrated above, for example, post-fission evaporation of nucleons from the fragments. Also a study of fission products gives only averaged information for the fission of the series of nuclei of different charge, mass, and excitation energy in the de-excitation chain.

Furthermore, as the bombarding energy is raised, the character of the initial nuclear interaction, which produces the excited nuclei whose de-excitation is to be studied, also changes. In addition to compound nucleus formation (2), characterized by the formation of a single nuclear type excited to a unique energy, reactions proceeding via direct interaction with individual nucleons (23) are observed. In some circumstances, the latter process occurs to a significant extent at energies as low as 14 Mev (14). It becomes more important with increasing energy and predominates above about 50 Mev.

Since such single nucleon reactions between target and projectile occur with the transfer of a variable amount of energy, generally less than the maximum available, and result in the prompt emission of a variable number of nucleons, de-excitation cascades such as that illustrated above begin from a range of nuclear charges, masses, and excitation energies.

Some previous attempts (1, 24) to interpret experimental data, making various assumptions regarding variation of Γ_f/Γ_{evap} with A, Z, and E, have suffered from lack of information regarding the nature of the prompt part of the nuclear interaction. The present work has the benefit of the results of detailed calculations which have been made both of the prompt initial nuclear interaction (17, 18) and of the evaporation process as it would occur in the absence of fission competition (5). It also differs from many previous studies in that it employs data on the nuclear charge distribution of fission products. The particular data used are those reported in the previous paper (20) for thorium irradiated with protons of 8- and 87-Mev energy, and those of Lavrukhina and Krasavina (15) for uranium with 480-Mev protons.

The following approach is used in the calculations. The distribution in nuclear charge, mass, and excitation energy at the end of the prompt interaction are obtained by assuming compound nucleus formation where appropriate, and elsewhere from the Monte Carlo calculations of Metropolis *et al.* (17, 18). These calculations, while being of the same general type and employing the same crude nuclear model (degenerate Fermi gas in a sharply defined nuclear potential) as previous calculations (10), nevertheless benefit from a three-dimensional relativistic treatment and good statistics. Their results are in reasonably good agreement with experiment (17, 18) and appear to be fairly reliable when used for the present purposes.

Next the Monte Carlo calculations of Dostrovsky *et al.* (5) are used to compute the course of evaporation cascades from each point in the A, Z, and E distribution at the end of the prompt cascade. These evaporation calculations have been made using the LeCouteur formalism (16) and do not take fission competition into account. The effect of the choice of input parameters for these calculations on the results obtained has not yet been completely investigated, and the results of the present analysis are uncertain to that extent. Parts (i) and (ii) of the calculations that follow (energies 8 and 87 Mev) are expected to be the least uncertain, since the nature of the evaporation reaction in heavy elements at excitation energies below 100 Mev (almost exclusively neutron emission) and the average de-excitation per particle emitted are not very sensitive to the choice of nuclear model and parameters that may reasonably be made. The same is not true for higher energies, and Part (iii) of the analysis, employing the results of

evaporation calculations for excitations of up to 480 Mev, has been made with those results obtained with a choice of parameters that seemed to lead to the best agreement with other experimental data. The parameters include a coulomb barrier independent of excitation energy with barrier penetration introduced in a manner similar to that used by LeCouteur (16), and a nuclear energy level density given by

$$w = C\, e^{2(0.14\times E)^{\frac{1}{2}}},$$

where A is the mass number and C is a constant. The results of Part (iii) should be considered in the light of this uncertainty in the evaporation reaction calculations.

Fission competition has been introduced in the present analysis by means of three assumptions:

(1) $\Gamma_f/(\Gamma_f+\Gamma_{evap})$ increases sharply from zero to unity as the Z^2/A ratio is raised through some critical value. This step-functional behavior is illustrated in Fig. 1*a*, and it may be compared with the previously reported experimental results shown in Fig. 1*b* where the solid line is taken from the data of Seaborg (1) and the broken line from those of Huizenga (13).

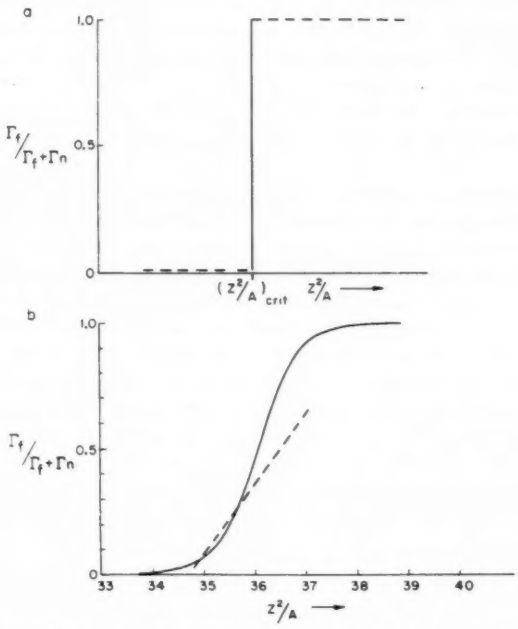

FIG. 1. Variation with Z^2/A of ratio of fission width to sum of fission and neutron widths for heavy elements. (*a*) Variation assumed in present calculations. (*b*) Experimental data (solid line from ref. (1), broken line from ref. (13)).

(2) Excitation energy of a fissioning nucleus is not (or is only to a small extent) transformed into kinetic energy of the fission fragments, or into electromagnetic radiation, but goes into excitation of the fragments (6) being divided between them in the ratio of their masses.

(3) On the average, 2.5 "fission" neutrons are emitted regardless of energy or fission mode. There is no information regarding the variation of the average number of fission neutrons ($\bar{\nu}$) with excitation energies above a few million electron volts, other than that given by Harding and Farey (11), who interpreted their experimental data for uranium bombarded with 147-Mev protons in terms of a $\bar{\nu}$ value of 2.5 ± 1.0. Further there exist few data on the variation of $\bar{\nu}$ with nuclear type (and then only for thermal energy or spontaneous fission (4, 12)) and there is no information regarding the variation of $\bar{\nu}$ with charge division mode. Thus the assumption of the constancy of $\bar{\nu}$ under all conditions seems the most reasonable working assumption that can be made at present. It should be noted that a change in $\bar{\nu}$ of unity would produce a change in fission product neutron-to-proton ratio of about 0.01 (see later).

In the calculations that follow, the results of the variation of several parameters will be investigated. These parameters include the critical Z^2/A value at which the sharp increase in the $\Gamma_f/(\Gamma_f+\Gamma_n)$ function occurs, the energy dependence of $\Gamma_f/(\Gamma_f+\Gamma_n)$ (assumed to be one of two limiting forms) and the mode of distribution of nuclear charge in fission. Experimental evidence has been cited in the literature for two charge distribution processes, namely the equal charge displacement (ECD) process (7, 8, 19) and the unchanged charge distribution (UCD) process (9). The former, observed to account well for independent yield data for the products from the fission of U^{235} at thermal energies and at 14 Mev (29), is based on the postulate that the most probable nuclear charges of complementary fragments will be equally displaced from the charge value corresponding to stability for their respective masses. That is to say

$$Z_p = Z_A - \tfrac{1}{2}[Z_A + Z_{(A_f - \bar{\nu} - A)} - Z_f],$$

where Z_p is the most probable charge for a fragment of mass A, Z_A is the stable charge for mass A, A_f and Z_f are the mass and charge of the fissioning nucleus, and $\bar{\nu}$ as before is the average number of prompt fission neutrons. This process implies a rearrangement of nucleons prior to or during the fission act, and is commonly assumed to be a low-energy process. The unchanged-charge-distribution mode of fission (first postulated by Goeckermann and Perlman (9) to occur in the fission of bismuth with 190-Mev deuterons) produces fragments whose most probable neutron-to-proton ratio is the same as that of the fissioning nucleus. This implies that the nucleonic rearrangement indicated in ECD-type fission does not take place, and UCD is considered characteristic of "fast" or "high-energy" fission (9).

Comparison between the predicted and observed neutron-to-proton ratios of primary fission products will then be made in order to determine which of the various choices of parameters best fits the data.

B. CALCULATIONS AND RESULTS

The n/p ratios resulting from calculations based on the assumptions described above are compared with the observed most probable n/p ratio for fission products in the mass range 130–135 as reported (20) for the systems

(i) Th^{232} + 8.0-Mev protons,
(ii) Th^{232} + 87-Mev protons,

and for fission products of masses 90 and 130 as reported (15) for

(iii) U^{238} + 480-Mev protons.

(*i*) Th^{232} + *8.0-Mev Protons*

The assumption of compound nucleus formation in this case is probably a good one. Consequently we must consider the de-excitation of Pa^{233} with an excitation energy

$$E^* = E_{\text{kinetic}} + E_{\text{proton binding}},$$
$$= 13.6 \text{ Mev},$$

since the proton-binding energy in Pa^{233} is 5.6 Mev (22). Thus we have the reaction scheme shown in Fig. 2; only neutron emission is considered for the evaporation reaction, since coulomb barrier effects render charged particle emission highly unlikely. The neutron-binding energies in Pa^{233} and Pa^{232} are 6.6 and 4.2 Mev (22) respectively so that formation of Pa^{231} is energetically possible. However, the evaporation calculations indicate that, in this region of charge, mass, and energy, the most probable de-excitation via neutron evaporation is greater than 9 Mev. Consequently the reaction would seldom proceed past Pa^{232}.

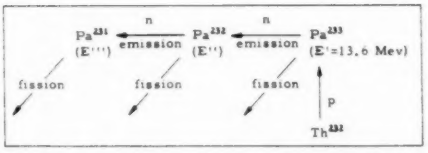

FIG. 2. De-excitation of Pa^{233} excited to 13.6 Mev.

Table I shows the n/p ratio calculated for both the ECD and the UCD mechanisms for the system of Fig. 2. The fission of Pa^{233} excited to 13.6 Mev is considered to lead to fission fragments sharing an excitation energy of about the same magnitude (see assumption (2)). Thus there is a significant probability for the evaporation of a neutron from each of the fission fragments, since the average neutron-binding energy in the iodine isotopes of mass 130–135 is about 7.4 Mev (22). This would reduce the n/p ratio calculated via ECD to 1.560 and via UCD to 1.514.

TABLE I

CALCULATED AND EXPERIMENTAL AVERAGE NEUTRON TO PROTON RATIOS FOR FRAGMENTS OF MASS 130–135 FROM THE FISSION OF Th^{232} WITH 8-MEV PROTONS

Fissioning nucleus	n/p Calculated via ECD	n/p Calculated via UCD	n/p observed
Pa^{233}	1.579	1.533	
Pa^{232}	1.570	1.522	1.566±0.004
Pa^{231}	1.560	1.511	

The experimental data in the preceding paper give a n/p ratio of 1.566±0.004. Thus they appear to be consistent with the fission of Pa^{232} via an ECD mechanism, perhaps with some contribution from ECD-type fission of Pa^{231} and Pa^{233}, and to be inconsistent with UCD-type fission.

(*ii*) Th^{232} + *87-Mev Protons*

The experimental data for this system will be compared with an analysis starting with the results of prompt cascade calculations for 83-Mev protons incident upon

U^{238}. (The difference in energy is neglected and the difference in target characteristics is taken into account by introduction of appropriate shifts in charges and masses of the reaction products.)

Figure 3 is a section of the chart of nuclides (Z plotted versus N) with the course of the reactions indicated on it. Immediately below the symbol and mass number for each nuclide are given its n/p and Z^2/A ratios. The Th^{232} target nucleus is enclosed by double lines, and the distribution of products from the prompt interaction (17) is given by the numbers (relative frequencies) in square boxes. The total number of cascades followed in the prompt interaction calculation was 1258 (in addition to those in which nuclear transparency was indicated). In addition to the number distribution given for each nuclide the excitation energy spectrum is available from the calculations (17). This is generally a continuous distribution except in the case of Pa^{233}, which is the compound nucleus product and is therefore excited to a unique energy.

The evaporation calculations (5) for heavy nuclei excited to 75 Mev indicate that 99.7% of the evaporated particles are neutrons. Consequently charged particle evaporation will be neglected. Also the average de-excitation per evaporated neutron is 9.2 Mev; the value shows no systematic trend with nuclear excitation in this energy region. Consequently a further simplification will be made, namely that all neutrons carry off exactly this energy. The evaporation reaction proceeds as indicated by the horizontal lines in Fig. 3, and leads to the final nuclide distribution shown by the unboxed numbers. (With the simplification used, the de-excitation of Pa^{233} leads to emission of $9\frac{1}{2}$ neutrons so that the 520 events are divided equally between Pa^{223} and Pa^{224}. Similar adjustments are made elsewhere as required.)

The incorporation of fission competition in the calculations must now be considered. The approximations made thus far would seem to make an analysis as sophisticated as that by Batzel (1) or Vandenbosch *et al.* (28) of doubtful value. Instead we shall examine two situations.

(1) The dependence of Γ_f/Γ_n on energy is greater than the dependence on nuclear type (specifically on the fissionability parameter Z^2/A). That is, increasing energy favors neutron emission sufficiently so that fission does not take place until the excitation energy is reduced below the neutron-binding energy at the end of the evaporation cascade.

(2) Γ_f/Γ_n is essentially independent of energy, but varies sharply with Z^2/A as described earlier and illustrated in Fig. 1*a*.

Again, both ECD- and UCD-type fission are to be considered, the n/p ratio resulting from the fission of each nuclide via the two mechanisms being calculated. The values are then weighted using the number distributions indicated for situations (1) and (2) above and averaged to give the mean n/p ratio expected for fission products of mass 130–135 in each case. The variation of total fission chain yield with mass number over the energy range and mass range considered is small enough to be neglected in the averaging.

The results of the calculation are compared with the experimental data in Table II. In Part 2 of Table II, the average n/p ratios calculated for fission fragments of mass 130–135 are listed both for the fragments initially formed by the fission act, still excited, and for these fragments after de-excitation by neutron emission. The average number of neutrons emitted was obtained by using average neutron-binding energy values appropriate to iodine nuclides in the indicated mass range (22) plus an estimated most probable

FIG. 3. Prompt cascade and evaporation reactions in thorium bombarded with 83-Mev protons.

neutron kinetic energy. In Part 1 fission is considered to take place in de-excited nuclei only, so that the fission fragments are considered to have excitation energies less than the neutron-binding energy.

TABLE II

CALCULATED AND EXPERIMENTAL AVERAGE n/p RATIOS FOR THE PRODUCTS OF THE FISSION OF Th^{232} WITH 87-MEV PROTONS—MASS NO. 130–135

1. Fission occurs after de-excitation by neutron emission in nuclides with greater than given Z^2/A value

Z^2/A greater than	ECD-type fission	UCD-type fission
37	1.478	1.423
36.6	1.491	1.435
36.3	1.497	1.441
36.0	1.499	1.445
35.5	1.506	1.450
35.0	1.511	1.458
34.5	1.512	1.459

Experimental value 1.502

2. Fission occurs at given Z^2/A value before complete de-excitation

	ECD-type fission		UCD-type fission	
Z^2/A	n/p ratio of initial fission fragments	n/p ratio of fragments after de-excitation	n/p ratio of initial fission fragments	n/p ratio of fragments after de-excitation
37.0	1.478	1.478	1.423	1.423
36.6	1.510	1.491	1.456	1.445
36.3	1.519	1.481	1.478	1.456
36.0	1.547	1.499	1.500	1.478
35.5	1.569	1.506	1.525	1.488
35.0	1.574	1.512	1.529	1.493
34.5	1.577	1.513	1.531	1.494

Experimental value 1.502

It is seen that the experimental n/p ratio is consistent with that calculated with the assumption that ECD-type fission occurs either during or at the end of de-excitation, in nuclides with Z^2/A values greater than 36.0. The n/p ratios calculated for UCD-type fission under various conditions are all inconsistent with the experimental value.

This conclusion is consistent with two other data. First, a Z^2/A value of 36.0 corresponds to a Γ_f/Γ_n value of nearly unity (1, 13), i.e. fission and neutron emission are roughly equally probable. Hence, that critical Z^2/A value of the step function assumed for $\Gamma_f/(\Gamma_f+\Gamma_n)$ which gives results most consistent with experiment, corresponds roughly to the mid-point of the $\Gamma_f/(\Gamma_f+\Gamma_n)$ functions reported previously which were based on other experimental evidence.

Second, we may calculate the cross section for the Th^{232} (p,f) reaction to be expected on the basis of the assumption that all nuclides of Z^2/A greater than 36.0 undergo fission. The total number of prompt interaction events followed in the Monte Carlo calculation (17) was 1336, of which 978 were found to give nuclides which were presumed to undergo fission. The geometric cross section for Th^{232} is 2.0×10^{-24} cm^2 for a nuclear radius parameter, $r_0 = 1.3\times10^{-13}$ cm. The fission cross section is then expected to equal

$$\sigma_f = \pi r^2 \times (978/1336)$$
$$= 1.4\times10^{-24} \text{ cm}^2$$

the value at 80 Mev is expected to be 1.1×10^{-24} cm^2 by extrapolation from published values at lower energies (26).

One further comparison with experiment may be made—namely the charge distribution for fragments of mass 130–135 may be calculated and compared with the charge distribution obtained from the mass distribution observed experimentally (20) for iodine isotopes. The calculation was made under the assumption that the charge distribution resulting from the fission of a single nuclide in this energy range is the same as that observed from the fission of U^{235} with thermal and with 14-Mev neutrons, with Z_p calculated via the ECD mechanism. The charge distribution resulting from the fission of a range of nuclides is then the sum of the separate distributions weighted by the number distribution for the fissioning nuclides (i.e. those of Z^2/A greater than 36.0) deduced from the above analysis. The calculated and observed distributions are shown in Fig. 4.

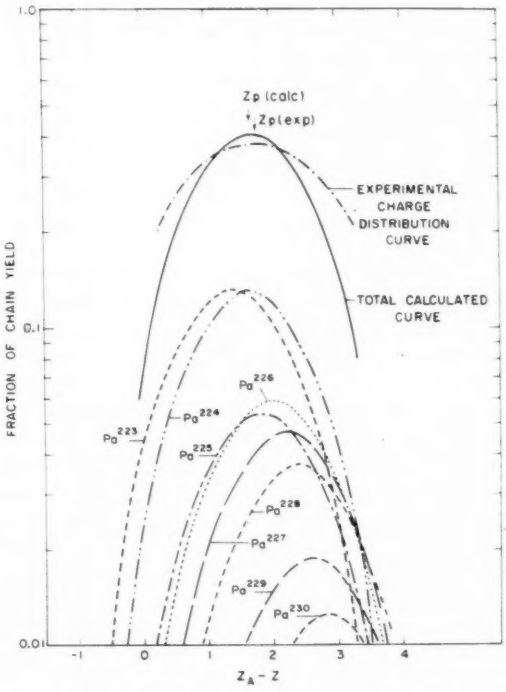

FIG. 4. Experimental and calculated fission product charge distributions in fission of Th^{232} induced by 83-Mev protons.

It is seen that the experimental distribution is wider than that calculated (although the Z_p values agree). This presumably reflects among other things the effect of one simplification made in this part of the analysis, namely that neutron-emission results in the loss of a constant amount of energy. Incorporation of a more realistic distribution of neutron-emission energies would presumably lead to a wider number distribution of fissioning nuclei, and hence a wider charge distribution.

(iii) U^{238} + *480-Mev Protons*

The experimental data for this system will be compared with the results of an analysis starting with the prompt cascade calculations for 450-Mev protons incident on U^{238} (18). Figure 5 shows again the Z versus N plot with the target nucleus enclosed in heavy lines. The frequency distribution from the prompt cascades is shown underlined in the top right-hand corner of each square.

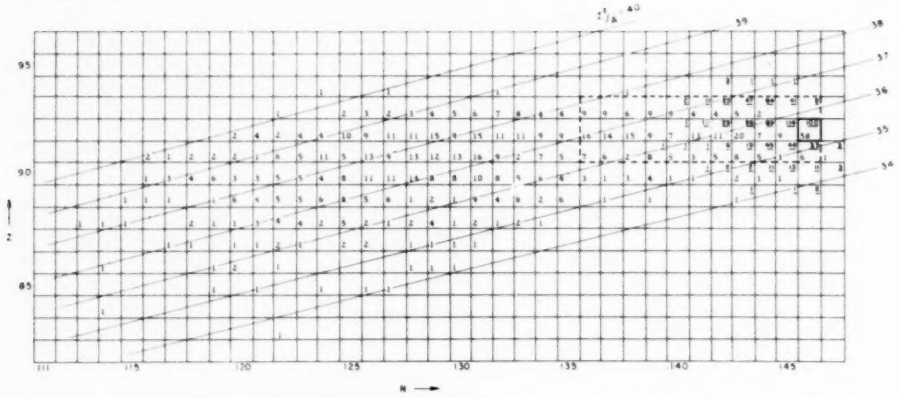

FIG. 5. Prompt cascade and evaporation reactions in uranium bombarded with 450-Mev protons.

At the excitation energies obtained in this system, charged particle emission from the product nuclei during the evaporation process is common, and no useful simplification in the treatment of that part of the reaction can be made. Consequently, from the evaporation–reaction calculations individual cascades have been chosen in which the initial A, Z, and E values match as closely as possible those for the products of individual prompt interaction cascades. These evaporation cascades have been used to specify the end product and intermediate products of the de-excitation process. The number of evaporation cascades that have been calculated is such that close matching is not difficult, and the sequence in which the data have been used is such as to ensure a random choice from among the prompt interaction and evaporation cascade data employed. The resulting number distribution of de-excited end products is shown in Fig. 5 in the bottom left-hand corner of each square. The region covered by Fig. 2 is shown enclosed in a dotted line to emphasize the much greater extent of particle emission induced at the higher bombarding energy. Also on Fig. 5 are shown lines connecting nuclides of equal Z^2/A value.

Additional information which may be obtained includes the number of de-excitation cascades which results in the transient formation of each nuclide and the spectrum of excitation energies with which it is formed.

Fission competition may now be introduced under the assumptions outlined earlier. The analysis is simplified by the general observation that the early part of a de-excitation cascade, when the excitation is highest, is characterized by emission of protons, neutrons, and alpha particles in such proportions that the evaporation "path" proceeds parallel to or towards the nuclear stability line. In the later, low-energy part of the cascade, however, coulomb effects predominate and neutron emission is favored. Consequently the Z^2/A value of nuclides successively formed in the de-excitation process generally decreases at first and then increases again, in a fairly smooth manner. Thus selection

of events producing nuclides of a given Z^2/A (particularly at the higher Z^2/A values) does not introduce serious error owing to the fact that a given event may be counted more than once.

Owing to the wide range of mass numbers produced, the variation of yield of fission fragments of a given mass with mass number can no longer be neglected. As an approximation, during the averaging of the product n/p ratios, weighting for mass yield will be accomplished using the over-all mass-yield curve given by Lavrukhina and Krasavina (15) in addition to weighting by the number distribution. The error made by use of the over-all mass-yield distribution rather than the distribution appropriate to fission of a single nucleus is probably small, since the effect of weighting for mass yield is in any case quite small.

In Part 2 of the analysis, in which fission is considered to take place from excited nuclei, it is again assumed that the total excitation of the system is unchanged during the fission process, and that, on the average, it divides among the products in the ratio of their masses. This division reduces the excitation energy per fragment in general to below 150 Mev, in which region the calculations of Dostrovsky *et al.* (5) predict a predominance of neutron emission. The de-excitation of the fission fragments is then presumed to take place in this manner with an energy loss per neutron evaporation of about 11 Mev, an average figure for this energy and mass region.

The results of the analysis are shown in Table III, with n/p ratios given for fission fragments of mass about 90 and about 130, calculated under the various parameter choices.

TABLE III

CALCULATED AVERAGE n/p RATIOS FOR THE PRODUCTS OF THE FISSION OF U^{238} WITH 450-MEV PROTONS

1. Fission occurs after de-excitation by particle evaporation in nuclides with greater than a given Z^2/A value

Z^2/A greater than	ECD-type fission		UCD-type fission	
	$A = 90$	$A = 130$	$A = 90$	$A = 130$
40	1.200	1.330	1.261	1.262
39	1.233	1.361	1.301	1.302
38	1.253	1.385	1.333	1.336
37	1.285	1.417	1.365	1.370
36	1.318	1.444	1.403	1.410
35	1.346	1.464	1.420	1.428

Experimental values: Mass 90 ~ 1.36
Mass 130 ~ 1.44–1.46

2. Fission occurs at given Z^2/A value before complete de-excitation

	ECD-type fission				UCD-type fission			
	$A = 90$		$A = 130$		$A = 90$		$A = 130$	
Z^2/A	n/p ratio of initial fragments	n/p after de-excitation	n/p before de-excitation	n/p after de-excitation	n/p before de-excitation	n/p after de-excitation	n/p before de-excitation	n/p after de-excitation
40	1.211	1.210	1.353	1.344	1.299	1.288	1.300	1.289
39	1.252	1.227	1.379	1.358	1.320	1.307	1.323	1.311
38	1.297	1.256	1.434	1.390	1.373	1.334	1.378	1.338
37	1.368	1.299	1.487	1.408	1.430	1.360	1.441	1.366
36	1.448	1.353	1.544	1.436	1.477	1.380	1.497	1.399
35	1.484	1.367	1.558	1.463	1.485	1.400	1.509	1.419

Experimental values: Mass 90 ~ 1.36
Mass 130 ~ 1.44–1.46

The most probable n/p ratios observed by Lavrukhina and Krasavina (15) are as follows: for mass 90, about 1.36; and for mass 130, 1.44 to 1.46 depending on which of the presentations of the data one uses. The agreement of the calculations with these figures is good for ECD-type fission and poor for UCD-type fission, being the best for the assumption that fission occurs before complete de-excitation and when a Z^2/A value between 35 and 36 is reached. However, a decision between the assumptions of Parts (1) and (2) of the analysis cannot be made as definitely as one between the two fission modes.

The value of Z^2/A found for best fit with experiment is close to that found in Part (ii) and is satisfactory for the same reasons.

If one calculates the fission cross section expected from the above results, in the same way as described in Section (ii), one obtains the value of 1.32 barns compared with an experimental value of 1.12 barns (15).

C. DISCUSSION

Within its limitations, the analysis described above leads to the conclusion that fission of nuclides with Z in the range 87–93 with excitation energies up to a few hundred Mev proceeds predominantly via a process described by the equal-charge displacement mechanism. There is also some indication (from Part (iii)) that fission of these nuclides begins to compete effectively with particle emission when the Z^2/A value is greater than about 36, in a fashion independent of energy. This last conclusion is generally in agreement with conclusions drawn from lower energy studies (1, 28), and in disagreement with the results of an analysis by Shamov (24).

The indication of an equal charge displacement mechanism in the fission of uranium and thorium with protons of energy up to 480 Mev, which is in disagreement with some previously published conclusions (15, 28), is at first surprising, since ECD has hitherto been considered a low-energy process. However, it may well be that ECD-type fission is characteristic of nuclides of specific charge and mass, rather than of specific energy. This is consistent with the observation by Porile and Sugarman (21) that ECD-type fission occurs when bismuth is bombarded with 450-Mev protons but that UCD-type fission occurs in tantalum bombarded with protons of the same energy.

D. ACKNOWLEDGMENTS

It is a pleasure to acknowledge the generosity of N. Metropolis *et al.* in making available to the author the material of references (17) and (18) prior to publication, and of I. Dostrovsky and G. Friedlander in providing access to the data of reference (5) prior to publication. The author is also very grateful to his colleagues in the Brookhaven National Laboratory Chemistry Department and to L. Yaffe for a number of stimulating discussions and for criticisms of the manuscript. The technical assistance of Mrs. E. McIver and Mrs. P. Payne with much of the tedious analysis is also gratefully acknowledged.

REFERENCES

1. Batzel, R. E. Univ. of Calif. Radiation Lab. Rept. UCRL 4303 (1954).
2. Bohr, N. Science, **86**, 161 (1937).
3. Bowles, B. J., Brown, F., and Butler, J. P. Phys. Rev. **107**, 751 (1957).
4. Crane, W. W. T., Higgins, G. H., and Bowman, H. R. Phys. Rev. **101**, 1804 (1956).
5. Dostrovsky, I., Rabinowitz, P., and Bivins, R. Phys. Rev. (1958) (In press).
6. Fong, P. Phys. Rev. **102**, 434 (1956).
7. Glendenin, L., Coryell, C. D., and Edwards, R. R. Phys. Rev. **75**, 337 (1949).
8. Glendenin, L. Ph.D. Thesis. Massachusetts Institute of Technology. 1949.
9. Goeckermann, R. H. and Perlman, I. Phys. Rev. **76**, 628 (1949).

10. GOLDBERGER, M. L. Phys. Rev. **74**, 1269 (1948).
11. HARDING, G. N. and FARLEY, F. J. M. Proc. Phys. Soc. (London), A, **69**, 853 (1956).
12. HICKS, D. A., ISE, J., JR., and PYLE, R. V. Phys. Rev. **101**, 1016 (1956).
13. HUIZENGA, J. R. Phys. Rev. **109**, 484 (1958).
14. IGO, G. and WEGNER, H. E. Phys. Rev. **102**, 1364 (1956).
15. LAVRUKHINA, A. K. and KRASAVINA, L. D. J. Nuclear Energy, **5**, 236 (1957).
16. LECOUTEUR, K. J. Proc. Phys. Soc. (London), A, **63**, 259 (1950).
17. METROPOLIS, N., BIVINS, R., STORM, M., TURKEVICH, A., MILLER, J. M., and FRIEDLANDER, G. Phys. Rev. **110**, 185 (1958).
18. METROPOLIS, N., BIVINS, R., STORM, M., MILLER, J. M., FRIEDLANDER, G., and TURKEVICH, A. Phys. Rev. **110**, 204 (1958).
19. PAPPAS, A. C. Ph.D. Thesis. Massachusetts Institute of Technology. 1953.
20. PATE, B. D., FOSTER, J. S., and YAFFE, L. Can. J. Chem. **36**, 1691 (1958).
21. PORILE, N. T. and SUGARMAN, N. Phys. Rev. **107**, 1410 (1957).
22. RIDDELL, J. Atomic Energy of Canada Ltd. Rept. No. CRP-654 (1956).
23. SERBER, R. Phys. Rev. **72**, 1114 (1947).
24. SHAMOV, V. P. J. Exptl. Theoret. Phys. (U.S.S.R.), **33**, 346 (1957). *Translated in* Soviet Phys. J. E. T. P. **6**, 268 (1958).
25. SPENCE, R. W. and FORD, G. P. Ann. Rev. Nuclear Sci. **2**, 399 (1953).
26. TEWES, H. A. and JAMES, R. A. Phys. Rev. **88**, 860 (1952).
27. VANDENBOSCH, R. and SEABORG, G. T. Univ. of Calif. Radiation Lab. Rept. UCRL-8047 (1957).
28. VANDENBOSCH, R., THOMAS, T. D., VANDENBOSCH, S. E., GLASS, R. A., and SEABORG, G. T. Univ. of Calif. Radiation Lab. Rept. UCRL-8032-Rev. (1958).
29. WAHL, A. C. Phys. Rev. **99**, 730 (1955).
30. WEISSKOPF, V. F. Phys. Rev. **52**, 295 (1937).

THE PREPARATION OF SOME DERIVATIVES OF D-RIBONO-1→4-LACTONE AND D-RIBITOL[1]

L. Hough,[2] J. K. N. Jones, and D. L. Mitchell[2]

ABSTRACT

Reaction of D-ribono-1→4-lactone with acetone gave the 2,3-*O*-isopropylidene derivative from which 5-*O*-methyl-D-ribitol, 5-deoxy-D-ribitol, and 2,3-*O*-isopropylidene-D-ribitol were prepared.

INTRODUCTION

5-Deoxy and 5-*O*-substituted derivatives of D-ribitol were required and consequently attempts were made to prepare from D-ribono-1→4-lactone (I) the 2,3-*O*-isopropylidene intermediate (II) for specific substitution of the primary alcohol group (e.g. methylation, tosylation), followed by reduction of the lactone function and finally hydrolysis of the ketal. D-Ribono-1→4-lactone (I) readily condensed with acetone, the reaction being catalyzed by concentrated and dilute mineral acid or anhydrous copper sulphate, although it also underwent condensation with acetone, without any added catalyst, because of the favored *cis*-configuration of the hydroxyls at carbons 2 and 3. The formation of the *O*-isopropylidene derivative was accompanied by a significant change in optical rotation which fell from an initial value of $[\alpha]_D$ 43° to an approximate value of $[\alpha]_D$ −80°. The rate and extent of the condensation reaction was dependent upon the catalyst selected and in particular on the concentration of the mineral acid. Hydrolysis of the lactone derivative (II) in water proceeded slowly in a manner typical of a 1→4 lactone, but the presence of an *O*-isopropylidene ring superimposed on the lactone ring may make this evidence unreliable. The position of the ketal ring was located by reaction of the sodium *O*-isopropylidene-D-ribonate (III), obtained by mild alkaline hydrolysis of the lactone derivative (II), with sodium metaperiodate which resulted in the consumption of 1.03 moles of oxidant and the formation of 1.02 moles of formaldehyde. The *O*-isopropylidene group must therefore be situated at carbons 2 and 3. This was confirmed by methylation of the 2,3-*O*-isopropylidene-D-ribonolactone (II), followed by mild acid hydrolysis of the mono-*O*-methyl derivative (IV) to produce in good yield 5-*O*-methyl-D-ribono-1→4-lactone (V); this compound was identical with the lactone obtained by the alkaline-bromine oxidation of 5-*O*-methyl-D-ribose (1). The methylation evidence is thus compatible with the presence of a 1→4 lactone ring in the *O*-isopropylidene derivative (II). The possibility that the change in optical rotation prior to or during ketal formation was due to a ring shift from a 1→5- to the 1→4-lactone was considered. However, the original D-ribonolactone slowly hydrolyzed in water at room temperature [$[\alpha]_D$ 17.8° (initial) → $[\alpha]_D$ 8° (13 days)], a property characteristic of 1→4-lactones (2) and the magnitude of the values recorded by Rehorst for L-ribono-1→4-lactone is similar (3). 2,3-*O*-Isopropylidene-D-ribono-1→4-lactone and D-ribonolactone possessed an infrared absorption maximum at 1790 cm^{-1} and 1793 cm^{-1} respectively, which is consistent with the 1→4-lactone structure (cf. reference 3 (*a*)). The stabilizing effect of the exocyclic double bond, thus making carbon 1 trigonal, must be a considerable influence in this case because the *cis*-hydroxyls at carbons 2 and 3 would be expected to create steric pressure as a result of the close proximity of these groups on a five-membered ring.

[1]*Manuscript received July 4, 1958.*
Contribution from the Department of Chemistry, Queen's University, Kingston, Ontario, and the Department of Organic Chemistry, The University, Bristol 8, England.
[2]*Present address: Department of Organic Chemistry, The University, Bristol 8, England.*

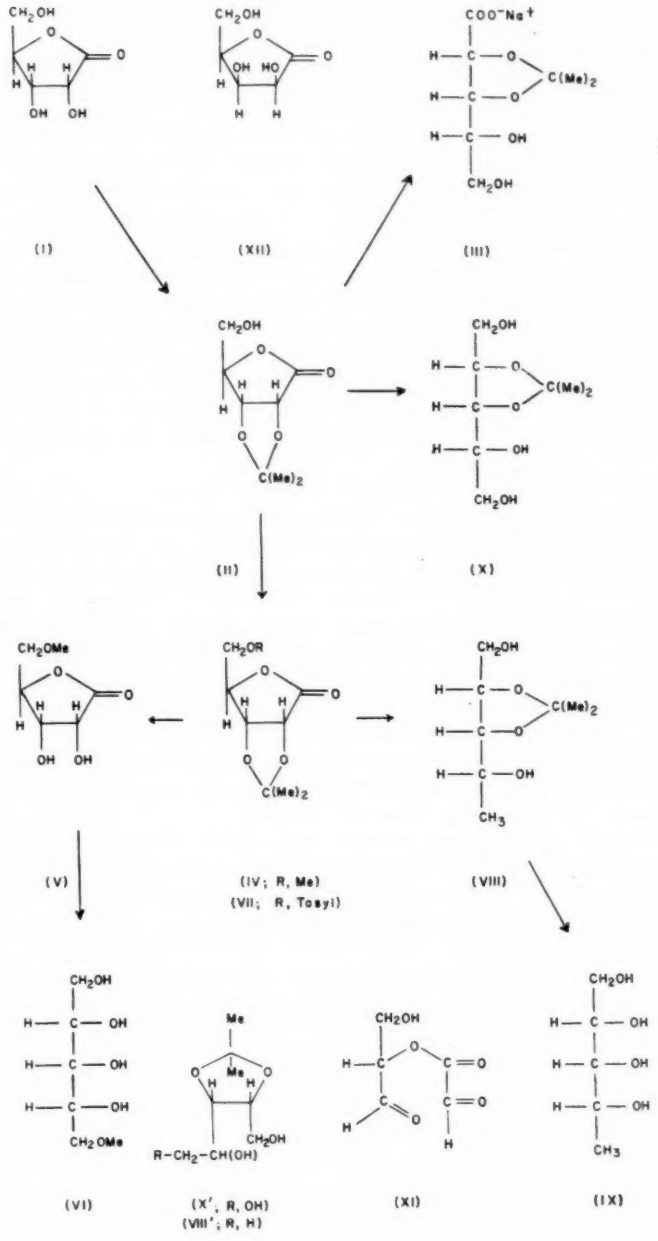
(I)
(XII)
(III)
(II)
(X)
(V)
(IV; R, Me)
(VII; R, Tosyl)
(VIII)
(VI)
(X', R, OH)
(VIII'; R, H)
(XI)
(IX)

Recent studies on the periodate oxidation of monosaccharides at pH 3.6 have revealed that they are oxidized almost completely in their ring forms with the formation of esters (formyl, glycollyl, and glyoxylyl) of glyceraldehyde and glycollaldehyde, further oxidation being dependent upon the rate of hydrolysis of the ester intermediates (4, 5). Similar oxidations of 1→4- and 1→5-pentonolactones would be expected to give rise to glyoxylic acid esters of glyceraldehyde (XI) and glycollaldehyde respectively. However, the former ester should be distinguished by a fairly rapid overoxidation reaction because the electrophilic hydroxyl group (from carbon 5) neighboring the ester linkage would facilitate its hydrolysis. In accord with this theory D-ribono-1→4-lactone and its 5-*O*-methyl derivative each consumed approximately one mole of periodate rapidly, which was followed by a slower but extensive oxidation, typical of 2-*O*-esters of glyceraldehyde to the approximate theoretical values (Fig. 1). Lactobiono-1→5-lactone behaved similarly after the initial rapid reaction with 3 moles of periodate (Fig. 1). The similarity between the oxidation curves of D-ribonolactone and 5-*O*-methyl-D-ribono-1→4-lactone would suggest that the former compound was indeed oxidized as a 1→4-lactone and it therefore seems likely that the change in optical rotation during acetonation cannot be ascribed to a ring shift (1→5- to 1→4-lactone), but must actually be related to the formation of the ketal ring.

1→4-Lactones are believed to be planar or nearly planar, but some degree of ring buckling might arise in the pentono- and hexono-lactones if the molecule possesses a bulky group at carbon 5 and substituents at carbons 2 and 3 in the true *cis*-configuration (XII) (cf. reference 5 (*a*)). Deviations from planarity have been observed in the D-ribofuranosyl ring system of crystalline adenosine (6) by X-ray analysis, but 1→4-lactol and 1→4-lactone ring systems are not precisely comparable. A shift in molecular rotation which should measure approximately the extent of ring buckling has been observed for 2,3-di-*O*-methyl-D-ribono-1→4-lactone and 2,3,5-tri-*O*-methyl-D-ribono-1→4-lactone (Table I). Such an effect is probably responsible for the large molecular rotational shift in the formation of 2,3-*O*-isopropylidene-D-ribono-1→4-lactone, although buckling of the lactone ring will result in a distortion of the *O*-isopropylidene ring which will then be asymmetric (cf. D-galactose and its 1,2-3,4-di-*O*-isopropylidene derivative). Asymmetrical *O*-isopropylidene rings have been suggested as being one of the factors responsible for molecular rotational shifts between methyl *O*-isopropylidene pyranosides and the corresponding methyl pyranosides (7). The substitution of a methoxyl group for the hydroxyl group at carbon 5 of various D-ribono-1→4-lactone derivatives results in a molecular rotational shift (in the positive direction) of approximately the same magnitude for each pair (Table I).

Tosylation of 2,3-*O*-isopropylidene-D-ribono-1→4-lactone (II) at a low temperature (*ca.* −20° C; 10 hours) produced the 5-*O*-tosyl derivative (VII) in quantitative yield.

TABLE I

ROTATIONS OF DERIVATIVES OF D-RIBONO-1→4-LACTONE IN WATER

	$[\alpha]_D$	M_D	Difference	Reference
D-Ribono-1→4-lactone	17.8	2636	+1809	(*)
5-*O*-Methyl-lactone	27.4	4445		(1)
2,3-Di-*O*-methyl-lactone	−31.5	−5538	+1754	(8)
2,3,5-Tri-*O*-methyl-lactone	−19	−3784		(9)
2,3-*O*-Isopropylidene-lactone	−57.5	−10820	+1900	(*)
2,3-*O*-Isopropylidene-5-*O*-methyl-lactone	−44.1	−8920		(*)

*Present paper.

When higher reaction temperatures and longer reaction periods were employed, lower yields and tarry products were often obtained. A simultaneous reduction of the lactone function to the primary alcohol and reductive cleavage of the tosyloxy group was effected in good yield by lithium aluminum hydride in tetrahydrofuran to give 2,3-*O*-isopropylidene-5-deoxy-D-ribitol (VIII). Hydrolysis of the product with cation exchange resin (H form) afforded 5-deoxy-D-ribitol (IX). Similarly, 5-*O*-methyl-D-ribono-1→4-lactone (V) and 2,3-*O*-isopropylidene-D-ribono-1→4-lactone (II) were reduced with lithium aluminum hydride to syrupy 5-*O*-methyl-D-ribitol (VI) and syrupy 2,3-*O*-isopropylidene-D-ribitol (X) respectively. The structures were verified by periodate oxidation experiments (Table III).

2,3-*O*-Isopropylidene-D-ribitol compounds are of interest because D-erythro hydroxyls are involved in the formation of a five-membered ketal ring of the αC-type (10, 11, 12) with bulky substituents in the *cis*-configuration at carbons 2 and 3. This unfavorable conformation (VIII′ and X′) would be expected to cause the ketal ring to be labile to acid, since deformation from the preferred zigzag conformation is considerable.

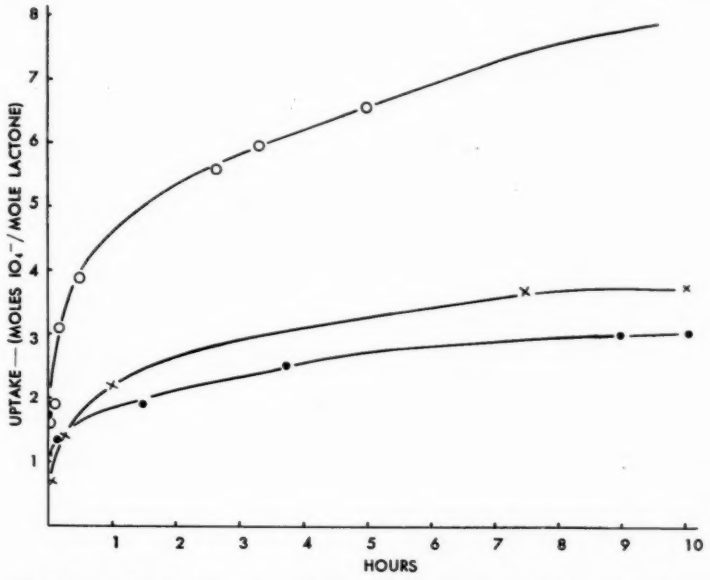

FIG. 1. Periodate oxidation of: —×— D-ribono-1→4-lactone (3.75–18.5 hours); —●— 5-*O*-methyl-D-ribono-1→4-lactone (3.05–21.0 hours); and —○— lactobiono-1→5-lactone (8.5–48 hours) (8.55–75 hours) at pH 3.7.

EXPERIMENTAL

Solutions were concentrated under reduced pressure (*ca.* 15 mm). Melting points were uncorrected and optical rotations were determined in water unless otherwise stated. Paper chromatography was carried out by the descending method (13) on Whatman No. 1 filter paper using the following solvent systems (v:v): (*a*) ethyl acetate – acetic acid – water (9:2:2); (*b*) ethyl acetate – acetic acid – formic acid – water (18:3:1:4); (*c*) butan-1-ol–ethanol–water (40:11:19); and (*d*) butan-1-ol–pyridine–water (10:3:3). Non-reducing compounds were detected on paper chromatograms with an alkaline

silver nitrate spray reagent (14). The rate of movement of the compound on paper chromatograms is quoted relative to that of the solvent front (R_f value). Wave numbers of infrared data are given to within $\pm 10\ cm^{-1}$.

*2,3-O-Isopropylidene-*D*-ribono-1→4-lactone*

(Assisted by R. J. Stoodley.) A solution of D-ribono-1→4-lactone (15 g) in acetone (600 ml) containing concentrated hydrochloric acid (6 ml) was shaken continuously for 18 hours at 25° C. The initial positive rotation decreased rapidly to reach a constant negative value (Table II). A control solution of D-ribono-1→4-lactone in dioxane and concentrated hydrochloric acid (2 drops) showed a relatively small change in optical rotation (Table II).

The solution was neutralized (silver or lead carbonate) and the inorganic salts were separated by filtration through a pad of cellulose. The combined filtrate and washings deposited crystals when concentrated. After trituration with cold acetone – light petroleum (b.p. 60–80° C), the crystals (14.0 g; 73.5%) were collected on a suction filter. They had a melting point of 138–139° C, $[\alpha]_D^{25°}$ −57.5° (initial value; *c*, 2.3) → −16.1° (20 days) and $[\alpha]_D^{24°}$ −65.7° (*c*, 2.13, pyridine; unchanged after 80 hours). ν_{max} 1790 cm^{-1} (chloroform; *C* = O for 1→4-lactone (15, 16)). D-Ribono-1→4-lactone gave an adsorption peak at 1793 cm^{-1} (nujol). Recrystallization from acetone–cyclohexane did not affect these constants. Anal. Calc. for $C_8H_{12}O_5$: C, 51.1; H, 6.4. Found: C, 51.4; H, 6.4.

When the condensation was catalyzed by 2 *N* hydrochloric acid (1% v:v), the rotation decreased less rapidly and reached a final rotation of $[\alpha]_D^{25°}$ −62.5° (30 hours).

A 5% solution of D-ribono-1→4-lactone in acetone revealed a polarimetric behavior similar to the acid-catalyzed reaction (Table II). After the optical rotation had reached a constant value, crystals of 2,3-*O*-isopropylidene-D-ribono-1→4-lactone were deposited, when the solution was concentrated.

TABLE II

OPTICAL ROTATION OF D-RIBONO-1→4-LACTONE IN VARIOUS SOLVENTS AT 25° C

Acidified acetone, *c* = 2.48	Hours:	0	0.33	0.5	2.8	3.8	15.8	18.3
	$[\alpha]_D$:	42.3°	−25°	−44.4°	−77.4°	−79°	−82.3°	−82.3°
Acidified dioxane, *c* = 2.5	Hours:	0	0.1	2.0	3.5	6.3	24.0	30.7
	$[\alpha]_D$:	52°	49.5°	48.5°	48°	46.8°	45°	43.6°
Water, *c* = 2.3	Hours:	0.25	23.0	42.5	66.2	90.5	138.5	322.8
	$[\alpha]_D$:	17.8°	17.4°	16.1°	14.8°	13.9°	11.7°	8.0°
Acetone, *c* = 5.0	Hours:	0.3	7	19	27	48	115	213
	$[\alpha]_D$ at 26° C:	39.8°	29.3°	7.4°	−3.9°	−24.2°	−48.7°	−65.2°

A solution of D-ribono-1→4-lactone (25 g) in acetone (500 ml) was heated under reflux in anhydrous conditions (calcium chloride tube). The optical rotation of the reaction mixture fell slowly, reaching a value of $[\alpha]_D^{25°}$ −8° after 92 hours. Anhydrous copper sulphate (5 g) was then added to the solution and the optical rotation fell to $[\alpha]_D^{25°}$ −77° (192.5 hours). The filtered solution was concentrated to a crystalline mass which was recrystallized from acetone – light petroleum (b.p. 60–80° C) to yield the *O*-isopropylidene derivative (21.5 g; 67%).

*2,3-O-Isopropylidene-5-O-methyl-*D*-ribono-1→4-lactone*

2,3-*O*-Isopropylidene-D-ribono-1→4-lactone (5.28 g) was treated three times with methyl iodide and active silver oxide (in the presence of anhydrous calcium sulphate), to aid solution chloroform was added to the first methylation. After filtration, the silver salts were thoroughly digested with chloroform. Concentration of the combined filtrates

yielded a pale yellow syrup (6.0 g) which was distilled at 90–100° C (bath temp.) and 10^{-5} mm to give the 5-*O*-methyl derivative [4.76 g; 84% with $n_D^{23°}$ 1.4490 at 90° C, $n_D^{23°}$ 1.4500 at 100° C, $[\alpha]_D^{27°}$ −56.8° (*c*, 3.0 ethanol), and $[\alpha]_D^{26°}$ −44.1° (*c*, 2.5)]. Anal. Calc. for $C_9H_{14}O_5$: C, 53.45; H, 7.0; OMe, 15.35. Found: C, 53.4; H, 7.5; OMe, 17.2.

*5-O-Methyl-*D*-ribono-1→4-lactone*

A mixture of a solution of 2,3-*O*-isopropylidene-5-*O*-methyl-D-ribono-1→4-lactone (4.5 g) in 40% aqueous acetone (100 ml) together with Amberlite resin IR-120 (H) (3 ml) was treated under reflux at 50° C. The initial specific rotation, $[\alpha]_D^{27°}$ −42.7°, rose to $[\alpha]_D^{27°}$ 9.5° (constant value; 60 hours). After it had been cooled, the solution was decanted from the resin, concentrated to a crystalline mass, and recrystallized from ethyl acetate to give 5-*O*-methyl-D-ribono-1→4-lactone (2.3 g; 63.5%) with m.p. 110–111° C, mixed m.p. 108.5–110° C, $[\alpha]_D^{25°}$ 26° (0.08 hours) → 19° (168 hours) (*c*, 0.94). R_f 0.71 (solvent *b*) and R_f 0.67 (solvent *d*). ν_{max} 1765 cm^{-1} (nujol) [lit. m.p. 109–110° C, $[\alpha]_D^{18°}$ 27.4° → 15.3° (7 hours; *c*, 9.0) (1)]. Anal.Calc. for $C_6H_{10}O_5$: C, 44.4; H, 6.2; OMe, 19.1. Found: C, 44.8; H, 6.2; OMe, 19.9.

*5-O-Methyl-*D*-ribitol*

A solution of 5-*O*-methyl-D-ribono-1→4-lactone (1.0 g) in anhydrous tetrahydrofuran (25 ml) was added dropwise to a suspension of lithium aluminum hydride (0.57 g) in tetrahydrofuran (25 ml). After the mixture had been heated under reflux for 4 hours, then cooled, ethyl acetate (2 ml) was added, followed by 70% aqueous alcohol (100 ml). The precipitate was separated by centrifugation and was washed twice with ethanol. The combined supernatants were percolated through Amberlite IR-120 (H) resin prior to concentration to a colorless syrup (0.78 g; 76%). Paper chromatographic examination of the compound revealed only a single spot with R_f 0.40 (solvent *b*), R_f 0.42 (solvent *d*), $[\alpha]_D^{25°}$ 10° (*c*, 1.0), and $n_D^{20°}$ 1.4802. Anal. Calc. for $C_6H_{14}O_5$: C, 43.4; H, 8.5; OMe, 18.7. Found: C, 43.5; H, 7.8; OMe, 20.6.

*2,3-O-Isopropylidene-5-O-toluene-p-sulphonyl-*D*-ribono-1→4-lactone*

2,3-*O*-Isopropylidene-D-ribono-1→4-lactone (1.13 g) was dissolved in cold (−20° C), anhydrous pyridine and toluene-*p*-sulphonyl chloride (2.38 g; 100% excess) was added in one portion. After the mixture had been kept for 10 hours at −20° C, with intermittent shaking, water (0.5 ml) was added and the solution was poured slowly into ice water (600 ml) with vigorous stirring. The crystals were collected by filtration and dried under reduced pressure at room temperature (2.07 g; 100%). Recrystallization from methanol gave prisms melting at 117.5–118° C and with $[\alpha]_D^{24°}$ −15.8° (*c*, 2.4 acetone). ν_{max} 1810 cm^{-1} (chloroform). Anal. Calc. for $C_{15}H_{18}O_7S$: C, 52.6; H, 5.3; S, 9.4. Found: C, 52.7; H, 5.3; S, 9.7.

*2,3-O-Isopropylidene-5-deoxy-*D*-ribitol*

To a suspension of lithium aluminum hydride (5.5 g) in anhydrous tetrahydrofuran (50 ml), a solution of 2,3-*O*-isopropylidene-5-*O*-toluene-*p*-sulphonyl-D-ribono-1→4-lactone (5.38 g) in tetrahydrofuran (50 ml) was added dropwise. The reaction mixture was heated under reflux for 5 hours, then ethyl acetate (20 ml) was slowly added dropwise, followed by 10% aqueous ethanol until the inorganic salts were precipitated. After filtration, the organic solvents were evaporated by repeated dilution with water and the product, obtained by continuous extraction with chloroform, was a syrup (2.38 g; 84%) with $n_D^{20°}$ 1.4510 and $[\alpha]_D^{27°}$ −15.5° (*c*, 2.7, ethanol). Anal. Calc. for $C_8H_{16}O_4$: C, 54.5; H, 9.15. Found: C, 52.9; H, 9.2.

TABLE III

RESULTS OF PERIODATE OXIDATION EXPERIMENTS

Compound	Determination	pH	Time (hours)								
			0.08	0.15	0.25	0.50	0.66	1.0	3.5	4.0	
D-Ribitol	Uptake*	7.5	4.0		4.0						(4.0–1.7 hr)
2,3-*O*-Isopropylidene-D-ribono-1→4-lactone	Uptake*	U	0.08		0.08		0.08	0.08			
Sodium 2,3-*O*-isopropylidene-D-ribonate	Uptake*	10		0.92	0.99	1.03		1.03	1.03		
	Formaldehyde*	10	0.94		0.95			1.02	1.02		
Sodium 5-*O*-methyl-D-ribonate	Uptake*		2.3		2.65	2.84		2.94	2.97	2.99	
	Formaldehyde*	10									(Nil–24 hr)
5-*O*-Methyl-D-ribono-l→4-lactone	Uptake*	3.7	1.38	1.34					2.52		(3.0–9.0 hr)
											(3.05–21 hr)
	Formaldehyde*	3.7									(Nil–13 hr)
5-*O*-Methyl-D-ribitol	Uptake*			2.23		2.38		2.48		2.50	
	Acid*									1.4	(1.5–20.5 hr)
	Formaldehyde*	U			0.88	0.88		0.89			
2,3-*O*-Isopropylidene-5-deoxy-D-ribitol	Uptake*	U		0.02	0.08	0.04		0.04			
5-Deoxy-D-ribitol	Uptake*	7.5	2.24			3.01			3.14	3.16	
	Uptake*	U	2.99			2.96					(2.96–2.0 hr)
											(2.96–22 hr)
	Acid*	U	1.78			1.85					(1.78–2.5 hr)
											(1.74–23 hr)
	Formaldehyde*	U			1.02	1.09				1.03	(0.99–16.5 hr)
2,3-*O*-Isopropylidene-D-ribitol	Uptake*	U		0.93		0.89		0.90			(0.92–18 hr)
	Formaldehyde*	U			1.05	1.0				1.0	(0.95–16 hr)

U = Unbuffered.
*In moles of periodate per mole substrate.

5-Deoxy-D-ribitol

The above *O*-isopropylidene compound (2.09 g) was hydrolyzed with Amberlite IR-120 (H) resin under the conditions previously described for the preparation of 5-*O*-methyl-D-ribono-1→4-lactone. The product (1.51 g; 93%) crystallized spontaneously when the solution was concentrated to dryness. Recrystallization from ethyl acetate – methanol (5:1 v:v) gave 5-deoxy-D-ribitol with m.p. 77–80° C. The product contained solvent of crystallization which could be removed under reduced pressure to give a product melting at 65–69° C and $[\alpha]_D^{25°}$ −10.6° (*c*, 1.7). Anal. Calc. for $C_5H_{12}O_4$: C, 44.1; H, 8.9. Found: C, 44.1; H, 8.6.

2,3-O-Isopropylidene-D-ribitol

2,3-*O*-Isopropylidene-D-ribono-1→4-lactone (1.50 g) was treated with lithium aluminum hydride by the method described for the preparation of 5-*O*-methyl-D-ribitol, except the reaction period was extended to 8 hours and the ion exchange resin, Amberlite IR-120, was used in the ammonium form. The syrupy product (1.6 g) moved on paper chromatograms as a single spot (R_f 0.39; solvent *b*) and had $[\alpha]_D^{26°}$ −4.3° (*c*, 2.8, ethanol), $n_D^{20°}$ 1.4730. Anal. Calc. for $C_8H_{16}O_5$: C, 50.0; H, 8.4. Found: C, 49.2; H, 8.0.

D-*Ribitol* (*Adonitol*)

2,3-*O*-Isopropylidene-D-ribono-1→4-lactone (130 mg) was dissolved in ethanol (5 ml) and sodium borohydride (93 mg) was added in one portion. The solution was heated at 50° C for 5 hours and then kept at room temperature overnight. After acidification with acetic acid, the solution was passed down a column of Amberlite resin IR-120 (H) and the effluent was evaporated to dryness. After removal of acetic and boric acids by repeated co-distillations with methanol, the syrupy product was hydrolyzed with 0.01 *N* sulphuric acid (10 ml, 3 hours, 95° C). The cooled solution was neutralized (barium carbonate), then filtered, and the filtrate concentrated to a syrup. Examination of the product in solvent systems (*a*) and (*c*) revealed a single component which had a rate of movement identical with that of an authentic specimen of adonitol. The syrup readily crystallized on seeding with adonitol (ribitol).

When the reduction was carried out using water as the solvent under the conditions described above, the major product was an acid (paper chromatography) and only a small amount of adonitol was detected.

Periodate Oxidation Experiments

All reactions were carried out in the dark and at room temperature (*ca.* 18°).

(i) *Determination of the Reacted Periodate*

The lactone or pentitol derivative (10–15 mg; accurately weighed) was dissolved in water or the required buffer solution containing 0.3 *M* sodium metaperiodate solution (1 or 2 ml). The total volume was made up to 10 ml with additional buffer solution. A blank was run concurrently. Aliquot portions (2 ml) were withdrawn at intervals and pipetted into phosphate buffer (pH 7.0; 25 ml) containing 20% potassium iodide solution (1–3 ml), and the liberated iodine was titrated with 0.01 *N* sodium thiosulphate solution using starch solution as indicator (17).

In some cases the lactone was hydrolyzed to the aldonic acid (sodium salt) with a slight excess of 0.01 *N* sodium hydroxide solution prior to the addition of the sodium metaperiodate solution and sufficient water to bring the total volume to 20 ml. (Buffer solutions: pH 7.5, 0.05 *M* sodium bicarbonate solution; pH 3.7, 0.05 *M* acetic acid – sodium acetate solution.)

(ii) *Estimation of the Formic Acid Produced*

Solutions containing *ca.* 5 mg of compound per milliliter of solution were oxidized with sodium metaperiodate solution under unbuffered conditions. At various intervals of time, ethylene glycol (1 ml) was added to aliquot portions (5 ml) and the acidic solution was titrated with 0.01 *N* sodium hydroxide solution using methyl red, screened with methylene blue as the indicator. A blank was run concurrently.

(iii) *Determination of the Formaldehyde Liberated*

Samples (2–4 mg; accurately weighed) were dissolved in water or buffer solution containing 0.3 *M* sodium metaperiodate solution (1 ml) and made up to 25 ml. At intervals, aliquot samples (1 ml) were withdrawn and the formaldehyde was estimated by the chromotropic acid method (18). A known weight of erythritol (periodate oxidized) was used as the source of formaldehyde for the preparation of the standard curve.

ACKNOWLEDGMENTS

The authors wish to thank Dr. G. R. Barker and Dr. D. C. C. Smith, of the University of Manchester, for a specimen of 5-*O*-methyl-D-ribono-1→4-lactone. They also wish to thank Mr. R. J. Stoodley for his assistance in the preparation of 2,3-*O*-isopropylidene-D-ribono-1→4-lactone, Messrs. B. S. Noyes and M. J. Graham for microanalyses, and Mr. M. C. B. Marshall for infrared absorption data. One of us (D.L.M.) thanks the Ontario Research Foundation for a grant which made this investigation possible.

REFERENCES

1. BARKER, G. R., NOONE, T. M., SMITH, D. C. C., and SPOORS, J. W. J. Chem. Soc. 1327 (1955).
2. DREW, H. D. K., GOODYEAR, E. H., and HAWORTH, W. N. J. Chem. Soc. 1237 (1927).
3. REHORST, K. Ann. **503**, 143 (1933). (*a*) BARKER, S. A., BOURNE, E. J., PINKARD, R. M., and WHIFFEN, D. H. Chem. & Ind. 658 (1958).
4. HOUGH, L., TAYLOR, T. J., THOMAS, G. H. S., and WOODS, B. M. J. Chem. Soc. 1212 (1958).
5. WARSI, S. A. and WHELAN, W. J. Chem. & Ind. 71 (1958). (*a*) COOKSON, R. C. Ann. Repts. (London), **54**, 173 (1957).
6. FURBERG, S. Acta Chem. Scand. **4**, 751 (1950).
7. REEVES, R. E. Advances in carbohydrate chemistry. Vol. 6. Academic Press, Inc., New York. 1951. p. 107.
8. BARKER, G. R. and SMITH, D. C. C. J. Chem. Soc. 1323 (1955).
9. LEVENE, P. A. and STILLER, E. T. J. Biol. Chem. **102**, 187 (1933).
10. BARKER, S. A. and BOURNE, E. J. J. Chem. Soc. 905 (1952).
11. BARKER, S. A., BOURNE, E. J., and WHIFFEN, D. H. J. Chem. Soc. 3865 (1952).
12. BARKER, S. A. and BOURNE, E. J. Advances in carbohydrate chemistry. Vol. 7. Academic Press, Inc., New York. 1952. p. 137.
13. PARTRIDGE, S. M. Biochem. J. **42**, 238 (1948).
14. TREVELYAN, W. E., PROCTOR, D. P., and HARRISON, J. S. Nature, **166**, 444 (1950).
15. ALI, M. E. and OWEN, L. N. J. Chem. Soc. 1074 (1958).
16. BELLAMY, L. J. The infra-red spectra of complex molecules. Methuen & Co. Ltd., London. 1954.
17. NEUMÜLLER, G. and VASSEUR, E. Arkiv Kemi, **5**, 235 (1953).
18. O'DEA, J. F. and GIBBONS, R. A. Biochem. J. **55**, 580 (1953).

THE REACTION OF 2,2-DIPHENYL-1-PICRYLHYDRAZYL WITH SECONDARY AMINES[1]

J. E. HAZELL[2] AND K. E. RUSSELL

ABSTRACT

The reaction of DPPH (2,2-diphenyl-1-picrylhydrazyl) with *N*-phenyl-1-naphthylamine, *N*-phenyl-2-naphthylamine, diphenylamine, and methylaniline has been studied and has been shown to be primarily a hydrogen abstraction process. Two moles DPPH react with 1–1.15 moles secondary amine to give 1.7–1.8 moles 2,2-diphenyl-1-picrylhydrazine and further products.

The reaction between DPPH and *N*-phenyl-1-naphthylamine is first order with respect to each reactant. The reaction of DPPH with the other amines is retarded by the major product 2,2-diphenyl-1-picrylhydrazine and the kinetics of the over-all reaction are complex. However second-order rate constants and activation energies have been obtained using initial rates of reaction. Possible reaction mechanisms are discussed.

This study of the reaction between 2,2-diphenyl-1-picrylhydrazyl (DPPH) and secondary amines forms part of a general investigation of the rates of hydrogen abstraction processes in solution using DPPH as the acceptor molecule. In spite of its existence as a stable free radical DPPH readily abstracts hydrogen atoms from mercaptans (1) and hydroaromatic compounds such as 1,4-dihydronaphthalene (2). A similar reactivity towards many secondary amines (3, 4), phenols, and hydrogen halides is observed. Rate studies on these reactions should give information concerning the influence of structure on the ease of hydrogen abstraction from the various donors.

As the acceptor molecule, DPPH has the advantage that it is a colored free radical which does not dimerize and its concentration can be estimated by its absorption in the visible region. However, it complexes with amines (3) and possibly with aromatic hydrocarbons (2) and such complexing may affect the kinetics of reaction. It may also be involved in steric effects which are not observed with small radicals.

In the present work the reactions between DPPH and certain secondary amines have been investigated with regard to stoichiometry and kinetics. It was hoped that the single hydrogen atom attached to nitrogen would be abstracted in the primary reaction. The secondary amines used were *N*-phenyl-1-naphthylamine, *N*-phenyl-2-naphthylamine, diphenylamine, and methylaniline. A few kinetic experiments were performed with di-*n*-propylamine.

EXPERIMENTAL

Materials

2,2-Diphenyl-1-picrylhydrazine and DPPH were prepared by the method of Goldschmidt and Renn (5). The hydrazyl crystals were heated to 75° *in vacuo* for 6 hours to break down a DPPH–chloroform complex.

Di-*n*-propylamine was distilled in a 20-plate column. Methylaniline was distilled under reduced pressure to give one sample. A second sample was obtained by conversion to the nitrosamine, followed by reduction with tin and hydrochloric acid and distillation. Diphenylamine was recrystallized from petroleum ether. The phenylnaphthylamines were recrystallized from 95% ethanol. The amines were stored in the dark.

[1]*Manuscript received in original form March 11, 1957, and, as revised, June 25, 1958.*
Contribution from the Department of Chemistry, Queen's University, Kingston, Ontario.
[2]*Milton Hersey Fellow 1955–56.*

Tetraphenylhydrazine was prepared by the oxidation of diphenylamine with lead dioxide (6). Diphenyldihydrophenazine was prepared by heating tetraphenylhydrazine in boiling toluene for 30 minutes (7); it was purified by dissolution in hot benzene and addition of 2 volumes of ethanol.

Alumina was deactivated by adding 500 g alumina to 20 cc water in a stoppered bottle.

Stoichiometry

Mixtures of DPPH and amine of varying ratio were made up in benzene, degassed, and heated to 55°. Reaction was virtually complete in less than an hour with the phenylnaphthylamines, but diphenylamine required some hours and methylaniline 2 days. If any significant amount of DPPH remained it gave a violet color to the solution. The results give an estimate of the number of moles DPPH reacting with 1 mole amine.

Benzene solutions of amine and DPPH, each at a known concentration (approximately 0.1 *M*), were heated to 55° until reaction was virtually complete, and were concentrated in an atmosphere of nitrogen. The products were separated on a column of deactivated alumina. Benzene was used as eluent.

The first fractions from the column contained the excess amine and part of the dehydrogenation products. The solvent was removed, and the amine was separated by careful treatment with small amounts of 95% ethanol in which the reaction products are almost insoluble; petroleum ether was used in the place of ethanol in the case of methylaniline. The phenylnaphthylamines and diphenylamine were identified by melting point and mixed melting point; methylaniline was identified by boiling point only. The excess amine was weighed in order to confirm the value of the DPPH to amine ratio determined colorimetrically.

The main fraction came down the column as a dark brown band. The solvent was removed from the eluate, the last traces of complexed benzene disappearing when the red solid was warmed *in vacuo*. The material was 1,1-diphenyl-2-picrylhydrazine, m.p. 170–171°, mixed m.p. 171–172°, and having an infrared spectrum identical with that of the pure hydrazine. It was weighed and the fraction of hydrazyl converted to hydrazine obtained. The infrared spectrum of the products in chloroform before separation on the column was compared with that of 1,1-diphenyl-2-picrylhydrazine at various concentrations. The results were consistent with the assumption that no hydrazine was produced or lost by reaction on the alumina column.

Further Products

In all cases a violet band of strongly adsorbed material appeared on the alumina column. It was removed by treating the alumina with ethanol. The yield was about 10% based on the amine reacting. The material was not identified, but a sample from the DPPH–diphenylamine reaction contained about 65% carbon suggesting that it was derived from the DPPH and was not simply a dehydrogenation product of the amine.

The first fractions from the column contained products derived from the dehydrogenated amine. The yields, based on the amine reacting, were 30%, 65%, 60%, and 40% respectively for methylaniline, diphenylamine, *N*-phenyl-1-naphthylamine, and *N*-phenyl-2-naphthylamine. In all cases some separation into bands occurred on the column, indicating the presence of more than one compound, but the separate fractions were impure judged by the wide temperature ranges over which they melted. A white solid, m.p. 128–132°, accounted for 40% of the amine reacting in the dehydrogenation of diphenylamine; the melting point was raised to 134–136° by admixture with tetra-

phenylhydrazine. Anal. Found: C, 86.37; H, 6.74. Calc. for $C_{24}H_{20}N_2$: C, 85.7; H, 6.00. Its infrared spectrum was almost identical with that of tetraphenylhydrazine; the absorption in the N–H stretching region was negligible, but weak bands below 1400 cm^{-1} indicate the possible presence of diphenyldihydrophenazine.

A yellow solid, m.p. 240–245°, accounted for 35% of the amine reacting in the dehydrogenation of *N*-phenyl-1-naphthylamine. Anal. Found: C, 87.4; H, 5.49. Calc. for $C_{32}H_{24}N_2$: C, 88.0; H, 5.54. Mol. wt. 480 (by Rast method). Oxidation of *N*-phenyl-1-naphthylamine with lead dioxide leads first to a red product and then to a yellow product, m.p. 266–268°, which gives the same analysis as the above solid. Infrared spectra of the two products are similar; a weak absorption at 3350 cm^{-1} is probably due to a minor impurity containing an N–H group. The yellow solid appears to be ultimately derived from two *N*-phenyl-1-naphthylamine molecules, but its structure is not known.

N-Phenyl-2-naphthylamine and methylaniline each gave a complex mixture of products. These were partially separated on the column but attempts to identify them were unsuccessful.

Kinetics

Reaction mixtures were prepared using measured amounts of benzene solutions of DPPH and amine. The reaction vessels were standard bore tubes of internal diameter 12 mm. The concentration of DPPH was followed by taking measurements of optical density with a Fisher electrophotometer. A 650 mμ filter was used because in this region the DPPH absorbs fairly strongly whereas the products of reaction absorb only weakly. The electrophotometer was adapted for constant temperature work by replacing the normal cell holder with a brass box with glass windows. Water from a Sargent thermostat was passed through the box by means of an Eastern Industries Circulating pump (Model B-1). Temperatures of 20°, 30°, 40°, and 50° were used and apart from the first 3 minutes of reaction the control was better than ±0.05°.

The experiments were normally performed in the presence of air. Experiments with degassed systems showed that oxygen had little or no effect on the initial rates of reaction. Degassing with the highly reactive phenylnaphthylamines was performed with the separate DPPH and amine solutions before they were mixed, so that the early stages of reaction could be observed.

For initial rate experiments, the amine concentrations used were in the range 1–5 $\times 10^{-4}$ *M* for the phenylnaphthylamines, 4–20$\times 10^{-4}$ *M* for diphenylamine, and 2–10$\times$ 10^{-3} *M* for methylaniline. The complete reactions were followed using concentrations some five times greater than these. The initial DPPH concentrations were in the range 6–30$\times 10^{-5}$ *M*.

No correction is required for the reaction of DPPH with the solvent, since experiments showed that the rate of this process is negligible at temperatures up to 50°.

TABLE I

STOICHIOMETRY OF REACTION OF DPPH WITH SECONDARY AMINES

Amine	DPPH (mM)	Amine reacting* (mM)	Amine reacting† (mM)	Hydrazine (mM)
N-Phenyl-1-naphthylamine	2.00	1.0	1.1	1.8
N-Phenyl-2-naphthylamine	2.00	1.0	1.1	1.8
Diphenylamine	2.00	1.15	1.2	1.76
Methylaniline	2.00	1.15	1.2	1.7

*From experiments involving disappearance of violet color of DPPH.
†From experiments involving isolation of excess amine.

RESULTS AND DISCUSSION

The results of the stoichiometric investigations are summarized in Table I.

The number of millimoles of amine reacting with 2 millimoles of DPPH was estimated (*a*) from experiments involving the disappearance of the violet color from reacting solutions, (*b*) from experiments involving the isolation of excess amine from solutions containing initially equimolar amounts of DPPH and amine. An uncertainty of up to 0.1 millimole arises in the first set of results because separate experiments have shown that some DPPH is removed by reaction with the products. The results of method (*b*) are maximum values, as the excess amine has probably not been completely isolated; 85–90% of the DPPH is recovered as 1,1-diphenyl-2-picrylhydrazine in each case.

The main process occurring is one of hydrogen abstraction by DPPH from the amine. In the case of diphenylamine the following evidence indicates that it is the amino hydrogen which is initially removed by the DPPH. Triphenylamine, a tertiary amine, does not react with DPPH at an appreciable rate. About 40% of the diphenylamine which reacts with DPPH is converted to tetraphenylhydrazine. Both lead dioxide and potassium permanganate oxidize diphenylamine to tetraphenylhydrazine showing that the amino hydrogen is most readily removed in related reactions. There is less definite evidence with the other amines. The yellow product from the *N*-phenyl-1-naphthylamine reaction shows only a weak N–H absorption in its infrared spectrum so that abstraction of the amino hydrogen certainly occurs in the reaction. Dimethylaniline reacts with DPPH at a very much lower rate than methylaniline. Whilst it is possible that attack by DPPH on a C–H bond does occur as a primary process in these reactions, attack on an N–H bond appears to be far more probable, and it is assumed here that it is the only important primary process.

The reactions are all retarded by the product 2,2-diphenyl-1-picrylhydrazine. Retardation is slight in the reaction of DPPH with *N*-phenyl-1-naphthylamine, but is quite considerable in other cases. For instance the addition of 2,2-diphenyl-1-picrylhydrazine at a concentration of 6×10^{-5} *M* to a solution containing *N*-phenyl-2-naphthylamine at a concentration of 5×10^{-4} *M* and DPPH at a concentration of 2×10^{-4} *M* reduces the initial rate of reaction by a factor of 3, and when the 2,2-diphenyl-1-picrylhydrazine concentration is increased to 15×10^{-5} *M* the rate is further reduced by a factor of 2. In order to obtain the rates of the unretarded reaction, the experimental results should be extrapolated back to zero reaction. However, the nature of the extrapolation is uncertain, and we have chosen to use as "initial rates" the rates of reaction after 3% reaction. These rates are close to the true values for *N*-phenyl-1-naphthylamine, but are less than the true values for the other amines.

The initial rate of reaction between DPPH and any of the amines is proportional to the concentration of DPPH and to the concentration of amine. This is readily understood if the primary process involves the attack of a molecule of DPPH on a molecule of amine, and this process is rate-determining in the initial stages of the reaction.

[1]

Rate constants (*k*) for this second-order reaction have been calculated from the rates of disappearance of DPPH, taking into account the stoichiometric results listed in Table I. The values of *k* at 20° have been recorded in Table II, together with activation energies (*E*) and frequency factors (*A*).

TABLE II

KINETIC RESULTS FOR THE REACTION OF DPPH WITH SECONDARY AMINES

Amine	k at 20° (cc/mole sec)	E (kcal/mole)	A (cc/mole sec)
N-Phenyl-1-naphthylamine	330	9.6	4.8×10^{9}
N-Phenyl-2-naphthylamine	580	11.0	1.1×10^{11}
Diphenylamine	53	12.8	2.3×10^{11}
Methylaniline	4.8	14.7	5.6×10^{11}

The value of E for the reaction with *N*-phenyl-1-naphthylamine is probably accurate to ±0.5 kcal/mole, but because of the difficulties associated with retardation by 2,2-diphenyl-1-picrylhydrazine, the other activation energies are not known to better than ±1 kcal/mole. The effect of structure on ease of abstraction of a hydrogen atom is clearly shown. The activation energies increase in going from the phenylnaphthylamines to methylaniline and this is associated with a considerable decrease in rate constant. Aliphatic amines are less reactive, the value of k at 20° for the reaction of DPPH with di-*n*-propylamine being approximately 0.2 cc/mole sec. The frequency factors are comparable to those obtained for reactions between DPPH and aliphatic mercaptans (1) and are of the same order as the frequency factors of hydrogen abstraction reactions involving methyl radicals (8). The relatively low value of the frequency factor for *N*-phenyl-1-naphthylamine is perhaps due to a steric effect.

The retardation of the reaction by the product 2,2-diphenyl-1-picrylhydrazine is explained by the reversal of reaction [1]; the concentration of amino radicals is reduced, and the over-all rate of reaction falls. The fall in rate can be adequately explained by the retarding effect of the diphenylpicrylhydrazine, and it is probable that complex formation between DPPH and amine, if it occurs, does not affect the kinetics of reaction.

Little information has been obtained in this study concerning the further reactions of the amino radicals. In the DPPH–diphenylamine reaction the following processes may be considered, among others:

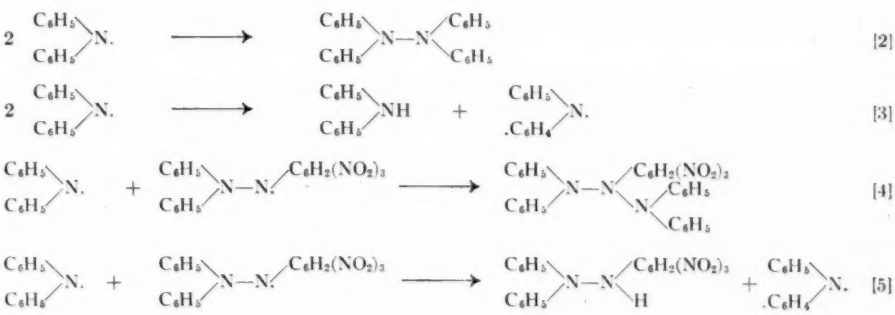

[2]

[3]

[4]

[5]

Reaction [2] occurs almost exclusively when diphenylamine is oxidized by lead dioxide at room temperature (6). It takes place to some extent in the dehydrogenation by DPPH as tetraphenylhydrazine accounts for about 40% of the products. It cannot occur exclusively, because this would require that 2 moles DPPH would react with 2 moles diphenylamine instead of the 1.2 moles diphenylamine observed experimentally. Reaction [3] involving the disproportionation of amino radicals probably occurs to some

extent at 55°, since tetraphenylhydrazine is slowly converted to diphenyldihydrophenazine in benzene solution at this temperature. Reaction [4] cannot be of great importance because 85–90% of the DPPH reacting is recovered as 2,2-diphenyl-1-picrylhydrazine. It is possible that the adduct is formed and then decomposes but infrared evidence indicates that such a decomposition does not take place on the alumina column. The disproportionation reaction [5] would help to explain the stoichiometric ratio of DPPH to diphenylamine observed experimentally. Attack at the ortho position may eventually lead to diphenyldihydrophenazine, but attack at the meta and para positions would give rise to more complex products. In the absence of a better knowledge of the dehydrogenation products further speculation on the secondary reactions does not appear to be warranted.

Two factors limit the accuracy of the kinetic results in Table II. In the first place, no allowance has been made for the possible primary attack of DPPH on C–H as well as on N–H bonds. Secondly, the retardation by 2,2-diphenyl-1-picrylhydrazine reduces the rate significantly with three of the amines even at 3% reaction, so that the rate constants quoted are less than the true values. Work in progress indicates that reactions involving phenols as donors are less subject to these limiting factors. It also shows that substituents in the aromatic ring may cause considerable changes in rates of dehydrogenation.

ACKNOWLEDGMENTS

The authors are grateful to the National Research Council and to the McLaughlin Research Fund of Queen's University for financial assistance.

REFERENCES

1. RUSSELL, K. E. J. Phys. Chem. **58**, 437 (1954).
2. BRAUDE, E. A., BROOK, A. G., and LINSTEAD, R. P. J. Chem. Soc. 3574 (1954).
3. BROOK, A. G., ANDERSON, R. J., and TISSOT VAN PATOT, J. Can. J. Chem. **36**, 159 (1958).
4. KUZ'MINSKIĬ, A. S. and ANGERT, L. G. Doklady Akad. Nauk S.S.S.R. **96**, 1187 (1954).
5. GOLDSCHMIDT, S. and RENN, K. Ber. **55**, 628 (1922).
6. WIELAND, H. and GAMBARJAN, S. Ber. **39**, 1499 (1906).
7. WIELAND, H. Ann. **381**, 200 (1911).
8. TROTMAN-DICKENSON, A. F. Quart. Revs. (London), **7**, 198 (1953).

DISSOCIATION CONSTANTS OF THE CYANOHYDRINS OF SOME TRITERPENE KETONES[1]

OWEN H. WHEELER[2] AND V. S. GAIND[3]

ABSTRACT

The reactivity of a number of triterpene ketones towards cyanohydrin formation is influenced by groups present in rings remote from the keto group. The results are interpreted as evidence of "conformational transmission" of the effects of the substituents.

INTRODUCTION

Barton and co-workers (1) have recently shown that the rate of condensation of a number of triterpene ketones with benzaldehyde is influenced by substituents in other rings. The effect does not seem to be electronic and Barton has suggested (1, 2) that the substituents cause small changes in valency angles and in the co-ordinates of the atoms, producing small distortions throughout the whole molecule, and effecting the reactivity of some substituent in the rings. The term "conformational transmission" has been introduced (3) for this new effect produced by substituents.

Similar effects have recently been observed in the formation of cyanohydrins from ring A keto steroids (4), and in their rates of reduction with sodium borohydride (5).

In the present work we have measured the dissociation constants of the cyanohydrins (in 80% dioxane–water) of a number of triterpene ketones. Most of these ketones were also used in the study of benzylidene derivative formation (1). The compounds used fall into four groups: (*a*) lanostan-3-one (I), lanost-8-en-3-one (II) and α-onoceradienedione (III), which lack an 8-methyl substituent; (*b*) germanicone (IV) and allobetulone (V), which have different substituents in ring E; (*c*) β-amyrone (VI), oleanonic acid (VII) and dehydro-β-amyrone (VIII), which have differences in rings C and D; and (*d*) α-amyra-9,11(12)-dien-3-one (IX) and α-amyra-12-en-3,11-dione (X), which have another carbon skeleton. The differences in reactivity (Table II) vary over a range of 2.1, while the corresponding values for benzylidene formation (1) differ within a range of 2.2.

DISCUSSION

If the effect was electrostatic in origin, those substituents with a greater charge separation, such as an acid or ketone group, would be expected to show the largest differences. However, oleanonic acid (VII) and allobetulone (V) are only a little more reactive than lanostan-3-one (I), in which there can be no electrostatic interaction. Moreover, the α,β-unsaturated ketone system of α-amyra-12-en-3,11-dione (X) has a smaller effect than the diene system of α-amyra-9,11(12)-dien-3-one (IX). On the other hand if the effect is due to changes in the conformation of the rings then double bonds would have the largest effect, since a double bond placed in a cyclohexane ring changes all its valency angles (6). In support of this lanost-8-en-3-one (II), β-amyrone (V), and germanicone (IV) show large differences in reactivity as compared to lanostan-3-one (I), and the greatest differences are shown by the homoannular dienes dehydro-β-amyrone (VIII) and α-amyra-9,11(12)-dien-3-one (IX).

[1]*Manuscript received May 15, 1958.*
Contribution from the Department of Chemistry, Dalhousie University, Halifax, N.S. Published as Part VII of Reactivity Studies on Natural Products. Part VI, Can. J. Chem. **36**, *1431 (1958).*
[2]*Present address: Department of Chemistry, University of Puerto Rico, Mayaguez, Puerto Rico.*
[3]*National Research Council Postdoctorate Fellow.*

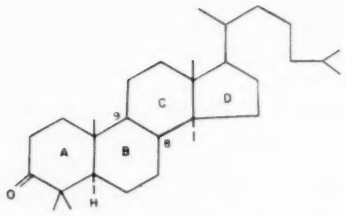

I; II $\Delta^{8(9)}$

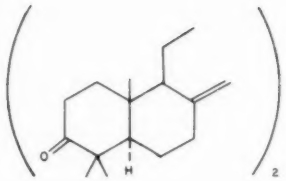

III

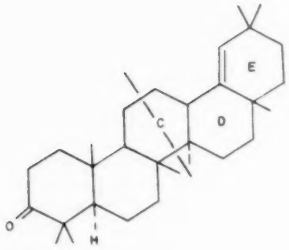

IV

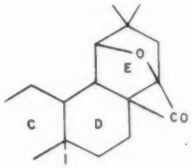

V

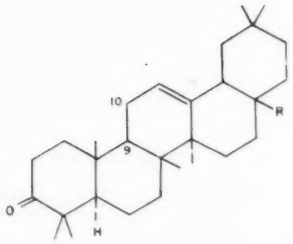

VI, R = Me
VII, R = CO_2H
VIII, $\Delta^{9(10)}$, R = Me

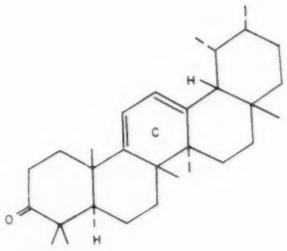

IX

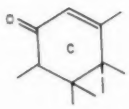

X, ring C

In cyclohexanone the α and γ axial groups are 2.37 Å apart (6), whereas in cyclohexane they are 2.53 Å apart (6). Thus in the triterpene ketones any interaction between the 4 and 10 axial methyl groups is reduced on forming the cyanohydrin, and in agreement with this lanostan-3-one (I) cyanohydrin is more stable than that of cholestanone.

A double bond placed elsewhere within the rings would be expected to increase the distortion in ring A, by "conformational transmission", and to increase the 1–3 axial methyl interference in the ketones. Such an effect would favor cyanohydrin formation

and the dissociation constants of the cyanohydrins of the unsaturated ketones are greater than those of the saturated ones. Moreover, those compounds having an axial methyl group at position 8, e.g. β-amyrone (VI), germanicone (IV), and dehydro-β-amyrone (VIII), form the more stable cyanohydrins. In these cases interaction between the 4, 10, and 8 axial methyl groups is possible.

The free-energy differences (calculated from $\Delta\Delta F = -RT \ln K_1/K$ at 25°) between the dissociation constant of the cyanohydrins of the various ketones are only small. Thus introducing a Δ^8 double bond (I and II) results in a difference of 0.11 kcal, in going from a double bond to a homoannular diene a difference of 0.17 kcal (VI and VIII), and changing a methyl group for a carboxylic acid grouping (VI and VII) a difference of 0.18 kcal. Changing the position of a double bond has little effect ($\Delta\Delta F = 0.05$ kcal for IV and VI).

The present results show a similar trend in the series of compounds studied as the results of Barton, Head, and May (1). However, the dissociation constant of the cyanohydrin of α-amyra-12-en-3,11-dione (X) shows a greater reactivity than expected. In this case the α,β-unsaturated ketone group may also have reacted with hydrogen cyanide (cf. cholest-4-en-3-one, ref. 4), and the measured dissociation constant may not be that of the 3-ketone cyanohydrin alone.

The experimental method was essentially that used in previous studies (4), but the equilibration time was increased to 20 to 25 hours. This will be more than sufficient, since Δ^5-lanosten-3-one reached equilibrium in some six hours (Table I).

TABLE I

REACTION LANOSTENONE WITH HYDROGEN CYANIDE*

Time, hours	Vol. 0.0020 *N* $Hg(NO_3)_2$, ml
0	0.98
1½	0.88
2½	0.85
3	0.83
3½	0.82
4½	0.78
6½	0.76
24	0.76, 0.75

*Initial concentrations, Δ^5-lanosten-3-one 0.00234 *M*, hydrogen cyanide, 0.00080 *M*, in 80% dioxane–water at 25.0°.

EXPERIMENTAL

Ketones

Many of the ketones were donated by Professor Barton.

Dehydro-β-amyrin was prepared by selenium dioxide oxidation of β-amyrin (7).

Lanost-8-en-3-one (II), β-amyrone (VI), and oleanonic acid (VII) were prepared by oxidation of the corresponding alcohols with chromium trioxide in pyridine (8).

Dissociation Constants

The triterpene ketones (25–30 mg) were dissolved in 80% aqueous dioxane (80 vol. purified dioxane + 20 vol. distilled water) (15 ml), and solutions of hydrogen cyanide (0.004 *M*, 5 ml) and 1% tri-*n*-propylamine (1 ml) in the 80% aqueous dioxane were added. The total volume was made up to 25 ml with the same solvent. The tightly stoppered flasks were allowed to equilibrate in a constant temperature bath, maintained at 25.0±0.1°, for 20–25 hours. Aliquots (5 ml) were then withdrawn and titrated with

aqueous mercuric nitrate solution (0.002 *N*), containing 5% nitric acid, using a capillary microburette. A freshly prepared solution of diphenylcarbazide in ethanol was used as indicator (9). The determinations were, in most cases, carried out in triplicate. The averaged results and their mean errors are given in Table II.

TABLE II

REACTIVITY OF TRITERPENE KETONES

	K_D^{HCN}*	k^{PhCHO}†
Dehydro-β-amyrone (VIII)	101±2	124
α-Amyra-9,11(12)-dien-3-one (IX)	110±1	115
Germanicone (IV)	125‡	—
β-Amyrone (VI)	135±3	108
α-Amyra-12-en-3,11-dione (X)	145±4	75
Lanost-8-en-3-one (II)	176±4	100
α-Onoceradienedione (III)	181±1	117
Allobetulone (V)	182±3	100
Oleanonic acid (VII)	185±2	97
Lanostan-3-one (I)	213±9	55
Cholestan-3-one	556±12	—

*Dissociation constants of cyanohydrins in 80% dioxane–water at 25.0°, from the present work.

†Rates of reaction with benzaldehyde at 25.0°, in 99% ethanol, relative to lanost-8-en-3-one = 100, ref. 1.

‡Only one determination.

Fredelin and 4,4-dimethylcholest-5-en-3-one were too insoluble in 80% aqueous dioxane for any measurements to be made. In aqueous dioxane containing less water, the dissociation constants were immeasurably high.

ACKNOWLEDGMENTS

The authors are very grateful to Professor D. H. R. Barton for initially suggesting this study and for generously supplying most of the compounds used. Dr. Estrada kindly furnished samples of germanicone, β-amyrin, and fredelin.

One of us (V.S.G.) is indebted to the National Research Council for the award of a Postdoctorate Fellowship.

REFERENCES

1. BARTON, D. H. R., HEAD, A. J., and MAY, P. J. J. Chem. Soc. 935 (1957).
2. BARTON, D. H. R. and HEAD, A. J. J. Chem. Soc. 932 (1956).
3. BARTON, D. H. R. XIVth Intern. Congr. Pure Appl. Chem. Experientia Suppl. II, 121 (1955).
4. WHEELER, O. H. and MATEOS, J. L. Can. J. Chem. **36**, 712 (1958).
5. WHEELER, O. H. and MATEOS, J. L. Can. J. Chem. **36**, 1049 (1958).
6. COREY, E. J. and SNEEN, R. A. J. Am. Chem. Soc. **77**, 2505 (1955).
7. RUZICKA, L. and JEGER, O. Helv. Chim. Acta, **24**, 1236 (1941).
8. POOS, G. I., ARTH, G. E., BEYLER, R. E., and SARETT, L. H. J. Am. Chem. Soc. **75**, 422 (1953).
9. PRELOG, V. and KOBELT, M. Helv. Chim. Acta, **32**, 1187 (1949).

NOTE ON THE INDUCTIVE AND MESOMERIC EFFECTS IN SUBSTITUTED BENZENE DERIVATIVES

C. SANDORFY

Inductive and mesomeric effects have become familiar terms with both organic and theoretical chemists since they were introduced by Ingold and others (1), and since the fundamental work of Wheland and Pauling (2). Among the numerous theoretical treatments we mention only those by Matsen (3, 4), who used an LCAO MO method combined with perturbation calculations, and by Murrell and Longuet-Higgins (5, 6), who used a simplified self-consistent field-molecular orbital method.

In 1949, the present author (7) published a series of diagrams of electronic charge distributions in monosubstituted benzene derivatives where, as in phenol or aniline, two electrons of the substituent can interact with the π-electrons of the benzene carbon atoms. The simple Hückel approximation of the LCAO MO method was used.

The extent of the mesomeric effect due to the addition of two more mobile electrons to the system depends in this approximation on the difference between the Coulombic integral, α_R, associated with the substituent, R, and α_C for a carbon atom. This difference is taken to be proportional to the corresponding difference in electronegativities or ionization potentials. The smaller these differences are, the easier it is for the electrons of the substituent to penetrate into the benzene ring orbitals.

The inductive effect is due to the fact that the presence of the substituent modifies the potential field in the benzene ring with the main result that the carbon linked to the substituent will have a somewhat increased electronegativity. This again may be represented by a supplement to its Coulombic integral, generally taken as a fraction of α_R.

It is interesting to see what would be the charge distribution if only the mesomeric or only the inductive effects are present. The purely mesomeric effect is obtained if we give an extra Coulombic integral to the substituent but none to the carbon linked to it. The purely inductive effect is obtained if we put the resonance integral between these two atoms, β, equal to zero and we give an extra Coulombic integral to the carbon atom linked to the substituent.

We have given $(\alpha_R - \alpha_C)$ the successive values of -2, -1, 0, 1, 2, and 3 in β units and to $(\alpha_{C_R} - \alpha_C)$ one tenth of the respective values of the former difference. All the resonance integrals were taken to be the same, β (except of course the one necessary to compute the pure inductive effect).

In Fig. 1, the first row represents the pure mesomeric effect, the second row the pure inductive effect, and the third row the combined effect of the two. Electron charge densities (at the atoms) and bond orders (at the bonds) are as defined by Coulson and Longuet-Higgins (8). Overlap was neglected. The unit for the charges is the charge of an electron. Values greater than one represent partial negative charges, values smaller than one (or two for the substituent) partial positive charges. The second and third rows are taken from (7) and in the third row the last decimal is uncertain.

The diagrams in the third row having respectively $\alpha_R = 1$, 2, and 3 are probably fairly close to aniline, phenol, and fluorobenzene. $\alpha_R = -1$ would be close to phenylphosphine.

Figure 1 needs little comment. For positive values of α_R the mesomeric and inductive effects are opposed and practically additive. The positive charge on the substituent is

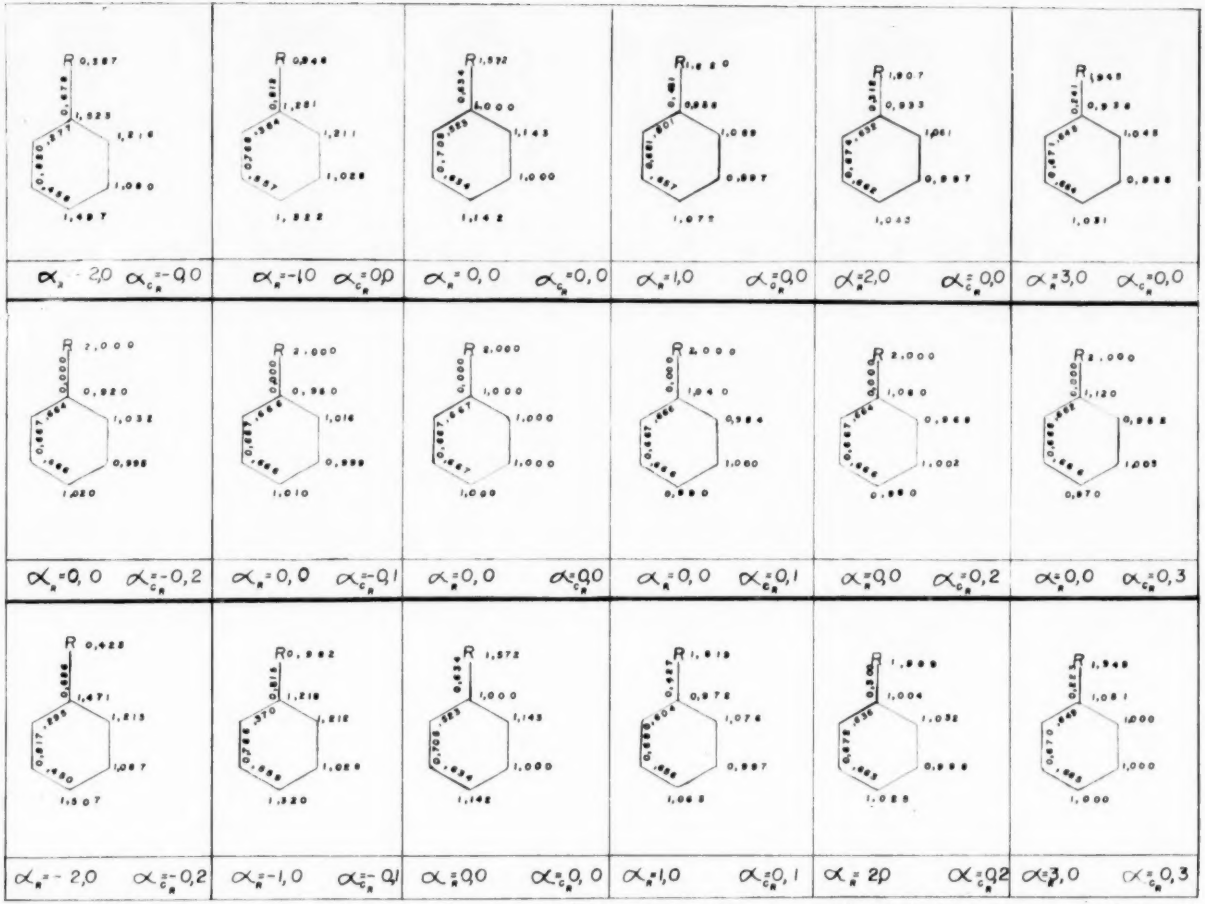
$\alpha_R = -2,0$ $\alpha_{C_R} = -0,0$
$\alpha_R = -1,0$ $\alpha_{C_R} = 0,0$
$\alpha_R = 0,0$ $\alpha_{C_R} = 0,0$
$\alpha_R = 1,0$ $\alpha_{C_R} = 0,0$
$\alpha_R = 2,0$ $\alpha_{C_R} = 0,0$
$\alpha_R = 3,0$ $\alpha_{C_R} = 0,0$
$\alpha_R = 0,0$ $\alpha_{C_R} = -0,2$
$\alpha_R = 0,0$ $\alpha_{C_R} = -0,1$
$\alpha_R = 0,0$ $\alpha_{C_R} = 0,0$
$\alpha_R = 0,0$ $\alpha_{C_R} = 0,1$
$\alpha_R = 0,0$ $\alpha_{C_R} = 0,2$
$\alpha_R = 0,0$ $\alpha_{C_R} = 0,3$
$\alpha_R = -2,0$ $\alpha_{C_R} = -0,2$
$\alpha_R = -1,0$ $\alpha_{C_R} = -0,1$
$\alpha_R = 0,0$ $\alpha_{C_R} = 0,0$
$\alpha_R = 1,0$ $\alpha_{C_R} = 0,1$
$\alpha_R = 2,0$ $\alpha_{C_R} = 0,2$
$\alpha_R = 3,0$ $\alpha_{C_R} = 0,3$

FIG. 1. First row: pure mesomeric effect. Second row: pure inductive effect. Third row: combined inductive and mesomeric effects. α_C is taken equal to zero.

determined only by the mesomeric effect, the negative charges in ortho and para by both effects. The ortho-para orienting character of the substituent is clearly brought out, as is the invariance of the meta position.

For negative values of α_R the situation is quite different. The very great positive charge appearing on the substituent because of the mesomeric effect is slightly diminished by the inductive effect, which from this point of view is again opposed to the mesomeric effect. The mesomeric effect sends a considerable negative charge into the para and ortho and even to the meta position, although much less to the last position. Curiously, the inductive effect leaves the ortho, meta, and para carbons practically unaffected.

Thus, while the inductive effect does not alter the charge on the substituent for positive values of $(\alpha_R - \alpha_C)$, it does influence the charges on the ring carbon atoms; the contrary is predicted for negative values of $(\alpha_R - \alpha_C)$ in this approximation.

The bond orders show that in the latter case, the benzene ring undergoes considerable deformation. The chemical behavior of the corresponding compounds should be interesting.

The inductive effect changes symmetrically if we change the sign of α_R but the mesomeric effect does not. The inductive effect affects not only the ortho position but also the para position.

As we know today, the simple approximation used to obtain these results is not very accurate. It has yielded, however, so many qualitatively correct results that our findings should have a relative interest even though the method does not correspond to the latest stage of development in theoretical chemistry.

The diagrams of the first row of Fig. 1 were obtained with the help of the Compution Centre of the University of Toronto. Free machine time was allotted by the National Research Council. The author wishes to express his thanks to these two institutions. Thanks are due to Professor D. Patterson for help in preparation of the manuscript.

RÉSUMÉ

Dans cet article on donne des diagrammes de répartition électronique représentant l'effet mésomère pur et l'effet inductif pur des substituants sur le noyau benzénique ainsi que leur effet simultané.

1. INGOLD, C. K. Chem. Revs. **15**, 225 (1934).
2. WHELAND, G. W. and PAULING, L. J. Am. Chem. Soc. **57**, 2086 (1935).
3. MATSEN, F. A. J. Am. Chem. Soc. **72**, 5243 (1950).
4. ROBERTSON, W. W. and MATSEN, F. A. J. Am. Chem. Soc. **72**, 5252 (1950).
5. MURRELL, J. N. and LONGUET-HIGGINS, H. C. Proc. Phys. Soc. A, **68**, 329 (1955).
6. MURRELL, J. N. Proc. Phys. Soc. A, **68**, 969 (1955).
7. SANDORFY, C. Bull. soc. chim. France, **16**, 615 (1949).
8. COULSON, C. A. and LONGUET-HIGGINS, H. C. Proc. Roy. Soc. A, **191**, 39 (1947).

RECEIVED AUGUST 18, 1958.
DEPARTMENT OF CHEMISTRY,
UNIVERSITY OF MONTREAL,
MONTREAL, QUEBEC.

THE CONFIGURATION OF GLYCOSIDIC LINKAGES IN OLIGOSACCHARIDES
VII. 4-*O*-β-D-GALACTOPYRANOSYL-D-GALACTOSE FROM WHITE BIRCH WOOD*

J. K. GILLHAM, A. S. PERLIN, AND T. E. TIMELL

Partial acid hydrolysis of an α-cellulose prepared from white birch (*Betula papyrifera*) wood has led to the isolation of a new disaccharide (1). The disaccharide is now shown to be 4-*O*-β-D-galactopyranosyl-D-galactose.

**Issued as N.R.C. No. 4963 and as Paper No. 256 on the Uses of Plant Products.*

The compound, isolated by chromatography on paper, crystallized from methanol. It had melting point 204°, $[\alpha]_D$ +68°, and a degree of polymerization (2) of 2.0. Complete acid hydrolysis with hot 0.1 *N* sulphuric acid required about 8 hours, indicative of the presence of a pyranosidic non-reducing end unit in the compound. The only detectable component sugar produced by hydrolysis was D-galactose, identified by its chromatographic behavior, specific rotation, and by conversion to crystalline galactose 1-methyl-1-phenylhydrazone.

In acetic acid solution the disaccharide consumed lead tetraacetate relatively slowly, 1.8 moles being taken up in 30 minutes, which is consistent with the oxidation of a 4-substituted aldohexose unit (3). When treated with 1.5 moles of oxidant it afforded a product which on hydrolysis yielded (chromatographic evidence) the expected products, i.e., galactose, lyxose, and threose (3, 4). In 90% acetic acid and in the presence of potassium acetate 1 mole of carbon dioxide was liberated at a rate almost identical with that for methyl α-D-galactopyranoside (5), suggesting that formic acid was produced only from the galactopyranosidic non-reducing end unit. Further, the corresponding figure for lead tetraacetate uptake was 3.9 moles, which allows for the required consumption of 2 moles by the non-reducing end unit and for degradation of the reducing end unit to a di-*O*-formyl tetrose derivative by cleavage of carbon–carbon bonds 1,2- and 2,3- (4). These data are consistent only with the formulation of a 1,4-D-galactopyranosyl-D-galactose structure for the disaccharide.

The new galactobiose is distinct from 4-*O*-D-galactopyranosyl-D-galactose derived from okra mucilage by Whistler and Conrad (6) and from pectic acid by Jones and Reid (7), since the latter disaccharide* gave a different X-ray powder diagram and has $[\alpha]_D$ +173°, in contrast to the current value of $[\alpha]_D$ +68°. It is clear, therefore, that the glycosidic linkage of galactobiose from birch possesses the β-configuration which, at the same time, confirms the presence of an α-linkage in the disaccharide from okra mucilage and pectic acid.

EXPERIMENTAL

Isolation of the Disaccharide

Alpha cellulose (400 g), prepared from white birch (*Betula papyrifera*) as described earlier (1), was heated with *N* sulphuric acid (2000 ml) at 95° C for 40 minutes. After neutralization with barium carbonate the hydrolyzate was deionized and the mixture of products formed was partially resolved by chromatography on Whatman 3 MM paper using ethyl acetate:acetic acid:water (9:2:2) as solvent. A second chromatographic separation, using butanol:pyridine:water (10:3:3), afforded five disaccharide fractions (1). After several weeks in methanol, one of these fractions (98 mg) yielded crystals (25 mg) having m.p. 204° C (corr.) and $[\alpha]_D^{20}$ +68° (equilibrium value; *c*, 1.0, water); degree of polymerization found by the end-group method of Peat, Whelan, and Roberts (2), 2.06. The X-ray powder diagram of the compound was distinct from that of 4-*O*-α-D-galactopyranosyl-D-galactose; interplanar lattice spacings in Å were as follows (relative intensities are given in parentheses): 7.85 (56), 6.56 (49), 5.40 (53), 4.50 (100), 3.76 (71), 3.50 (47), 3.05 (44), 2.7 (diffuse) (51), 2.3 (diffuse) (44), 2.15 (23), 2.05 (30), 1.84 (14), 1.60 (8), 1.46 (9), 1.40 (4).

D-*Galactose 1-Methyl-1-phenylhydrazone*

The disaccharide (2.74 mg) was taken up in 0.5 ml of 0.1 *N* sulphuric acid (found, $[\alpha]_D^{25}$ +66°, equilibrium value) and heated on the steam bath to constant rotation (α_D^{25} +0.22°±0.01°, 0.5 dm tube), which required 7.5 hours. After neutralization with Dowex-1

*The authors are grateful to Prof. R. L. Whistler for providing a sample of this compound.

resin (bicarbonate form) the hydrolyzate was examined by paper chromatography using three solvent systems, each chromatogram suggesting that galactose was the only product formed and showing the presence of a trace of unhydrolyzed disaccharide. Accordingly, the specific rotation of the sugar produced on hydrolysis was $[\alpha]_D^{25}$ +77° (*c*, 0.576, 0.1 *N* sulphuric acid); (D-galactose has $[\alpha]_D^{20}$ +80°).

To the neutral hydrolyzate 0.5 ml of ethanolic 1-methyl-1-phenylhydrazine acetate (8) was added; the solution was stored in the dark at 35° C for 12 hours and then at 4° C for 9 hours. Crystals which formed were filtered off, washed with cold ethanol, and dried. Melting point 189–190° C (corr.), undepressed on admixture with authentic D-galactose 1-methyl-1-phenylhydrazone, m.p. 190–191° C. The known and unknown derivatives gave X-ray powder diagrams which were indistinguishable from each other.

Lead Tetraacetate Oxidation of the Disaccharide

(*a*) The galactobiose (1.0 mg), in 0.04 ml of water, was taken up in acetic acid (1.0 ml) and a solution of lead tetraacetate (5.0 mg) in acetic acid (1.0 ml) was added at room temperature. At 10, 20, and 30 minutes aliquots (0.5 ml) were withdrawn and the lead tetraacetate consumption measured by microtitration. Found: 1.0, 1.5, and 1.8 moles/mole, respectively. Under the same conditions maltose consumed 0.8, 1.3, and 1.5 moles/mole, respectively.

(*b*) In another experiment the galactobiose (1.1 mg) was treated with an aliquot of the lead tetraacetate solution equivalent to 1.5 moles of oxidant/mole. A negative starch–iodide test was obtained within two hours, water (2.0 ml) was added, divalent lead was removed with excess Amberlite IR-120, and the suspension was heated on the water bath for 2 hours. Examination of the hydrolyzate on a paper chromatogram, using two solvent systems and aniline oxalate spray (9), showed the presence of products corresponding to threose, lyxose, and galactose, in addition to unhydrolyzed material.

(*c*) On oxidation in the Warburg respirometer in 90% acetic acid and in the presence of potassium acetate (5), the galactobiose (1.1 mg) yielded carbon dioxide (formic acid) at the following rate (comparative data is given for methyl α-D-galactopyranoside oxidized simultaneously), in moles/mole:

Time (minutes)	15	20	40	60	80	140
Galactobiose	0.33	0.80	0.97	1.02	1.04	1.09
Methyl galactoside	0.32	0.73	0.89	0.98	1.01	1.01

At 140 minutes the total consumption of lead tetraacetate was 4.95 moles/mole which, corrected for the oxidant used in converting formic acid to carbon dioxide (1.09 moles/mole), corresponds to a lead tetraacetate uptake of 3.86 moles/mole by the disaccharide.

1. Gillham, J. K. and Timell, T. E. Can. J. Chem. **36**, 1467 (1958).
2. Peat, S., Whelan, W. J., and Roberts, J. G. J. Chem. Soc. **2258** (1956).
3. Charlson, A. J. and Perlin, A. S. Can. J. Chem. **34**, 1200 (1956).
4. Perlin, A. S. Anal. Chem. **27**, 396 (1955).
5. Perlin, A. S. J. Am. Chem. Soc. **76**, 5505 (1954).
6. Whistler, R. L. and Conrad, H. E. J. Am. Chem. Soc. **76**, 1673 (1954).
7. Jones, J. K. N. and Reid, W. W. J. Chem. Soc. 1890 (1955).
8. Hirst, E. L., Jones, J. K. N., and Woods, E. A. J. Chem. Soc. 1048 (1947).
9. Horrocks, R. H. Nature, **164**, 444 (1949).

Received August 1, 1958.
McGill University and Pulp and Paper Research Institute of Canada,
Montreal, Quebec;
and
Prairie Regional Laboratory,
National Research Council of Canada,
Saskatoon, Saskatchewan.

ADDITION OF PYRROLES TO 1,4-BENZOQUINONE*

E. BULLOCK†

Several workers have observed the formation of colored products from quinones and pyrroles (1, 2). In the reaction, four hydrogens are lost between two molecules of pyrrole and one of quinone, hydroquinone being a by-product. The structure I (2) is incompatible with the infrared spectra of the benzoquinone adducts of 2,4-dimethylpyrrole (I*a*) and cryptopyrrole (I*b*), since these show a "bonded" NH band at 3360 cm^{-1}.

The cryptopyrrole adduct must therefore possess structure II*b* and since the ultraviolet and visible spectra of the two adducts are almost identical, the product from 2,4-dimethylpyrrole is formulated as II*a*. Structure II gives a satisfactory explanation of the intense color of the compounds and their behavior with acid.

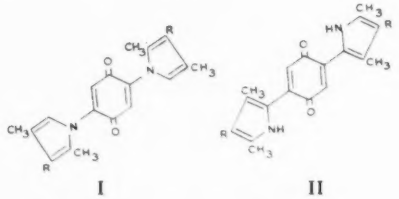

I II

I*a*, R = H
I*b*, R = C_2H_5

II*a*, R = H
II*b*, R = C_2H_5

EXPERIMENTAL

The adducts were prepared according to Pratesi (2) and recrystallized from chloroform.

2,5-bis(2′,4′-Dimethyl-5′-pyrryl)p-benzoquinone (II*a*)

Calc. for $C_{18}H_{18}O_2N_2$: C, 73.41; H, 6.17; N, 9.97. Found: C, 73.26; H, 6.01; N, 9.55. λ_{max} (chloroform): 324, 545–552 mμ; log ε: 4.45, 4.37. Infrared spectrum: (saturated solution in chloroform, 1-mm cell) absorbed at 3360, 1618, 1385, 986, 965 cm^{-1}. Solution in *N,N*-dimethyl formamide was violet, turning yellow on addition of concentrated hydrochloric acid, the color being restored after neutralization.

2,5-bis(2′,4′-Dimethyl-3′-ethyl-5′-pyrryl)p-benzoquinone (II*b*)

Calc. for $C_{22}H_{26}O_2N_2$: C, 75.39; H, 7.49; N, 7.99. Found: C, 74.94; H, 7.36; N, 8.22. λ_{max} (chloroform): 327, 560–575 mμ; log ε: 4.49, 4.41. Infrared spectrum: (approximately 50% saturated solution in chloroform, 1-mm cell) absorbed at 3360, 1615, 1387, 1066, 993, 968 cm^{-1}.

Solution in *N,N*-dimethyl formamide was blue, turning very pale green on acidification; the solution became blue again on neutralization.

The analyses are by Mr. H. Seguin and the infrared determinations by Mr. R. Lauzon.

1. MOHLAU, R. and REDLICH, A. Ber. **44**, 3605 (1911).
2. PRATESI, P. Gazz. chim. ital. **66**, 215 (1936).

RECEIVED AUGUST 28, 1958.
DIVISION OF PURE CHEMISTRY,
NATIONAL RESEARCH COUNCIL OF CANADA,
OTTAWA, CANADA.

*Issued as N.R.C. No. 4947.
†*National Research Council Postdoctorate Fellow.*

AN INFRARED CELL FOR SMALL GAS SAMPLES*

D. S. RUSSELL

During the examination of some organic reaction products and the fractions from gas chromatographic separations, it was necessary to obtain the infrared spectra of very small gas samples. The conventional cylindrical gas cell usually provided for infrared work has a relatively large volume, most of which is not in the effective light path. A wedge-shaped metal cell has recently been available for small samples which provides much more efficient absorption of the light beam. Although the shape of this cell is quite satisfactory, there is no convenient method of transferring a gas sample to the cell completely from a vacuum system.

In order to overcome this problem, a glass cell was made whose volume conformed roughly to the shape of the converging light beam of a Perkin–Elmer model 21 spectrophotometer. In addition a small freeze-out tube was added to the bottom so that a small gas sample could be condensed from a vacuum system. Thus quantities of the order of 0.03 ml could be completely transferred to give satisfactory spectra in compounds which exhibited a normal absorption coefficient. Using a spectrophotometer equipped with scale expansion this limit could be extended considerably further.

The cell walls were constructed from flat pieces of pyrex glass fused together at the corners. A similar result could probably be obtained by flattening a slightly conical glass tube of appropriate dimensions. The ends were ground flat on abrasive paper on a plane surface. The sodium chloride windows were then sealed in place by a lead gasket which had been wetted with mercury. The cell assembly was clamped together in the usual way between two metal plates, and adjusted so that the light column fell on the slit when the cell was in place in the instrument.

The cell as illustrated has a light path of 5.0 cm and a total volume of 7.5 ml, which is approximately 1/10th the volume of the 5.0-cm conventional cell. Although some

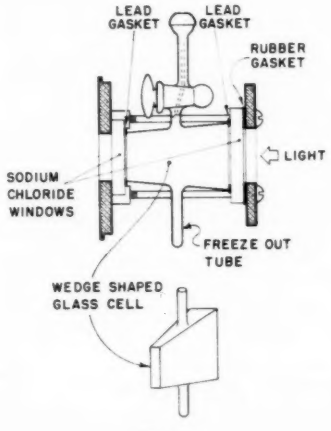

FIG. 1.

*Issued as N.R.C. No. 4940.

Can. J. Chem. Vol. 36 (1958)

light was lost by the cell, it did extend the lower sample limit by at least a factor of five.

In use, packets of silica were fastened over the windows while the sample was being condensed into the cell by liquid nitrogen to prevent condensation of moisture on them.

RECEIVED SEPTEMBER 19, 1958.
DIVISION OF APPLIED CHEMISTRY,
NATIONAL RESEARCH COUNCIL,
OTTAWA, CANADA.

CONTENTS OF VOLUME 36

Abraham, R. J., Pople, J. A., and **Bernstein, H. J.** The analysis of nuclear magnetic resonance spectra. IV. Four nuclei: AB_3, 1302.

Abramovitch, R. A. The infrared spectra of malonate esters, 151.

Tryptamines, carbolines, and related compounds. Part IV. Attempted synthesis of the physostigmine ring system, 354.

Abramovitch, R. A. and **Gear, J. R.** Unsymmetrically substituted 3,3′-methylene bridged 2,2′-dihydroxychromones, 1501.

Adams, G. A. Structure of an arabogalactan from white spruce (*Picea glauca* (Moench) Voss), 755.

Allan, F. J., Allan, G. G., and **Thomson, J. B.** The condensation of rhodanine with aromatic dialdehydes and some related compounds, 1579.

Allan, G. G. See Allan, F. J., 1579.

Amberg, C. H. Gas–liquid partition chromatography of organic sulphur compounds, 590.

Anderson, R. J. See Brook, A. G., 159.

Anet, F. A. L. and **Bavin, P. M. G.** Studies in the Wagner–Meerwein rearrangement. Part III, 763.

Anet, F. A. L. and **Eves, C. R.** Lycodine, a new alkaloid of *Lycopodium annotinum*, 902.

Anet, F. A. L. and **Isabelle, E.** The reduction of some halogenated compounds by chromous chloride, 589.

Anet, R. Fused heterocyclics. Part II. Synthesis of quinolino-(2:3:3′:2′)-quinoline: an isomer of calycanine, 1449.

Anet, R. and **Marion, L.** Some structural features of delcosine, 766.

Archambault, J. and **Rivest, R.** Donor acceptor reactions of titanium tetrachloride with formamide and N,N-dimethyl formamide, 1461.

Armstrong, W. A. and **Grant, G. A.** Radiation chemistry of solutions. II. Dose-rate, energy, and temperature dependence of a leuco triarylmethane dosimeter solution, 1398.

Arnot, C. and **McDowell, C. A.** The quenching of the iodine fluorescence spectrum, 114.

Quenching and vibrational-energy transfer of excited iodine molecules, 1322.

Atkinson, G. F. and **McBryde, W. A. E.** Treatment of experimental data in the study of chelation, 393.

Aubin, R. and **Rivest, R.** Sur les réactions des polyesters avec le tétrachlorure de titane. I. La réaction de l'oxalate de diéthyle avec le tétrachlorure de titane, 915.

Ausloos, P. The photolysis of alkyl esters, 383.

The liquid phase photolysis of diethyl ketone and methyl ethyl ketone, 400.

Bailey, R. A. See Campbell, A. N., 518.

Balla, G. A. See Heard, R. D. H., 1260.

Bannard, R. A. B. See Hawkins, L. R., 220.

Bannard, R. A. B., Casselman, A. A., Cockburn, W. F., and **Brown, G. M.** Guanidine compounds. II. Preparation of mono- and N,N-di-alkylguanidines, 1541.

Bannard, R. A. B. and **Hawkins, L. R.** Cyclohexane compounds. II. Synthesis and structure of two stereoisomeric 3-amino-1,2-cyclohexanediols, 1241.

Barth, F. W. and **Timell, T. E.** Separation of carbohydrates on cocoanut charcoal columns, 1321.

Barton, G. M. See Gardner, J. A. F., 1612.

Barton, S. S. and **Mason, S. G.** Physical adsorption in the benzene–polystyrene system, 1126.

Bavin, P. M. G. The preparation of amines and hydrazo compounds using hydrazine and palladized charcoal, 238.

See also Anet, F. A. L., 763.

Bavin, P. M. G. and **Scott, J. M. W.** Some chemistry of 2,6-diethylaniline, 1284.

Bayley, C. H. See Gingras, B. A., 1320.

Becker, H. A. An interpretation of the moisture desorption isotherm of wheat, 1416.

Bednas, M. E. and **Russell, D. S.** A study of silver nitrate solutions in gas chromatography, 1272.

Belleau, B. See Marchini, P., 581.

Benoît, H. See Bushuk, W., 1616.

Benson, G. C. See White, P., 1135.

Berg, O. W., Lay, W. P., Rodgman, A., and **Wright, G. F.** Deoxymercuration, 358.

Berisford, R. and **Le Roy, D. J.** Reaction of deuterium atoms with ethane—mechanism of methane exchange, 983.

Berlinguet, L. See Talbot, G., 593.

Berman, S. S. and **Ironside, R.** A spectrophotometric determination of rhodium with tin (II) bromide, 1151.

Berman, S. S. and **McBryde, W. A. E.** Separations of the platinum metals by ion exchange, 835.

The separation of rhodium and iridium by ion exchange, 845.

Bernstein, H. J. See Abraham, R. J., 1302.

Berry, P. J. See Roy, J. C., 731.

Betts, E. E. and **MacLean, D. B.** Lycopodium alkaloids. VI. Reactions of the diphenyl derivative of desoxodihydroannotinine, 473.

Bigelow, C. C. and **Cragg, L. H.** Critical concentration effects in polymer–polymer–solvent systems, 199.

Blades, A. T. The kinetics of the thermal decomposition of ethyl bromide and ethyl bromide-d_5, 1043.

The mechanism of the pyrolysis of primary alkyl bromides, 1129.

Blanchfield, R. See Grant, G. A., 242.
Bock, E. See Campbell, A. N., 330, 1277.
Bock, E., Ferguson, J., and **Schneider, W. G.** Photoconductivity and absorption and fluorescence spectra of 9,10-dichloroanthracene, 507.
Boivin, J. L. Synthesis of N-substituted diisopropanolamines, their sebacate polyesters and polyurethane elastomers, 1405.
See also Gagnon, P. E., 737, 1436.
Boivin, J. L. and **Tremblay, M.** Synthesis of guanidine from urea, ammonium benzenesulphonate, and ammonium sulphamate, 378.
Boivin, P. A. See Gagnon, P. E., 737.
Bowering, W. D. S. and **Timell, T. E.** An alternative synthesis of 2-*O*-methyl-D-xylose, 283.
Brassard, P. and **L'Écuyer, P.** L'arylation des quinones par les sels de diazonium. I. Sur la synthèse des monoaryl-*p*-benzoquinones, 700.
L'arylation des quinones par les sels de diazonium. II. Sur la synthèse des 2,5-bisaryl-*p*-benzoquinones, 709.
L'arylation des quinones par les sels de diazonium. III. Sur la synthèse des aryl-chloro-*p*-benzoquinones, 814.
L'arylation des quinones par les sels de diazonium. IV. Sur la réaction de ces sels avec la 2,5-dihydroxy-*p*-benzoquinone et la synthèse de la 3-hydroxy-2,5-bisphenyl-*p*-benzoquinone, 1346.
Bright, N. F. H., Rowland, J. F., and **Wurm, J. G.** The compound $CaO.Ti_2O_3$, 492.
Bright, N. F. H. and **Wurm, J. G.** Some new fluoride complexes of trivalent titanium, 615.
Brook, A. G., Anderson, R. J., and **Van Patot, J. T.** Hydrogen abstraction reactions of diphenylpicrylhydrazyl, 159.
Brown, G. M. See Bannard, R. A. B., 1541.
Brown, W. H. and **French, W. N.** Synthesis of porphyrinogen-like compounds (mixed quaterenes), 371.
The condensation of furan with carbonyl compounds, 537.
Bullock, E. The structure of pyrrole salts and the basic strengths of some simple pyrroles, 1686.
Addition of pyrroles to 1,4-benzoquinone, 1744.
Burditt, A. M. See Douglas, D. E., 1256.
Bushuk, W. and **Benoît, H.** Light-scattering studies of copolymers. I. Effect of heterogeneity of chain composition on the molecular weight, 1616.
Bywater, S. See Worsfold, D. J., 1141.
Campbell, A. N. and **Bailey, R. A.** The system lithium nitrate – ethanol – water and its component binary systems, 518.
Campbell, A. N. and **Bock, E.** The limiting equivalent conductances of ammonium chloride, ammonium bromide, and ammonium nitrate at 35.00° C., 330.
The limiting conductance of potassium iodate and of iodate ion at 25.00° C, 1277.
Campbell, A. N. and **Kartzmark, E. M.** The systems Li_2SO_4–K_2SO_4–H_2O and Li_2SO_4–Na_2SO_4–H_2O at 25° C., 171.
Campbell, A. N., Kartzmark, E. M., and **Falconer, W. E.** The system: nicotine – methylethyl ketone – water, 1475.
Campbell, A. N., Kartzmark, E. M., and **Lovering, E. G.** Reciprocal salt pairs, involving the cations Li_2, Na_2, and K_2, the anions SO_4 and Cl_2, and water, at 25° C, 1511.
Campbell, A. N., Kartzmark, E. M., and **Sherwood, A. G.** Conductances of concentrated aqueous solutions of mixed electrolytes, 1325.
Campbell, A. N. and **Paterson, W. G.** The conductances of aqueous solutions of lithium chlorate at 25.00° C. and at 131.8° C., 1004.
Canady, W. J. and **Laidler, K. J.** Microcalorimetric and kinetic studies of the α-chymotrypsin – hydrocinnamic ester – hydrocinnamic acid system, 1289.
Casselman, A. A. See Bannard, R. A. B., 1541.
Cerfontain, H. and **Kutschke, K. O.** The photolysis of azoethane, 344.
Chao, T. S. See Lieber, E., 1441.
Chenon, B. and **Sandorfy, C.** Hydrogen bonding in the amine hydrohalides. I. General aspects, 1181.
Chisholm, M. J. and **Hopkins, C. Y.** Fatty acids of the seed oil of *Cardiospermum halicacabum*, 1537.
Cockburn, W. F. See Bannard, R. A. B., 1541.
Coffman, R. and **McClure, D. S.** The electronic spectra of crystalline toluene, dibenzyl, diphenylmethane, and biphenyl in the near ultraviolet, 48.
Coldwell, B. B. and **McLean, S. R.** A new spot test for nitrate ion, 652.
Connelly, B. T. and **Porter, G. B.** Kinetics of excited molecules. I. Ketene, 1640.
Constantin, R. and **L'Écuyer, P.** Sur la synthèse de quelques xanthones polysubstituées, 1381.
Sur la synthèse de formyldiphényl éthers polysubstitués, 1627.
Cragg, L. H. See Bigelow, C. C., 199; Manson, J. A., 858.
Craig, B. M. and **Murty, N. L.** The separation of saturated and unsaturated fatty acid esters by gas–liquid chromatography, 1297.
Cvetanović, R. J. Molecular rearrangements in the reactions of oxygen atoms with olefins, 623.
See also Dewing, J., 678; Sato, S., 279, 970, 1668.
Dearden, J. C. and **Forbes, W. F.** Light absorption studies. Part XII. Ultraviolet absorption spectra of benzaldehydes, 1362.
Dewing, J. and **Cvetanović, R. J.** The decomposition of nitrous oxide at low pressures on nickel oxide catalysts, 678.
Dickson, J. H. See Gagnon, P. E., 737.

DiGiorgio, V. E. See Robinson, G. W., 31.
Douglas, D. E. and **Burditt, A. M.** The reaction of cyanogen bromide with the sodium salts of carboxylic acids. II. The reaction of cyanogen bromide with the sodium salts of aliphatic acids, 1256.
Dunn, J. R. and **Kutschke, K. O.** Photooxidation of ketones in an O^{18} enriched environment, 421.
Dutton, G. G. S. and **Yates, K.** Methylation of sugar mercaptals. I. Introduction and D-glucose diethyl mercaptal, 550.
Dyne, P. J. and **Kennedy, J. M.** The kinetics of radical reactions in the tracks of fast electrons. A detailed study of the Samuel–Magee model for the radiation chemistry of water, 1518.
Edwards, O. E., Marion, L., and **Palmer, K. H.** The interrelation of delpheline and lycoctonine, 1097.
Elofson, R. M. The polarographic reduction of diazotized aromatic amines, 1207.
Elsdon, W. L. See McKenzie, D. E., 1233.
Eves, C. R. See Anet, F. A. L., 902.
Eyring, H., Stewart, G., and **Parlin, R. B.** Diabatic reactions, 72.
Falconer, W. E. See Campbell, A. N., 1475.
Falk, M. See Giguère, P. A., 883.
Falk, M. and **Giguère, P. A.** On the nature of sulphurous acid, 1121.
Infrared spectra and structure of selenious acid, 1680.
Favre, H. and **Marinier, B.** Sur la transformation de la dihydrohétéroconessine en dihydroconessine, 429.
Ferguson, J. See Bock, E., 507.
Ferguson, J. and **Schneider, W. G.** The polarized fluorescence of very thin anthracene crystals, 1070.
On the spectral response of photoconduction in thin single crystals of anthracene, 1633.
Flengas, S. N. and **Ingraham, T. R.** Voltaic cells in fused salts. Part III. The system silver – silver chloride, cadmium – cadmium chloride, 780.
Voltaic cells in fused salts. Part IV. Electrode potentials of the systems: Tl/TlCl (KCl–NaCl), Cu/C· Cl (KCl–NaCl), Cu/$CuCl_2$ (KCl–NaCl), Cr/$CrCl_2$ (KCl–NaCl), and Cr/$CrCl_3$ (KCl–NaCl). Redox potentials of the systems: Pt/CuCl, $CuCl_2$ (KCl–NaCl), and Pt/$CrCl_2$, $CrCl_3$ (KCl–NaCl), 1103.
Voltaic cells in fused salts. Part V. The systems Sn/$SnCl_2$ (KCl–NaCl), Fe/$FeCl_2$ (KCl–NaCl), and Mn/$MnCl_2$ (KCl–NaCl), 1662.
Fletcher, J. W. See McKenzie, D. E., 1233.
Flood, E. A. Some thermodynamic considerations of the effects of stress on metal electrode potentials, 1332.
Forbes, W. F. Light absorption studies. Part XI. Electronic absorption spectra of nitrobenzenes, 1350.
See also Dearden, J. C., 1362.
Forbes, W. F. and **Leckie, I. R.** Light absorption studies. Part XIII. The electronic absorption spectra of ring-substituted anilines, 1371.
Forbes, W. F., Ralph, A. S., and (in part) **Gosine, R.** Light-absorption studies. Part X. Ultraviolet spectra in acid and basic media—some further observations on the ortho effect, 869.
Forbes, W. F. and **Templeton, J. F.** The study of hydrogen bonding and related phenomena by ultraviolet light absorption. Part I. Introduction, 180.
Forrest, T. P. and **Ryan, D. E.** Sulphinic acids as analytical reagents, 1674.
Forst, W. Second-order unimolecular kinetics in the thermal decomposition of hydrogen peroxide vapor, 1308.
Foster, J. S. See Pate, B. D., 1691.
French, W. N. See Brown, W. H., 371, 537.
Frost, D. C. and **McDowell, C. A.** Excited states of the molecular ions of hydrogen fluoride, hydrogen iodide, water, hydrogen sulphide, and ammonia, 39.
Frost, G. B. See McAdie, H. G., 635.
Gagnon, P. E., Boivin, J. L., Boivin, P. A., and **Dickson, J. H.** Alkylguanidine nitrates and alkylnitroguanidines, 737.
Gagnon, P. E., Boivin, J. L., and **Zauhar, J.** Syntheses of substituted guanidines, 1436.
Gagnon, P. E., Keirstead, K. F., and **Newbold, B. T.** The relation between the sulphate and nitrogen content of unstabilized cellulose nitrate, 212.
A contribution to the chemistry of unstabilized cellulose nitrate, 215.
Determination of sulphate acid ester in unstabilized cellulose nitrate by the hydrolysis method, 291.
Slurry titrations of unstabilized cellulose nitrate, 672.
Gagnon, P. E., Keirstead, K. F., Newbold, B. T., and **Thomas, J.** Influence of water concentration on the hydrolysis of unstabilized cellulose nitrate in acetone/water solution, 695.
Hydrolysis of sulphate acid ester in unstabilized cellulose nitrates, 1039.
Gaind, V. S. See Wheeler, O. H., 1735.
Gardner, J. A. F. and **Barton, G. M.** Occurrence of β-dolabrin (4-isopropenyltropolone) in Western red cedar (*Thuja plicata* Donn.), 1612.
Garmaise, D. L. See McKay, A. F., 147.
Gaudry, R. See Talbot, G., 593.
Gavin, G. See Winthrop, S. O., 722, 879.
Gayer, K. H. and **Thompson, L. C.** The solubility of uranium peroxide in acidic and basic media at 25° C, 1649.
Gayer, K. H., Thompson, L. C., and **Zajicek, O. T.** The solubility of aluminum hydroxide in acidic and basic media at 25° C, 1268.
Gear, J. R. See Abramovitch, R. A., 1501.

George, M. V. and **Wright, G. F.** The electric moments of some N,N′-disubstituted piperazines, 189.
George, Z. M., Wright, A. N., and **Winkler, C. A.** The reactions of dimethyl- and trimethyl-amines with atomic hydrogen, 1171.
Georgieff, K. K. and **Richard, Y.** Diacetylene: preparation, purification, and ultraviolet spectrum, 1280.
Giacometti, G. and **Steacie, E. W. R.** The gas phase reactions of perfluoro-*n*-propyl radicals with methane and ethane, 1493.
Giguère, P. A. See Falk, M., 1121, 1680.
Giguère, P. A., Knop, O., and **Falk, M.** Hydrogen peroxide and its analogues. VIII. Excess functions for the binary systems H_2O–H_2O_2 and D_2O–D_2O_2, 883.
Giguère, P. A. and **Zengin, N.** Spectre infrarouge de HF à l'état cristallin, 1013.
Gill, E. K. and **Laidler, K. J.** Reactions involving electronically-excited oxygen, 79.
Theoretical aspects of the unimolecular decomposition of nitrous oxide, 1570.
Gillham, J. K., Perlin, A. S., and **Timell, T. E.** The configuration of glycosidic linkages in oligosaccharides. VII. 4-*O*-β-D-Galactopyranosyl-D-galactose from white birch wood, 1741.
Gillham, J. K. and **Timell, T. E.** The hemicellulose of white elm (*Ulmus americana*). I. Identification of 2-*O*-(4-*O*-methyl-D-glucopyranosyluronic acid)-D-xylopyranose, 410.
The hemicellulose of white elm (*Ulmus americana*). II. Constitution of the methyl glucurono-xylan, 1467.
Gingras, B. A. and **Bayley, C. H.** Polyoxyethyleneglycol ethers. Part II, 1320.
Goldman, G. K. See Rao, C. N. R., 1596.
Goodings, J. M. See Lake, P. E., 1089.
Gorin, P. A. J. and **Perlin, A. S.** D-Apiose, 480.
Hydrogenolysis of carbohydrates. IV. 1,2-*O*-*Iso*propylidene-D-glucofuranose, 661.
The configuration of glycosidic linkages in oligosaccharides. VI. Degradation of 4-*O*-methyl-D-glucopyranuronsyl-aldobiuronic acids to 2-*O*-(4-*O*-methyl-D-glucopyranosyl)-glycerols, 999.
Goring, D. A. I. See Huque, M. M., 952.
Goring, D. A. I. and **Rezanowich, A.** Physicochemical studies of ligninsulphonates. III. Properties of fractions prepared by successive sulphonation of periodate lignin, 1653.
Gosine, R. See Forbes, W. F., 869.
Goton, R. and **Whalley, E.** The thermodynamic properties of benzoic acid, 720.
Graham, G. D. and **Maass, O.** A modification of the direct current conductance method, 315.
Grant, G. A. See Armstrong, W. A., 1398; McIvor, R. A., 820.
Grant, G. A., Blanchfield, R., and **Smith, D. M.** Triarylmethane compounds as redox indicators in the Schoenemann reaction. III. The dyes and their spectra, 242.
Greenblatt, J. H. Note on the rate of evolution of hydrogen at a magnesium anode, 1138.
Grey, A. A. See McIvor, R. A., 820.
Grivas, J. C. and **Taurins, A.** Reaction of trichloroacetonitrile with primary and secondary amines. Part I. Preparation of some trichloroacetamidines, 771.
Gunning, H. E. Primary processes in reactions initiated by photoexcited mercury isotopes, 89.
Habgood, H. W. The kinetics of molecular sieve action. Sorption of nitrogen–methane mixtures by Linde Molecular sieve 4A, 1384.
Hamblin, M. C. See Lee, C. C., 1597.
Hawkins, L. R. See Bannard, R. A. B., 1241.
Hawkins, L. R. and **Bannard, R. A. B.** Ammonolysis of 1,2-epoxycyclohexane and *trans*-2-bromocyclohexanol, 220.
Hazell, J. E. and **Russell, K. E.** The reaction of 2,2-diphenyl-1-picrylhydrazyl with secondary amines, 1729.
Heacock, R. A. and (in part) **Mahon, M. E.** The chemistry of the "aminochromes". Part II. The preparation, paper chromatography, and spectroscopic properties of pure adrenolutin; the infrared spectrum of adrenochrome, 1550.
Heacock, R. A., Nerenberg, C., and **Payza, A. N.** The chemistry of the "aminochromes". Part I. The preparation and paper chromatography of pure adrenochrome, 853.
Heard, R. D. H., Balla, G. A., Jamieson, J. R., and **Ziegler, P.** Studies on the mechanisms of cyclization of ring A of steroids during the Reformatsky reaction, 1260.
Herron, J. T. and **Schiff, H. I.** A mass spectrometric study of normal oxygen and oxygen subjected to electrical discharge, 1159.
Heyding, R. D. See Taylor, J. B., 597.
Hites, R. D. See Lieber, E., 801.
Holbrook, K. A. and **Ouellet, L.** The non-enzymatic hydrolysis of *p*-nitrophenyl phosphate, 686.
Hopkins, C. Y. See Chisholm, M. J., 1537.
Hough, L., Jones, J. K. N., and **Mitchell, D. L.** The preparation of some derivatives of D-ribono-1→4-lactone and D-ribitol, 1720.
Hubley, C. E. See McIvor, R. A., 820.
Huque, M. M., Goring, D. A. I., and **Mason, S. G.** Molecular size and configuration of cellulose trinitrate in solution, 952.
Hyde, J. C. See Leger, A. E., 1584.
Ingraham, T. R. See Flengas, S. N., 780, 1103, 1662.
Ironside, R. See Berman, S. S., 1151.
Isabelle, E. See Anet, F. A. L., 589.
Isabelle, M. E. and **Leitch, L. C.** Organic deuterium compounds. XIX. Synthesis of some deuterated lauric acids and their methyl esters, 440.
Isfendiyaroğlu, A. N. See Talât-Erben, M., 1156.

Iveković, H. See Vrbaški, T., 1410.
Ives, D. A. J. and **O'Neill, A. N.** The chemistry of peat. Part I. The sterols of peat moss (*Sphagnum*), 434.
The chemistry of peat. II. The triterpenes of peat moss (*Sphagnum*), 926.
James, N. See Lee, C. C., 1597.
Jamieson, J. R. See Heard, R. D. H., 1260.
Jones, J. K. N. See Hough, L., 1720.
Jones, J. K. N. and **Mitchell, D. L.** The synthesis of ω-deoxy-ω-*S*-ethyl-polyols, 206.
Jones, R. N. and **Spinner, E.** The infrared carbonyl stretching bands of acetophenones substituted in the methyl group, 1020.
Kabayama, M. A. and **Patterson, D.** The thermodynamics of mutarotation of some sugars. II. Theoretical considerations, 563.
Kabayama, M. A., Patterson, D., and **Piche, L.** The thermodynamics of mutarotation of some sugars. I. Measurement of the heat of mutarotation by microcalorimetry, 557.
Kartzmark, E. M. See Campbell, A. N., 171, 1325, 1475, 1511.
Keirstead, K. F. See Gagnon, P. E., 212, 215, 291, 672, 695, 1039.
Kennedy, J. M. See Dyne, P. J., 1518.
Kim, J. S. See Pinkus, A. G., 296.
Kirby, P. and **Maass, O.** A study of the conductivity of certain acids and alkali halides in glycol and the influence of the addition of a second solvent, 456.
Klassen, N. V., Onyszchuk, M., McCabe, J. C., and **Winkler, C. A.** The reactions of active nitrogen with cyclopropane, cyclobutane, and cyclopentane, 1217.
Knop, O. See Giguère, P. A., 883.
Kommandeur, J., Korinek, G. J., and **Schneider, W. G.** The change of photoconduction and semiconduction in aromatic hydrocarbons on melting, 513.
Photoconductivity of some polynuclear aromatic hydrocarbons, 607.
Korinek, G. J. See Kommandeur, J., 513, 607.
Kouris, M., Ruck, H., and **Mason, S. G.** The effect of water removal on the crystallinity of cellulose, 931.
Kreling, M.-E. and **McKay, A. F.** Some new sulphonamides and derivatives of bicyclic guanidines, 775.
Kulka, M. Seven- and eight-membered rings containing carbon and two sulphur atoms, 750.
Kutschke, K. O. See Cerfontain, H., 344; Dunn, J. R., 421.
Laidler, K. J. Kinetic laws for surface reactions in flow systems, 1081.
See also Canady, W. J., 1289; Gill, E. K., 79, 1570; Papée, H. M., 1338.
Laidler, K. J. and **Ramsay, D. A.** A report on a symposium held by the Physical Chemistry Division of the Chemical Institute of Canada, 1.
Lake, P. E. and **Goodings, J. M.** The nature of the cadmium ions in hydroxide and carbonate solutions, 1089.
Lang, A. A. and **Sukava, A. J.** The system $KOH–K_2CO_3–H_2O$ at low temperatures. I. Phase equilibria, 1064.
Lay, W. P. See Berg, O. W., 358.
Leckie, I. R. See Forbes, W. F., 1371.
L'Écuyer, P. See Brassard, P., 700, 709, 814, 1346; Constantin, R., 1381, 1627.
Lee, C. C., Hamblin, M. C., and **James, N.** Rearrangement studies with C^{14}. VI. The Friedel–Crafts alkylation of benzene with ethyl-β-C^{14} iodide, 1597.
Leger, A. E., Hyde, J. C., and **Sheffer, H.** Light-scattering studies on aluminum distearate, 1584.
Leitch, L. C. See Isabelle, M. E., 440.
Le Roy, D. J. See Berisford, R., 983.
Lieber, E., Rao, C. N. R., Chao, T. S., and **Rubinstein, H.** The ultraviolet and infrared spectra of vicinal-triazole derivatives, 1441.
Lieber, E., Rao, C. N. R., Pillai, C. N., Ramachandran, J., and **Hites, R. D.** The infrared spectra of 4-substituted-thiosemicarbazides and diazotization products, 801.
Linnett, J. W. Equivalent orbitals and the shapes of excited species, 24.
Lounsbury, M. See McFadden, W. H., 990.
Lovering, E. G. See Campbell, A. N., 1511.
Maass, O. See Graham, G. D., 315; Kirby, P., 456; Thomas, D. K., 449, 744; Weinberger, M. A., 1455.
McAdie, H. G. and **Frost, G. B.** Studies of the mechanism of the formation and decomposition of the molecular complex between solid urea and *n*-octane vapor, 635.
McBryde, W. A. E. See Atkinson, G. F., 393; Berman, S. S., 835, 845.
McCabe, J. C. See Klassen, N. V., 1217.
McCallum, K. J. See Nelson, D. H., 979.
McClure, D. S. Energy transfer in molecular crystals and in double molecules, 59.
See also Coffman, R., 48.
McDowell, C. A. See Arnot, C., 114, 1322; Frost, D. C., 39.
McDowell, C. A. and **Sharples, L. K.** The photochemical oxidation of aldehydes in the gaseous phase. Part I. The kinetics of the photochemical oxidation of acetaldehyde, 251.
The photochemical oxidation of aldehydes in the gaseous phase. Part II. The kinetics of the photochemical oxidation of propionaldehyde, 258.
The photochemical oxidation of aldehydes in the gaseous phase. Part III. The absolute values of the velocity constants for the propagating and terminating steps in the photochemical oxidation of acetaldehyde and propionaldehyde, 268.

McElcheran, D. E., Wijnen, M. H. J., and **Steacie, E. W. R.** The photolysis of methyl cyanide at 1849 Å, 321.
McFadden, W. H., Lounsbury, M., and **Wahrhaftig, A. L.** The mass spectra of three deuterated butanols, 990.
McIvor, R. A., Hubley, C. E., Grant, G. A., and **Grey, A. A.** The infrared spectra of organo-phosphorus compounds. II. The 1–2.6 μ region, 820.
McKay, A. F. See Kreling, M.-E., 775; Tarlton, E. J., 496.
McKay, A. F., Skulski, M., and **Garmaise, D. L.** Reaction of amino alcohols with carbon disulphide, 147.
McKenzie, D. E., Elsdon, W. L., and **Fletcher, J. W.** The extraction of plutonium from neutron-irradiated uranium by uranium trichloride and by magnesium chloride, 1233.
McKinley, J. D., Jr. and **Polanyi, J. C.** Chemiluminescence in the system atomic sodium plus atomic hydrogen, 107.
MacLean, D. B. See Betts, E. E., 473; Perry, G. S., 1146.
McLean, S. R. See Coldwell, B. B., 652.
McMillan, G. and **Wijnen, M. H. J.** Reactions of alkoxy radicals. V. Photolysis of di-*t*-butyl peroxide, 1227.
Mahon, M. E. See Heacock, R. A., 1550.
Manske, R. H. F. See Perry, G. S., 1146.
Manson, J. A. and **Cragg, L. H.** A study of graft copolymers. I. Preparation and viscosity behavior, 858.
Marchini, P. and **Belleau, B.** The synthesis of cryptopleurine and related phenanthroquinolizidines, 581.
Marcus, R. A. Studies of chemical reactions of excited species using intense light sources, 102.
Marinier, B. See Favre, H., 429.
Marion, L. See Anet, R., 766; Edwards, O. E., 1097; Seaton, J. C., 1031; Wiehler, G., 339.
Mason, S. G. See Barton, S. S., 1126; Huque, M. M., 952; Kouris, M., 931; Murray, F. E., 415.
Mateos, J. L. See Wheeler, O. H., 712, 1049, 1431.
Merritt, W. F. Radiochemical analysis for long-lived fission products in environmental materials, 425.
Miller, M. L. Block and graft polymers. I. Graft polymers from acrylamide and acrylonitrile, 303.
Block and graft polymers. II. Block polymers from acrylamide and acrylonitrile and acrylamide and acrylic acid, 309.
Minkoff, G. J. Excited states of acetylene and their role in pyrolysis, 131.
Mitchell, D. L. See Hough, L., 1720; Jones, J. K. N., 206.
Moore, A. M. Ultraviolet irradiation of pyrimidine derivatives. II. Note on the synthesis of the product of reversible photolysis of uracil, 281.
Morris, W. and **Pidgeon, L. M.** The vapor pressure of lithium in the reduction of lithium oxide by silicon, 910.
Mousseau, T. J. See Weinberger, M. A., 1455.
Mulliken, R. S. The lower excited states of some simple molecules, 10.
Murray, F. E. and **Mason, S. G.** Coexistence phenomena in the critical region. V. The gravity effect in the binary liquid system aniline–cyclohexane from light scattering, 415.
Murty, N. L. See Craig, B. M., 1297.
Nelson, D. H. and **McCallum, K. J.** Chemical effects of the $Br^{81}(\gamma, \alpha)As^{77}$ reaction in bromides, 979.
Nerenberg, C. See Heacock, R. A., 853.
Newbold, B. T. See Gagnon, P. E., 212, 215, 291, 672, 695, 1039.
Novak, A. and **Whalley, E.** The structures of α- and β-parachloral, 1116.
Okabe, H. and **Steacie, E. W. R.** The fluorescence and its relationship to photolysis in hexafluoroacetone vapor, 137.
O'Neill, A. N. See Ives, D. A. J., 434, 926.
Onyszchuk, M. See Klassen, N. V., 1217.
Ouellet, L. See Holbrook, K. A., 686; Pelletier, G. E., 896.
Palmer, K. H. See Edwards, O. E., 1097.
Papée, H. M. On the preparation and sintering of cloud precipitating agents. Lead di-iodide microcrystals, 1443.
Papée, H. M. and **Laidler, K. J.** Microcalorimetry of the adsorption of water vapor on sodium chloride, 1338.
Parlin, R. B. See Eyring, H., 72.
Pate, B. D. Fission of excited heavy nuclei, 1707.
Pate, B. D., Foster, J. S., and **Yaffe, L.** Distribution of nuclear charge in the proton-induced fission of Th^{232}, 1691.
Paterson, W. G. See Campbell, A. N., 1004.
Patterson, D. See Kabayama, M. A., 557, 563.
Pavlović, D. See Vrbaški, T., 1410.
Payza, A. N. See Heacock, R. A., 853.
Pelletier, G. E. and **Ouellet, L.** Influence of calcium ions on the myosin-catalyzed hydrolysis of adenosine triphosphate, 896.
Perlin, A. S. Radiochemical evidence for heterogeneity in wheat starch, 810.
See also Gillham, J. K., 1741; Gorin, P. A. J., 480, 661, 999.
Perlin, A. S., von Rudloff, E., and **Tulloch, A. P.** Hydrogenolysis of carbohydrates. V. Isomerization of methyl β-L-arabopyranoside, 921.
Perry, G. S., MacLean, D. B., and **Manske, R. H. F.** Lycopodium alkaloids. VII. The reaction of annotinine with phenyl lithium, 1146.

Piche, L. See Kabayama, M. A., 557.
Pidgeon, L. M. See Morris, W., 910.
Pillai, C. N. See Lieber, E., 801.
Pinkus, A. G. and **Kim, J. S.** The reaction of carbon disulphide with alumina, 296.
Podleschka, P., Westland, L., and **Wright, G. F.** Some anomalous electrical polarizations, 574.
Polanyi, J. C. Quenching and vibrational-energy transfer of excited iodine molecules, 121.
See also McKinley, J. D., Jr., 107.
Pople, J. A. See Abraham, R. J., 1302.
Porter, G. B. See Connelly, B. T., 1640.
Puddington, I. E. See Sirianni, A. F., 543; Tremblay, R., 725.
Ralph, A. S. See Forbes, W. F., 869.
Ramachandran, J. See Lieber, E., 801.
Ramsay, D. A. See Laidler, K. J., 1.
Rao, C. N. R. See Lieber, E., 801, 1441; Smith, P., 1174.
Rao, C. N. R. and **Goldman, G. K.** Resonance parameters from reactivity constants, 1596.
Reeves, L. W. and **Schneider, W. G.** Nuclear magnetic resonance measurements of proton transfers in acetylacetone in diethylamine and triethylamine, 793.
Reichmann, M. E. Potato X virus. Part I. The size and size distribution of potato X virus in tobacco sap, 1603.
Rezanowich, A. See Goring, D. A. I., 1653.
Richard, Y. See Georgieff, K. K., 1280.
Rivest, R. See Archambault, J., 1461; Aubin, R., 915.
Robinson, G. W. and **DiGiorgio, V. E.** The nature of formaldehyde in its low-lying excited states, 31.
Rodgman, A. See Berg, O. W., 358.
Rowland, J. F. See Bright, N. F. H., 492.
Rowlinson, H. C. The effect of addition of potash to nickel chromite catalysts, 1053.
Roy, J. C., Berry, P. J., and **Roy, L. P.** Reactor neutron-capture cross section of 18-minute Rb^{88}, 731.
Roy, J. C. and **Wuschke, D.** Neutron capture cross section of I^{129} and I^{130}, 1424.
Roy, L. P. See Roy, J. C., 731.
Rubinstein, H. See Lieber, E., 1441.
Ruck, H. See Kouris, M., 931.
von Rudloff, E. Synthesis of some hexanediols, 486.
See also Perlin, A. S., 921.
Russell, D. S. An infrared cell for small gas samples, 1745.
See also Bednas, M. E., 1272.
Russell, K. E. See Hazell, J. E., 1729.
Ryan, D. E. See Forrest, T. P., 1674.
Sandorfy, C. Note on the inductive and mesomeric effects in substituted benzene derivatives, 1739.
See also Chenon, B., 1181.
Sandri, R. On the decomposition flame of ozone at high pressure, 1210.
Sato, S. and **Cvetanović, R. J.** Long-wavelength limit of photooxidation of butene-1 by nitrogen dioxide, 279.
Photoöxidation of butene-1 and isobutene by nitrogen dioxide, 970.
Photooxidation of butenes by nitrogen dioxide at different wave lengths, 1668.
Sawatzky, H. and **Wright, G. F.** The electrical polarizations of *bis*-mercurials, 1555.
Schierholtz, O. J. The crystallization of calcium sulphate dihydrate, 1057.
Schiff, H. I. See Herron, J. T., 1159.
Schneider, W. G. See Bock, E., 507; Ferguson, J., 1070, 1633; Kommandeur, J., 513, 607; Reeves, L. W., 793; Waddington, T. C., 789.
Scott, J. M. W. See Bavin, P. M. G., 1284.
Seaton, J. C., Tondeur, R., and **Marion, L.** The structure of mitraphylline, 1031.
Sharples, L. K. See McDowell, C. A., 251, 258, 268.
Sheffer, H. See Leger, A. E., 1584.
Sherwood, A. G. See Campbell, A. N., 1325.
Singh, L. Classical approach to the structure of condensed-ring aromatic compounds—a rejoinder to the problem of dibenzo(*cd,mn*)pyrene, 1028.
Sirianni, A. F. See Tremblay, R., 725.
Sirianni, A. F., Tremblay, R., and **Puddington, I. E.** The molecular weight of polyvinyl acetate, 543.
Skulski, M. See McKay, A. F., 147.
Smith, D. M. See Grant, G. A., 242.
Smith, F. G. Gaseous and liquid states of aggregation in the supercritical region, 1131.
Smith, P. and **Rao, C. N. R.** Prediction of some thermodynamic properties employing the isoelectronic principle, 1174.
Sobering, S. E. and **Winkler, C. A.** The reactions of active nitrogen with chloromethanes, 1223.
Spinner, E. See Jones, R. N., 1020.
Steacie, E. W. R. See Giacometti, G., 1493; McElcheran, D. E., 321; Okabe, H., 137.
Stevens, B. Some effects of intramolecular vibrational energy transfer in complex fluorescent molecules 96.
Stewart, G. See Eyring, H., 72.
Stonhill, L. G. The determination of UO_3 and U_3O_8 in brown oxide, 1487.
Sukava, A. J. See Lang, A. A., 1064.
Symposium on the structure and reactivity of electronically-excited species, 1–146.

Talât-Erben, M. and **Isfendiyaroğlu, A. N.** The extent of the abnormal recombination of cyanisopropyl free radicals from 2,2′-azo-bis-isobutyronitrile, 1156.
Talbot, G., Gaudry, R., and **Berlinguet, L.** Synthesis of 4-aminobutyric acid and 2,4-diaminobutyric acid from butyrolactone, 593.
Tarlton, E. J. and **McKay, A. F.** Amino acids. IV. The reaction of glycine and β-alanine with carbon disulphide, 496.
Taurins, A. Nitrimino-(1H)pyridinium and nitrimino-(3H)thiazolium inner salts. The structure of some nitrimines in the light of infrared study, 465.
See also Grivas, J. C., 771.
Taylor, G. W. Peroxides in the combustion of isobutane, 1213.
Taylor, J. B. and **Heyding, R. D.** Arsenates of the transition metals. The arsenates of cobalt and nickel, 597.
Templeton, J. F. See Forbes, W. F., 180.
Thomas, D. K. and **Maass, O.** Electrolytic conductance in hydrogen peroxide – water mixtures. Part I. The alkali chlorides, 449.
Electrolytic conductance in hydrogen peroxide – water mixtures. Part II. Some monobasic and dibasic acids, 744.
Thomas, J. See Gagnon, P. E., 695, 1039.
Thompson, L. C. See Gayer, K. H., 1268, 1649.
Thomson, J. B. See Allan, F. J., 1579.
Tickner, A. W. The determination in situ of the carbon content of solid products in reaction vessels, 718.
Timell, T. E. See Barth, F. W., 1321; Bowering, W. D. S., 283; Gillham, J. K., 410, 1467, 1741.
Tondeur, R. See Seaton, J. C., 1031.
Tremblay, M. See Boivin, J. L., 378.
Tremblay, R. See Sirianni, A. F., 543.
Tremblay, R., Sirianni, A. F., and **Puddington, I. E.** The molecular weight of polyethylene and of other high-molecular-weight organic compounds, 725.
Tulloch, A. P. See Perlin, A. S., 921.
Van Patot, J. T. See Brook, A. G., 159.
Vrbaški, T., Iveković, H., and **Pavlović, D.** The spontaneous precipitation of hydrated alumina from aluminate solutions, 1410.
Waddington, T. C. and **Schneider, W. G.** The effect of the ambient gases on the surface photocurrent in anthracene, 789.
Wahrhaftig, A. L. See McFadden, W. H., 990.
Weinberger, M. A., Mousseau, T. J., and **Maass, O.** Electrolysis of lithium hydride, 1455.
Westland, L. See Podleschka, P., 574.
Whalley, E. Conformational effects and the influence of pressure on reaction rates, 228.
See also Goto, R., 720; Novak, A., 1116.
Wheeler, O. H. Étard reaction. I. Its scope and limitation with substituted toluenes, 667.
Étard reaction. II. Polycyclic aromatic and heterocyclic compounds, 949.
Wheeler, O. H. and **Gaind, V. S.** Dissociation constants of the cyanohydrins of some triterpene ketones, 1735.
Wheeler, O. H. and **Mateos, J. L.** Reactivity studies on natural products. IV. Dissociation constants of the cyanohydrins of some steroid ketones, 712.
Reactivity studies on natural products. V. Rates of borohydride reduction of some ring A and B steroid ketones, 1049.
Stereochemistry of reduction of ketones by complex metal hydrides, 1431.
Wheeler, O. H. and **Zabicky, J. Z.** Structure and properties of cyclic compounds. XI. Dissociation constants of the cyanohydrins of some methylcyclohexanones, 656.
White, P. and **Benson, G. C.** Ultrasonic absorption in butyric acid, 1135.
Wiehler, G. and **Marion, L.** (–)-Homostachydrine, a new alkaloid isolated from the seeds of *Medicago sativa* L. Grimm, 339.
Wijnen, M. H. J. Photolysis of acetone in the presence of methyl-d_3 acetate, 176.
Photolysis of *n*- and *i*-propyl propionate, 691.
See also McElcheran, D. E., 321; McMillan, G., 1227.
Wiles, D. R. Exchange between thallous and thallic ions in the presence of sulphate ion, 167.
Wilmshurst, J. K. The infrared and Raman spectrum of dimethoxymethane, 285.
Winkler, C. A. See George, Z. M., 1171; Klassen, N. V., 1217; Sobering, S. E., 1223.
Winthrop, S. O. and **Gavin, G.** 1-Arylsulphonyl-3-*n*-butyl-2-methyl-2-thiopseudoureas, 722.
2-Benzhydrylimino-4-thiazolidones and related compounds, 879.
Worsfold, D. J. and **Bywater, S.** Anionic polymerization of α-methylstyrene. Part II. Kinetics, 1141.
Wright, A. N. See George, Z. M., 1171.
Wright, G. F. See Berg, O. W., 358; George, M. V., 189; Podleschka, P., 574; Sawatzky, H., 1555.
Wurm, J. G. See Bright, N. F. H., 492, 615.
Wuschke, D. See Roy, J. C., 1424.
Yaffe, L. See Pate, B. D., 1691.
Yates, K. See Dutton, G. G. S., 550.
Zabicky, J. Z. See Wheeler, O. H., 656.
Zajicek, O. T. See Gayer, K. H., 1268.
Zauhar, J. See Gagnon, P. E., 1436.
Zengin, N. See Giguère, P. A., 1013.
Ziegler, P. See Heard, R. D. H., 1260.

CORRECTIONS

Volume 36, 1958.

Page 371. Figure 1 should be replaced by the figure appearing below.

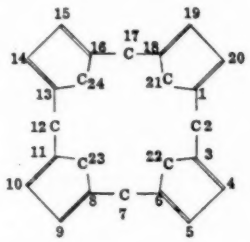

QUATERENE NUCLEUS

Page 857. Reference 20 should read: "HARLEY-MASON, J. and BU'LOCK, J. J. Chem. Soc. 712 (1951)."

Page 1026. On line 13 "on this unnecessary detail" should read: "on this in unnecessary detail".

Page 1317. On the first line "contribution of the homogeneous reaction" should read: "contribution of the heterogeneous reaction".

Page 1318. On the eighth line from the bottom of the page "E_A and s are experimental quantities" should read "E_A and a are experimental quantities".

Page 1558. On line 13 "orientation polarization" should read: "distortion polarization".

Volume 35, 1957.

Page 513. In footnote 3 "3×10^{10}" should read: "2×10^{10}".

HELVETICA CHIMICA ACTA

SCHWEIZERISCHE
CHEMISCHE GESELLSCHAFT
Verlag Helvetica Chimica Acta
Basel 7 (Schweiz)

Seit 1918 **40** Jahre

Abonnemente: **Jahrgang 1958, Vol. XLI $22.10 incl. Porto**

Es sind noch lieferbar:

Neudruck ab Lager
Vol. I–XIV (1918–1931)
Vol. XVII–XX (1934–1937)

Vol. XV, XVI, XXI–XXV (1932, 1933, 1938–1942) in Vorbereitung.

Originalausgaben, druckfrisch und antiquarisch.
Vol. XXVI–XL (1943–1957)

Diverse Einzelhefte ab Vol. XXI
Preise auf Anfrage. Nur solange Vorrat

Das wissenschaftliche Organ der SCHWEIZERISCHEN CHEMISCHEN GESELLSCHAFT

CANADIAN JOURNAL OF CHEMISTRY

Notes to Contributors

Manuscripts

(i) ***General.*** Manuscripts, in English or French, should be typewritten, double spaced, on paper 8½×11 in. **The original and one copy are to be submitted.** Tables and captions for the figures should be placed at the end of the manuscript. Every sheet of the manuscript should be numbered.

Style, arrangement, spelling, and abbreviations should conform to the usage of recent numbers of this journal. Names of all simple compounds, rather than their formulas, should be used in the text. Greek letters or unusual signs should be written plainly or explained by marginal notes. Superscripts and subscripts must be legible and carefully placed.

Manuscripts and illustrations should be carefully checked before they are submitted. Authors will be charged for unnecessary deviations from the usual format and for changes made in the proof that are considered excessive or unnecessary.

(ii) ***Abstract.*** An abstract of not more than about 200 words, indicating the scope of the work and the principal findings, is required, except in Notes.

(iii) ***References.*** These should be designated in the text by a key number and listed at the end of the paper, with the number, in the order in which they are cited. The form of the citations should be that used in this journal; in references to papers in periodicals, titles should not be given and only initial page numbers are required. The names of periodicals should be abbreviated in the form given in the most recent *List of Periodicals Abstracted by Chemical Abstracts*. All citations should be checked with the original articles and each one referred to in the text by the key number.

(iv) ***Tables.*** Tables should be numbered in roman numerals and each table referred to in the text. Titles should always be given but should be brief; column headings should be brief and descriptive matter in the tables confined to a minimum. Vertical rules should not be used. Numerous small tables should be avoided.

Illustrations

(i) ***General.*** All figures (including each figure of the plates) should be numbered consecutively from 1 up, in arabic figures, and each figure referred to in the text. The author's name, title of the paper, and figure number should be written in the lower left corner of the sheets on which the illustrations appear. Captions should not be written on the illustrations (see Manuscripts (i)).

(ii) ***Line Drawings.*** Drawings should be carefully made with India ink on white drawing paper, blue tracing paper, or co-ordinate paper ruled in blue only; any co-ordinate lines that are to appear in the reproduction should be ruled in black ink. Paper ruled in green, yellow, or red should not be used. All lines should be of sufficient thickness to reproduce well. Decimal points, periods, and stippled dots should be solid black circles large enough to be reduced if necessary. Letters and numerals should be neatly made, preferably with a stencil (**do NOT use typewriting**), and be of such size that the smallest lettering will not be less than 1 mm high when reproduced in a cut of suitable size.

Many drawings are made too large; originals should not be more than 2 or 3 times the size of the desired reproduction. Wherever possible two or more drawings should be grouped to reduce the number of cuts required. In such groups of drawings, or in large drawings, full use of the space available should be made; the ratio of height to width should conform to that of a journal page (5½×7¾ in.) but allowance must be made for the captions.

The original drawings and one set of clear copies (e.g. small photographs) are to be submitted.

(iii) ***Photographs.*** Prints should be made on glossy paper, with strong contrasts. They should be trimmed so that essential features only are shown and mounted carefully, with rubber cement, on white cardboard, with no space between them. In mounting, full use of the space available should be made to reduce the number of cuts required (see Illustrations (ii)). Photographs or groups of photographs should not be more than 2 or 3 times the size of the desired reproduction.

Photographs are to be submitted in duplicate; if they are to be reproduced in groups one set should be mounted, the duplicate set unmounted.

Reprints

A total of 50 reprints of each paper, without covers, are supplied free. Additional reprints, with or without covers, may be purchased at the time of publication.

Charges for reprints are based on the number of printed pages, which may be calculated approximately by multiplying by 0.5 the number of manuscript pages (double-space typewritten sheets, 8½×11 in.) and including the space occupied by illustrations. An additional charge is made for illustrations that appear as coated inserts. Prices and instructions for ordinary reprints are sent out with the galley proof.

Any reprints required in addition to those requested on the author's reprint requisition form must be ordered officially as soon as the paper has been accepted for publication.

Contents

M. E. Reichmann—Potato X virus. Part I. The size and size distribution of potato X virus in tobacco sap - - - - - - - - - - - - - - - 1603

J. A. F. Gardner and G. M. Barton—Occurrence of β-dolabrin (4-isopropenyltropolone) in western red cedar (*Thuja plicata* Donn.) - - - - - - 1612

W. Bushuk and H. Benoît—Light-scattering studies of copolymers. I. Effect of heterogeneity of chain composition on the molecular weight - - 1616

R. Constantin and P. L'Écuyer—Sur La synthèse de formyldiphényl éthers polysubstitués - - - - - - - - - - - - - - - - - - - 1627

J. Ferguson and W. G. Schneider—On the spectral response of photoconduction in thin single crystals of anthracene - - - - - - - - - - 1633

B. T. Connelly and Gerald B. Porter—Kinetics of excited molecules. I. Ketene 1640

Karl H. Gayer and Lancelot C. Thompson—The solubility of uranium peroxide in acidic and basic media at 25° C - - - - - - - - - - - 1649

D. A. I. Goring and A. Rezanowich—Physicochemical studies of lignin-sulphonates. III. Properties of fractions prepared by successive sulphonation of periodate lignin - - - - - - - - - - - - - - - - - 1653

S. N. Flengas and T. R. Ingraham—Voltaic cells in fused salts. Part V. The systems Sn/$SnCl_2$ (KCl-NaCl), Fe/$FeCl_2$ (KCl-NaCl), and Mn/$MnCl_2$ (KCl-NaCl) - 1662

S. Sato and R. J. Cvetanović—Photooxidation of butenes by nitrogen dioxide at different wave lengths - - - - - - - - - - - - - - - - - 1668

T. P. Forrest and D. E. Ryan—Sulphinic acids as analytical reagents - - 1674

Michael Falk and Paul A. Giguère—Infrared spectra and structure of selenious acid - 1680

E. Bullock—The structure of pyrrole salts and the basic strengths of some simple pyrroles - 1686

B. D. Pate, J. S. Foster, and L. Yaffe—Distribution of nuclear charge in the proton-induced fission of Th^{232} - - - - - - - - - - - - - 1691

B. D. Pate—Fission of excited heavy nuclei - - - - - - - - - - - 1707

L. Hough, J. K. N. Jones, and D. L. Mitchell—The preparation of some derivatives of D-ribono-1→4-lactone and D-ribitol - - - - - - - - - 1720

J. E. Hazell and K. E. Russell—The reaction of 2,2-diphenyl-1-picrylhydrazyl with secondary amines - - - - - - - - - - - - - - - - 1729

Owen H. Wheeler and V. S. Gaind—Dissociation constants of the cyanohydrins of some triterpene ketones - - - - - - - - - - - - - - - 1735

Notes:

C. Sandorfy—Note on the inductive and mesomeric effects in substituted benzene derivatives - - - - - - - - - - - - - - - - - - 1739

J. K. Gillham, A. S. Perlin, and T. E. Timell—The configuration of glycosidic linkages in oligosaccharides. VII. 4-*O*-β-D-Galactopyranosyl-D-galactose from white birch wood - - - - - - - - - - - - - - - - - 1741

E. Bullock—Addition of pyrroles to 1,4-benzoquinone - - - - - - - 1744

D. S. Russell—An infrared cell for small gas samples - - - - - - - 1745

Contents of Volume 36 - - - - - - - - - - - - - - - - - - - 1747

Printed in Canada *by* University of Toronto Press